Slx5/Slx8-dependent Ubiquitin Hotspots on Chromatin Contribute to Stress Tolerance in *Saccharomyces Cerevisiae*

Dissertation der Fakultät für Biologie
der Ludwig-Maximilians-Universität München

Zur Erlangung des Doktorgrades vorgelegt von
Mag. rer. nat. Markus Höpfler

Mai 2019

Eidesstattliche Erklärung

Hiermit erkläre ich an Eides statt, dass ich die vorliegende Dissertation selbstständig und ohne unerlaubte Hilfe angefertigt habe. Ich habe weder anderweitig versucht eine Dissertation einzureichen oder eine Doktroprüfung durchzuführen, noch habe ich diese Dissertation oder Teile derselben einer anderen Prüfungskommission vorgelegt.

München, den 7. 5. 2019 Markus Höpfler

1. Gutachter: Prof. Dr. Peter Becker

2. Gutachter: Prof. Dr. Christof Osman

Tag der Abgabe: 7. 5. 2019

Tag der mündlichen Prüfung: 27. 6. 2019

Die vorliegende Arbeit wurde zwischen Oktober 2013 und Mai 2019 unter der Anleitung von Prof. Dr. Stefan Jentsch und Dr. Boris Pfander am Max-Planck-Institut für Biochemie in Martinsried durchgeführt.

Wesentliche Teile dieser Arbeit, insbesondere Resultate und Abbildungen, sowie eine überarbeitete Fassung von Teilen des Textes, sind in folgender Publikation veröffentlicht und zusammengefasst:

Markus Höpfler, Maximilian J. Kern, Tobias Straub, Roman Prytuliak, Bianca H. Habermann, Boris Pfander, and Stefan Jentsch (2019). Slx5/Slx8-dependent ubiquitin hotspots on chromatin contribute to stress tolearance. *EMBO J:* e100368.

"A discovery is like falling in love and reaching the top of a mountain after a hard climb all in one, an ecstasy not induced by drugs but by the revelation of a face of nature that no one has seen before and that often turns out to be more subtle and wonderful than anyone had imagined."

Max F. Perutz

Table of Contents

Summary

Chromatin is a tightly controlled cellular environment and protein association with chromatin is often regulated by post-translational modifications (PTMs), including modification with SUMO and ubiquitin. In the last decades, both these modifications and their corresponding enzymatic machineries have emerged as pivotal regulators involved in nuclear quality control, DNA repair and transcriptional regulation. More recently, SUMO-targeted ubiquitin ligases (STUbLs) were discovered to provide an important link between those pathways, as they recognize SUMOylated proteins and catalyze their ubiquitylation. However, many of the physiological functions of STUbLs and how exactly they recognize specific substrates, while SUMOylated proteins are highly prevalent on chromatin, remained elusive.

In this study, my analysis of the genome-wide distribution of the yeast STUbL Slx5/Slx8 demonstrates a remarkably specific localization of Slx5/Slx8 to seven loci of strong ubiquitin accumulation, so-called “ubiquitin hotspots”. My data show that Slx5/Slx8 is recruited to ubiquitin hotspots by the uncharacterized transcription factor-like protein Ymr111c/Euc1. Slx5/Slx8 recruitment relies on a bipartite interaction between Ymr111c/Euc1 and Slx5, which involves the Slx5 SUMO-interacting motifs and a novel, uncharacterized substrate recognition domain of Slx5 directly interacting with Ymr111c/Euc1. Importantly, the Euc1–ubiquitin hotspot pathway and Slx5/Slx8 are required for the cellular response to various stresses like temperature shifts, in particular when general gene expression control is impaired by mutation of members of the H2A.Z and Rpd3L pathways.

Thus, my data suggest that the STUbL-dependent ubiquitin hotspots shape chromatin during stress adaptation, and the bipartite recruitment mechanism exemplifies how specificity can be generated in the STUbL pathway. These findings can guide future research elucidating how different substrate recognition domains control the diverse STUbL functions, which range from the response to DNA damage to early embryonic development.

1. Introduction

1.1 Post-translational Modification by Ubiquitin and UBLs

Post-translational modifications (PTMs) represent an essential way for all eukaryotic cells to modify protein function and virtually all cellular pathways can be regulated and fine-tuned by PTMs. Many PTMs like phosphorylation, acetylation or methylation expand the chemical repertoire of the twenty regular amino acids by addition of a small chemical group to side chains or to protein N- or C-termini. In contrast, modifications by ubiquitin (referred to as ubiquitylation or ubiquitination) and ubiquitin-like proteins (UBLs, e. g. SUMO) are distinct, because they involve the covalent attachment of a small protein to the substrate protein (Varshavsky, 2012). The ubiquitin-family proteins of eukaryotic cells comprise nearly twenty proteins that share a typical β-grasp fold and that are highly diverse in their cellular functions (Van der Veen & Ploegh, 2012). The founding member ubiquitin is most well-known for its function in targeting proteins for degradation by the 26S proteasome (Finley *et al*, 2012). However, already in the early days of ubiquitin research, it had been revealed that ubiquitin functions not only in protein degradation pathways, but also in DNA repair and cell cycle regulation (Jentsch *et al*, 1987; Goebl *et al*, 1988). Over the last three decades, it became clear that ubiquitin achieves these functions by both proteolytic and nonproteolytic means, and numerous additional pathways and signaling events in all eukaryotic cells have been described to be regulated by the ubiquitin system (Oh *et al*, 2018). Similarly, other UBLs are involved in a wide range of cellular processes, including proteolysis, nuclear transport, autophagy, antiviral defense, tRNA-modification or splicing (Van der Veen & Ploegh, 2012). The molecular mechanisms of UBLs range from covalent attachment to substrate proteins similar to ubiquitylation (e. g. SUMO, Urm1, Nedd8/Rub1, Atg12) over covalent modification of lipids with Atg8 in autophagy, to non-covalent functions of Hub1 in splicing, or extracellular signaling functions of soluble ISG15 (Van der Veen & Ploegh, 2012). These variegated molecular mechanisms vividly reflect the diversity of cellular UBL functions.

Besides the ubiquitin proteasome system (UPS), the small ubiquitin-like modifier (SUMO) pathway is of specific relevance to this study. It has been shown to be particularly active within the nucleus and targets many DNA-associated proteins (Jentsch & Psakhye, 2013; Flotho & Melchior, 2013). SUMO and ubiquitin together regulate many chromatin-associated processes like DNA repair, replication or transcription (Gareau & Lima, 2010; Geng *et al*, 2012; Dantuma & van Attikum, 2016; Schwertman *et al*, 2016; Rosonina *et al*,

2017), and both systems with their specific functions at chromatin will be discussed in the following sections in more detail, with particular focus on the model organism *Saccharomyces cerevisiae*.

1.2 The Ubiquitin Pathway

1.2.1 Covalent Modification of Substrate Proteins by Ubiquitin

Ubiquitylation is achieved by the covalent attachment of the 8.5 kDa protein ubiquitin to substrate proteins, usually to ε-amino groups of lysine residues via its C-terminal di-glycine motif that is exposed upon initial processing. The enzymatic cascade required for ubiquitylation (Fig. 1) is initiated by an E1 enzyme for ubiquitin activation (Uba1), which forms a high-energy thioester-bond between the ubiquitin C-terminal carboxyl group and a cysteine residue in an ATP-dependent manner. In a transesterification reaction, activated ubiquitin is then transferred to the cysteine residue of a ubiquitin-conjugating enzyme (E2, Ubc-enzymes). Finally, ubiquitin ligases (E3) catalyze the isopeptide bond formation between the ubiquitin C-terminus and the ε-amino group of lysine residues of substrate proteins (Varshavsky, 2012; Finley *et al*, 2012; Deshaies & Joazeiro, 2009). The enzymes are organized in a hierarchical manner, with a single E1 in yeast (up to two in other species), eleven E2s (>30 in mammalian cells), and 60–100 E3s (>600 in mammalian cells) (Finley *et al*, 2012; Oh *et al*, 2018). Because many E3s act in concert with E2s, several hundred E2–E3 complexes are possible in yeast, which is the basis for substrate specificity of ubiquitin ligases (Kerscher *et al*, 2006). Typically, specific recognition by ubiquitin ligases is conferred by linear or structural motifs on the surface of substrate proteins, which are called degrons if proteins are destined for degradation (Varshavsky, 2012). The ubiquitin pathway repertoire is enriched by E4 enzymes, which are E3 ligases that specifically act on monoubiquitylated substrates to attach polyubiquitin chains (Koegl *et al*, 1999).

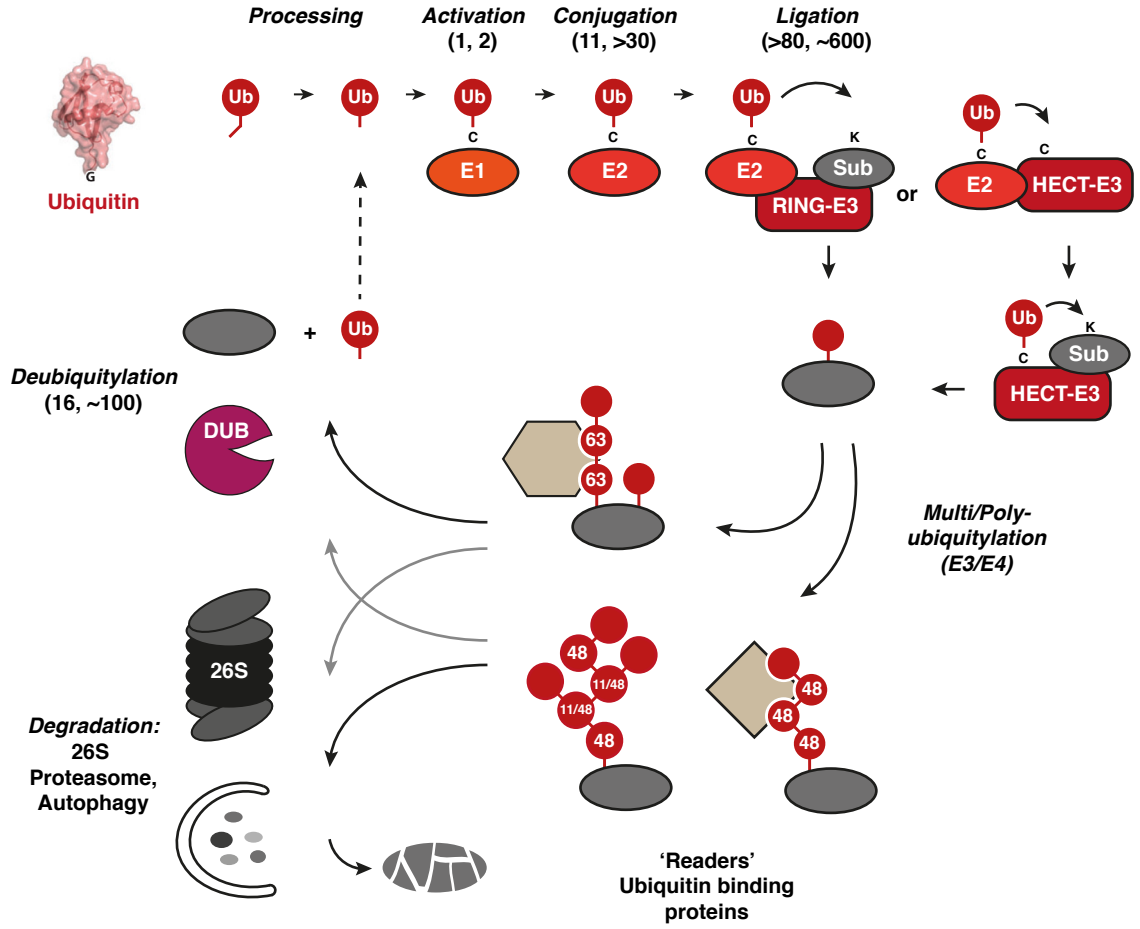

Figure 1. The ubiquitin pathway.
Ubiquitin (Ub) is translated as a precursor that needs C-terminal processing and for ubiquitylation, an enzymatic cascade involving enzymes for activation (E1), conjugation (E2) and finally ligation (E3) to substrate lysines (K) is required (top). RING-type E3s catalyze transfer of ubiquitin from an E2 to substrates (Sub), while HECT-type ligases first transfer ubiquitin to an internal cysteine (C) residue (top right). Monoubiquitylated substrates can be further modified resulting in multi- or polyubiquitylation (center). Polyubiquitylation can result in different chain topologies and while mono- or K63-linked chains often signal nonproteolytic functions (center, top branch), K11, K48 or mixed chain types often result in degradation via the 26S proteasome or the autophagy pathway (bottom left). Specific recognition of chain topologies is mediated by ubiquitin-binding proteins, or "readers" (shown in light brown). Finally, deubiquitylation enzymes (DUBs) can cleave ubiquitin to recycle free ubiquitin and unmodified substrates (center left). Numbers in brackets indicate number of enzyme family members in *S. cerevisiae* and in *H. sapiens*, respectively.

Ubiquitin Ligases

Within E3 ligases, three distinct families have been described to date: (1) RING (really interesting new gene), (2) HECT (homologous to E6AP C-terminus) and (3) RBR (RING-between-RING) domain ligases (Morreale & Walden, 2016; Zheng & Shabek, 2017). RING domain ligases act in concert with E2s and catalyze ubiquitin transfer directly from the E2 to the substrate by positioning them in a conformation that allows efficient ubiquitylation (Fig. 1) (Deshaies & Joazeiro, 2009). Adding to the complexity of the ubiquitylation enzyme machinery, RING-ligases often form homo- and heterodimers as well as oligomeric structures (Deshaies & Joazeiro, 2009). On the other hand, HECT and RBR domain ligases, which are RING-HECT hybrid enzymes, contain a catalytic cysteine

residue that accepts ubiquitin from the E2 and subsequently transfer it to the substrate protein (Fig. 1) (Scheffner *et al*, 1995; Finley *et al*, 2012; Morreale & Walden, 2016). RING domain ligases constitute the majority of E3s in yeast, with only five HECT domain and two putative RBR ligases encoded in the yeast genome (Finley *et al*, 2012). Importantly, many ubiquitin ligases act in complex with regulatory or adaptor subunits, with the anaphase promoting complex or cyclosome (APC/C) representing probably the most complex ligase composed of 13 subunits (McLean *et al*, 2011). A large class of multi-subunit ligases is the Cullin-RING ligase (CRL) family, for which a wide range of substrate specificity is achieved by a modular architecture featuring at least four subunits (RING protein, cullin-scaffold, linker protein and substrate receptor). For full activity, CRLs require modification by the UBL Rub1 (NEDD8 in humnas) (Deshaies & Joazeiro, 2009; Skaar *et al*, 2013; Liakopoulos *et al*, 1998).

Functions of Polyubiquitylation

Ubiquitin ligases differ not only in their substrate specificity, but also in the pattern of substrate ubiquitylation, because after initial monoubiquitylation all of the seven lysine residues within ubiquitin (K6, K11, K27, K29, K33, K48, K63) and its N-terminal amino group (M1) can be used for chain formation (polyubiquitylation) (Finley *et al*, 2012; Komander & Rape, 2012). In principle all chain types can lead to proteasomal degradation, although K11- and K48-linked chains appear to be the major degradation signals (Fig. 1). M1- and K63-chains often serve as signaling platforms in DNA repair, NFκB-signaling or protein synthesis, and K6-chains are important in mitophagy (Oh *et al*, 2018; Komander & Rape, 2012). Specific functions of the less abundant K27-, K29- and K33-chains are largely unexplored. Recently, new research has also shed light on specific functions of mixed and branched chain types. For example, K11/K48-branched chains have been demonstrated to act as a priority signal for proteasomal degradation of conjugated substrates (Meyer & Rape, 2014; Yau *et al*, 2017), further expanding the "ubiquitin code" (Komander & Rape, 2012).

Besides canonical conjugation to amino groups of lysine residues or the ubiquitin N-terminus, ubiquitin can also be attached to thiol or hydroxyl groups in cysteine, serine or threonine residues (Pao *et al*, 2018; Cadwell & Coscoy, 2005; Shimizu *et al*, 2010; Wang *et al*, 2012). Recent findings also demonstrated the ability of bacterial effector proteins to transfer ubiquitin to substrate serines in a phosphoribosylation-dependent manner, bypassing the eukaryotic E1-E2-E3 cascade (Qiu *et al*, 2016; Bhogaraju *et al*, 2016).

Taken together, the immense complexity of the enzymatic machinery catalyzing ubiquitylation allows specific recognition of a wide range of substrates and generates a variegated pattern of substrate ubiquitylation. Consequently, to mediate proper downstream recognition or processing of substrates, an equally diversified set of "readers" of this code is required.

1.2.2 Consequences of Protein Ubiquitylation

Once a protein is covalently modified with ubiquitin, the mark can be recognized to mediate a plethora of biological functions, which can be conceptually separated into substrate processing and signaling events. Major substrate processing events triggered by ubiquitin are further modifications with other PTMs, proteasomal or autophagic degradation (discussed in more detail below) or deubiquitylation by specific proteases (deubiquitylating enzymes, DUBs) to balance ubiquitylation (Fig. 1) (Dikic, 2017; Mevissen & Komander, 2017; Pickles *et al*, 2018). Signaling by ubiquitin is highly diverse and ranges from endolysosomal receptor sorting over the establishment of signaling platforms in immune reactions or in DNA repair, to the recruitment of other modifying enzymes to establish epigenetic marks on chromatin (Höhfeld & Hoppe, 2018; Oh *et al*, 2018).

Ubiquitin Binding Domains

Both processing and signaling functions are mediated by proteins harboring specific ubiquitin binding domains (UBDs) (Dikic *et al*, 2009; Husnjak & Dikic, 2012). Not surprisingly, there is a wide range of UBDs, most of which recognize a hydrophobic patch around isoleucine 44 on the surface of ubiquitin. Around twenty distinct UBDs can be grouped according to structural features: (1) α-helical (e.g. ubiquitin-interacting motif (UIM), ubiquitin-associated (UBA)), (2) zinc finger (ZnF, e.g. ubiquitin-binding zinc finger (UBZ)), (3) plekstrin homology (PH) domain, (4) ubiquitin-conjugating (Ubc)-like domain, and (5) other structures (Dikic *et al*, 2009; Husnjak & Dikic, 2012). The basis for specific recognition of certain chain-types by UBDs is the distinct structural topology that arises due to linkage via different lysine residues. For example, UBDs can act as rulers to measure the distance between ubiquitin moieties in a chain: Two tandem UIMs in RAP80 separated by a seven-residue helix recognize the extended conformation of K63-linked chains, but not compact K48-linked chains (Sato *et al*, 2009; Sims & Cohen, 2009). On the other hand, two closely spaced UIMs in Ataxin-3 separated by only two residues mediate preference for the compact K48 chains. In this case, swapping the linkers is sufficient to

change the preference for K48- versus K63-linked chains (Sims & Cohen, 2009). A different mode of binding is applied by the UBA domain of the proteasome shuttling factor RAD23A (Rad23 in yeast) to recognize K48 chains. Here, the UBA domain is sandwiched by two closely spaced K48-linked ubiquitin moieties and has contacts with both molecules and the linkage, which gives it selectivity over monoubiquitin (Varadan *et al*, 2005).

Combination of different UBDs could also allow the specific recognition of branched chains or chains with different linkage types. For the case of K11/K48 branched chains, however, the increased local ubiquitin concentration was suggested to support more efficient binding by the proteasome and the ubiquitin-specific segregase p97/VCP (Cdc48 in yeast, see below) (Yau *et al*, 2017).

Deubiquitylation

UBDs are also essential for the specificity of DUBs (~20 in yeast, ~100 in humans), which counteract ubiquitylation by cleaving off individual ubiquitin moieties, partial or complete chains (Mevissen & Komander, 2017; Harrigan *et al*, 2018). So far, six families of DUBs can be distinguished based on structural features of their catalytic domain: (1) USP (ubiquitin specific protease), (2) OTU (ovarian tumor protease), (3) UCH (ubiquitin C-terminal hydrolase), (4) Josephin, (5) MINDY (motif interacting with ubiquitin DUB family), and (6) JAMM-type (JAB1/MPN/MOV34). The first five DUB families are all cysteine proteases, while JAMM-type DUBs are Zn-dependent metalloproteases. Related to DUBs are also ubiquitin-like proteases (ULPs) that cleave UBLs like SUMO (see below) or NEDD8 (Mevissen & Komander, 2017; Harrigan *et al*, 2018).

1.2.3 Proteasomal Protein Degradation

The 26S proteasome is the endpoint of the ubiquitin-proteasome system because it degrades ubiquitylated substrates and achieves recycling of their amino acid components (Bard *et al*, 2018). Depending on the nature of the substrate and the ubiquitin chain type, substrates can also be degraded by autophagy-mediated delivery to the lysosome (vacuole in yeast) (Dikic, 2017; Lu *et al*, 2014; 2017). However, the fact that autophagy is dispensable in yeast under normal growth conditions, while proteasome function is essential, underscores the importance of the proteasome for cellular physiology. This is especially true for nuclear proteins that are largely inaccessible to autophagy.

The proteasome is a large 2.5 MDa complex composed of a barrel-shaped 20S core particle (CP) and one or two 19S regulatory particles (RP) attached to either side that regulate entry to the central pore (Finley *et al*, 2012; Bard *et al*, 2018). Altogether, 33

proteins constitute the largest and most complex ATP-dependent protease in eukaryotes. The protease activity is mediated by three subunits of the two CP central β-rings (β1, β2 and β5), which are shielded by adjacent α-rings that regulate substrate entry and serve as docking sites for RPs on either side (Finley *et al*, 2012; Bard *et al*, 2018). The RP is essential for substrate selection and delivery to the proteolytic cavity and is composed of a 9-subunit base and a 9-subunit lid subcomplex, linked by an additional factor (Rpn10). As part of the base, the heterohexameric Rpt1–Rpt6 AAA+-type motor (ATPases associated with various cellular activities) provides the energy to unfold and thread substrates into the catalytic center.

Substrate recognition is achieved by intrinsic or extrinsic ubiquitin receptors (Bard *et al*, 2018). At least three intrinsic receptors (Rpn1, Rpn10 and Rpn13) are part of the RP (Schreiner *et al*, 2008; Husnjak *et al*, 2008; van Nocker *et al*, 1996; Deveraux *et al*, 1994; Elsasser *et al*, 2002), while extrinsic receptors, also called shuttling factors (Rad23, Dsk2 and Ddi1 in yeast, more paralogs in humans), dynamically associate with the proteasome (Hofmann & Bucher, 1996; Schauber *et al*, 1998; Kaplun *et al*, 2005; Elsasser *et al*, 2002; Funakoshi *et al*, 2002). This is achieved by a domain organization featuring a UBA domain for ubiquitin binding and a ubiquitin-like (UBL) domain that is in turn bound by the intrinsic proteasome receptors Rpn1 or Rpn13. Together, these receptors allow recognition of ubiquitylated substrates, especially K11-, K48-, K29-, but also K63-linked chains (Lu *et al*, 2017). Interestingly, the *in vivo* preference of the proteasome for substrates modified with K48-linked ubiquitin chains might be largely due to the linkage type specificity of upstream processing by the AAA+ enzyme Cdc48 and associated factors (Richly *et al*, 2005; Tsuchiya *et al*, 2017).

Preceding degradation, substrates are usually deubiquitylated by proteasome-associated DUBs to allow recycling of ubiquitin. Of those, the JAMM-type metalloprotease Rpn11 of the lid subcomplex is essential and it cleaves off ubiquitin chains between substrates and the first ubiquitin moiety en bloc (Bard *et al*, 2018; Maytal-Kivity *et al*, 2002; Verma *et al*, 2002). Additionally, the non-essential DUBs Ubp6 and Uch37 (no homolog in *S. cerevisiae*) act at the proteasome (Bard *et al*, 2018; Verma *et al*, 2000; Leggett *et al*, 2002).

1.2.4 The Ubiquitin-targeted Segregase Cdc48

A key component of the UPS involved in both proteolytic and nonproteolytic functions is the AAA+-type ATPase Cdc48 (p97 or valosin-containing protein/VCP in humans). The

main function of Cdc48 is the physical dissociation of ubiquitylated substrates from their local subcellular environment, like large protein complexes, membranes or chromatin, often leading to proteasomal degradation of substrates (Jentsch & Rumpf, 2007; Meyer *et al*, 2012; van den Boom & Meyer, 2017). Like other AAA+-type ATPases (e.g. the Rpt1–Rpt6 complex of the RP), Cdc48 utilizes the chemical energy of ATP to create physical movement of its subunits, ultimately resulting in a pulling force on substrates. Each subunit of the homohexameric ring-shaped structure consists of a lateral, N-terminal N-domain and two ATPase subunits (D1 and D2) stacked on top of each other and surrounding the central pore (DeLaBarre & Brunger, 2003; Buchberger *et al*, 2015; Banerjee *et al*, 2016).

For long, it had been thought that substrates cannot enter the narrow central pore of Cdc48 and are only remodeled due to structural rearrangements on the outer surface of Cdc48. However, recently it has been demonstrated that model substrates are unfolded and even threaded through the pore, shedding new light on how Cdc48 could provide a continuous pulling force, which is required e.g. for its function in the translocation of proteins over membranes (Bodnar & Rapoport, 2017; Blythe *et al*, 2017). So far, this threading mechanism has only been demonstrated *in vitro*, and whether and to what extent this also applies to substrates *in vivo* still needs further investigation (Bodnar & Rapoport, 2017).

Regulation of Cdc48 Functions by Cofactors

The molecular segregase function of Cdc48 is applicable to a wide range of substrates, due to its association with a number accessory proteins or cofactors (around 40 in mammals) (Buchberger *et al*, 2015). Conceptually, Cdc48 cofactors can be separated into two major groups: substrate recruiting cofactors and substrate processing cofactors (Jentsch & Rumpf, 2007; Buchberger *et al*, 2015). Most cofactors bind to the N-domain via distinct Cdc48-binding domains or motifs, including the UBX (ubiquitin regulatory X) or UBXL (UBX-like) domains or the short linear binding motifs VIM (VCP-interacting motif), VBM (VCP-binding motif) and SHP box (suppressor of high-copy PP1). In contrast, PUB (PNGase/UBA or UBX containing proteins) and PUL (PLAP, Ufd3, and Lub1) domains mediate binding to the Cdc48 C-terminus (Buchberger *et al*, 2015).

Three basic Cdc48 complexes can be distinguished based on association with substrate-recruitment cofactors: (1) Most functions in protein segregation upstream of proteasomal degradation are mediated by the $Cdc48^{Ufd1\text{-}Npl4}$ complex; (2) $Cdc48^{Shp1}$ ($p97^{p47}$

in mammals) regulates homotypic membrane fusion events; (3) with UBXD1, which is only found in mammalian cells, $p97^{UBXD1}$ is involved in sorting of ubiquitylated cargo in the endocytic pathway (Buchberger *et al*, 2015; Ritz *et al*, 2011; Hetzer *et al*, 2001). Additional cofactors can associate with these basic complexes to better control substrate specificity or cellular localization of Cdc48/p97.

Substrate processing cofactors can modify the ubiquitylation status of substrates, exemplified for Spt23 ubiquitylation by the antagonistic action of the Ufd2 ubiquitin ligase and the Otu1 DUB, which fine-tune Spt23 degradation kinetics (Richly *et al*, 2005; Rumpf & Jentsch, 2006; Jentsch & Rumpf, 2007). Other processing activities include the PNGase function (peptide N-glycanase) for deglycosylation of misfolded glycoproteins in mammalian cells (Li *et al*, 2006) and the recently described protease function of Wss1 acting on DNA–protein crosslinks, although the exact function of Cdc48 in this pathway is still elusive (Stingele *et al*, 2014; Stingele & Jentsch, 2015). The latest addition to this group of diverse enzymatic functions is the peptidyl-tRNA hydrolase or tRNA-cleavage activity of Vms1 that facilitates release of aberrant tRNA-linked peptides from stalled ribosomes (Verma *et al*, 2018; Rendón *et al*, 2018; Kuroha *et al*, 2018).

In addition to substrate recruitment and processing cofactors, a third distinct group comprising regulatory cofactors that modulate Cdc48 activity has been suggested recently, which includes TUG (also known as ASPL or UBXD9, Ubx4 in yeast), UBXD4 and SVIP in mammalian cells (Hänzelmann & Schindelin, 2017).

Cellular Functions of Cdc48

The wide range of cofactors and their distinct activities imply diverse biological functions of Cdc48. Indeed, Cdc48 is involved in cell cycle progression, homotypic membrane fusion, endoplasmic reticulum-associated degradation (ERAD), mitochondria-associated degradation, autophagy, ribosome-associated quality control, transcription factor (TF) processing and various chromatin-associated functions (the latter will be discussed in more detail as part of the next section) (van den Boom & Meyer, 2017; Franz *et al*, 2016). As an example for TF processing, the activation mechanism of the transcription factor Spt23 of the oleic acid pathway in yeast has greatly contributed to a mechanistic understanding of Cdc48: Spt23 is synthesized as an inactive precursor (p120) and has a transmembrane domain that tethers it to the ER. Upon activation it is ubiquitylated and cleaved by the proteasome, but stays attached to its uncleaved homodimer binding partner. Separation of this complex to allow translocation of the active p90 fragment into the nucleus requires the

activity of $Cdc48^{Ufd1\text{-}Npl4}$. This has led to the proposition of Cdc48 as a molecular segregase (Rape *et al*, 2001; Jentsch & Rumpf, 2007).

Another well-studied example of Cdc48-function is its role in ERAD. Here, $Cdc48^{Ufd1\text{-}Npl4}$ is required to translocate misfolded proteins across the ER membrane, which is assisted by the transmembrane cofactor Ubx2 and Ubx4. ERAD substrates first get ubiquitylated on the cytoplasmic surface of the ER membrane and then Cdc48 is required to fully translocate them across the membrane to allow proteasomal degradation (Berner *et al*, 2018). Like for many proteolytic functions of Cdc48, the shuttling factors Rad23 and Dsk2 facilitate substrate handover to the proteasome (Berner *et al*, 2018; Richly *et al*, 2005).

1.2.5 Chromatin-related Functions of Ubiquitin and Cdc48/p97

Nuclear functions of ubiquitin can be separated in quality control (QC) functions similar to cytoplasmic QC pathways, and functions related to DNA metabolism and chromatin, which will be discussed in more detail due to their relevance to this study (Finley *et al*, 2012; Ulrich & Walden, 2010; Shibata & Morimoto, 2014; Gallagher *et al*, 2013). Historically, the ubiquitin system is tightly linked to DNA transactions: histone H2A was the first identified ubiquitin substrate (Goldknopf *et al*, 1977); the first cloned E2 enzymes Rad6 and Cdc34 play pivotal roles in DNA repair and cell cycle regulation, respectively (Jentsch *et al*, 1987; Goebl *et al*, 1988); and the first physiological substrate for ubiquitin dependent proteasomal degradation was the transcription factor Matα2 (Hochstrasser & Varshavsky, 1990; Hochstrasser *et al*, 1991). Over the last three decades, both proteolytic and nonproteolytic functions of ubiquitin have been demonstrated in a wide range of chromatin-related processes. These include (1) regulation of replication by controlling crucial factors in initiation, origin licensing, replication fork protection, replication termination and chromosome segregation (Finley *et al*, 2012; Abbas & Dutta, 2017; Dewar & Walter, 2017); (2) various DNA repair pathways, like postreplicative DNA repair, global genome repair or transcription coupled repair (Bergink & Jentsch, 2009; Ulrich & Walden, 2010); and (3) the regulation of chromatin structure and epigenetic marks, transcription, mRNA processing and export (Tutucci & Stutz, 2011; Geng *et al*, 2012; Hammond-Martel *et al*, 2012; Yao & Ndoja, 2012; Braun & Madhani, 2012).

Importantly, Cdc48/p97 has emerged as a crucial downstream processing factor thanks to its ability to remove ubiquitylated proteins that are tightly associated with chromatin (Franz *et al*, 2016; Dantuma & Hoppe, 2012). The first examples for chromatin

targets of Cdc48/p97 include the Aurora B kinase that is extracted from chromatin by p97 at the end of mitosis to allow reformation of the nucleus (Ramadan *et al*, 2007), and the replication licensing factor CDT1 (and CDT-1 in *C. elegans*) that needs to be removed from chromatin to ensure a single round of replication origin firing per cell cycle (Raman *et al*, 2011; Franz *et al*, 2011). More recently, it has been discovered that also replication termination involves Cdc48/p97: After DNA replication is finished, the Mcm7 subunit of the CMG helicase (Cdc45, minichromosome maintenance [MCM] subunits 2–7, GINS complex) is marked with K48-linked ubiquitin chains (by the E3 ligase complexes SCF^{DIA2} in yeast and $CRL2^{LRR1}$ in vertebrates) and disassembled from DNA by Cdc48/p97 (Maric *et al*, 2014; Moreno *et al*, 2014; Maculins *et al*, 2015; Dewar *et al*, 2017). Cdc48 not only acts on DNA replication components, but is also critically involved in transcription by targeting TFs (Wilcox & Laney, 2009; Ndoja *et al*, 2014) or subunits of stalled/defective RNA polymerases II and III (Verma *et al*, 2011; Wang *et al*, 2018). Cdc48 plays another important role in the response to various sources of DNA damage (reviewed in (Franz *et al*, 2016)), where it has been shown to also act in non-conventional ways by targeting not only ubiquitylated, but also SUMOylated proteins (Nie *et al*, 2012; Bergink *et al*, 2013).

Taken together, it is now well accepted that the UPS and in particular Cdc48 play crucial roles in the control and maintenance of chromatin composition throughout the cell cycle and in interphase cells. Importantly, ubiquitin-mediated functions can interfere and crosstalk with other PTMs at chromatin to ensure accurate regulation and responses to changing cellular conditions. One of these is modification with the related SUMO, which is known to be particularly active in the nucleus and has been shown to be involved in numerous protein–DNA transactions.

1.3 The SUMO pathway

1.3.1 Protein Modification with SUMO

At first glance, the SUMO and ubiquitin pathways share striking similarities: The chemistry of covalent attachment of SUMO to substrates (SUMOylation) is analogous to that of ubiquitin, relying on initial processing to expose a C-terminal di-glycine motif, activation by an E1-enzyme (the heterodimeric Aos1/Uba2 in *S. cerevisiae*), transfer to a cysteine residue of an E2 conjugating enzyme and transfer to substrates aided by E3 ligases (Fig. 2) (Gareau & Lima, 2010). Like ubiquitylation, SUMOylation can lead to formation of SUMO chains (polySUMOylation), but can also be reversed

(deSUMOylation) by the activity of specific proteases of the Ulp or SENP-family (ubiquitin-like specific protease or sentrin specific protease), and deSUMOylating Isopeptidase-1 (Fig. 2) (Mevissen & Komander, 2017; Kunz *et al*, 2018). SUMO is essential in most eukaryotes, and while a single gene encodes SUMO in *S. cerevisiae* (*SMT3*), there are at least three distinct isoforms in higher eukaryotes (SUMO1–3) (Flotho & Melchior, 2013).

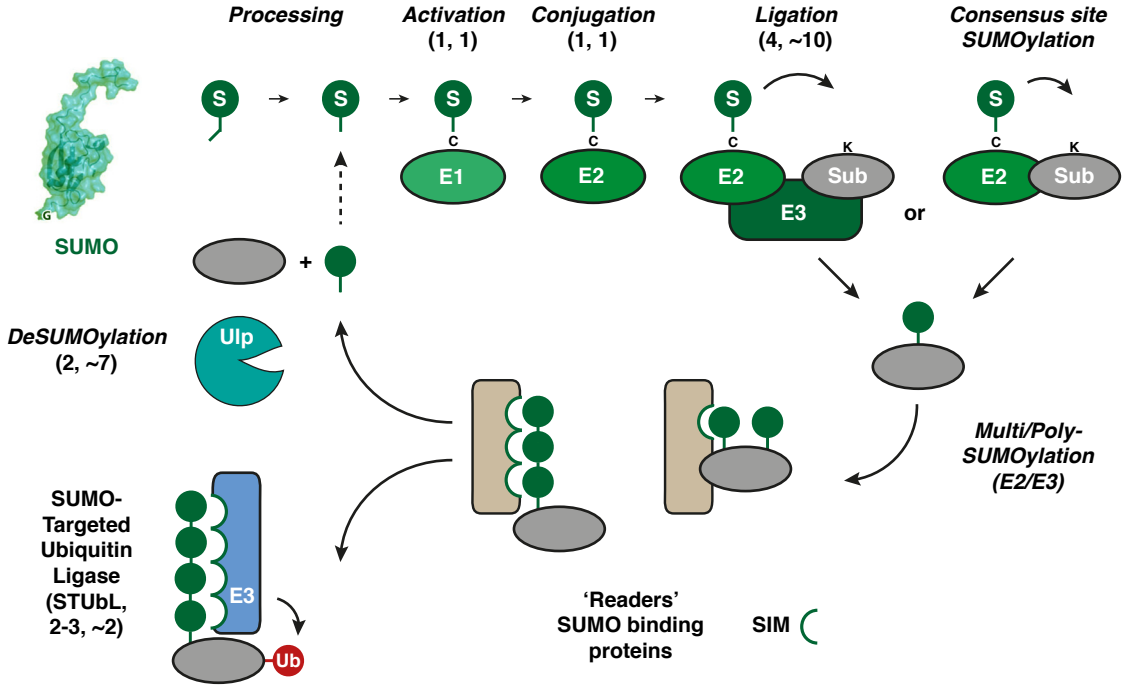

Figure 2. The SUMO pathway.
As for ubiquitin, the SUMO (S) is translated as a precursor and needs C-terminal processing and an enzymatic cascade for activation (E1), conjugation (E2) and ligation (E3) to lysines within substrate (Sub) proteins (top). Lysines within SUMOylation consensus sites (ΨKx(D/E), Ψ is a large hydrophobic residue) can also be modified by the E2 enzyme without the need of E3s (top right). Center: SUMOylation often provides additional protein–protein interaction sites for binding partners with SUMO-interacting motifs (SIMs, SUMO binding proteins shown in light brown). Multi-SIM proteins have increased specificity for multi/polySUMOylated proteins, like some SUMO-targeted ubiquitin ligases (STUbLs), which transfer SUMO-substrates to the ubiquitin pathway (bottom left). Alternatively, deSUMOylation by ubiquitin-like specific proteases (Ulp) leads to recycling of free SUMO and substrates (center left). Numbers in brackets indicate number of enzyme family members in *S. cerevisiae* and in *H. sapiens*, respectively.

Despite these parallels, the enzymatic outfit of the SUMO pathway reveals an obvious difference to the ubiquitin pathway: While multiple E2 and myriads of E3 enzymes and DUBs promote substrate specificity in the ubiquitin pathway (see above), Ubc9 is the sole E2 in both yeast and mammalian cells, only very few E3 enzymes exist (Siz1, Siz2, Mms21, and Zip3 in yeast, around ten are described in mammalian cells), and only two specific proteases are present in yeast (7 in mammalian cells) (Jentsch & Psakhye, 2013; Kunz *et al*, 2018; Mevissen & Komander, 2017). Interestingly, many proteins with the consensus SUMOylation site ΨKx(D/E), where ψ is a large hydrophobic

residue, can be modified by Ubc9 alone, bypassing the need for E3s altogether (Gareau & Lima, 2010). Therefore, for many target proteins it currently remains enigmatic if and how the limited number of enzymes allow specific targeting by the SUMO pathway.

The apparent lack of high substrate specificity, together with the observation that in many cases multiple proteins of a macromolecular complex or functional pathway are simultaneously SUMOylated led to the proposition of the concept of "protein group SUMOylation" (Psakhye & Jentsch, 2012; Jentsch & Psakhye, 2013). First demonstrated for the homologous recombination (HR) DNA repair pathway (Psakhye & Jentsch, 2012), according to this idea, SUMOylation happens in waves upon specific triggers or confined to subcellular localizations, and targets multiple members of a protein complex with low specificity, e.g. HR repair proteins that assemble on DNA double strand breaks (Jentsch & Psakhye, 2013). SUMO-mediated protein–protein interactions can then help to both propagate the SUMOylation wave and act as a molecular glue to stabilize complexes. Other examples of protein groups targeted by SUMOylation include yeast septin proteins that assemble at the bud neck, telomeres, ribosome biogenesis factors, or promyelocytic leukemia (PML) bodies in mammalian cells (Johnson & Blobel, 1999; Potts & Yu, 2007; Panse *et al*, 2006; Shen *et al*, 2006). Although for protein group SUMOylation individual modified sites often seem dispensable or redundant, SUMOylation can also target highly specific lysine residues to achieve distinct outcomes.

1.3.2 Consequences of SUMOylation

On a molecular level, protein modification with SUMO can have three main consequences for target proteins (Jentsch & Psakhye, 2013): First, SUMOylation can compete with other PTMs that target lysine residues, like ubiquitylation, which can lead to protein stabilization (e.g. for of IκBα (Desterro *et al*, 1998)), or acetylation, which in the case of MEF2A affects its activity as transcription factor (Shalizi *et al*, 2006). Second, addition of the 11 kDa SUMO moiety to a protein can block interactions with other proteins, as demonstrated for proliferating cell nuclear antigen (PCNA) K127 SUMOylation that prevents the interaction with Eco1 (Moldovan *et al*, 2006). Third, SUMOylation can enhance protein–protein interactions, which seems to be the most prevalent function (Gareau & Lima, 2010). This mechanism is usually brought about by a moderate-affinity interaction between SUMO and SUMO-interacting motifs (SIMs), which consist of a short stretch of hydrophobic residues (often (V/I)x(V/I)(V/I)), sometimes flanked by acidic residues (Song *et al*, 2004). This interaction can stabilize weak interactions or achieve specificity for

SUMO-modified binding partners, as exemplified by the preferential binding of the Srs2 helicase to K164-SUMOylated PCNA during S-phase (Pfander *et al*, 2005; Papouli *et al*, 2005; Armstrong *et al*, 2012). Crucially, SUMO–SIM interactions also contribute to the proposed glue-like function and protein group SUMOylation, because most SUMO E3s harbor SIMs and are therefore attracted to SUMOylated proteins or complexes. An additional SUMO–SIM mediated function can be intramolecular contacts that change protein conformation, as for thymine DNA glycosylase (Steinacher & Schär, 2005).

Like for ubiquitin chains, polySUMO chains can also be recognized by proteins that harbor multiple SIMs, although there seems to be little specificity towards linkage types, and increased avidity is the basis for recognition of multi- or polySUMOylated proteins by multi-SIM proteins (Cappadocia & Lima, 2018). A prominent example of multi-SIM proteins are SUMO-targeted ubiquitin ligases (STUbLs) that recognize SUMOylated proteins and catalyze their ubiquitylation, which can ultimately lead to their degradation (Fig. 2, see also below) (Sriramachandran & Dohmen, 2014). Mixed chains can also be recognized by reader proteins that feature both SUMO- and ubiquitin-binding domains, as exemplified by RAP80 being recruited to DNA damage sites by STUbL-generated mixed chains (Guzzo *et al*, 2012).

Taken together, like all PTMs, SUMOylation expands and fine-tunes the functions of modified proteins, however, alteration of protein–protein interactions plays a central role for SUMO-mediated functions.

1.3.3 Cellular Functions of SUMO

In contrast to ubiquitin, SUMO signals primarily nonproteolytic functions. Consistent with the relatively low specificity of the enzymatic machinery, many proteins can be modified with SUMO, evidenced by estimates of ~10% of the yeast proteome being targeted by SUMOylation under different conditions (Jentsch & Psakhye, 2013); a similar fraction was reported for the human proteome (>3600 proteins) (Hendriks & Vertegaal, 2016). Notably, dramatic responses of global SUMOylation patterns can be induced by certain cellular stress conditions, including heat shock (where SUMOylation increases in most organisms), oxidative stress, or hypoxia (Tempé *et al*, 2008). Importantly, SUMOylation is essential for cellular survival under some of these stress conditions, but the molecular basis is largely unclear (Flotho & Melchior, 2013). Although examples for dedicated SUMO functions in the cytoplasm have been described (e.g. the above-mentioned septins), SUMO

primarily acts in the nucleus and most SUMOylation enzymes localize to the nucleus (Jentsch & Psakhye, 2013).

Consistently, SUMO substrates are enriched for nuclear and DNA-binding proteins (Wohlschlegel *et al*, 2004; Hannich *et al*, 2005; Lewicki *et al*, 2014). Several nuclear substructures are regulated or maintained by SUMOylation, including DNA repair foci, telomeres, nucleoli, centromeres and kinetochores, polycomb group bodies and PML-bodies as well as processes like DNA repair, cell cycle progression, transcription, pre-mRNA splicing, nucleo-cytoplasmatic transport and ribosome biogenesis (Cubeñas-Potts & Matunis, 2013; Zhao, 2018). Historically, early on after the discovery of SUMO in the mid-1990s (Matunis *et al*, 1996; Mahajan *et al*, 1997), SUMO pathway mutants were linked to nuclear anomalies and chromosome segregation defects (Biggins *et al*, 2001; Hari *et al*, 2001). Since then, SUMO emerged as a central player in several DNA-repair pathways, including homolgous recombination (HR), non-homologous end joining (NHEJ), base excision repair (BER), and nucleotide excision repair (NER), orchestrating repair proteins often in concert with other PTMs like ubiquitylation (Bergink & Jentsch, 2009; Ulrich & Walden, 2010). Also in the context of DNA repair, SUMOylation is required for chromosome movements and the relocation of certain types of DNA lesions to the nuclear pore complex or nuclear envelope (Nagai *et al*, 2008; Horigome *et al*, 2016; Kalocsay *et al*, 2009).

SUMO in Transcriptional Regulation

Additionally, proteins linked to transcription are amongst the most prominent SUMO substrates (Fig. 3) (Wohlschlegel *et al*, 2004; Hannich *et al*, 2005; Lewicki *et al*, 2014). In most cases, SUMOylation was shown to have a negative effect on transcription, although examples for SUMO-mediated activation are emerging (Chymkowitch *et al*, 2015a). Global regulators of transcription, including DNA methyltransferases or histone deacetylases (HDACs), which mediate mostly repressive effects, have been shown to be regulated by SUMO. For example, SUMOylated histones or TFs can recruit HDAC1 and HP1 (heterochromatin protein 1) (Shiio & Eisenman, 2003), and SUMOylation of HDAC1 and HDAC4 is required for full transcriptional repression of target promoters (David *et al*, 2002; Kirsh *et al*, 2002; Cheng *et al*, 2004).

For gene-specific TFs, SUMOylation can modulate their effect on transcription in numerous ways (Rosonina *et al*, 2017). Conceptually, SUMOylation can on the one hand directly affect TF activity on DNA by interfering with other regulatory PTMs like

acetylation and phosphorylation, or by mediating recruitment of corepressors (like HDACs) or coactivators (Fig. 3A–C). On the other hand, in many cases SUMOylation influences TF association with DNA, e.g. by regulating shuttling of TFs into the nucleus, regulating DNA-binding, promoting TF clearance from DNA, or by triggering STUbL-mediated TF degradation (Fig. 3D–H) (Rosonina *et al*, 2017; Sri Theivakadadcham *et al*, 2019).

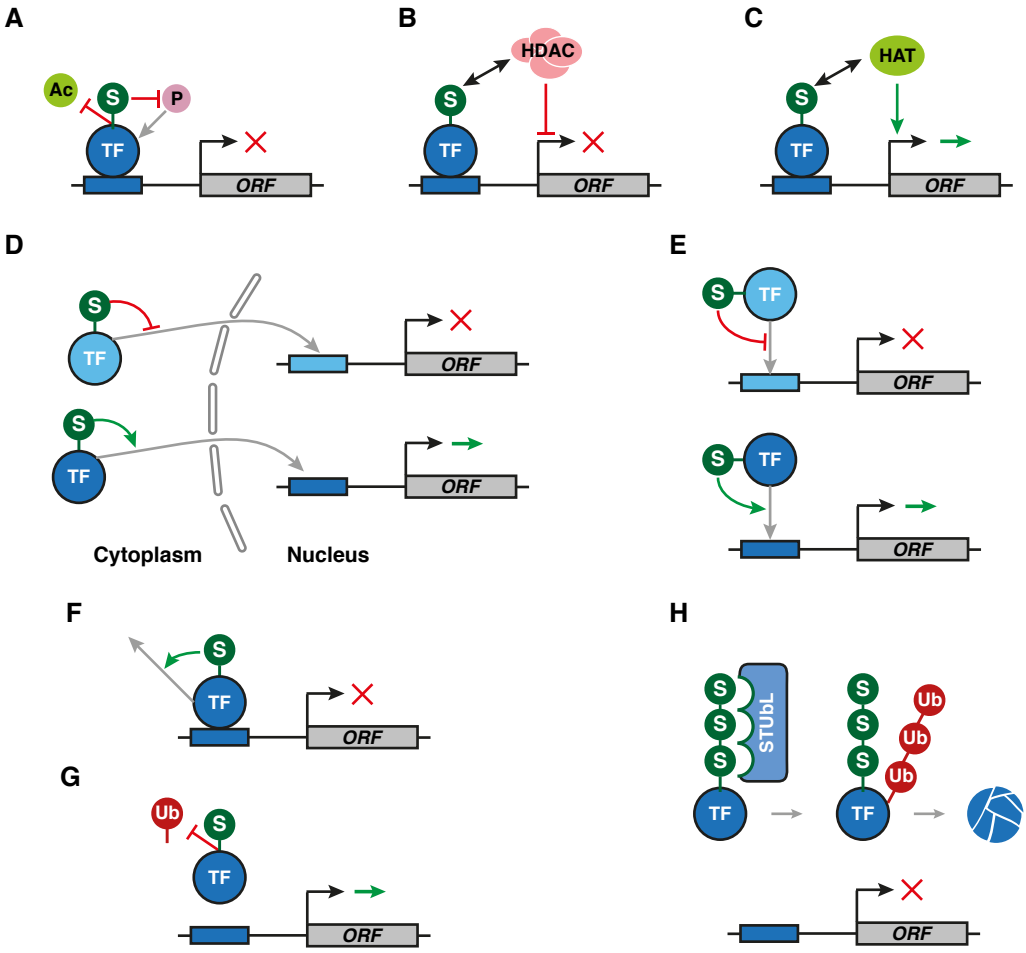

Figure 3. SUMO in transcriptional regulation.
(A-C) SUMOylation can modulate transcription factor (TF) activity, e.g. by (A) blocking other modifications like acetylation (Ac) or phosphorylation (P), or by mediating histone deacetylase (HDAC, (B)) or histone acetyl transferase (HAT, (C)) recruitment.
(D-H) SUMOylation can regulate the association of TFs with DNA. SUMOylation can promote or block nuclear transport of TFs (D) or their binding to promoter sequences (E). (F) SUMOylation can signal removal of TFs from DNA. SUMOylation can compete with ubiquitylation and thus stabilize TFs (G) or lead to STUbL-mediated ubiquitylation and degradation of TFs (H). Note that effects on transcription rates (red cross: down, green arrow: up) are based on the scenario of an activating TF. For transcriptional repressors, the reverse outcome is expected. ORF: open reading frame.
Figure inspired by (Rosonina *et al*, 2017).

Well-studied examples for transcriptional regulation in S. cerevisiae include Gcn4, a TF induced by amino acid starvation. Specifically, SUMOylation is required to promote eviction of Gcn4 to shut down transcription of e.g. *ARG1* upon re-availability of amino

acids (Rosonina *et al*, 2010; 2012). Additionally, SUMOylation of the Tup1 corepressor also contributes to *ARG1* deactivation (Ng *et al*, 2015). Conversely, Tup1 in complex with the coactivator Ssn6 maintains the galactose inducible gene *GAL1* in a repressed state. Upon induction, the NPC-associated SUMO protease Ulp1 deSUMOylates Ssn6 to allow full *GAL1* transcription (Texari *et al*, 2013). Another study found many pro-growth genes like ribosomal protein genes (RPGs) and RNA Pol III-transcribed genes positively regulated by SUMO (Chymkowitch *et al*, 2015b). For RPGs, this effect relied on enhanced SUMOylation of the TF Rap1, which leads to recruitment of TFIID and consequently RNA Pol II.

Besides the multiple effects of SUMOylation on transcriptional regulation, ever more novel SUMO-mediated regulatory mechanisms continue to be discovered for the thousands of cellular SUMO substrates. What is understudied in many cases, however, is the fate of SUMOylated proteins. Besides deSUMOylation by SUMO-specific isopeptidases to recycle unmodified proteins, another major pathway is STUbL-mediated ubiquitylation.

1.4 SUMO-targeted Ubiquitin Ligases (STUbLs)

1.4.1 Proteolytic Control of SUMOylated Proteins

STUbLs modify SUMOylated proteins with ubiquitin and thereby transfer substrates from the SUMO to the ubiquitin pathway, often leading to proteasomal degradation (Fig. 2, bottom left, Fig. 3H). STUbLs orchestrate multiple functions in DNA repair, quality control, transcriptional regulation and beyond (Sriramachandran & Dohmen, 2014). To achieve this, STUbLs combine binding to SUMOylated proteins via SUMO-interacting motifs (SIMs) with ubiquitin ligase activity, STUbL mutants accumulate high molecular weight (HMW) SUMOylated proteins, and are hypersensitive to DNA damage and replication stress (Uzunova *et al*, 2007; Prudden *et al*, 2007; Sun *et al*, 2007; Xie *et al*, 2007). Among eukaryotes, the STUbL family is highly diversified, although the basic enzymatic activity is conserved from yeast to mammalian cells, evidenced by the ability of the mammalian STUbLs RNF4 or Arkadia (RNF111) to complement the replication stress phenotypes of yeast STUbL mutants (schemes Fig. 4) (Uzunova *et al*, 2007; Sun *et al*, 2007; Prudden *et al*, 2007).

S. Cerevisiae STUbLs

Slx5/Slx8. The main STUbL enzyme in yeast is formed by the heterodimeric Slx5/Slx8, of which both subunits harbor C-terminal RING-domains, which are essential for ubiquitylation *in vitro*, and for *in vivo* functions (Fig. 4) (Ii *et al*, 2007; Xie *et al*, 2007). Slx5 harbors 5 SIMs, 4 of which cluster in the N-terminal part and are most important for recruitment of the Slx5/Slx8 complex to polySUMOylated proteins (Xie *et al*, 2010). Slx8 contains one putative SIM and its N-terminal part exhibits non-specifc DNA-binding activity (Yang *et al*, 2006).

Consistent with DNA-binding activity and the predominant role of SUMO inside the nucleus, Slx5/Slx8 primarily localizes to the nucleus and to nuclear pore complexes (Nagai *et al*, 2008; Cook *et al*, 2009), and most of the substrates are nuclear proteins. Initially, the Slx5/Slx8 complex has been identified for its role in genome stability, which manifests in a synthetic lethal phenotype with the DNA helicase Sgs1 (hence the name Synthetic lethal of unknown [X] function (Mullen *et al*, 2001)), and hypersensitivity to replication stress (Xie *et al*, 2007). Slx5/Slx8 is also involved in the repositioning of different types of DNA lesions to nuclear pore complexes (Nagai *et al*, 2008; Horigome *et al*, 2016; Churikov *et al*, 2016; Su *et al*, 2015), and has recently been demonstrated to contribute to the cell cycle regulation of the Yen1 nuclease, which acts on HR intermediates (Talhaoui *et al*, 2018). Several DNA-associated proteins have been shown to be Slx5/Slx8 substrates, including the centromeric histone variant Cse4 (Ohkuni *et al*, 2016; 2018), the chromosomal passenger complex proteins Bir1 and Sli15 (Thu *et al*, 2016), the kinetochore-protein Kar9 (Schweiggert *et al*, 2016), the rDNA silencing protein Tof2 (Liang *et al*, 2017) and RNA polymerase III (Wang *et al*, 2018). Furthermore, transcription factors such as a mutant variant of Mot1 and the mating type regulator Matα2 are substrates for Slx5/Slx8 (Wang & Prelich, 2009; Xie *et al*, 2010). Interestingly, in the latter case, Matα2-SUMOylation is dispensable for Slx5/Slx8 targeting, however, the SIMs of Slx5 and Matα2 DNA-binding are required (Xie *et al*, 2010; Hickey *et al*, 2018). Ubiquitylation is not only important for targeting Matα2 for proteasomal degradation, but also signals recruitment of the Cdc48 complex for extraction (Wilcox & Laney, 2009). Noteworthy, Cdc48 can be recruited not only to ubiquitylated, but also to SUMOylated proteins (Bergink *et al*, 2013).

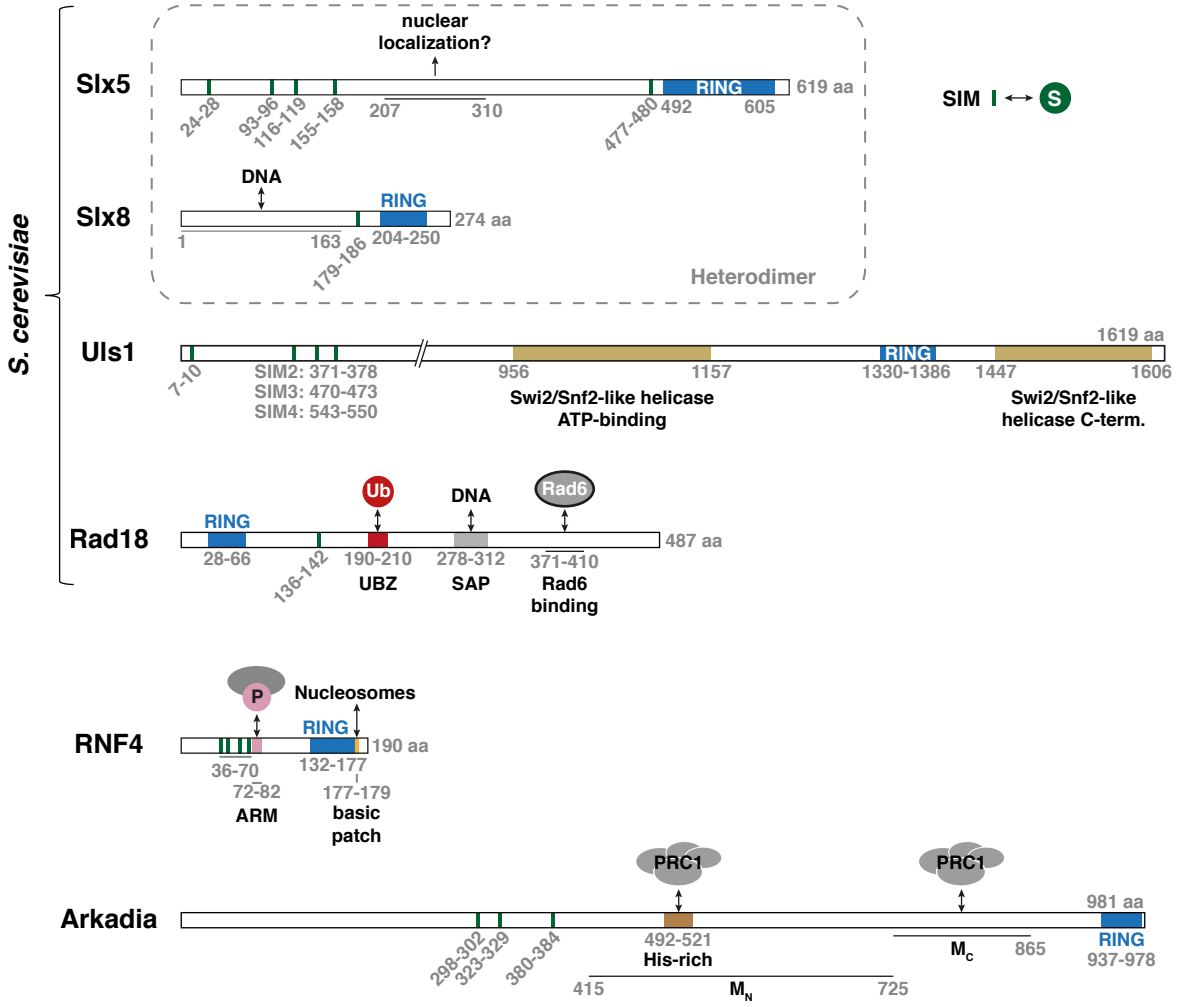

Figure 4. SUMO-targeted ubiquitin ligases (STUbLs).
Schematic representation of selected STUbLs. SUMO-interacting motifs (SIMs) are marked by green bars. Functional features and interaction sites to recognize specific substrates or binding partners are highlighted. For RNF4, aminoacid (aa) positions are given for the *H. sapiens* protein, for Arkadia for the *M. musculus* variant. For Uls1, the N-terminal part is not drawn to scale. UBZ: ubiquitin-binding zinc finger; SAP: SAF-A/B, Acinus, PIAS-domain (DNA-binding); ARM: arginine rich motif; (P): phosphorylation; PRC1: polycomb repressive complex 1; His: histidine; $M_{N/C}$: middle-domain N-/C-terminal.

Uls1. Uls1 (also known as Ris1/Dis1/Tid4) is a complex 1619 aa protein with 4 SIMs in the N-terminal part and a RING domain sandwiched between a Swi2/Snf2-like (switch/sucrose non-fermentable) translocase/helicase ATP-binding motif and the C-terminal helicase domain (Fig. 4). Uls1, like Slx5/Slx8, contributes to the clearance of HMW SUMO conjugates (Uzunova *et al*, 2007), however, a direct biochemical proof of STUbL activity is still elusive. The Swi2/Snf2-like translocase function, which mediates ATP-dependent repositioning or removal of proteins from DNA, is essential for most Uls1 functions. A major function is partially overlapping with other Swi2/Snf2-like translocases (Rad54, Rdh54) for the removal of Rad51 from undamaged DNA (Shah *et al*, 2010). Uls1 also prevents detrimental NHEJ of telomeres by curbing the accumulation of polySUMOylated Rap1 at telomeric DNA. Both the Swi2/Snf2-like translocase and RING

domains contribute to this function (Lescasse *et al*, 2013). Similarily, NHEJ of Rap1-bound double-strand breaks (DSBs) is prevented by Uls1, likely by a similar mechanism (Marcomini *et al*, 2018).

Interestingly, Rrp2, the *S. pombe* homolog of Uls1, has been termed a "SUMO targeted DNA translocase" for its activity on SUMOylated Top2 that is trapped by Top2 poisons. Notably, the translocase function, but not the RING domain, is essential for this function (Wei *et al*, 2017). In fact, the authors propose that Rrp2 safeguards SUMOylated Top2 from ubiquitylation by the *S. pombe* STUbL formed by Slx8 and Rfp1 or Rfp2, and show similar behavior in *S. cerevisiae.* Indeed, several studies reported physical or genetic interactions between Uls1 and Slx5/Slx8 and proposed antagonistic functions, suggesting a complex interplay between the two STUbLs (Cal-Bąkowska *et al*, 2011; Tan *et al*, 2013; Kramarz *et al*, 2014).

Although the requirement for intact SIMs, Swi1/Snf2-like translocase and RING domain has not been deteremined for all Uls1 functions, it seems likely that Uls1 acts as a multi-purpose protein that is recruited to SUMOylated proteins on DNA to translocate and/or ubiquitylate them.

Rad18. Rad18 (Fig. 4) has been suggested to have STUbL-like activity for its substrate PCNA, however, in this case the interaction of a single SIM with monoSUMOylated PCNA only enhances Rad18 activity, but is not strictly required (Parker & Ulrich, 2012). Also, the mechanism does not seem to be conserved, since the SIM is absent from human Rad18.

Mammalian STUbL Enzymes

RNF4. With 190 aa, RNF4 is the smallest STUbL described to date (Fig. 4). It forms a homodimeric ligase and is the best-studied family member so far. The first physiological substrate described for RNF4 was the PML protein, which gets polySUMOylated upon exposure to arsenic and RNF4-mediated ubiquitylation subsequently leads to its degradation (Tatham *et al*, 2008). Although it is unclear whether RNF4 a is direct homolog of yeast STUbLs (*S. pombe* Rfp1/Rfp2 or *S.pombe/S. cerevisiae* Slx8 have been suggested as distant homologs (Prudden *et al*, 2007; Sriramachandran & Dohmen, 2014)), RNF4 and its yeast counterparts act in similar biological pathways.

RNF4 has crucial functions in DNA repair and both proteolytic and nonproteolytic functions are relevant in this case, as well as generation of SUMO/ubiquitin hybrid chains

(Galanty *et al*, 2012; Yin *et al*, 2012; Luo *et al*, 2012; Guzzo *et al*, 2012). Other substrates include the kinetochore protein CENP-I (Mukhopadhyay *et al*, 2010), misfolded and quality control substrates (Ahner *et al*, 2013; Guo *et al*, 2014), transcriptional regulators and oncogenes (Guo & Sharrocks, 2009; van Hagen *et al*, 2010; Kuo *et al*, 2014; Thomas *et al*, 2016; Costanzo *et al*, 2018), and even SUMOylation enzymes (Kumar *et al*, 2017). The wide range of RNF4 functions is also underscored by the ability to cooperate with multiple E2s to catalyze mono-ubiquitylation as well as K11-, K33-, K48- and K63-linked ubiquitin chains (Plechanovová *et al*, 2011; Branigan *et al*, 2015; Thomas *et al*, 2016).

Arkadia (RNF111). Arkadia has functions in the repair of UV-induced DNA lesions by targeting polySUMOylated XPC (Xeroderma pigmentosum C), a central damage recognition factor in NER (Poulsen *et al*, 2013). Furthermore, Arkadia has overlapping functions with RNF4 in PML degradation (Erker *et al*, 2013). However, its best-studied and possibly major function lies in transcriptional control of the TGFβ (transforming growth factor β) pathway, where it promotes TGFβ signaling through degradation of negative regulators (Smad7, c-Ski, SnoN) (Inoue & Imamura, 2008). Binding and degradation of c-Ski and SnoN seem to be independent of SIMs (Erker *et al*, 2013), but SUMO-binding has been shown to contribute to localization to Polycomb bodies and thereby transcriptional regulation of the TGFβ pathway (Fig. 4) (Sun & Hunter, 2012; Sun *et al*, 2014).

Other STUbL Enzymes

Degringolade/Dgrn is an RNF4 homolog in *Drosophila melanogaster* and has been shown to mediate transcriptional repression in early embryonic development or transcriptional activation in the innate immune response (Abed *et al*, 2011a; Koltun *et al*, 2017). Furthermore, like *S. cerevisiae* Slx5/Slx8, it contributes to relocalization of DNA breaks to the nuclear periphery and their repair (Ryu *et al*, 2015).

Besides the eukaryotic members, two viral STUbLs have been identified: ICP0 of Herpes simplex virus 1 and the related ORF61p of Varicella zoster virus, which target SUMOylated host proteins for degradation to promote viral infectivity (Everett *et al*, 2013).

1.4.2 Specificity in the STUbL Pathway

The initial characterization of STUbL enzymes showed an accumulation of HMW SUMO conjugates, and that multiple SIMs were necessary for STUbL-mediated clearance and to

alleviate replication stress hypersensitivity (Uzunova *et al*, 2007; Xie *et al*, 2007; Tatham *et al*, 2008). Multiple SUMO–SIM interactions have been demonstrated to provide increased avidity and therefore preference for polySUMOylated over monoSUMOylated substrates (Xu *et al*, 2014; Keusekotten *et al*, 2014), and many substrates accumulate in a polySUMOylated form in the absence of STUbLs (Tatham *et al*, 2011; Lescasse *et al*, 2013; Ohkuni *et al*, 2016). Consistent with a shared role in keeping substrate SUMOylation in check, STUbLs also compete or cooperate with deSUMOylation enzymes for certain substrates (Kosoy *et al*, 2007; Xie *et al*, 2007; Uzunova *et al*, 2007). Additionally, polySUMO chains have been shown to activate STUbLs and contribute to homodimerization of RNF4 (Rojas-Fernandez *et al*, 2014), which is required for catalysis (Plechanovová *et al*, 2012). Therefore, the prevailing view is that STUbLs are ligases with specificity for polySUMOylated proteins.

However, how STUbLs select their proper substrates amongst myriads of SUMOylated proteins is still largely unclear. Enzyme localization likely contributes to specificity, e.g. RNF4 is recruited to PML bodies (in a SUMO-dependent manner (Geoffroy *et al*, 2010)) and Slx5/Slx8 is targeted to the nuclear pore complex (Nagai *et al*, 2008). More recently, it has been reported that STUbLs also use SUMO-independent substrate interactions (highlighted in Fig. 4): RNF4 interacts with nucleosomes via a basic patch and can target non-SUMOylated, but phosphorylated proteins via an arginine-rich motif (ARM) (Groocock *et al*, 2014; Thomas *et al*, 2016; Kuo *et al*, 2014). Similarily, substrate-specific interactions have been described for Arkadia and Degringolade (Sun *et al*, 2014; Abed *et al*, 2011a). In contrast, for the prototypical *S. cerevisiae* STUbL Slx5/Slx8, substrate specificity is rather unexplored. As mentioned, for Matα2 turnover, SUMOylation is dispensable, but Slx5-SIMs are still required and it has been suggested that SUMO-like features of Matα2 and its DNA binding contribute to recognition by Slx5/Slx8 (Xie *et al*, 2010; Hickey *et al*, 2018). Also, it was demonstrated, that Slx5/Slx8 can target binding partners of SUMOylated proteins *in trans*, suggesting that SUMOylation of the substrate is not a prerequirement for ubiquitylation.

Taken together, since their discovery in 2007, STUbLs have emerged as critical effectors at the crossroads of the SUMO and ubiquitin pathways that are involved in a plethora of cellular, predominantly nuclear functions, reflecting the versatility of the SUMO pathway. However, a clear mechanistic understanding of how substrate specificity is achieved in the STUbL pathway is still elusive.

2 Aims of this Study

2.1 Rationale

Extensive evidence suggests that STUbLs play pivotal roles in controlling the functions of proteins on chromatin. Many SUMOylated proteins associate with chromatin and, by using chromatin immuno-precipitation (ChIP), it has recently been demonstrated that SUMO associates with hundreds of regions in *S. cerevisiae* cells, and thousands of regions in human cells (Chymkowitch *et al*, 2015b; Neyret-Kahn *et al*, 2013; Seifert *et al*, 2015; Niskanen *et al*, 2015). However, what remains completely unexplored is whether STUbLs play a global role in turnover of SUMOylated proteins on chromatin. In this context, a crucial question is whether STUbLs are recruited to all SUMOylated proteins on chromatin, or if additional features define and select *bona fide* substrates. Therefore, a detailed study on the role of STUbLs on chromatin is expected to not only further our understanding of SUMO metabolism on chromatin, but is also likely to give insights into mechanisms of STUbL recruitment and potentially novel biological functions.

2.2 Preliminary Data

In a previous PhD project in the Jentsch laboratory, a novel approach to study protein turnover on chromatin on a genome-wide scale in *S. cerevisiae* has been developed by Maximilan J. Kern (Kern, 2013). To this end, ChIP with ubiquitin-specific antibodies was paired with genome-wide tiling arrays (ChIP-chip). Critically, nine genomic sites with high enrichment of ubiquitylated proteins ("ubiquitin hotspots") stood out because of a marked increase of ubiquitin signal in mutants of the $Cdc48^{Ufd1\text{-}Npl4}$ complex and its cofactors Ubx4 and Ubx5. Seven of those intergenic ubiquitin hotspots share a common mechanism, involving a DNA sequence motif (ub-HS-motif) bound by the transcription factor-like protein Ymr111c, now named Euc1: Enriches ubiquitin on chromatin 1 (Fig. 5). Euc1 gets SUMOylated and then recruits the STUbL Slx5/Slx8 to mediate ubiquitylation at ubiquitin hotspots. Although SUMOylation-deficient Ymr111c/Euc1 exhibited transactivation function when artificially targeted to reporter genes, it did not seem to regulate genes adjacent to ubiquitin hotspots. Hence, the biological function of ubiquitin hotspots remained elusive (Kern, 2013).

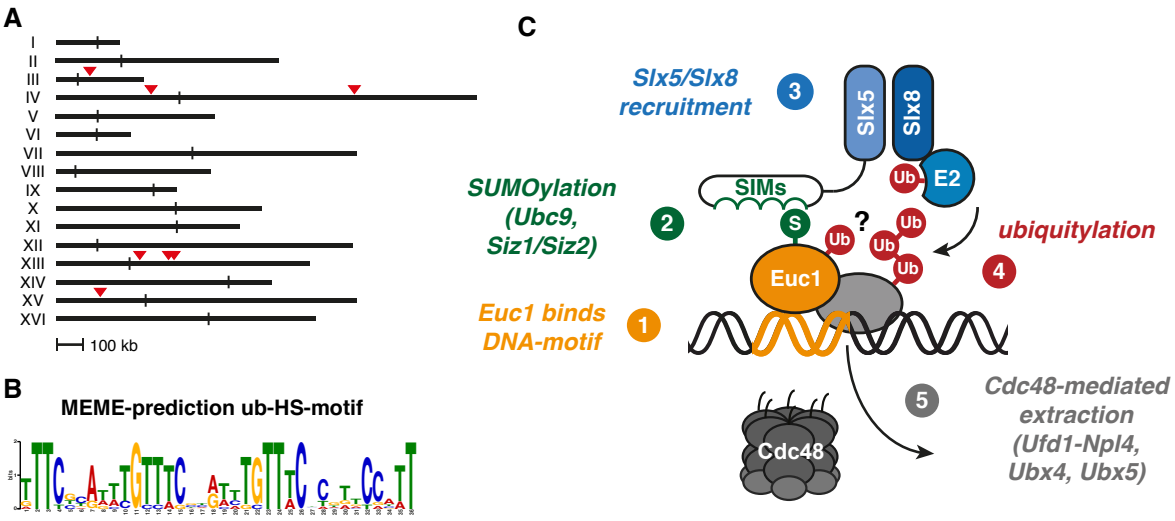

Figure 5. Seven "ubiquitin hotspots" across the yeast genome.
(A) Schematic representation of the *S. cerevisiae* genome with positions of seven related "ubiquitin hotspots" indicated by red triangles. (B) The ubiquitin hotspots (ub-HS) contain a shared sequence motif that was used in a yeast one-hybrid screen, which identified Ymr111c/Euc1 as a specific interactor (Kern, 2013). (C) Working model for the ubiquitin hotspot pathway: (1) Euc1 binds to the DNA sequence motif (2) and gets SUMOylated by Ubc9 together with Siz1 or Siz2; (3) SUMOylation recruits the yeast STUbL Slx5/Slx8 to (4) catalyze modification of Euc1 itself or associated proteins with K48-linked ubiquitin chains; (5) the ubiquitin-specific segregase Cdc48 in complex with Ufd1-Npl4 and the cofactors Ubx4 and Ubx5 are required to remove ubiquitylated proteins from ubiquitin hotspots. Figure adapted from (Kern, 2013).

2.3 Aims of this Study

Several questions remained open after the initial characterization of ubiquitin hotspots: First, what is the biological function of ubiquitin hotspots? A sophisticated mechanism seemed to be at work to establish ubiquitin hotspots and control protein turnover at these sites, suggesting that they have evolved to serve an important physiological function. However, strains deleted for *EUC1* did not exhibit any obvious growth phenotypes. Additionally, the identity of the ubiquitylated proteins remained elusive. Second, what is the global function and distribution of Slx5/Slx8 across the yeast genome? It was demonstrated that Slx8 is highly enriched at ubiquitin hotspots, but the genome-wide distribution was unexplored. Third, how can Slx5/Slx8 be specifically recruited by Euc1, while SUMOylation is highly prevalent on chromatin? Euc1 seemed to be predominantly monoSUMOylated, so recruitment of Slx5/Slx8 might involve other, polySUMOylation independent mechanisms. Since the apparent lack of substrate specificity in both the SUMO and STUbL pathways is a major unresolved question, gaining insight into Slx5/Slx8 recruitment is expected to contribute to our understanding of both pathways.

3 Results

3.1 Euc1 and Slx8 Bind to Ubiquitin Hotspots with High Specificity

Ubiquitin hotspots (ub-hotspots, ub-HS in figures) have previously been shown to be the major sites of Cdc48-mediated extraction of ubiquitylated proteins from chromatin within the *S. cerevisiae* genome (Kern, 2013). Furthermore, for selected ub-hotspot sites it has been demonstrated that both Slx8 and the ub-hotspot factor Euc1 are enriched by performing chromatin immunoprecipitation combined with quantitative real-time PCR (ChIP-qPCR). However, the genome-wide distribution of Euc1 and Slx8 remained unexplored. Therefore, and to gain further insight into the biological functions of Slx5/Slx8 and Euc1, I performed ChIP experiments combined with genome-wide tiling arrays (ChIP-chip, Fig. 6A–D).

Using a chain-type specific antibody (ub-K48, clone Apu2), I could confirm the specific enrichment of K48-linked ubiquitin chains at ub-hotspots, that ub-hotspots are enhanced in *cdc48* mutants (*cdc48-3*), and lost in the absence of Euc1 (Fig. 6B, *cdc48-3 euc1*Δ). Consistent with a crucial function at ub-hotspots, Euc1 was detected at all ub-hotspots in wild-type (WT) cells, but not in *euc1*Δ cells (Fig. 6C). ChIP-chip data for tagged Slx8 (*Slx8-9myc*) revealed a marked enrichment at most ub-hotspots, that was mildly enhanced in *cdc48-3* cells, reduced in cells with impaired SUMOylation (*ubc9-1*), and lost in the absence of Euc1 (*euc1*Δ, Fig. 6D). Notably, with few exceptions as described below, the localization not only of Euc1, but also of Slx8 was confined to ub-hotspots, arguing that these are prominent sites of STUbL activity within the yeast genome. All ub-hotspots are situated in intergenic regions, do not seem to be linked with any annotated features within the yeast genome, and are spread across the sixteen yeast chromosomes (Fig. 5A) in an apparently random way. No common genetic pathway or function could be identified for ub-hotspot adjacent genes, and no physical association was apparent in publicly available chromosome conformation capture datasets (Duan *et al*, 2010).

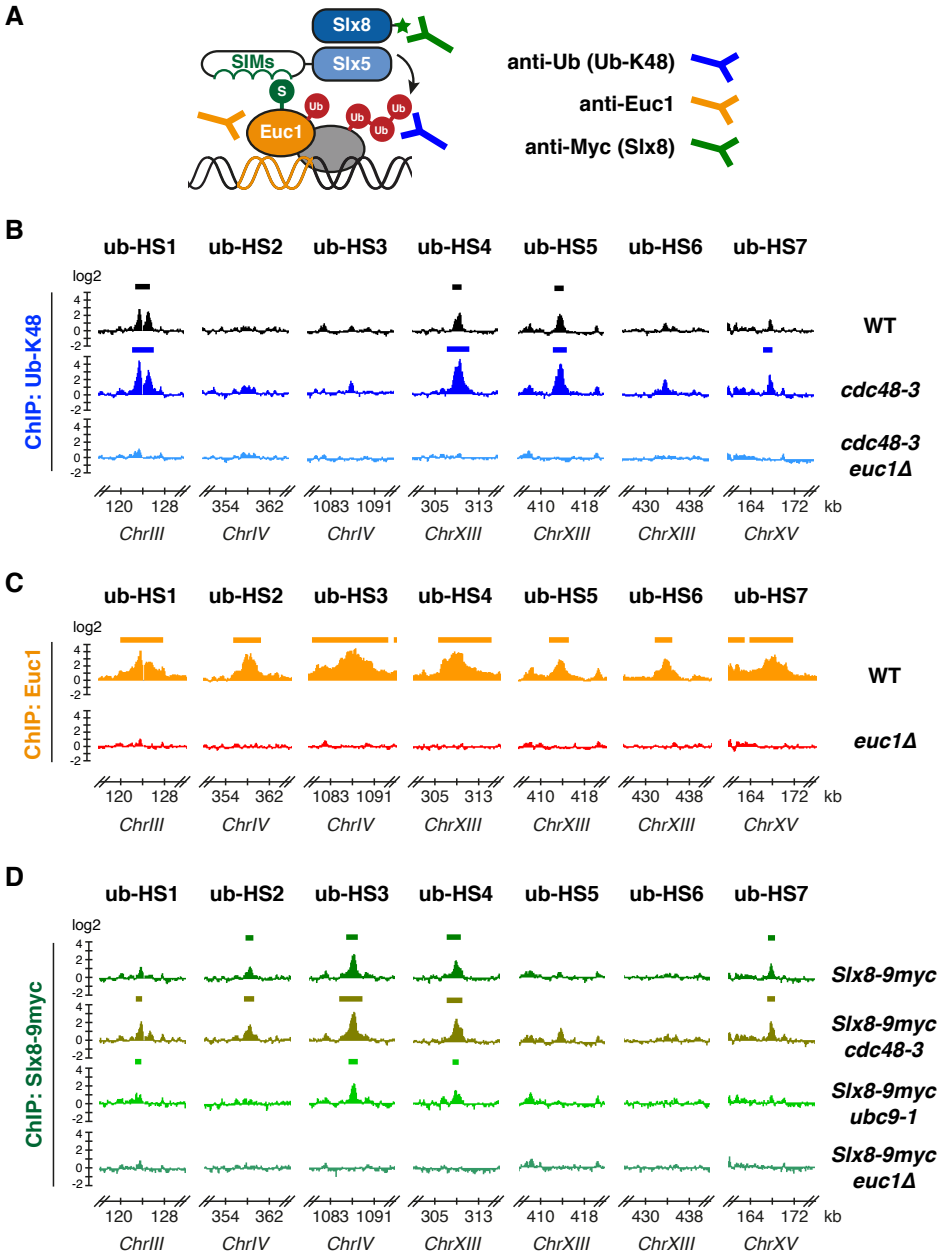

Figure 6. Ubiquitin hotspots are the main binding sites for Euc1 and Slx8 in the *S. cerevisiae* genome.
(A) Schematic representation of the strategy used to probe proteins bound at ubiquitin hotspots (ub-hotspots, ub-HS) using chromatin immuno-precipitation combined with NimbleGen genome-wide tiling arrays (ChIP-chip).
(B) Ub-hotspots depend on Euc1. 16-kb windows of the indicated regions centered around the seven ub-hotspots of ChIP-chip tracks for ub-K48 directed ChIP-experiments. Significantly enriched regions are marked by bars above the respective ChIP-chip tracks, DNA from non-specific IgG-ChIP experiments served as background control (not shown). Genotypes of the used strains are indicated on the right. Data represent means from two independent replicates. All experiments, including those using *cdc48-3* and *ubc9-1* temperature-sensitive (ts) alleles, were performed at 30°C (semipermissive temperature for ts-alleles) unless stated otherwise.
(C) Euc1 binds to ub-hotspots. Genome-wide binding profiles of Euc1 were obtained in ChIP-chip experiments as described in (B). Euc1 ChIP experiments were performed with a polyclonal antibody raised against Euc1 aa 292–462. The wider peaks of Euc1 compared to ubiquitin peaks are likely due to very strong enrichments of Euc1 over background signals and the limited resolution of the tiling arrays. Data represent means from two independent replicates.
(D) Slx8 is specifically recruited to ub-hotspots. Genome-wide binding profiles of Slx8-9myc probed with a Myc-tag specific antibody. ChIP-chip was performed as described in (B). Data represent means from two independent replicates.

Besides ub-hotspots, I could detect only three additional sites of major Euc1 enrichment, two of which also contained a ub-HS-motif and coincided with Slx8 binding sites (Euc1-sites1–3, Fig. 7). However, these sites did not show any accumulation of ubiquitylated proteins (Fig. 7). Conversely, two of the nine originally identified Cdc48-controlled ub-hotspots did not show Euc1 or Slx8 localization, arguing for a different pathway acting at those positions (ub-only-sites1–2, Fig. 7).

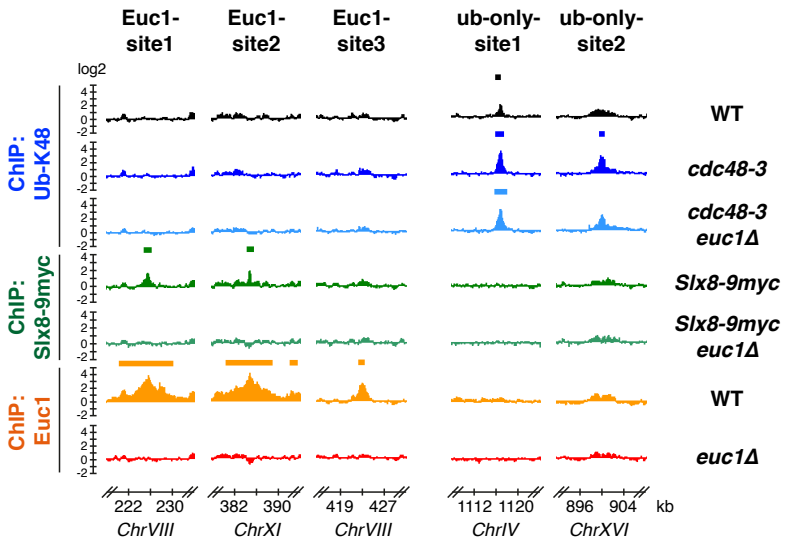

Figure 7. Major non-ub-hotspot binding sites of ubiquitin, Slx8 and Euc1.
ChIP-chip data for sites with major Euc1 enrichment without ubiquitin enrichment, two of which also show Slx8-accumulation (Euc1-sites, left panels) and sites with major ubiquitin enrichment in *cdc48* mutants (*cdc48-3*) without Slx8 and Euc1 enrichment (ub-only-sites, right panels). ChIP-chip experiments were performed as described in Fig. 6.
Of note, in agreement with a previous study (van de Pasch *et al*, 2013), I did not observe any binding of Slx8-9myc to centromeres in ChIP-chip or ChIP-qPCR. In contrast to that study, however, I also did not detect any Slx5 enrichments at centromeres when probed by qPCR for 3HA-Slx5 or endogenous Slx5 (not shown). The discrepancies might be due to a non-functional *SLX5* allele that had been used by van de Pasch *et al* (2013), as stated in their methods section.

I confirmed the binding of Slx8 to selected ub-hotspots using ChIP-qPCR, which also highlighted a strong variability in the relative amount of bound Slx8 at the different loci (*Slx8-9myc*, Fig. 8A). Importantly, Slx5 (*3HA-Slx5*) also associated with ub-hotspots in a similar pattern (Fig. 8B), suggesting that both STUbL subunits are recruited together. Data from ChIP experiments using antibodies raised against endogenous Slx5 or Slx8 were in good agreement with the results for epitope-tagged proteins (Fig. 8C).

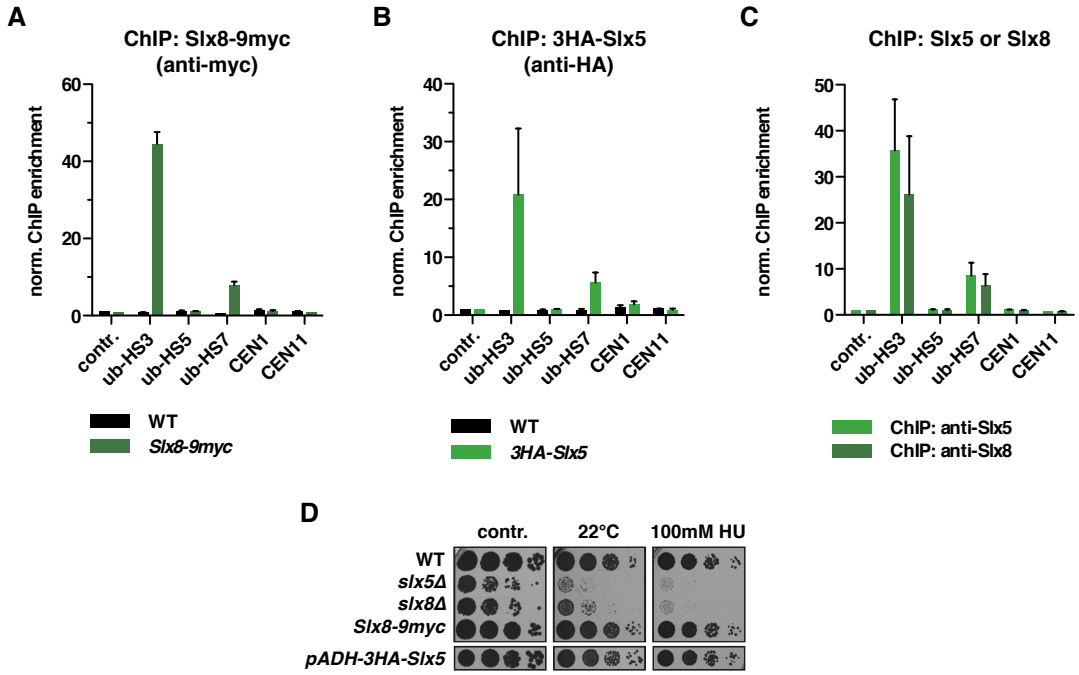

Figure 8. Slx5 and Slx8 localize to ub-hotspots in similar patterns.
(A–C) ChIP followed by quantitative real-time PCR (ChIP-qPCR) with primers specific for the indicated ub-hotspot sites or at centromeres (CEN1, CEN11). ChIP was performed using antibodies for epitope-tagged Slx8-9myc (A) and 3HA-Slx5 (B), or endogenous Slx5 or Slx8 using specific antibodies (C). In contrast to a previous study (van de Pasch *et al*, 2013), no signals for Slx5 were detected at centromeres. Data were normalized to an unrelated control region (contr.) on *ChrII* (*TOS1* promoter region, see Materials and Methods), i.e. background levels are defined as 1. The control region is omitted from plots of normalized ChIP-qPCR experiments for clarity hereafter.
(D) Spotting assay to compare relative growth and survival rates of the indicated strains. Cells were diluted to OD_{600} = 0.5 and 5-fold serial dilutions were spotted on YPD plates, supplemented with 100 mM hydroxyurea (HU) as indicated. Plates were incubated at 30°C or 22°C for 3 days. Note that tagged Slx8 and Slx5 allels do not show the typical *slx5Δ/slx8Δ* phenotypes upon cold stress or replication stress (HU).

A previous study investigating genome-wide binding of Slx5 and Slx8 reported specific localization of Slx5 to centromeres, and no specific enrichment sites for Slx8 (van de Pasch *et al*, 2013). I tested enrichment of Slx5 and Slx8 at centromeres (CEN1, CEN11), however, did not detect any specific signal for either subunit (Fig. 8A–C). The discrepancies might be due to technical reasons, or due to the fact that van de Pasch *et al* (2013) used a non-functional variant of Slx5 (Slx5-GFP), as stated in their methods section. Possibly, accumulation of kinetochore-bound Slx5/Slx8 substrates could have led to trapping of non-functional Slx5 at centromeres (Schweiggert *et al*, 2016). Manual inspection of the data revealed signals for both Slx5-GFP and Slx8-GFP at some of the ub-hotspots, however, these might not have fulfilled the bioinformatics criteria for peak definition (van de Pasch *et al*, 2013). Importantly, all tagged WT Slx5 and Slx8 variants used in this study did not show any growth defects or STUbL-specific phenotypes, like sensitivity to cold or replication stress induced by hydroxyurea (HU, Fig. 8D).

Taken together, my ChIP-chip data indicate that Euc1 localizes to ub-hotspots in a highly specifc manner, which is required for recruitment of Slx8. Site-specific enrichment

of Slx8 on a genome-wide level seems to be confined to ub-hotspots, and Slx5 appears to be recruited together with Slx8.

3.2 SUMOylated Euc1 Recruits Slx5/Slx8 to Ub-hotspots

Besides Euc1, which is likely binding to the ub-HS-motif directly, a Y1H screen also identified SUMO to associate with ub-hotspots in an Euc1-dependent manner (Kern, 2013). Large-scale proteomic studies have previously reported Ymr111c/Euc1 as a candidate SUMOylation substrate (Zhou *et al*, 2004; Denison *et al*, 2005; Hannich *et al*, 2005) and Euc1 immunoprecipitation (IP) suggested that Euc1 is SUMOylated in a highly specific manner on lysine 231 (K231, see scheme Fig. 9A). Replacement of this residue with arginine (K231R mutant, *euc1-KR* hereafter) seemed to abolish Euc1 SUMOylation (Kern, 2013). Therefore, SUMOylation might be a crucial regulator of the ub-hotspots.

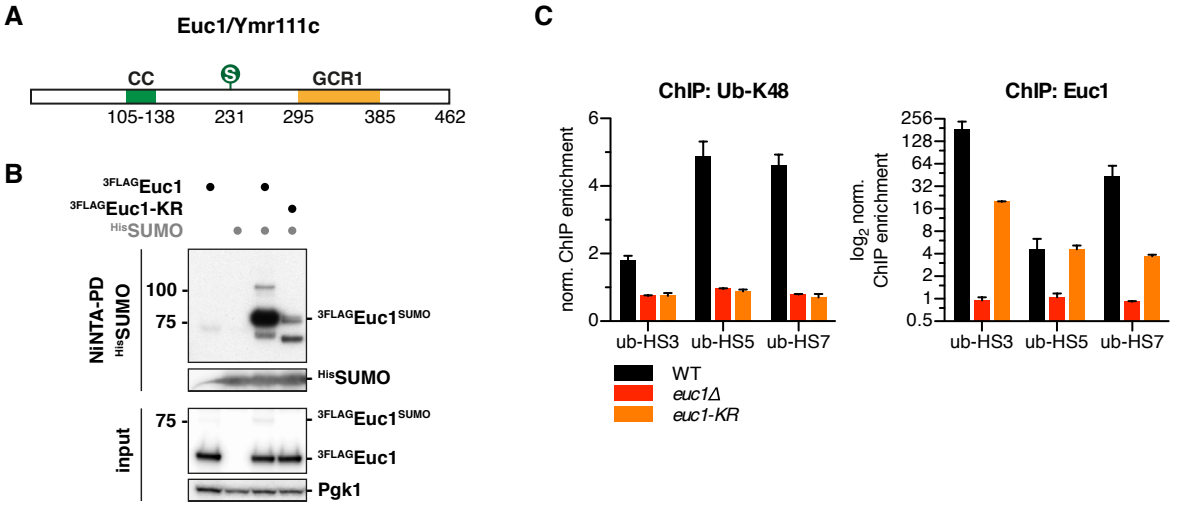

Figure 9. Euc1 SUMOylation is required for ub-hotspot formation.
(A) Schematic representation of the Euc1/Ymr111c domain structure. A coiled-coil domain (CC, green) and a GCR1 domain with predicted DNA-binding activity (orange) are indicated. A single lysine residue has been identified as the major SUMOylation site (K231, (Kern, 2013) and (B)).
(B) Euc1 is predominantly monoSUMOylated on lysine 231. Denaturing NiNTA-pulldowns (NiNTA-PD) with strains expressing 7-histidine-tagged SUMO (^{His}SUMO) as indicated and ^{3FLAG}Euc1 constructs under the control of an *ADH* promoter. Covalently SUMO-modified proteins were enriched and eluates probed with a FLAG antibody to visualize SUMOylated Euc1. Eluates were probed for SUMO to control for equal pull-down efficiency; to control for equal input levels, input samples were probed with FLAG and Pgk1 antibodies (top to bottom). Euc1-KR denotes the K231R mutation here and hereafter.
(C) Left: Euc1 and its SUMOylation are required for ub-hotspot formation. Ub-K48 ChIP followed by qPCR for the indicated sites and strains. Right: Euc1 binding to ub-HSs drops in *euc1-KR* cells. In parallel to ub-K48 ChIP, ChIP against Euc1 was performed and quantified by qPCR. Data represent means ± SD (n = 2).

To corroborate these initial findings and demonstrate a direct, covalent modification of Euc1 with SUMO, I performed NiNTA pull-downs (NiNTA-PDs) of His-tagged SUMO (^{His}SUMO) in cells expressing 3FLAG-tagged Euc1 (^{3FLAG}Euc1). Using denaturing conditions, only covalently SUMO-modified proteins are enriched and associated proteins are washed off. The NiNTA-PD experiments followed by western blot

(WB) revealed an up-shifted Euc1 band corresponding to monoSUMOylated Euc1 and a weaker band further up-shifted, likely representing diSUMOylation (Fig. 9B). SUMOylation was strongly reduced in cells expressing Euc1-KR, confirming that K231 is the major SUMOylation site of Euc1 (Fig. 9B).

Importantly, Euc1-K231 SUMOylation is required for ub-hotspot formation (Fig. 9C, left panel, (Kern, 2013)). Curiously, Euc1 binding at ub-hotspots itself was also reduced by up to ten-fold in *euc1-KR* cells for several selected sites (Fig. 9C, right panel). Hence, SUMOylation seems to regulate ub-hotspot formation through modulating Euc1 binding and/or Slx5/Slx8 recruitment.

To address the possibility that Euc1 is an Slx5/Slx8 substrate, I established denaturing NiNTA-PDs to probe for covalently His-ubiquitin-modified proteins (^{His}Ubi, Fig. 10A). A WB against ^{3FLAG}Euc1 revealed an up-shifted smear likely representing polyubiquitylated Euc1, which was reduced for Euc1-KR and entirely lost in cells expressing a catalytically dead Slx8 RING domain variant (*slx8-CD*, Fig. 10A), and in *slx5*Δ cells (Fig. 10B).

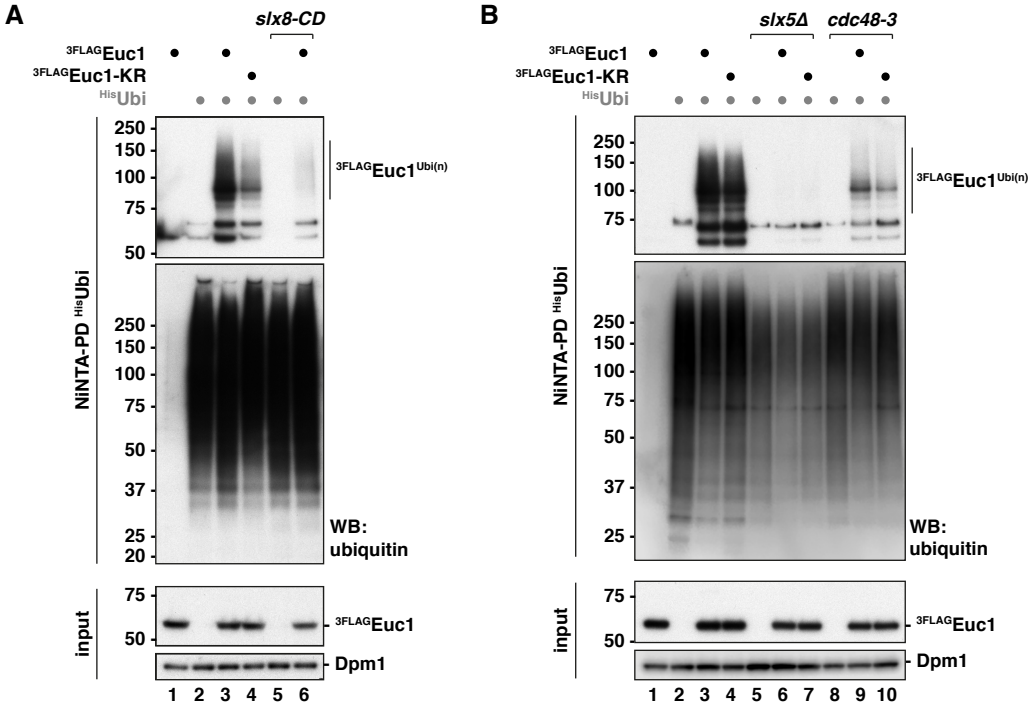

Figure 10. Euc1 is ubiquitylated in an Slx5/Slx8-dependent manner.
(A) Euc1 ubiquitylation depends on Slx8 and partly on Euc1 SUMOylation. Denaturing NiNTA-PDs as described for Fig. 9B, but with strains expressing 6-histidine-tagged ubiquitin (^{His}Ubi) and ^{3FLAG}Euc1 constructs under the control of the *ADH* promoter. WBs were developed with a FLAG antibody to probe for ^{3FLAG}Euc1 (PD and input), a ubiquitin blot served as NiNTA-PD control and Dpm1 as input control. The catalytic dead *slx8-CD* allele carries the C206S, C209S mutations (Xie *et al*, 2007).
(B) Slx5 is required for Euc1 ubiquitylation. Denaturing NiNTA-PDs with ^{His}Ubi as in (A). Note that Euc1-ubiquitylation levels are abolished in *slx5*Δ cells, but also reduced in *cdc48-3* cells.

Based on these data, it would be an appealing hypothesis that Euc1 is the main Slx5/Slx8 ubiquitylation substrate at ub-hotspots, and therefore the subject of Cdc48-mediated extraction, and possibly subsequent degradation. Consequently, Euc1 levels should be enhanced or turnover kinetics slowed down when the ub-hotspot pathway is impaired.

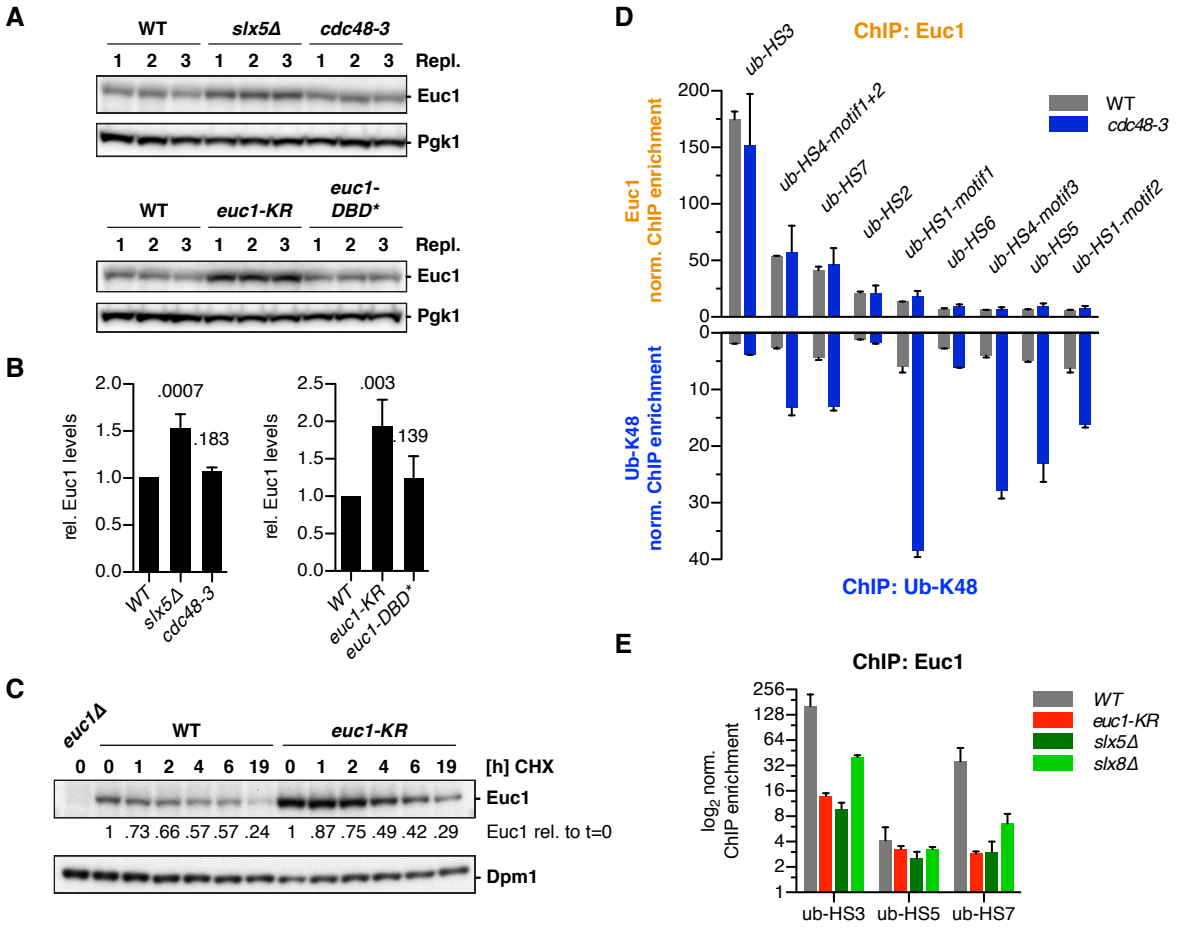

Figure 11. Slx5/Slx8-mediated ubiquitylation does not lead to fast Euc1 degradation.
(A–B) Euc1 levels increase in *slx5*Δ and for *euc1-KR*. Euc1 levels were quantified from WBs of three replicate samples (A) using a LI-COR Odyssey Fc imaging system and were normalized to Pgk1 and wild-type levels (B). Pgk1 served as loading control. Data represent means ± SD (n = 3). p-values of Student's t-tests for comparisons to WT are indicated above the bars. *euc1-DBD** signifies a DNA binding-deficient mutant variant (W333A, R334A, see also Fig. 18).
(C) Euc1 shows slow degradation kinetics. Cells were treated with 0.5mg/ml cycloheximide (CHX) to shut down protein translation and samples were taken at the indicated times. Quantification was done as in (A–B). Relative Euc1 signals were normalized to Dpm1 levels and to t = 0.
(D) Euc1 and ub-K48 ChIP signal strengths do not correlate. ChIP against Euc1 (top) and ub-K48 (bottom) analyzed by qPCR for all ub-HSs. Separate primer pairs were used for distinct motif occurrences within ub-HS1 and ub-HS4. Note that Euc1 signals did not increase in a *cdc48-3* strain. Data represent means ± SD (n = 2).
(E) Euc1 binding to ub-HS sites is reduced, rather than increased, in *slx5*Δ and *slx8*Δ cells. ChIP against Euc1 was quantified by qPCR in the indicated strains. Note that the binding defect for Euc1 is similar for the *euc1-KR* and *slx5*Δ strains. Data represent means ± SD (n = 2).

Probing total protein amounts, steady-state levels of Euc1 were mildly increased in *slx5*Δ and *euc1-KR* cells, but not in *cdc48-3* cells (Fig. 11A–B). To test turnover, I used cycloheximide to shut down protein synthesis and followed Euc1 levels. Interestingly, WT Euc1 is a rather stable protein and degradation rates seemed similar for Euc1-KR (Fig.

11C). Also, Euc1 stability did not change in *slx5*Δ or *cdc48-3* cells (not shown). These results indicate that ubiquitylation by Slx5/Slx8 does not cause rapid Euc1 degradation, or that only a small fraction of Euc1 undergoes Slx5/Slx8-mediated ubiquitylation.

Additional evidence suggests that Euc1 is not the only or main ubiquitylation substrate at ub-hotspots: First, ubiquitylated Euc1 species were reduced, rather than enhanced in *cdc48-3* cells in denaturing NiNTA-PDs (Fig. 10B). Second, Euc1 signals at different ub-hotspots did not correlate with ubiquitin signals, and Euc1 did also not accumulate at these sites in *cdc48* mutant strains—in contrast to ubiquitin (Fig. 11D). Third, Euc1 enrichment at ub-hotspots in ubiquitylation-deficient *slx5*Δ and *slx8*Δ strains was decreased, arguing against Slx5/Slx8-dependent degradation of Euc1 at ub-hotspots (Fig. 11E).

If it is not the substrate for turnover at ub-hotspots, what then is the role of Euc1? As an alternative hypothesis, SUMOylated Euc1 could act as a cofactor to signal Slx5/Slx8 localization to ub-hotspots, given that Euc1 (and SUMOylation) are required for Slx8 recruitment (Fig. 6D). As a first step to elucidate how Euc1 might achieve the highly specific recruitment of Slx5/Slx8 (Fig. 6D), I decided to investigate recruitment of both heterodimer subunits separately in different genetic backgrounds. Signals for tagged Slx5 and Slx8 were mildly enhanced in *cdc48-3* cells when probed by ChIP-qPCR (Fig. 12A–B). Notably, Slx5 and Slx8 levels correlated well with WT Euc1 enrichment patterns at the tested sites (compare Fig. 12A–B and Fig. 11E). Consistent with a strict dependence on Euc1 and its SUMOylation, both Slx5 and Slx8 were entirely lost from ub-hotspots in *euc1*Δ and *euc1-KR* strains (Fig. 12A–B). Furthermore, the data suggested that Slx5 was

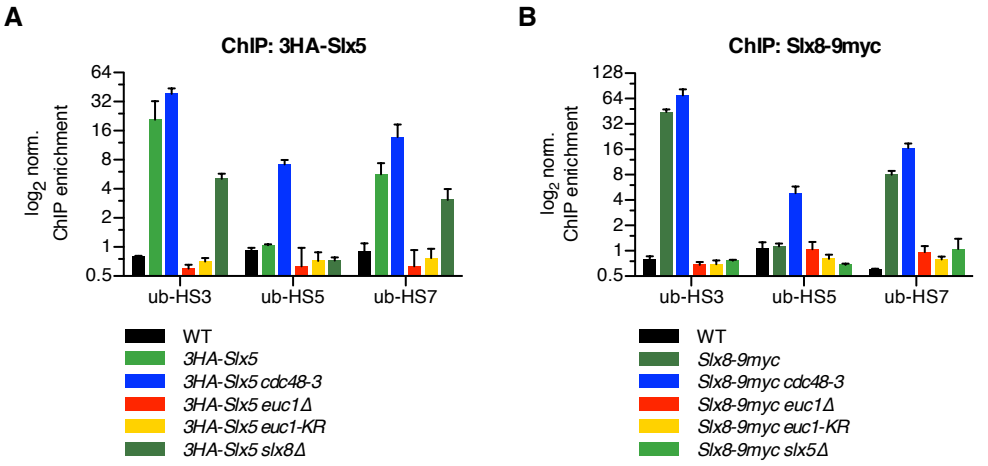

Figure 12. SUMOylated Euc1 recruits Slx5/Slx8 via the Slx5 subunit to ub-hotspots.
ChIP against 3HA-Slx5 (A) and Slx8-9myc (B) in the indicated genetic backgrounds were quantified by qPCR. Note that Slx5 is still partially recruited in the absence of Slx8 (*3HA-Slx5 slx8*Δ), but not vice versa (*Slx8-9myc slx5*Δ). Data represent means ± SD (n = 2).

still recruited in the absence of Slx8 (*3HA-Slx5 slx8*Δ, Fig. 12A), albeit to a lower extent, while Slx8 recruitment to ub-hotspots was strictly Slx5 dependent (*Slx8-9myc slx5*Δ, Fig. 12B).

Taken together, these data demonstrate that Euc1 and its SUMOylation play major roles in controlling ub-hotspots by enabling Slx5/Slx8 recruitment. Additionally, they identify Euc1 as a novel Slx5/Slx8 ubiquitylation substrate, but it appears likely that additional proteins bind and get ubiquitylated at ub-hotspots. These proteins are putative Slx5/Slx8 ubiquitylation substrates, which get extracted from chromatin by Cdc48.

3.3 Specific Interaction Sites Mediate SUMO–SIM-independent Euc1–Slx5 Binding

A hallmark of many STUbL substrates is modification with polySUMO chains (polySUMOylation) or multiple SUMO moieties (multiSUMOylation), which is thought to facilitate STUbL recruitment through polyvalent SUMO–SIM contacts (Sriramachandran & Dohmen, 2014). However, Euc1 seems to be predominantly monoSUMOylated (Fig. 9B), and expressing lysine-free SUMO (*SUMO-KRall*) as only copy of SUMO to block chain formation did not affect ub-hotspots (Fig. 13A). This raises the question of how Slx5/Slx8 can be targeted to ub-hotspots with high specificity, while SUMOylation on chromatin is prevalent (Chymkowitch *et al*, 2015a)?

ChIP-qPCR data suggested that Slx5 could be recruited by SUMOylated Euc1 independently of its dimerization partner Slx8 (Fig. 12), and I could show an interaction between Euc1 and Slx5 using a yeast two-hybrid (Y2H) assay (Fig. 13B, bottom row, Appendix Fig. A1A–C) (Yu *et al*, 2008). This interaction was mildly enhanced upon truncation of the C-terminal Slx5 RING domain (Slx5-RINGΔ, aa 1–487), and was still detectable for a SUMOylation-deficient Euc1-KR construct (Fig. 13B, bottom rows). To map an interaction site within Euc1, I expressed truncations spanning the N-terminal half of Euc1 and found that amino acids 81-183 were required and sufficient for interaction with Slx5 (Fig. 13B, Appendix Fig. A1A–C). Of note, $Euc1^{81\text{-}183}$ does not contain the SUMOylation site, but spans a CC domain that mediates Euc1 homodimerization in Y2H assays (Appendix Fig. A1D–E). A SUMO-independent interaction was also substantiated by direct binding of unmodified recombinant Euc1 to purified Slx5 in *in vitro* GST-pulldown assays (Fig. 13C). Similarly, the *in vivo* binding did not strictly depend on Euc1 SUMOylation, as ^{3FLAG}Euc1 and ^{3FLAG}Euc1-KR both interacted similarly with Slx5 in co-immunoprecipitation (co-IP) experiments. A recent study demonstrated that DNA

binding of Matα2 was required for degradation by Slx5/Slx8 (Hickey *et al*, 2018). However, even an Euc1 DNA binding-deficient mutant variant interacted with Slx5 (Fig. 13D, lane 4, ^{3FLAG}Euc1-DBD*, W333A, R334A, see also Fig. 18). In summary, these data argue for the existence of SUMO–SIM independent binding sites between Euc1 and Slx5.

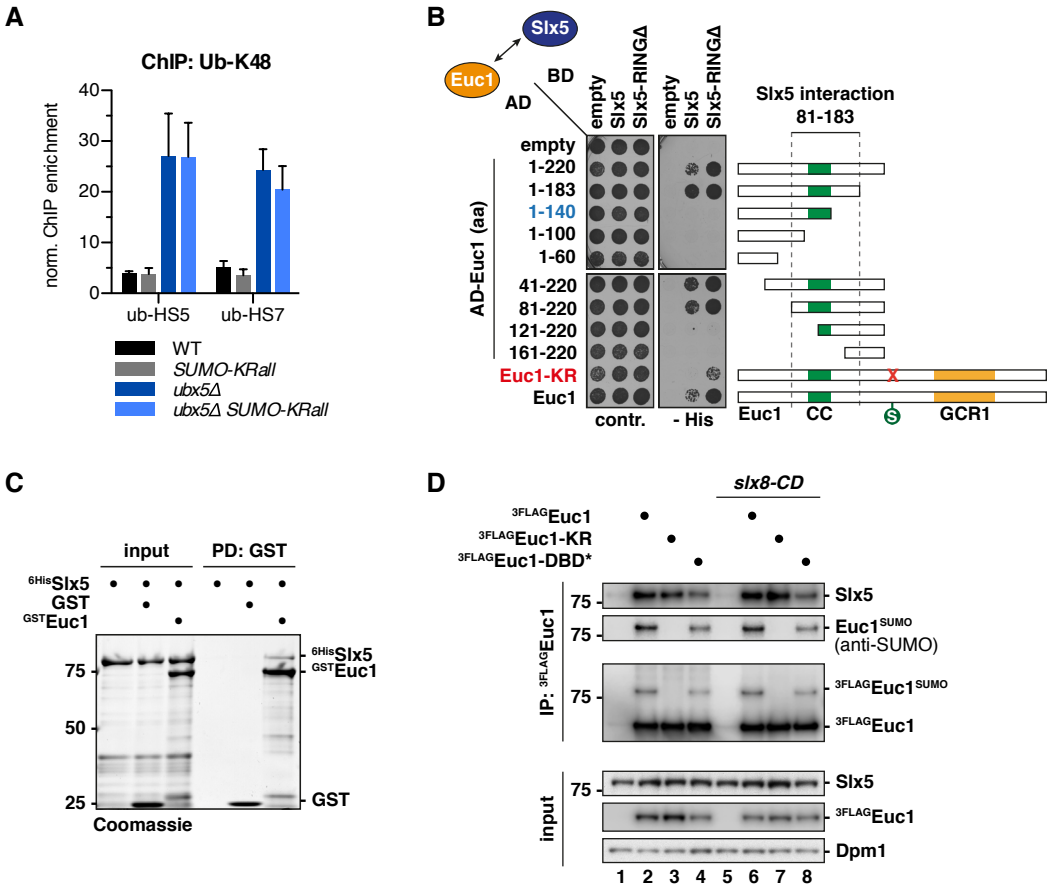

Figure 13. SUMOylation independent interactions of Slx5 with Euc1.
(A) PolySUMO-chain formation is not required for ub-hotspot formation. ChIP against ub-K48 in strains expressing a SUMO variant with all lysines mutated to arginines (*SUMO-KRall*) as the only source of SUMO. *ubx5*Δ cells were used to enhance ubiquitin signals, as Ubx5 is required for Cdc48-dependent extraction of ubiquitylation substrates. Enriched DNA was analyzed by qPCR. Data represent means ± SD (n = 3). Data courtesy of Maximilian J. Kern.
(B) The region of Euc1 required for interaction with Slx5 maps to aa 81–183. Yeast two-hybrid (Y2H) assay to map the Slx5 interaction site on Euc1. A Y2H reporter strain (PJ69-7a) was transformed with Gal4 DNA-binding domain (BD) and Gal4 activation domain (AD) fusion constructs in the indicated combinations. Note that SUMOylation-deficient Euc1-KR still interacts with Slx5-RINGΔ (Δaa 488–619), albeit weaker than wild-type Euc1 (bottom 2 rows). Cells were spotted on control media or selective media (- His) and grown at 30°C for 2 days. See also Appendix Fig. A1A–C.
(C) Euc1 binds to Slx5 *in vitro*. Recombinant purified GST or ^{GST}Euc1 were used in GST pull-down assays to coprecipitate recombinant ^{6His}Slx5.
(D) Euc1 binds to Slx5 *in vivo*. Cell lysates from an *euc1*Δ strain expressing the indicated ^{3FLAG}Euc1 constructs from plasmids (under *EUC1* promoter) were subjected to immunoprecipitation (IP) using anti-FLAG beads. IP-eluates were probed by WB with Slx5, SUMO and Euc1 antibodies, inputs were probed with Slx5, FLAG and Dpm1 antibodies (top to bottom). Note that the Euc1–Slx5 interaction is independent of the Slx8 ligase activity (*slx8-CD*, lanes 5–8).

To identify potential binding motifs, a customized version of the software HH-MOTiF (Prytuliak *et al*, 2017) for *de novo* motif prediction was employed[1]. With

[1] in collaboration with Roman Prytuliak and Bianca Habermann, MPI Computational Biology Group/CNRS, IBDM UMR 7288 Marseille, France

Euc1$^{81-183}$ and a set of putative Slx5 substrates[2] as input data, three potential binding sites were predicted within Euc1$^{81-183}$. Mutation of two of those sites indeed led to a reduction in interaction with Slx5 in Y2H and co-IP experiments (Fig. 14A and B (lanes 2–5), Slx5-binding mutants SBM1 and SBM2, SBM1: aa 139–143 ENQKK>ANAAA, SBM2: aa 162–165 KEVF>AAAA, see also Appendix Fig. A2A). Of note, additional mutation of the Euc1 SUMOylation site had little effect on Slx5 binding in co-IP (Fig. 14B, lanes 6–9). In Y2H experiments, the stretch between Euc1 aa 140–183 was required for interaction with Slx5, but not for dimerization (Fig. 13B, Appendix Fig. A1D). In agreement with that, the SBM1/SBM2 mutations left Euc1 dimerization intact (Appendix Fig. A2B), suggesting that impaired dimerization did not account for the loss of Slx5 interaction.

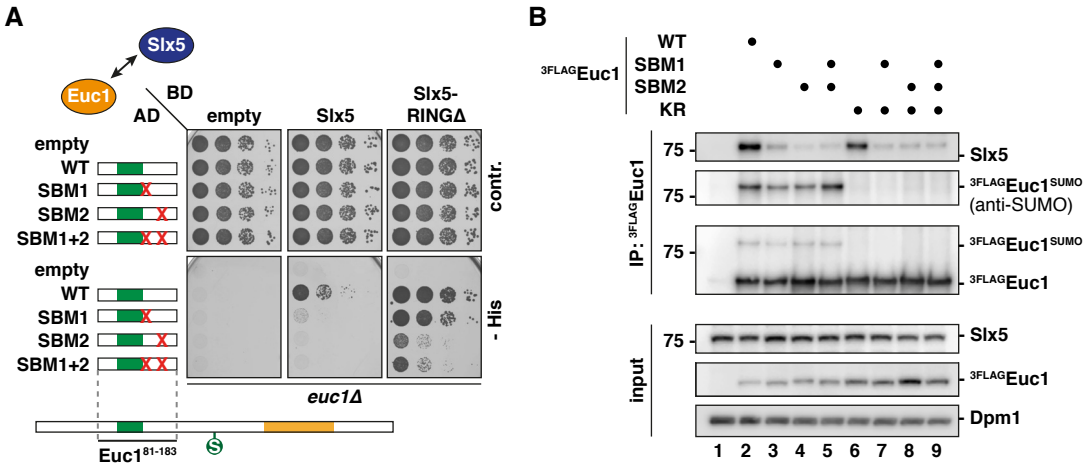

Figure 14. Euc1 interaction with Slx5 is mediated by specific interaction sites.
(A) Euc1 Slx5-binding mutants (SBM1, SBM2) affect Euc1–Slx5 interaction in Y2H assays. AD-Euc1$^{81-183}$ constructs harboring mutations in the region required for Slx5 binding were probed for interaction with BD-Slx5 constructs as described in Fig. 13B. Mutations: SBM1: aa 139–143 ENQKK>ANAAA, SBM2: aa 162–165 KEVF>AAAA. Serial dilutions were spotted and cells were grown at 30°C for 2 days. See Appendix Fig. A2A for expression levels.
(B) Euc1-SBM constructs show defective Slx5 binding *in vivo*. Mutations described in (A) were introduced into full-length ^{3FLAG}Euc1 constructs (with or without the K231R mutation) and FLAG IPs were performed as described in Fig. 13D. WB analysis showed strong Slx5-binding defects for the SBM1/SBM2 and SBM1+2 constructs (top panel, immunoprecipitated Slx5). IP-eluates were probed by WB with Slx5, SUMO and Euc1 antibodies, inputs were probed with Slx5, FLAG and Dpm1 antibodies (top to bottom).

So far, all characterized Slx5/Slx8 substrates required the Slx5 SIMs for their recognition, but the interaction with Euc1 did not comprise the Euc1 SUMOylation site. To identify which features within Slx5 were required for interaction with Euc1, I truncated Slx5 constructs and performed Y2H assays to assess interaction with Euc1. Consistent with a SUMO–SIM-independent interaction, the mapped fragment between aa 201–335 did not contain any SIM (Fig. 15A). This part of the protein was poorly characterized, and I designated it the Slx5 middle domain (Slx5-Md). The Slx5-Md is required and sufficient

[2] unpublished data kindly provided by Ivan Psakhye, FIRC Institute of Molecular Oncology, Milan

for interaction with the Euc$^{81-183}$ fragment (Fig. 15B) and Slx5-binding-deficient mutants of Euc1 (SBM1/2) strongly diminished the interaction (Fig. 15C).

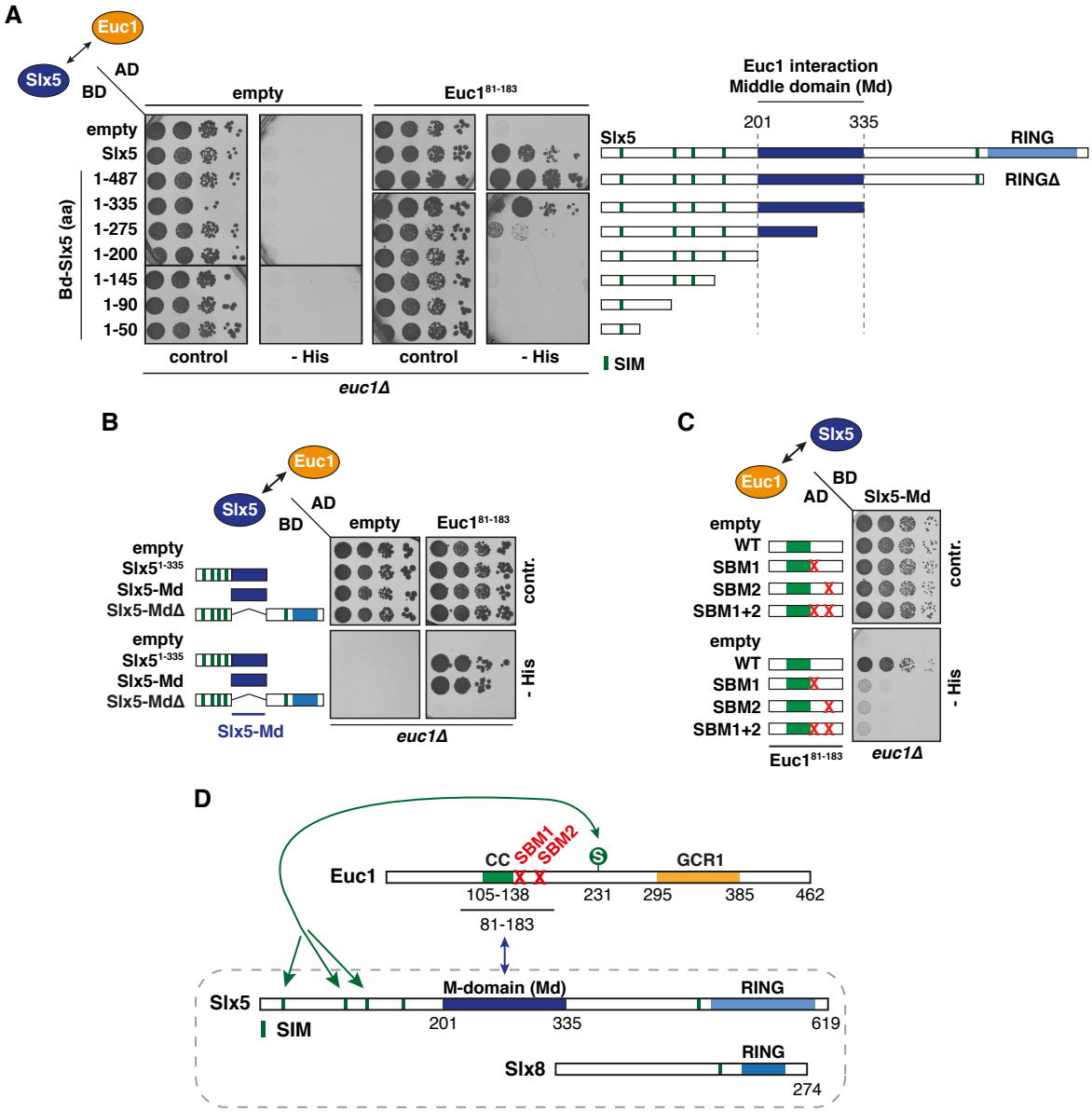

Figure 15. The Slx5 middle domain (Slx5-Md) interacts with Euc1.
(A) The region of Slx5 required to interact with Euc1 maps to aa 201–335 (Slx5-Md). C-terminal Gal4-BD-Slx5 truncation constructs were probed for interaction with AD-Euc1$^{81-183}$ in Y2H. Note that the interaction gradually decreased when truncations between aa 201 and 487 were introduced. The Slx5-Md was defined to be the minimal region required for robust interaction with Euc1, however, the region between aa 336–487 also contributes to the interaction (compare Slx5-RINGΔ and Slx5-Md in Fig. 14A and 15C, respectively). Cells were grown at 30°C for 3 days.
(B) The Slx5-Md is sufficient for interaction with Euc1. Y2H assays with AD-Euc1$^{81-183}$ and BD-Slx5 constructs. Slx5-Md: aa 201–335, Slx5-MdΔ: Δaa 201–338. Serial dilutions were spotted and cells were grown at 30°C for 4 days.
(C) Euc1-SBM constructs show defective binding to the Slx5-Md. Y2H assay with the indicated constructs as in Fig. 14A. See Appendix Fig. A2A for expression levels.
(D) Schematic representation of Euc1, Slx5 and Slx8, domain features and interactions. Domains and protein lengths are drawn to scale, numbers below schemes denote amino acid positions. The mapped interaction between Euc1 and Slx5 is indicated by an arrow. CC: coiled-coil domain, SBM: Slx5-binding mutant, Md: middle domain, S: SUMO, SIM: SUMO interacting motif.

In conclusion, the interaction between Euc1 and Slx5 is independent of polySUMO chains and involves contacts between Euc1$^{81\text{-}183}$ and the Slx5-Md, possibly requiring Euc1 dimerization. SUMO–SIM contacts are not strictly required, but likely contributing to the interaction *in vivo*, suggesting bipartite substrate recognition (summarized in Fig. 15D).

3.4 Specific Euc1–Slx5 Interaction Sites are Required for Ub-hotspots

To validate the functional relevance of the SUMO-independent contacts between Euc1 and Slx5, I tested whether ubiquitylation of Euc1 or ub-hotspot formation would be affected by mutations of the respective interaction sites. Using denaturing NiNTA-PDs with His-ubiquitin, I found that both Euc1 Slx5-binding mutants (SBM1, SBM2), as well as the double mutant exhibited reduced Euc1 ubiquitylation (Fig. 16A, lanes 3–6). Adding the SUMOylation site mutation (KR) to these constructs further decreased the ubiquitylation efficiency (lanes 7–10), suggesting that both specific contact sites and SUMOylation contribute to Slx5/Slx8 recruitment.

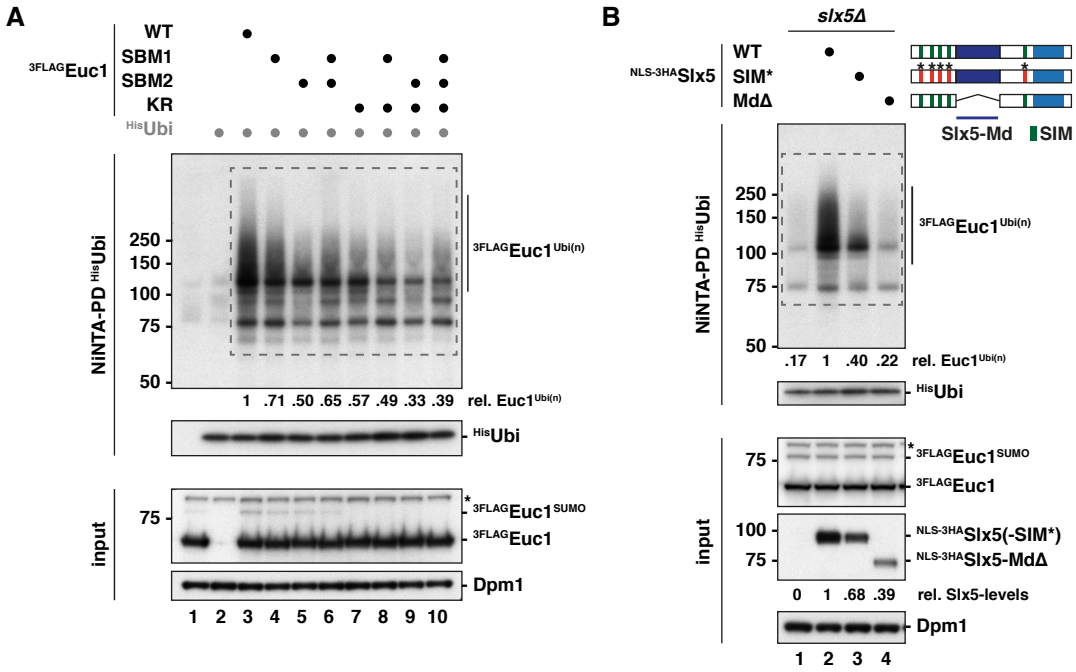

Figure 16. Euc1 ubiquitylation depends on specific Slx5-interaction sites.
(A) Euc1 Slx5-binding mutations impair Euc1 ubiquitylation. His-ubiquitin-modified proteins were enriched by denaturing NiNTA-PDs as described in Fig. 10. 3FLAG-tagged Euc1 constructs with the indicated mutations were expressed from plasmids under the control of the *ADH* promoter. NiNTA-PD eluates were probed with FLAG and ubiquitin (P4D1) antibodies. Whole cell lysates (input) were probed with FLAG and Dpm1 antibodies. Asterisk denotes a non-specific band. For quantification of relative Euc1$^{Ubi(n)}$ levels in NiNTA-PD samples, signals were quantified using ImageStudio Lite from the section indicated by dashed lines, normalized to free ubiquitin (^{His}Ubi) and WT ^{3FLAG}Euc1.
(B) The Slx5-SIMs and Slx5-Md are required for Euc1 ubiquitylation. NiNTA-PDs for His-ubiquitin as in (A). All strains expressed WT ^{3FLAG}Euc1 from plasmids under the *ADH* promoter and His-ubiquitin. Slx5 constructs were expressed from plasmids under control of the endogenous promoter. WBs were probed as described in (A), Slx5 levels were probed using an hemagglutinin (HA) antibody. Slx5-SIM*: SIMs 1–4 were mutated as described (Xie *et al*, 2010), for SIM5, aa 477–479 (IIV) were mutated to alanines. To avoid possible mislocalization by deletion of the Slx5-Md,

(Figure 16, continued)
which overlaps with a putative nuclear localization signal (NLS) (Westerbeck *et al*, 2014), an N-terminal NLS was fused to all constructs. See Appendix Fig. A3C for HU complementation. Quantification of relative Euc1$^{Ubi(n)}$ as in (A) with normalization to (^{His}Ubi) and WT $^{NLS\text{-}3HA}$Slx5. For quantification of relative Slx5 levels, signals were normalized to WT $^{NLS\text{-}3HA}$Slx5.

Moreover, when I performed NiNTA-PDs of His-tagged ubiquitin with *slx5*Δ cells, plasmid-borne expression of a WT Slx5 construct restored Euc1 ubiquitylation (Fig. 16B, lane 2). In contrast, expressing Slx5-SIM* with all SIMs mutated led to reduced Euc1 ubiquitylation, and Slx5-MdΔ failed to restore Euc1 ubiquitylation (Fig. 16B, lanes 3–4).

The central region of Slx5, part of which overlaps with the Slx5-Md (aa 201–335), has previously been implicated in mediating Slx5 nuclear localization, shows interactions with Slx8 and Slx5 itself (Westerbeck *et al*, 2014), and comprises a so-called "lysine desert", a lysine-free stretch that separates the N-terminal SIM-containing region from the RING domain and apparently protects from auto-ubiquitylation (Sharma *et al*, 2017). To rule out that Slx5-MdΔ was generally defective or comprised in its catalytic function, I tested whether the different *SLX5* alleles would be able to complement *slx5*Δ growth phenotypes when challenged with replication stress by HU, or upon exposure to low temperatures (Xie *et al*, 2007). As expected, the Slx5-SIM* construct was deficient in *slx5*Δ complementation, but Slx5-MdΔ restored WT growth (Appendix Fig. A3A–C). Fusion of an N-terminal nuclear localization signal led to reduced protein levels, but did not influence the complementation in growth assays (Appendix Fig. A3A–C). Additionally, I followed turnover of a known Slx5/Slx8 substrate in CHX chase experiments. A Matα2 fragment previously described as model substrate (Hickey & Hochstrasser, 2015) was stabilized in *slx5*Δ cells compared to WT cells, but both WT Slx5 and Slx5-MdΔ constructs fully restored substrate degradation (Appendix Fig. A3D). This argues that Slx5-MdΔ, likely in complex with Slx8, is functional as a STUbL and that the Slx5-Md is required only for ubiquitylation of a subset of substrates, including Euc1.

Consequently, I tested whether Euc1–Slx5 binding defects would affect ub-hotspots. Ub-K48 ChIP-qPCR experiments revealed a reduced ubiquitylation signal for *euc1-SBM1* cells, while it was entirely lost in *euc1-SBM2* and *euc1-SBM1+2* cells (Fig. 17A). In agreement with compromised Slx5 interaction, the signals for Slx5 at ub-hotspots were reduced in *euc1-SBM1* cells and abolished in *euc1-SBM2* and *euc1-SBM1+2* cells (Fig. 17B). Interestingly, Euc1 binding was also reduced in the same pattern (Fig. 17C), reminiscent of defective binding in SUMOylation-deficient *euc1-KR* cells (Fig. 9C).

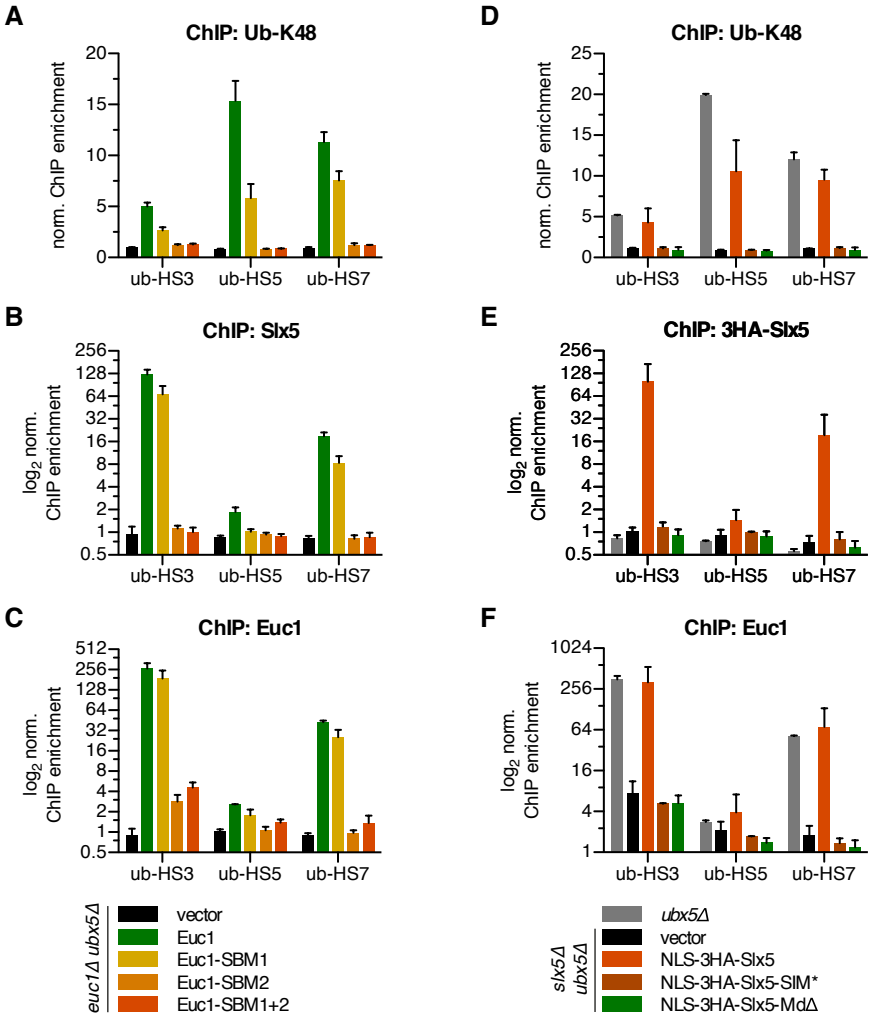

Figure 17. Ub-hotspots depend on specific Euc1–Slx5 interactions.
(A–C) Euc1 Slx5-binding mutations (SBM1/SBM2) reduce/abolish ub-hotspots (A), recruitment of Slx5 (B) and Euc1 (C) to ub-hotspots. ChIP-qPCR for ub-K48, Slx5 (using Slx5 antibody) or Euc1 (Euc1 antibody) in *euc1*Δ *ubx5*Δ cells expressing the indicated Euc1 constructs from plasmids under the control of the *EUC1* promoter. Note that Euc1 Slx5-binding mutants (SBM1, especially SBM2, SBM1+2) show reduced binding to ub-hotspots (C). ChIP for (A–C) was performed using the same cell lysates. Data represent means ± SD (n = 3). See also Appendix Fig. A3E–F for expression levels and Y1H DNA-binding assay of Euc1-SBM1/2 constructs.
(D–F) Slx5-SIMs and the Slx5-Md are required for the formation of ub-HSs and recruitment of Slx5. ChIP-qPCR for ub-K48 (D), Slx5 (anti-HA ChIP, E) and Euc1 (F) in *ubx5*Δ cells or *slx5*Δ *ubx5*Δ cells complemented with plasmids expressing the indicated Slx5 constructs under control of the *SLX5* promoter. Note that also Euc1 recruitment to ub-HS sites is impaired when Slx5-SIMs are mutated or the Slx5-Md is deleted. ChIP for (D–F) was performed using the same cell lysates. Data represent means ± SD (n = 2).

Vice versa, to test whether the Slx5-Md and -SIMs would be required for ub-hotspot formation, I complemented an *slx5*Δ *ubx5*Δ strain with different *SLX5* encoding plasmids. The WT *SLX5* allele restored ubiquitylation and the protein was recruited to ub-hotspots, while *slx5-SIM** and *slx5-Md*Δ alleles were deficient in ubiquitylation and ub-hotspot binding (Fig. 17D–E). Like for the Euc1 Slx5-binding mutants (SBM1/2), recruitment of WT Euc1 was eliminated in *slx5-SIM** and *slx5-Md*Δ cells (Fig. 17F), suggesting mutually dependent binding of Slx5/Slx8 and Euc1 and possibly formation of a stable Euc1^{SUMO}–Slx5/Slx8 complex at ub-hotspots.

Overall, these data indicate that Euc1 SUMOylation and SUMO–SIM mediated interactions, as well as specific contacts between Euc1 and the Slx5-Md are required for proper recruitment of Slx5/Slx8. Therefore, it appears likely that Slx5/Slx8 targeting to ub-hotspots is facilitated by a bipartite or multivalent substrate recognition mode that is distinct from STUbL-typical mechanisms relying primarily on multiple SUMO–SIM contacts.

3.5 The Transcription Factor-like Euc1 Shows Transactivation in Reporter-gene Assays

Prior to the discovery of its role in ub-hotspot formation, Euc1 had been uncharacterized. It features a predicted coiled-coil (CC) domain in its N-terminal part and a GCR1 domain at its C-terminus (Fig. 9A), a domain found to confer sequence-specific DNA-binding in Gcr1 and the related transcription factors (TFs) Msn1 and Hot1 (Huie *et al*, 1992; Hohmann, 2002). Gcr1 acts as a transcriptional regulator of glycolytic genes, while Msn1 and Hot1 mediate transcriptional responses to osmotic and other environmental stress conditions (Hohmann, 2002). Another GCR1 domain is predicted for Cbf2, which is also a DNA-binding protein and part of the CBF3 complex that is required for kinetochore attachment to centromeres (Espelin *et al*, 2003).

For Euc1, structure prediction suggested a myb-like DNA-binding fold within the GCR1 domain (Fig. 18A) (Kelley *et al*, 2015; Biedenkapp *et al*, 1988). To map the region of Euc1 required for DNA binding, I used a yeast one-hybrid (Y1H) strategy to test specific association of Euc1 constructs with the ub-hotspot motif (ub-HS-motif). The yeast one-hybrid strain carried a stably integrated reporter construct with three copies of the ub-HS-motif of ub-hotspot 4 cloned in the promoter region of *HIS3* (*3x ub-HS4-HIS3*, Fig. 18B, scheme on top right, (Kern, 2013)). Plasmids encoding Euc1 truncation constructs fused to a Gal4 transactivation domain (AD) were transformed into cells to assay growth on media lacking histidine (-His), which indicates DNA binding and *HIS3* activation. My mapping results establish that the complete GCR1 domain and C-terminus are essential for Euc1 association with the ub-HS-motif (amino acid (aa) 291–462, Fig. 18B). Mutations introduced in the predicted, conserved DNA-binding loop (W333A, R334A, *euc1-DBD**) led to a loss of binding to ub-HS-motifs in Y1H assays (Fig. 18C). When I replaced endogenous *EUC1* with *euc1-DBD**, Euc1 binding to endogenous ub-hotspots was lost in ChIP experiments, as was ubiquitin enrichment (Fig. 18D–E).

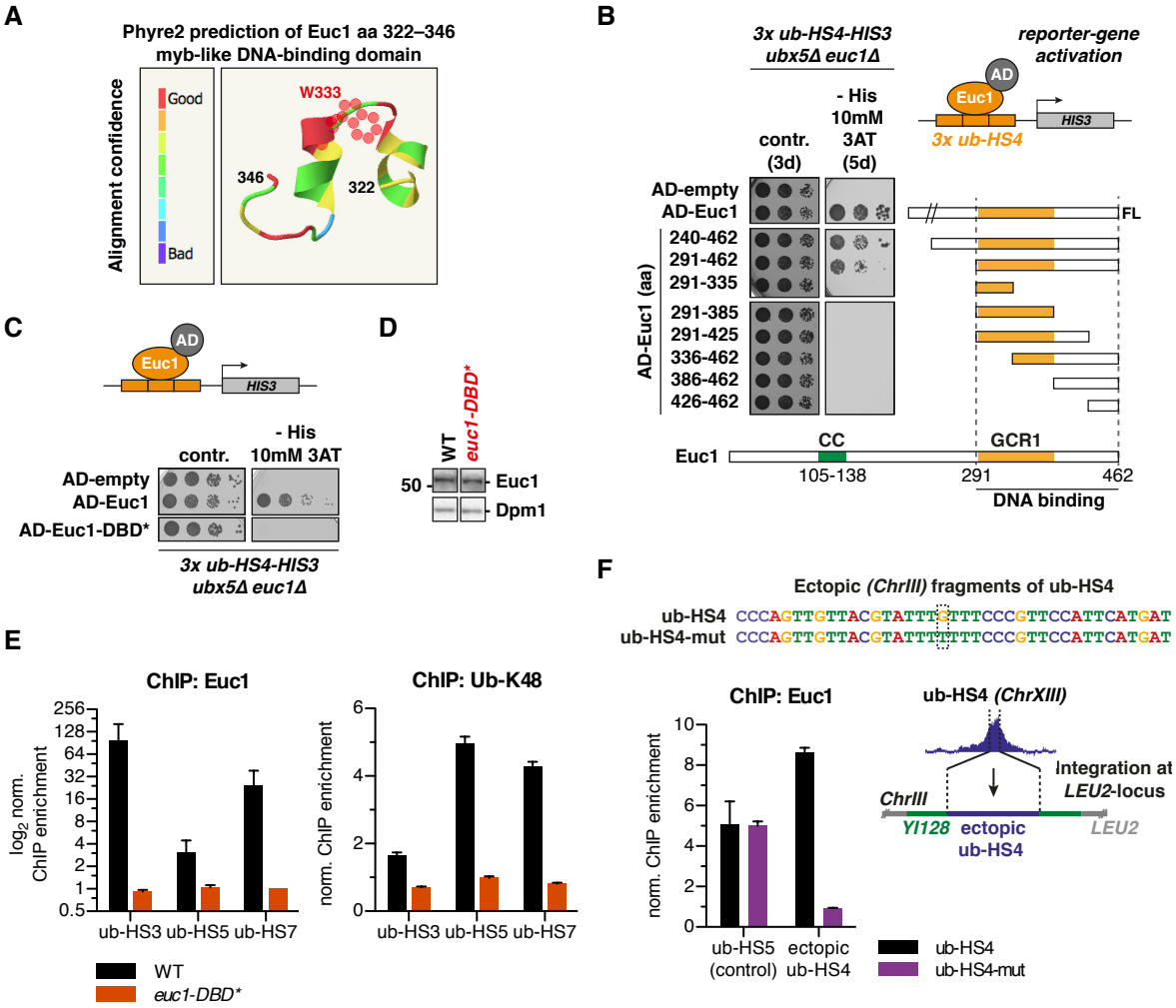

Figure 18. Euc1 binds to the ubiquitin hotspot motif via its GCR1 domain.
(A) Phyre2 structural prediction result (Kelley *et al*, 2015) for part of the Euc1 GCR1 domain (aa 322–346) that shows homology to the DNA/RNA-binding 3-helical bundle fold of myb-like DNA-binding domains (DBD) of the homeodomain family. Structural prediction is color-coded for the alignment confidence with PDB-entry d1x58a1 (*Mus musculus* Terb1). A conserved tryptophan (W333) predicted to display strong mutational sensitivity is highlighted in red.
(B) The GCR1 domain and C-terminus (aa 291–462) of Euc1 are required and sufficient for DNA binding in yeast one-hybrid (Y1H) assays. A growth-based Y1H assay was established by cloning three copies of the ub-HS4-motif upstream of a minimal promoter followed by a *HIS3* reporter-gene and integrated at the *URA3* locus (*3x ub-HS4-HIS3*, top right). Gal4-AD- or Gal4-AD-Euc1-encoding plasmids harboring the indicated Euc1 truncations were transformed into the Y1H reporter strain and serial dilutions were spotted on control plates and plates lacking histidine supplemented with 3-amino-1,2,4-triazole (3AT) to suppress background activation. Cells were grown at 30°C for 3–5 days as indicated (3d/5d). The Y1H strain also carried a deletion of the Cdc48 cofactor *UBX5*, which leads to accumulation of ubiquitylated proteins bound at ub-hotspots.
(C) Mutation of the myb-like DNA-binding domain leads to loss of Euc1 binding to the ub-HS-motif in Y1H assays. The W333A, R334A-mutation (hereafter *euc1-DBD**) led to a complete loss of Euc1 DNA binding. Assay was performed as in (B), cells were grown for 3 days at 30°C.
(D) Expression levels of Euc1 in WT and *euc1-DBD** strains used in (E) as probed by WB. The *euc1-DBD** allele was integrated at the endogenous *EUC1* locus. Euc1 was probed with the Euc1 antibody and Dpm1 levels served as loading control. Sections were cropped from the same exposure.
(E) The Euc1-DBD is required for Euc1 binding and ubiquitin enrichment at endogenous ub-HS sites. ChIP followed by qPCR quantification of selected ub-hotspots using an Euc1-specific or ub-K48 antibody was performed in either WT or *euc1-DBD** cells. Data represent means ± SD ($n = 2$).
(F) A single point mutation within the ub-HS-motif abolishes Euc1 enrichment. Schemes: A 39-bp stretch of WT or a mutated ub-HS4 sequence was cloned and integrated at the *LEU2* locus (grey) using the integrative YIplac128 vector (green) (Kern, 2013). For ub-HS4-mut, a G>T mutation was introduced in one of the conserved TGTT repeats. ChIP-qPCR for Euc1 demonstrated that Euc1 binding was lost upon mutation of the ub-HS-motif. Experiments were performed in *cdc48-6* strains. Data represent means ± SD ($n = 2$).

Supporting direct binding of Euc1 to the ub-HS-motif, I found that Euc1 no longer bound to a mutated ub-hotspot 4 motif that was integrated at an ectopic chromosomal location (Fig. 18F). Here, a single point mutation had been introduced in one of the central, conserved TGTT repeats of the ub-HS-motif (Fig. 18F, top). Using the same strategy, it had previously been demonstrated that ubiquitin was enriched at the ectopically integrated WT ub-HS4, but was lost at the mutated ub-HS4-mut (Kern, 2013). Taken together, these experiments demonstrate that Euc1 binds the ub-HS-motif via its GCR1 domain and that both Euc1 binding and ubiquitin enrichment depend on the ub-HS-motif. Importantly, Euc1 binding and ub-hotspot formation are independent of the genomic location of the ub-HS-motif.

To investigate the evolutionary conservation of Euc1, I performed phylogenetic analysis, which identified *EUC1*-like genes in several other *Saccharomyces* species with most pronounced sequence similarity in the CC and GCR1 domains (Fig. 19A–B). Likewise, ub-hotspot-related sequences were found in those yeast species, where intergenic regions corresponding to ub-hotspot loci could be identified (Fig. 19C). Of interest, the residues most conserved within the *S. cerevisiae* ub-HS-motifs also showed the highest degree of homology in other yeasts, suggesting that Euc1 orthologs might bind them and fulfill a related function at those sites (Fig. 19C, right panels). Using standard sequence alignment and homology search tools like BLAST, no homologs of Euc1 could be identified in distantly related yeast species or higher eukaryotes. Hence, it remains elusive whether Euc1 or its function is conserved in higher eukaryotes.

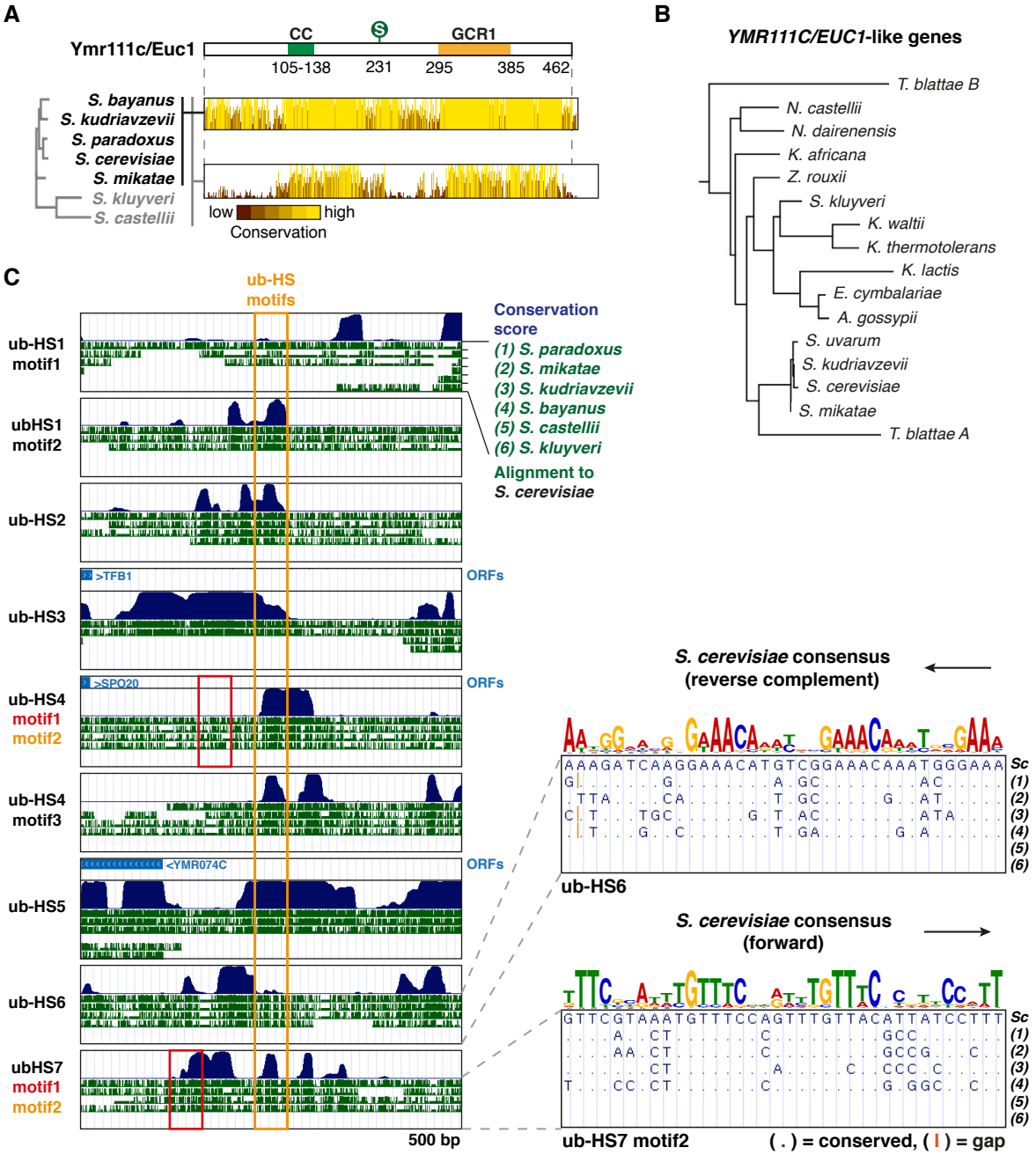

Figure 19. Euc1 and the ub-hotspots are conserved in closely related yeast species.
(A) Conservation of Euc1 domains. Euc1-like protein sequences from closely related *Saccharomyces* species were aligned and a phylogenetic tree was generated using Clustal Omega. Jalview was used to graphically display the degree of sequence conservation.
(B) Phylogenetic tree of *YMR111C/EUC1*-like genes. The Yeast Gene Order Browser was used to identify orthologs of *YMR111C/EUC1* in other yeasts and to generate a phylogenetic tree with the MUSCLE algorithm and PhyML (http://ygob.ucd.ie/ (Byrne & Wolfe, 2005)).
(C) The ub-HS-motif is conserved in closely related yeast species. The 7 yeast Multiz Alignment & Conservation tool of the UCSC Genome Browser was used to retrieve alignments of sequences corresponding to ub-HS-motifs from other *Saccharomyces* species. Local conserved stretches within the mostly intergenic regions are marked by dark blue peaks of the Conservation score track (left panel) and examples for two ub-HS-motifs are highlighted at base-pair resolution (right panels). Note that several ub-hotspots harbor multiple ub-HS-motifs. Dot (.) indicates a conserved base, (|) denotes a gap. *Sc*: *Saccharomyces cerevisiae.*

To explore whether Euc1 itself, like three of the other GCR1 domain proteins, could also function as a TF in cells, I deleted the endogenous *EUC1* gene in the *3x ub-*

HS4-HIS3 Y1H strain, which led to reduced background activation of the *HIS3* reporter in *euc1*Δ cells (Fig. 20A). Reciprocally, complementing the *euc1*Δ reporter strain with *EUC1* encoding plasmids (under the control of the endogenous *EUC1* promoter) restored reporter gene expression and growth on selective -His plates (Fig. 20B–C). The presence of an acidic patch (aa 19–28) in the Euc1 N-terminus, together with several aromatic residues hinted at a possible function of this part of the protein in transactivation, since this feature combination often mediates transcriptional activation (Fig. 20B, bottom, (Sigler, 1988; Ravarani *et al*, 2018)). Consistently, truncation of the first 15 or 30 amino acids led to strong defects in *HIS3* activation by Euc1 (Fig. 20B), and fusion of Euc1$^{1\text{-}30}$ to the Gal4 BD was sufficient for activation of a *GAL1*-promoter controlled reporter gene (Fig. 20D).

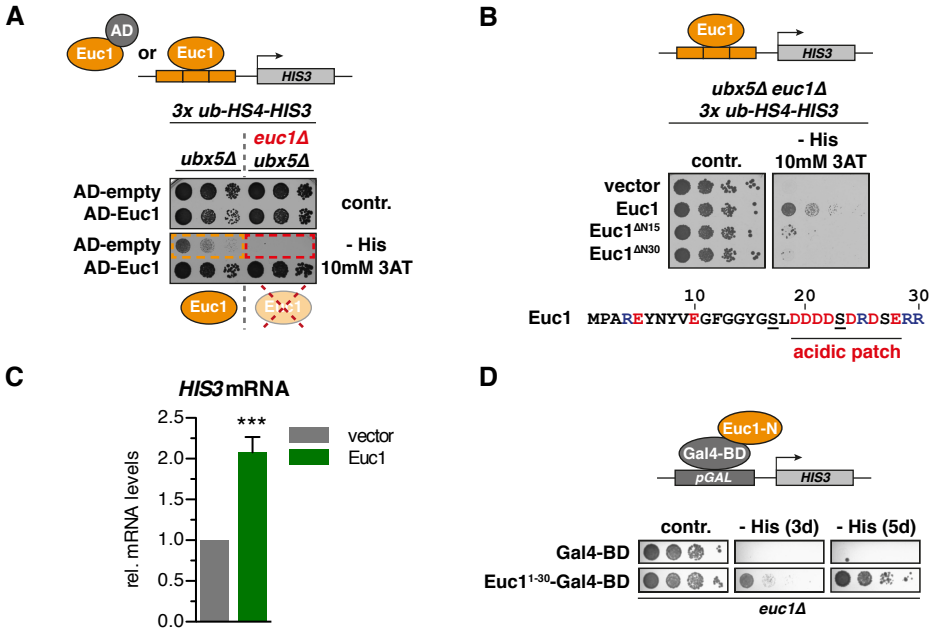

Figure 20. Euc1 can mediate transactivation via its N-terminus.
(A) Endogenous Euc1 acts as a TF in reporter-gene assays. The Y1H reporter strain described in Fig. 18B (*3x ub-HS4-HIS3 ubx5*Δ) or the same strain with *EUC1* deleted (*euc1*Δ) was transformed with the indicated plasmids and a growth assay was performed as described in Fig. 18B. Note that endogenous Euc1 weakly drives activation of the *HIS3* reporter gene (compare orange and red dashed boxes). Cells were grown at 30°C for 5 days.
(B) Euc1 can induce transactivation via its N-terminal 30 amino acids. Euc1 constructs under control of the endogenous *EUC1* promoter were transformed in a reporter strain as described for Fig. 18B and serial dilutions were spotted on control or selective media to test *HIS3* activation. Note that no Gal4 AD was fused to Euc1 constructs. Cells were grown at 30°C for 3 days. Bottom: Euc1 aa 1–30 are shown with negatively charged residues shaded in red and positively charged residues in blue. Underlined residues have been annotated to be phosphorylation sites in UniProt.
(C) Quantification of *HIS3* mRNA levels from strains used in (B). Cells with full-length Euc1 or empty vector were grown in liquid media with selection for the transformed plasmids (SC-Leu medium), harvested in logarithmic growth phase and total mRNA was prepared. After reverse transcription, *HIS3* mRNA levels were quantified using qPCR (RT-qPCR), normalized first to *ACT1* mRNA and then to the empty vector control strain. Data represent means ± SD (n = 4). $p = 2.43*10^{-5}$ (Student's t-test).
(D) The Euc1 N-terminal 30 amino acids are sufficient for transactivation. The Gal4-BD was C-terminally fused to Euc1$^{1\text{-}30}$ and the activation of a *GAL1* promoter controlled *HIS3* reporter gene was monitored. The PJ69-7a Y2H strain with *EUC1* deleted was used.

These data suggest that Euc1 might act as transcription factor at ub-hotspots. However, it remains a possibility that Euc1 is required to establish a particular chromatin domain or structure at ub-hotspots for different purposes, like Cbf2 does at centromeres.

3.6 Euc1 in Transcriptional Regulation

Inspired by the data obtained in the reporter-gene assays (Fig. 20), a plausible hypothesis for Euc1 function is that it acts as a transcription factor, and the ub-hotspot pathway could regulate transactivation by Euc1.

To investigate a potential role of Euc1 as TF, I performed RNA sequencing (RNAseq) to compare transcriptome alterations in *euc1*Δ cells and *EUC1* overexpression cells (*pGAL-EUC1*) to WT/control strains[3]. Out of 15 genes in direct proximity to ub-hotspots, only 2 showed a significant change in expression levels in *euc1*Δ cells, with

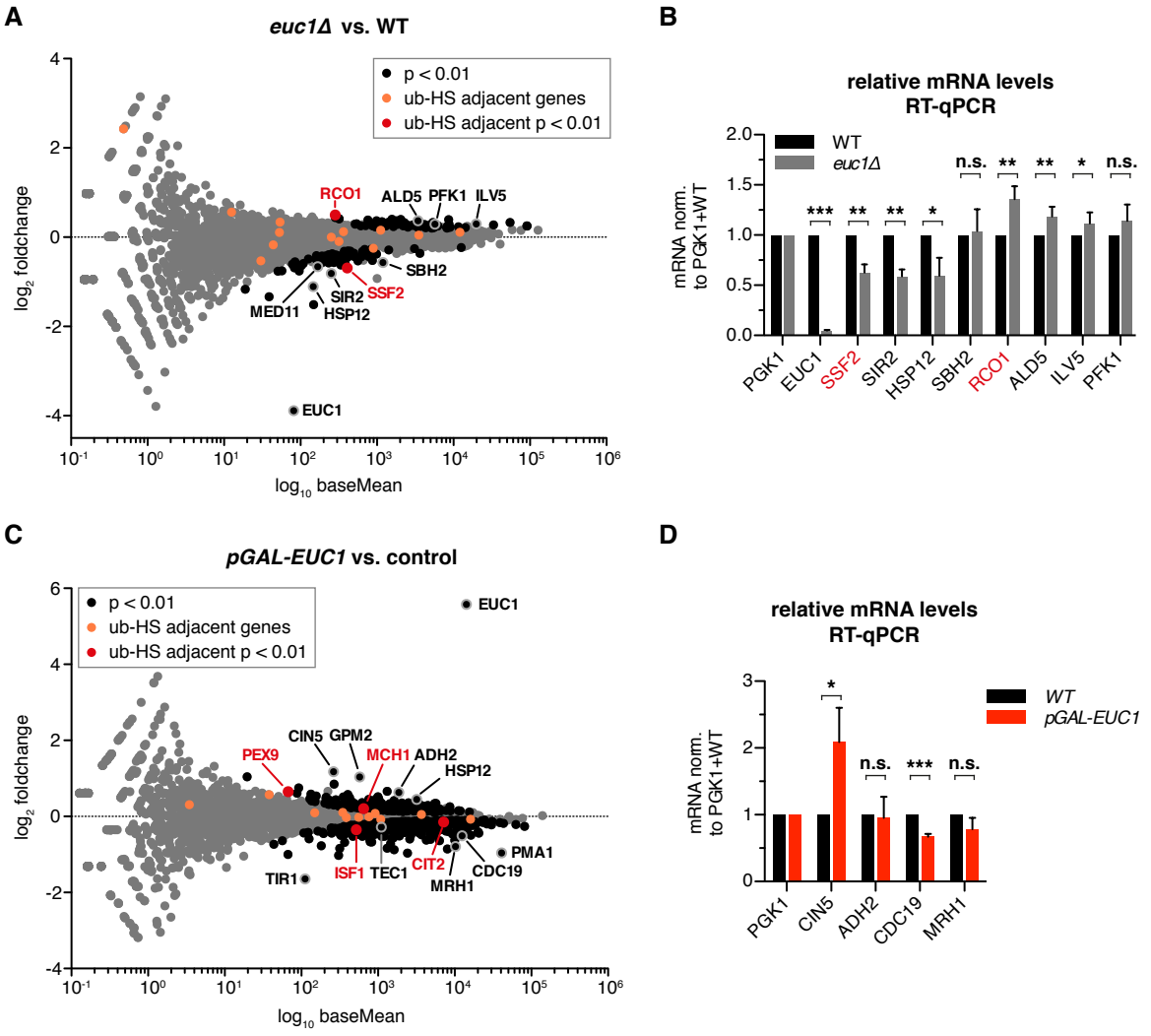

[3] Sequencing was performed with help from Marja Driessen, MPI Biochemistry Core Facility, Bioinformatic analysis was performed in collaboration with Tobias Straub, BMC/LMU, Munich

Figure 21 (previous page). Euc1 has only minor effects on ub-hotspot adjacent gene transcription.
(A) Deletion of *EUC1* does not lead to ub-HS adjacent gene deregulation, but rather widespread transcriptome changes. Total RNA isolated from WT and *euc1*Δ cells grown under standard growth conditions was polyA enriched and sequenced (RNAseq in triplicates). Significance testing was based on the Wald test, see Materials and Methods for details. baseMean: mean expression levels across all samples.
Highlighted transcripts: *RCO1*: Rpd3S histone deacetylase subunit; *SSF2*: ribosomal large subunit maturation factor; *MED11*: RNA Pol II mediator subunit (ORF adjacent to *EUC1*, *MED11* downregulation likely contributes to some *euc1*Δ phenotypes, see Appendix Fig. A6C–F); *SIR2*: Sirtuin family histone deacetylase; *HSP12*: plasma membrane protein involved in membrane organization.
Metabolic functions: *ALD5*: mitochondrial aldehyde dehydrogenase; *PFK1*: phosphofructokinase subunit; *ILV5*: acetohydroxyacid reductoisomerase and mitochondrial DNA binding protein.
(B) RT-qPCR quantification of selected transcripts deregulated in the *euc1*Δ transcriptome (A). Quantification was performed as for Fig. 20C, but normalization was performed with *PGK1*, because *ACT1* appeared mildly upregulated in *euc1*Δ cells in RNAseq. RT-qPCR was performed on the same three replicate samples as used for RNAseq. Data represent means ± SD ($n = 3$), for statistical analysis an unpaired, two-tailed Student's *t*-test was performed. For (B) and (D): (*): $p \leq 0.05$, (**): $p \leq 0.01$, (***): $p \leq 0.001$, n.s.: not significant.
(C) RNAseq transcriptome analysis of *EUC1* overexpression as in (A). Δ*euc1* cells with *pGAL-EUC1* (overexpression) or *pEUC1-EUC1* (control) integrated at the *URA3*-locus (YIplac211) were grown to mid-log phase and 2% galactose was added for 3h.
Highlighted transcripts: *PEX9*: peroxisomal membrane signal receptor for peroxisomal matrix proteins; *MCH1*: protein with similarity to mammalian monocarboxylate permeases; *ISF1*: serine-rich, hydrophilic protein, molecular function uncharacterized; *CIT2*: peroxisomal citrate synthase, involved in glyoxylate cycle; *CIN5*: basic leucine zipper TF of the yAP-1 family, mediates pleotropic drug and salt tolerance; *TIR1*: cell wall mannoprotein; *TEC1*: TF targeting filamentation genes and Ty1 expression; *MRH1*: membrane protein related to Hsp30, localizes primarily to plasma membrane; *PMA1*: plasma membrane P2-type H+-ATPase, major regulator of cytoplasmic pH.
Metabolic functions: *GPM2*: nonfunctional phosphoglycerate mutase homolog; *ADH2*: glucose-repressible alcohol dehydrogenase II; *CDC19*: pyruvate kinase; *MCH1*, *CIT2*.
(D) RT-qPCR quantification of genes misregulated in the *pGAL-EUC1* transcriptome (C). Data was obtained from samples independent of the RNAseq experiment. Data represent means ± SD ($n = 3$), for statistical analysis an unpaired, two-tailed Student's *t*-test was performed.

opposing trends (*RCO1* up, *SSF2* down, Fig. 21A–B). In total, around 150 genes were significantly deregulated (up or down) in *euc1*Δ cells ($p < 0.01$), possibly reflecting a more general function of Euc1 in transcriptional regulation, or indicating an adaptation response to loss of *EUC1*. When functional categories of the deregulated genes were analyzed, gene ontology (GO) term enrichments identified an upregulation of small molecule metabolic processes (e.g. organic, carboxylic and amino acid metabolism). These data overall do not seem to support a model whereby Euc1 directly activates transcription of ub-hotspot adjacent genes.

In agreement with this notion, *EUC1* overexpression did not lead to strong deregulation of ub-hotspot adjacent genes as well (Fig. 21C). Four of them showed mild up- or downregulation, while in contrast many other genes showed stronger changes in expression levels (Fig. 21C–D), especially genes involved in cellular metabolism (e.g. carboxylic and organic acid metabolism were upregulated; and translation, peptide biosynthesis and ribosome biogenesis appeared downregulated). These results from RNAseq experiments largely agree with a previous characterization of Euc1-mediated transcriptional regulation using microarrays, in particular in that ub-hotspot adjacent genes did not exhibit strong deregulation (Kern, 2013).

Interestingly, in reporter gene assays Euc1-KR exhibited higher activity than WT Euc1, suggesting that SUMOylation might negatively regulate transactivation (Kern, 2013). Confirming these results, Euc1 constructs with the endogenous DBD replaced with Gal4-BD showed a similar behavior: Abolishing Euc1 SUMOylation by introducing the K231R mutation or interfering with the SUMOylation machinery (*siz1*Δ *siz2*Δ) led to enhanced reporter gene activation (Appendix Fig. A4A–B). However, similar assays with endogenous Euc1 and different ub-hotspot sequences in the promoter region of a reporter gene did not give consistent results regarding the regulation by the ub-hotspot pathway machinery (Appendix Fig. A4C–D), or when different Euc1 mutants were tested (Appendix Fig. A4E–F). Additionally, transcriptome analysis of *euc1-KR* cells failed to reveal any strongly deregulated genes or activation of ub-hotspot adjacent genes (Kern, 2013).

A previous study addressing transcriptome changes in *slx5*Δ and *slx8*Δ cells found several hundred genes deregulated (321 and 132, respectively, with fold-change > 1.7 and $p < 0.05$, (van de Pasch *et al*, 2013)). Of note, only 2 ub-hotspot adjacent genes were significantly changed (*ATG34* and *ATG19* around ub-HS7 upregulated), while other ub-hotspot adjacent genes showed minor changes, both up- or downregulation. The authors conclude that most changes observed in *slx5*Δ/*slx8*Δ transcriptomes arise from genome instability-induced stress, rather than direct effects on transcriptional regulation by Slx5/Slx8 (van de Pasch *et al*, 2013).

Taken together, genes around the endogenous Euc1 binding sites at ub-hotspots do not appear to underlie direct regulation by Euc1 or Slx5/Slx8. This suggests that Euc1's primary function might not be in transcriptional regulation of ub-hotspot adjacent genes, at least not under the conditions tested.

3.7 The Slx5/Slx8-dependent Ub-hotspot Pathway Controls Aberrant Euc1

To gain insight into physiological functions of Euc1 and the ub-hotspot pathway, I tested cellular fitness of strains deleted for *EUC1* or overexpressing *EUC1* in growth assays under various conditions. While *euc1*Δ cells did not exhibit any noticeable growth defect compared to WT cells, overexpression of *EUC1* (*pGPD-EUC1*, *pGAL-EUC1*) led to lethality at high temperatures or upon treatment with the membrane-fluidizing drug benzyl alcohol (Lone *et al*, 2015) (Fig. 22A–B). Highlighting a crucial role for Slx5/Slx8 in the control of overexpressed *EUC1*, the toxicity was increased when *EUC1* overexpression

was paired with *slx5*Δ or *slx8*Δ via mating and tetrad analysis, even under normal growth conditions (Fig. 22C). Interestingly, *EUC1* alleles deficient in ub-hotspot formation, like SUMOylation-deficient *euc1-KR* or Euc1 Slx5-binding mutants (*euc1-SBM1/2*), showed the same toxicity as overexpressed WT *EUC1* (Fig. 22D, Appendix Fig. A5A). In contrast, alleles deficient in DNA binding (*euc1-DBD**) and/or transactivation (*euc1-N30*Δ, *-CC*Δ, see also Appendix Fig. A4E–F) caused milder or no toxicity (Fig. 22D, Appendix Fig. A5A). As Euc1-WT, -KR and -DBD* all show a similar nuclear localization, it is unlikely that a change in cellular localization could explain the different growth phenotypes (Appendix Fig. A5B). Together, these data indicate that *EUC1* overexpression toxicity does not arise from over-active ub-hotspots formation.

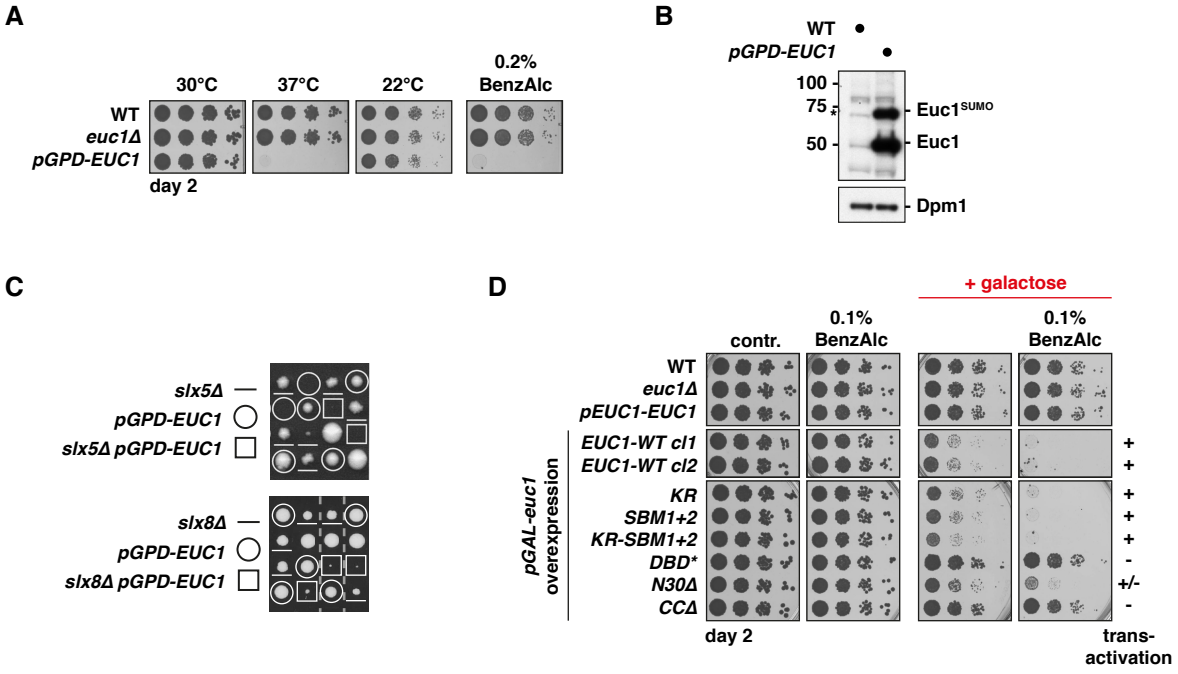

Figure 22. *EUC1* overexpression is toxic.
(A) *EUC1* overexpression is toxic at elevated temperatures and upon exposure to the membrane fluidizing drug benzyl alcohol (BenzAlc). Serial dilutions of the indicated strains were spotted and grown on YPD control (30°C) or under conditions as indicated.
(B) Western blot against Euc1 (and Dpm1 as loading control) to compare expression levels in WT and *pGPD-EUC1* cells. Asterisk denotes an unspecific band.
(C) *EUC1* overexpression leads to strong phenotypes or lethality in *slx5*Δ and *slx8*Δ cells. Individual cells from tetrads (arranged in vertical columns) of *pGPD-EUC1 slx5*Δ or *pGPD-EUC1 slx8*Δ diploid cells were grown on YPD plates at 30°C for 3 days. Data for top panel courtesy of Julian Stingele.
(D) *EUC1* overexpression toxicity depends on DNA binding and transactivation. The indicated *EUC1* alleles with endogenous (*pEUC1*) or galactose-inducible promoters (*pGAL*) were integrated at the *URA3* locus (YIplac211, *euc1*Δ background) and spotted on glucose control or galactose plates to induce *EUC1* overexpression, supplemented with benzyl alcohol as indicated. See also Appendix Fig. A4E–F and A5A.

To address how then the observed toxicity arises, I performed ChIP-chip experiments to monitor genomic binding sites of Euc1 upon overexpression. Compared to control conditions, overexpressed Euc1 bound to additional loci, including the *STI1-CIN5*

intergenic and the *TEC1*-upstream (us) region (Fig. 23A). ChIP-qPCR experiments showed a marked increase in Euc1 binding to unrelated control regions ("contr.", Fig. 23B, top), suggesting higher background binding across the genome. Yet, ChIP-qPCR also confirmed significant additional enrichment of Euc1 at *STI1-CIN5* and *TEC1-us* (Fig. 23B, top). The additional binding to those sites was strongly reduced in *euc1-DBD** and *euc1-N30*Δ cells, offering a rationale for the weaker growth phenotypes of those mutants. Importantly, no additional ubiquitin enrichments were detected at the aberrantly bound loci, supporting the hypothesis that *EUC1* overexpression toxicity is unrelated to ub-hotspot formation on chromatin (Fig. 23B, bottom).

The observed widespread transcriptome changes in *pGAL-EUC1* cells could indicate direct Euc1-dependent transcriptional deregulation of additionally bound genes, but also indirect effects are conceivable. Of note, *CIN5* (a TF involved in pleiotropic drug resistance and salt tolerance) and *TEC1* (a TF controlling filamentation genes), which are in close proximity to abnormally bound regions, were deregulated in the *pGAL-EUC1* transcriptome (Fig. 21C–D). Since both genes encode transcriptional regulators, they could also further propagate transcriptional aberrations.

Importantly, overexpression of *SLX5/SLX8* (*pADH-SLX5+SLX8*) mitigated spurious Euc1 binding at *STI1-CIN5* and *TEC1-us* loci and could relieve Euc1 toxicity (Fig. 23C–D, Appendix Fig. A5C). In contrast, overexpression toxicity of the SUMOylation- and Slx5-binding-deficient *euc1-KR-SBM1+2* could only be alleviated to a minor extent by additional *SLX5/SLX8* overexpression (Fig. 23C–D, Appendix Fig. A5C).

Taken together, the data indicate that Euc1 needs to be tightly controlled by Slx5/Slx8 in order to confine its action to sites of ub-hotspots. Aberrant Euc1 leads to transcriptome changes, likely via its transactivation function, and probably by a combination of direct effects on abnormally bound genes and indirect effects. In contrast, the primary function of endogenous Euc1 appears independent of transcriptional activation of ub-hotspot adjacent genes.

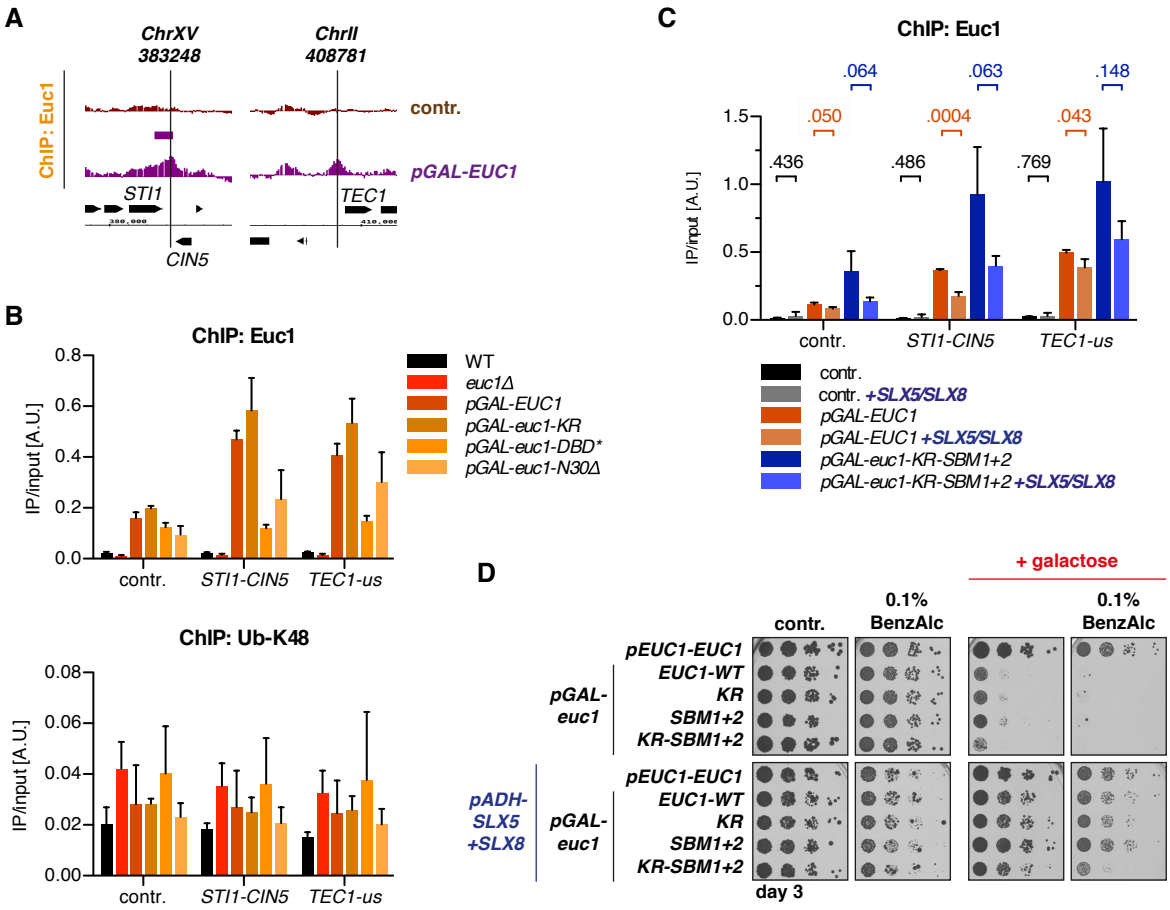

Figure 23. *SLX5/SLX8* rescue aberrant Euc1 binding and overexpression toxicity.
(A) Snapshots of ChIP-chip tracks from regions showing additional *EUC1* binding signals upon *EUC1*-overexpression (*pGAL-EUC1*, 3h induction). *pGAL-EUC1* or an empty plasmid (contr.) was integrated at the *URA3* locus (YIplac211). Data represent means from two independent replicates.
(B) Top: Binding of overexpressed *EUC1* to aberrant loci depends on Euc1 DNA binding. ChIP-qPCR for Euc1 after 3h galactose induction. Note that IP/input ratios of Euc1 signals are shown, also for the control locus (contr.: *TOS1* promoter) to highlight Euc1 binding at non-ub-HS sites upon overexpression. *STI1-CIN5*: intergenic region. *TEC1-us*: upstream (promoter) region of *TEC1*. Bottom: Ubiquitin (ub-K48) ChIP-qPCR for the same samples. Data represent means ± SD (n = 3).
(C) Simultaneous overexpression of *SLX5* and *SLX8* leads to a reduction of aberrant Euc1 binding to non-ub-HS loci. Experiment as in (B, top), but with concomitant plasmid-borne overexpression (*ADH* promoter) of *SLX5* and *SLX8*. ChIP-qPCR analysis of selected strains from (D) as indicated, after 3h galactose induction. Data represent means ± SD (n = 3). p-values from Student's t-tests for the indicated comparisons are shown.
(D) *SLX5/SLX8* overexpression rescues *EUC1* toxicity. Experiment as in Fig. 22D, but with concomitant plasmid-borne overexpression (*ADH* promoter) of *SLX5* and *SLX8* (bottom panels) and on media selecting for *SLX5/SLX8* plasmids. See also Appendix Fig. A5C.

3.8 *EUC1* Shows Genetic Interactions with Regulators of Gene Expression upon Thermostress

As mentioned above, *euc1*Δ cells did not show any growth defect when compared to WT cells, even in a wide range of stress conditions, including cold, heat and oxidative stress, exposure to reducing agents, ER protein folding stress, hypoxia, DNA-damage inducing agents, drugs targeting lipid biosynthesis, and growth on various different carbon sources (not shown). Although this might suggest that *EUC1* is not required for growth in any of

those conditions, another possibility is that redundant pathways compensate for loss of *EUC1*.

Supporting the notion of redundancy, other studies using high-throughput genetic screens have reported a number of genetic interactions of *EUC1* with genes showing GO-term enrichments for genetic pathways including chromatin organization, negative regulation of transcription, histone deacetylation, and related processes (Zheng *et al*, 2010; Costanzo *et al*, 2010; 2016). I could confirm some of these interactions, for example deleting *EUC1* markedly enhanced phenotypes of strains deleted for *HTZ1*, the gene encoding the histone variant H2A.Z, specifically upon exposure to thermostress (heat or cold) and when challenged with dimethyl sulfoxide (DMSO) or HU (Fig. 24A). Similar genetic interactions were observed with *SWR1* and *YAF9*, which encode for members of the H2A.Z remodeling complex SWR1-C (Appendix Fig. A6A–B). The H2A.Z–SWR1-C axis has previously been ascribed to functions in the regulation of inducible promoters, heterochromatin maintenance and genome stability (Billon & Côté, 2013). Of note, H2A.Z itself was proposed to act as a nucleosomal "thermosensor", in *Arabidopsis thaliana* and *S. cerevisiae*, and several studies described a requirement for H2A.Z and associated remodelers for resistance to DMSO (Lindstrom *et al*, 2006; Zhang *et al*, 2005; Gaytán *et al*, 2013; Kumar & Wigge, 2010). On a molecular level, the causes of DMSO toxicity are not well understood, however, perturbation of membrane organization and weak inhibition of histone deacetylases (HDACs) have been reported (Gurtovenko & Anwar, 2007; Marks & Breslow, 2007). Additional genetic interactions were found with *NPL3*, which is required for proper mRNA splicing and processing, and *STB5* encoding for a TF mediating oxidative and multidrug stress responses (Fig. 24A, Appendix Fig. A6A, C–F).

Most prominently, deletion of *EUC1* led to a strong aggravation of the described heat sensitivity of cells deleted for accessory members of the Rpd3L HDAC complex (*dep1*Δ, *rxt2*Δ*, sds3*Δ*,* Fig. 24B–C) (Ruiz-Roig *et al*, 2010). The catalytic subunit Rpd3 is a homolog of human class I HDACs and is a shared component of three distinct HDAC complexes in yeast (Carrozza *et al*, 2005; McDaniel & Strahl, 2013): (i) Rpd3L, which is primarily recruited to gene promoters to mediate repression, but also activation in some stress conditions, such as heat stress (de Nadal *et al*, 2004; Carrozza *et al*, 2005; Ruiz-Roig *et al*, 2010); (ii) Rpd3S, which is primarily recruited to transcribed regions, where it binds to methylated H3K36 and suppresses cryptic intragenic transcription by deacetylating histones (Carrozza *et al*, 2005); and (iii) Rpd3µ, a less-well-described complex (formed by

Rpd3/Snt2/Ecm5) mediating transcriptional regulation related to oxidative stress resistance (Baker *et al*, 2013).

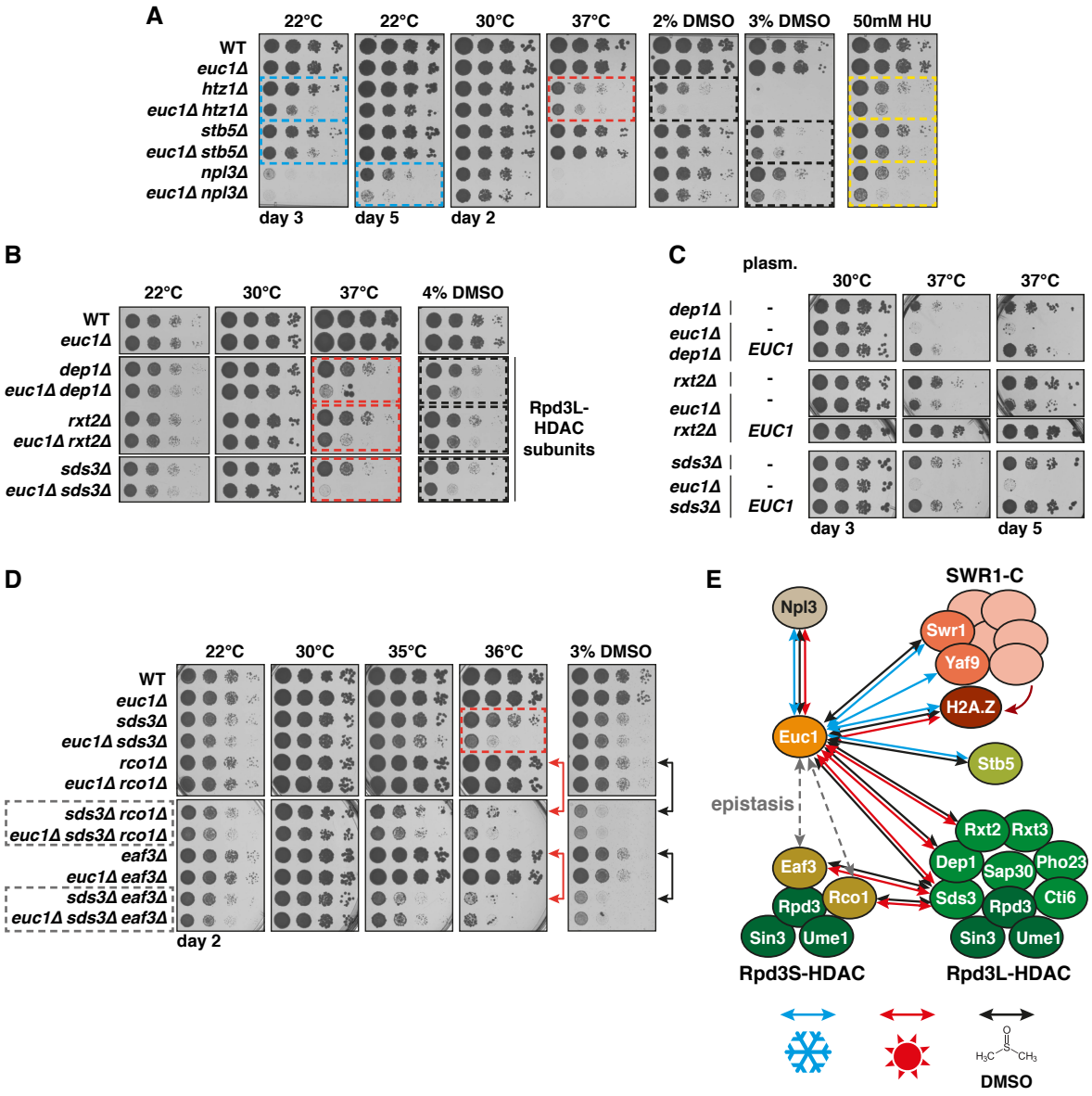

Figure 24. *EUC1* shows genetic interactions with regulators of gene expression upon thermostress and DMSO exposure.

(A–B) *EUC1* displays negative genetic interactions with genes involved in general and specific transcriptional regulation (A), and in particular with members of the Rpd3L histone deacetylase complex (B). For (A–D), serial dilutions of the indicated strains were spotted and grown on YPD control or selective media plates, or under conditions as indicated. Dashed boxes highlight genetic interactions with *EUC1*, color code as in (E). Note that all strains used in (A–D) contained an extra copy of *MED11*, see Fig. 21A and Appendix Fig. A6C–F for details.

(C) Plasmid-borne *EUC1* complements genetic interactions with Rpd3L subunits. Empty vector (-) or a plasmid encoding *EUC1* with its endogenous promoter were transformed in the indicated strains and spotted on selective media.

(D) *EUC1* and Rpd3S act in a common pathway which is redundant with Rpd3L. *rco1*Δ and *eaf3*Δ (Rpd3S) show similar phenotypes when paired with *sds3*Δ (Rpd3L complex, genetic interaction indicated by arrows) as *euc1*Δ (dashed box) and are epistatic with *euc1*Δ.

(E) Graphic summary of *EUC1* genetic interactions as tested in (A–D) and Appendix Fig. A6. Arrows indicate negative genetic interactions upon cold (blue), heat (red) or DMSO stress (black), dashed grey arrows indicate epistatic relationships.

Notably, mutant cells deleted for common Rpd3L and Rpd3S subunits (*rpd3*Δ*, sin3*Δ) showed strong heat and DMSO sensitivity, which was not further enhanced by *euc1*Δ (Appendix Fig. A6G–H). Similarly, no genetic interactions of *EUC1* were observed with Rpd3S-specific deletion strains (Fig. 24D, *rco1*Δ*, eaf3*Δ). Interestingly, when mutations for Rpd3S subunits (*rco1*Δ*, eaf3*Δ) were combined with Rpd3L mutations (*sds3*Δ), enhanced heat and DMSO sensitivity became apparent (Fig. 24D, red/black arrows), suggesting overlapping functions of the Rpd3L and Rpd3S complexes. Strikingly, these genetic interactions were reminiscent of *euc1*Δ *sds3*Δ phenotypes (Fig. 24D, red dashed box), and additional deletion of *EUC1* did not further enhance Rpd3L/Rpd3S combination phenotypes (Fig. 24D, labels highlighted with dashed grey boxes). This epistatic relationship between *EUC1* and Rpd3S places them in a common genetic pathway (Fig. 24D–E). Consistent with shared functions between *EUC1* and Rpd3S, significant correlations of gene sets downregulated in *euc1*Δ cells were identified not only with genes downregulated in published *rpd3*Δ transcriptome data, but also with genes downregulated in *set2*Δ datasets, which is an upstream regulator of H3K36 methylation and the Rpd3S pathway (Appendix Fig. A7)[4] (McKnight *et al*, 2015; McDaniel *et al*, 2017). Overall, I therefore conclude that Euc1 works in a common pathway with Rpd3S that counteracts cellular stress induced by exposure to heat or DMSO.

3.9 Euc1-mediated Ub-hotspots are Crucial during Stress Responses when Gene Expression Control is Impaired

To substantiate a possible role of Euc1 in the response to heat stress, I performed Euc1 and ub-K48 ChIP experiments in cells shifted from 30°C (control) to 37°C (mild heat stress) and detected a significant increase of Euc1 binding to ub-hotspots, especially in *sds3*Δ cells (Fig. 25, left panel, Appendix Fig. A8A). In contrast, ubiquitin signals were reduced at 37°C, but this effect was also observed for an Euc1-independent ubiquitin-bound region (ub-only-site1), possibly because free ubiquitin becomes limiting at higher temperatures (Fig. 25A, right panel) (Finley *et al*, 1987).

Noteworthy, Euc1 recruitment to ub-hotspots was also significantly increased in *sds3*Δ cells compared to WT cells at 37°C (Fig. 25, left panel). Similar effects were observed for *htz1*Δ cells, and for *npl3*Δ cells at 25°C (Appendix Fig. A8B–D). Together, this indicates that Euc1 occupancy at ub-hotspots is increased in conditions or genetic backgrounds where its function becomes critical (Fig. 24). Although ubiquitin levels

[4] Data analysis performed by Tobias Straub, LMU/BMC, Munich

themselves did not show consistent changes under these conditions (Fig. 25, Appendix Fig. A8), these data support a model whereby Euc1 serves a role in gene expression control or chromatin maintenance. This function becomes critical upon exposure to thermo- and other stress conditions, in particular when other factors controlling gene expression are impaired.

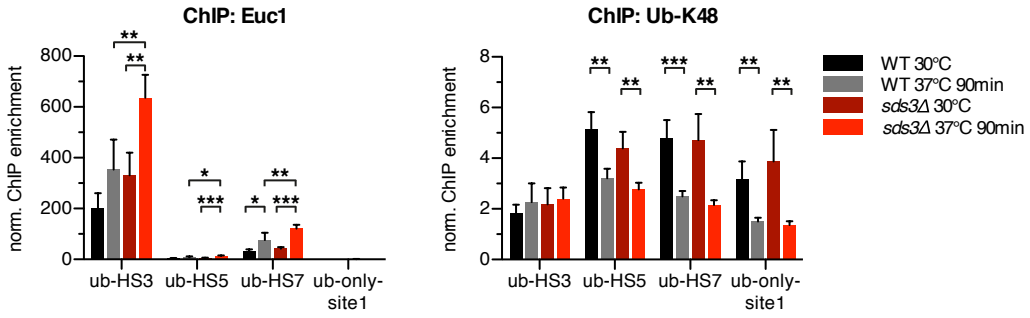

Figure 25. Euc1 is recruited to ub-hotspots upon mild heat stress in *sds3*Δ cells.
ChIP-qPCR experiments for Euc1 and ub-K48 with strains and conditions as indicated. For mild heat stress, cells were grown at 30°C to mid-log phase and shifted to 37°C for 90 minutes. Data represent means ± SD (n = 4). For statistical analysis an unpaired, two-tailed Student's t-test was performed, see Appendix Fig. A8A for detailed results. (*): $p \leq 0.05$, (**): $p \leq 0.01$, (***): $p \leq 0.001$.

Therefore, I tested which features of Euc1 would be required for rescuing the observed genetic interaction phenotypes of *euc1*Δ cells using a plasmid-based complementation approach. Interestingly, the ability of the *EUC1* alleles to alleviate the heat and DMSO sensitivity of *euc1*Δ *sds3*Δ or *euc1*Δ *npl3*Δ cells fully depended on the ability to restore ub-hotspots, but not on the N-terminal transactivation domain: ub-hotspot proficient WT *EUC1* and *euc1-N30*Δ restored growth, but not the ub-hotspot deficient *KR, SBM1+2, KR-SBM1+2, DBD** and *CC*Δ alleles (Fig. 26A, Appendix Fig. A9A–B). Furthermore, I found that abolishing ub-hotspots by deletion of *SLX5* or *SLX8* enhanced *sds3*Δ heat sensitivity as well (Fig. 26B, red dashed box, Appendix Fig. S12C). Deletion of *EUC1* did not further exacerbate these phenotypes, and these genetic interactions are most likely dependent on ub-hotspot function, since they could be alleviated by plasmid-borne expression of WT *SLX5*, but not by *slx5-SIM**, and only to a minor extent by *slx5-Md*Δ (Fig. 26C).

In conclusion, Euc1 and Slx5/Slx8-dependent ub-hotspots are critical for thermotolerance and the response to other stresses, and Euc1 is functionally linked to chromatin regulation by the Rpd3S HDAC complex. Overall, my data support a model that places *EUC1* and *SLX5/SLX8* together with Rpd3S in a common genetic pathway, which acts redundantly with the Rpd3L complex.

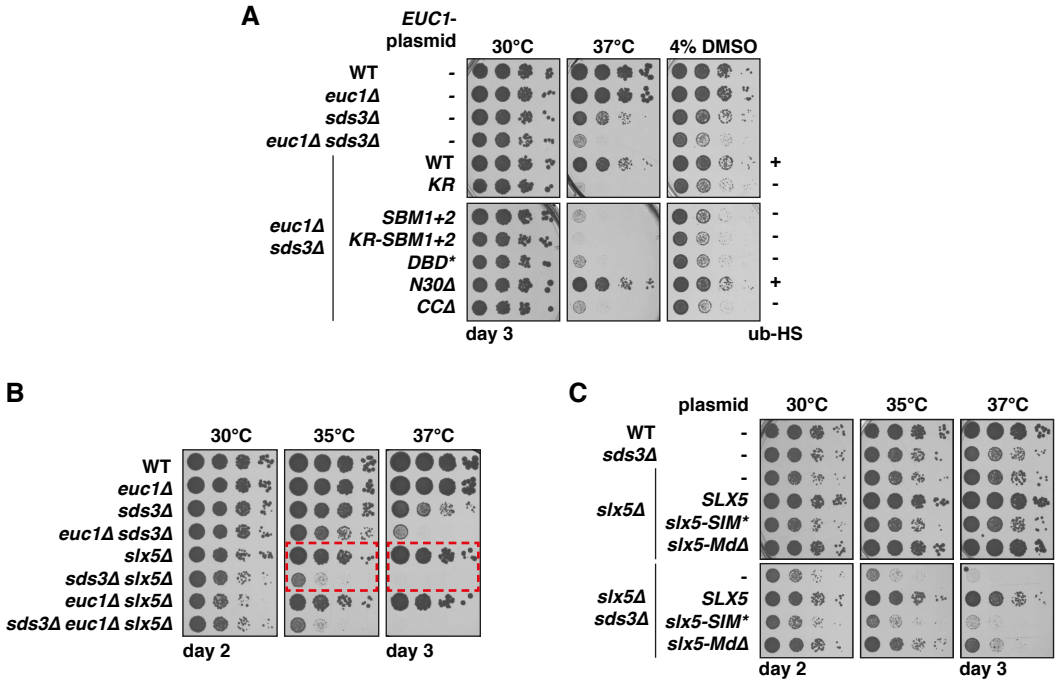

Figure 26. The ub-hotspot pathway is required to complement genetic interactions of *EUC1*.
(A) The ability to form ub-hotspots is crucial for endogenous *EUC1* function. The genetic interaction of *EUC1* with *SDS3* (Rpd3L complex) was rescued with plasmid-borne *EUC1* alleles and serial dilutions were spotted on selective media. (-) denotes empty vector. See also Appendix Fig. A9A–B.
(B) *SLX5* shows negative genetic interactions with *SDS3* upon heat stress. Serial dilutions of the indicated strains were spotted on YPD and incubated as indicated, dashed boxes highlight the *sds3*Δ *slx5*Δ synthetic sickness in this case. See also Appendix Fig. A9C.
(C) The Slx5-SIMs and Slx5-Md are required for full complementation of *slx5*Δ *sds3*Δ phenotypes. Strains were transformed with plasmids expressing *SLX5* alleles under control of the endogenous promoter and spotted on selective media and grown as indicated. Note that all strains used in (A–C) contained an extra copy of *MED11*, see Fig. 21A and Appendix Fig. A6C–F for details.

4 Discussion

4.1 An Euc1- and Slx5/Slx8-dependent Pathway Controls Protein Turnover at Ub-hotspots

Protein–DNA transactions and chromatin composition underlie extensive regulation by various mechanisms, including post-translational protein modifications, and global as well as local turnover of chromatin proteins. Removal or degradation of proteins is typically achieved by the ubiquitin–proteasome system and within this framework, the Cdc48/p97 segregase and STUbLs take key positions, as evidenced by the identification of numerous critical substrates over the last years (Ramadan *et al*, 2007; Wilcox & Laney, 2009; Maric *et al*, 2014; Ndoja *et al*, 2014; Franz *et al*, 2016; Nie & Boddy, 2016). By profiling the genome-wide binding landscape of ubiquitin, Slx8 and Euc1, I could extend the understanding of the complex mechanism at work at ub-hotspots. Furthermore, my data demonstrate that ub-hotspots are not only major enrichment sites for ubiquitin on budding yeast chromosomes, but also for Slx8 and Euc1, and genetic analysis established important connections between these factors and cellular physiology related to environmental stress adaptation.

Together with data from a previous PhD project that originally identified the ub-hotspots (Kern, 2013), a refined picture of the cascade of events at ub-hotspots emerges (summarized in Fig. 27, (Höpfler *et al*, 2019)): (1) Euc1 binds to the ub-hotspot DNA motif via its GCR1 domain. (2) Euc1 is SUMOylated by Ubc9, Siz1 or Siz2, which supports Euc1 binding to DNA. (3) Slx5/Slx8 is recruited via multivalent interactions that rely on both direct Euc1–Slx5 contacts and SUMO–SIM interactions. (4) Slx5/Slx8 recruitment leads to ubiquitylation of Euc1, and likely other substrates at ub-hotspots. (5) Cdc48 in complex with Ufd1–Npl4, and assisted by the cofactors Ubx4 and Ubx5, segregates K48-linked ubiquitylated proteins from chromatin. After extraction, these ubiquitylated proteins could be handed over to the proteasome for degradation, as it is typical for proteins modified with K48-linked ubiquitin chains (Finley *et al*, 2012). Alternatively, deubiquitylation could facilitate substrate recycling, as it has been found for other DNA-binding proteins like TFs, even when marked with K48-linked ubiquitin chains (Inui *et al*, 2011; Flick *et al*, 2004).

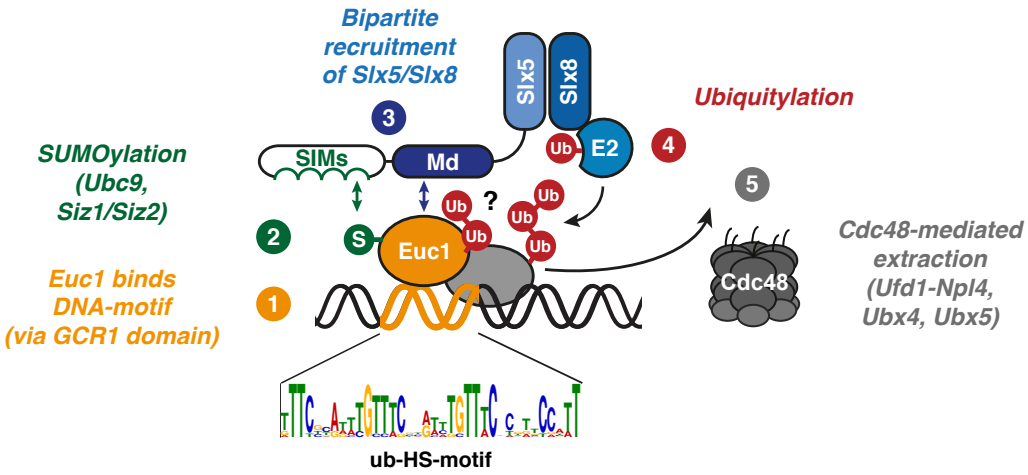

Figure 27. Refined model of the molecular mechanism of ub-hotspot formation.
See text for details. S: SUMO, Ub: ubiquitin, SIM: SUMO-interacting motif. Figure modified from (Kern, 2013).

Of note, while the described mechanism (Fig. 27) applies for all seven ub-hotspots, there are strong variations regarding the relative amounts of bound Euc1, Slx5/Slx8 and ubiquitylated proteins between individual ub-hotspots. Signals for Euc1 and Slx5/Slx8 seem to correlate well, consistent with direct STUbL recruitment by Euc1 (Fig. 17), but ubiquitylation signals deviate from that pattern (Fig. 11D). This discrepancy could be due to variable ubiquitylation efficiencies, or due to alternative complexes forming with accessory proteins or ubiquitylation substrates at the different sites. Of note, Euc1 might not be the main ubiquitylaton substrate, as it is a rather stable protein and does not seem to underlie strong STUbL-dependent turnover, nor does it accumulate in *cdc48* mutants at ub-hotspots or on total protein level (Fig. 11). Despite extensive efforts to identify ubiquitylation substrates at ub-hotspots other than Euc1, including mass spectrometry based proteomics approaches and a Y2H screen designed to identify physical Euc1 interactors, it remains enigmatic whether other proteins are bound at ub-hotspots.

If so, these proteins are likely to be targets of Slx5/Slx8-dependent ubiquitylation and subsequent Cdc48-mediated extraction. In line with this "*in trans* ubiquitylation" model, other studies have found that Slx5/Slx8 and other STUbLs can target binding partners of SUMOylated proteins (Abed *et al*, 2011a; Schweiggert *et al*, 2016). Notably, following this "*in trans* ubiquitylation" model, ubiquitylation substrates might not necessarily be the same for all ub-hotspots. Euc1 is ubiquitylated by Slx5/Slx8, but if Euc1 were not the primary Slx5/Slx8 target, a role for Euc1 as an Slx5/Slx8-recruitment factor or cofactor for ubiquitylation of a specific subset of target proteins would also be consistent with this model.

Overall, the ub-hotspot pathway exemplifies a complex pathway where the SUMO and ubiquitin pathways converge on chromatin to control protein abundance at highly specific loci in the yeast genome. As discussed in the following sections, open questions remain, especially regarding the exact molecular mechanism by which Euc1 exerts its functions in stress adaptation, opening up new research questions. Importantly, this work provides rich insight into a novel STUbL-recruitment mechanism, and is likely to contribute to a better understanding of STUbL specificity in general.

4.2 High Local Enrichment of Ub-hotspot Factors at Seven Genomic Sites

Two particular features seem to distinguish the ub-hotspots most from previously published chromatin binding events of UBLs or UPS components: First, the remarkably low number of ub-hotspots; and second, the specific and high local enrichment of ubiquitin and other ub-hotspot factors. In this section, I will discuss the potential reasons for such highly localized signals, and I will compare ub-hotspots with data from the literature on genome-wide binding studies of UPS components and UBLs

During the initial characterization of ub-hotspots, hundreds of regions with local enrichment of ubiquitin had been identified with a ubiquitin antibody (clone FK2) that recognizes a wide range of ubiquitin conjugates (mono-ubiquitylation, K29-, K48-, K63-linked chains), most of which could be attributed to histone H2B ubiquitylation (Kern, 2013). Some of the ub-hotspots stood out in WT cells, but the seven ub-hotspots, along with the two ub-only-sites (Fig. 6–7), showed a dramatic increase of ubiquitin signal in *cdc48* mutant cells, while other ubiquitin peaks were lost or diminished. This effect might be due to overall lower H2B ubiquitylation levels in *cdc48* mutant cells (Kern, 2013), or due to the depletion of free ubiquitin in *cdc48* mutant cells. Surprisingly however, these results also demonstrated that ub-hotspots seem to be the major sites of Cdc48-dependent extraction of ubiquitin conjugates from chromatin in yeast, although several other proteins were described to rely on Cdc48 for extraction from chromatin (Wilcox & Laney, 2009; Verma *et al*, 2011; Maric *et al*, 2014).

What could be the reasons for the prominent appearance of ub-hotspots in ChIP-chip profiles over other protein turnover events on chromatin? In part, this phenomenon can be explained by the apparent constant presence of ubiquitylated proteins at ub-hotspots in normal growth conditions and throughout the cell cycle (data not shown). Additionally, the ChIP-chip methodology has certain constraints in its resolution, and the necessary

PCR-based amplification steps could potentially introduce biases during sample preparation with regards to signal intensity readouts. State-of-the-art ChIP-seq techniques could provide a more differentiated picture.

Moreover, several known chromatin-bound Cdc48 substrates might not lead to highly localized ubiquitin signals, because they do not bind DNA in a sequence-specific manner. Prominent examples include RNA Pol II, which is extracted upon transcriptional stalling at DNA lesions, or Mcm7 that is removed to disassemble the replicative helicase after termination (Verma *et al*, 2011; Maric *et al*, 2014). Cdc48-dependent extraction of sequence-specific TFs has been described for a model TF and Matα2, however, in the latter case extraction of Matα2 was specifically triggered by changing growth conditions (Wilcox & Laney, 2009; Ndoja *et al*, 2014). The low number of ubiquitin peaks in the *cdc48-3* ChIP-chip data does not suggest a widespread function for Cdc48 in extraction of TFs from chromatin, though. In contrast, many TFs appear be removed from DNA directly by the proteasome ((Auld *et al*, 2006), see below). Hence, it seems reasonable to speculate that ub-hotspots do not mark TF turnover sites, but might represent a genomic region with particular chromatin composition or a specific chromatin domain (see section 4.5.2).

4.2.1 Ub-hotspots Compared to Genome-wide UPS-component- and UBL-binding Studies

Cdc48-dependent turnover of proteins from chromatin has not been investigated on a genome-wide level by other laboratories so far. Other studies addressing protein turnover on chromatin in human cells have reported over 33,000 ubiquitin peaks in control conditions, and over 46,000 peaks upon proteasome inhibition, indicating thousands of sites of active protein turnover (Catic *et al*, 2013). Most of the sites overlapped with promoter regions, and transcription start or termination sites, which is in agreement with other studies showing that transcriptional regulators often underlie rapid turnover (Schwanhäusser *et al*, 2011). Although the identity of the ubiquitylated proteins remained largely elusive, one study specifically identified the transcriptional corepressor NCoR1 as ubiquitylation substrate (Catic *et al*, 2013). In line with widespread proteasomal turnover of transcriptional regulators also in yeast, genome-wide binding profiles of proteasome subunits identified several hundred peaks, which largely correlated with highly transcribed ORFs and their regulatory regions (Auld *et al*, 2006).

Similar to ubiquitin, SUMO ChIP experiments identified numerous peaks in yeast (670), and from 13,000 up to 46,000 peaks in human cells, depending on the experimental

conditions and setup (Neyret-Kahn *et al*, 2013; Seifert *et al*, 2015; Niskanen *et al*, 2015; Chymkowitch *et al*, 2015b). Although the effect of SUMO on transcription rates seems context dependent, these studies largely agree in that SUMOylated proteins predominantly also bind in gene regulatory and intergenic regions. In particular, binding of RNA Pol III-dependent tRNA gene promoters seems to be conserved between yeast and human cells (Chymkowitch *et al*, 2015b; Neyret-Kahn *et al*, 2013).

Previous ChIP experiments for Slx5 and Slx8 did not identify specific binding regions other than centromeres for Slx5, however, these results might be influenced due to the use of a non-functional Slx5 allele in that study (van de Pasch *et al*, 2013). Highly localized signals for Slx5/Slx8 are somewhat unexpected, as the STUbL most likely does not directly bind DNA at specific sequences and ubiquitin ligases often modify their substrates in a touch-and-go fashion. This could also explain why Slx5/Slx8 is not enriched at the 670 SUMO peaks, of which only 3 overlap with ub-hotspots. At ub-hotspots, the apparent presence of a relatively stable Euc1–SUMO–Slx5/Slx8 complex is probably responsible for the remarkably specific signals for Slx5/Slx8. Taken together, both the low number of ubiquitin peaks in *cdc48* mutant cells and the almost exclusive localization of Slx8 (and presumably Slx5) to ub-hotspots are surprising findings.

4.3 Specificity in the STUbL Pathway is Achieved by Multivalent Substrate–Ligase Contacts

STUbL recruitment is thought to primarily rely on recognition of polySUMO chains by multiple SIMs, however, how STUbLs select their substrates amongst abundant SUMOylated proteins in the nucleus remains largely enigmatic. So far, all currently known Slx5/Slx8 substrates require Slx5-SIMs for ubiquitylation, and in the majority of cases substrate SUMOylation is indeed a prerequisite for recognition. A notable exception to the latter rule is Matα2: Here, Matα2 DNA binding and Slx5-SIMs are required for its STUbL-dependent ubiquitylation, but not SUMOylation (Xie *et al*, 2010; Hickey *et al*, 2018). The authors speculated that Slx5-SIMs could interact with hydrophobic Matα2 features (Xie *et al*, 2010).

Interestingly, although the primary sequence and domain organization of the mammalian STUbLs RNF4 and Arkadia (RNF111) are only distantly related to Slx5 and Slx8 (Fig. 4), both enzymes (or variants thereof) can complement certain phenotypes observed for *slx5*Δ and *slx8*Δ cells: In particular, the accumulation of high molecular weight conjugates and the typical sensitivity to hydroxyurea-induced replication stress can

be alleviated by the mammalian homologs (Uzunova *et al*, 2007; Prudden *et al*, 2007; Sun *et al*, 2007; 2014). In both cases, complementation strictly requires multiple SIMs within the heterologous ligase. Hence, complementation might depend primarily on a "polySUMO–SIM interaction mode" for recognition of yeast substrates, rather than specific substrate interactions.

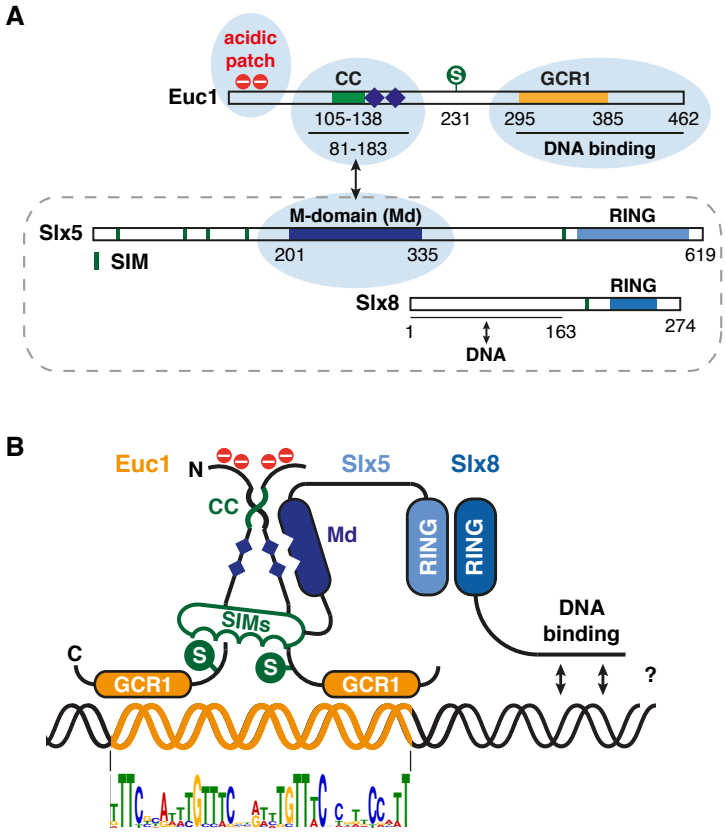

Figure 28. Bipartite recognition of Euc1 by Slx5/Slx8.
(A) Schematic domain structures of Euc1, Slx5 and Slx8 with features highlighted. Light blue shading highlights domains characterized in this study.
(B) Close-up view of a model for Slx5/Slx8 recruitment to ub-hotspots by Euc1. Two Euc1 molecules might bind to the repetitive ub-HS-motif (orange DNA) via their GCR1 domains (orange) and dimerize via the coiled-coil (CC) domains (black/green). Besides SUMO, Slx5 recognizes interaction surfaces close to the dimerization site (blue diamonds) via its middle domain (Md). Slx5 and Slx8 likely dimerize via their ring domains, as previously demonstrated for other RING ligases (Plechanovová *et al*, 2011; 2012). All components are required for formation of a stable Euc1–SUMO–Slx5/Slx8 complex. Slx8 DNA binding might contribute to recruitment and stability (Yang *et al*, 2006).

Interestingly, RNF4 and Arkadia were unable to complement ub-hotspot formation in *slx5*Δ cells, even when fused to the Slx5-Md (not shown). Moreover, for Euc1 there is currently no evidence for modification with long polySUMO chains (Fig. 9B, 13A). Therefore, it is unlikely that such a "polySUMO–SIM interaction mode" is sufficient for recognition of Euc1. In contrast, my data suggest that in addition to a SUMO–SIM interaction, direct contacts between the Slx5-Md and Euc1 are required for Slx5/Slx8 recruitment and ubiquitylation of Euc1, and possibly other substrates at ub-hotspots. For

such a “bipartite recognition mode” (Höpfler *et al*, 2019), multiple interactions likely provide the required affinity/avidity for accurate recognition specifically of SUMOylated Euc1 (Fig. 28). Such bipartite recognition would not be without precedent, as SUMOylation had previously been described to allow specific recognition of modified binding partners in other contexts, e.g. the selective recruitment of the Srs2 helicase by SUMOylated PCNA (Pfander *et al*, 2005; Papouli *et al*, 2005; Armstrong *et al*, 2012).

Even within the STUbL protein family, bipartite substrate recognition might be the rule, rather than the exception: For RNF4, a basic patch enables interactions with nucleosomes to allow recognition of chromatin bound SUMOylated proteins (Groocock *et al*, 2014), and recognition of phosphorylated substrates is facilitated by an arginine-rich motif (Kuo *et al*, 2014; Thomas *et al*, 2016). Arkadia relies on its Mn/Mc domains comprising a His-rich motif for proper localization to Polycomb bodies and its role in transcriptional regulation of the TGFβ-pathway, which additionally requires SIMs (Sun *et al*, 2014). Drosophila Degringolade/Dgrn interacts with the transcriptional repressor Hairy via its RING domain, and its SIMs simultaneously interact with the SUMOylated transcriptional corepressor Gro. Ultimately, this mechanism leads to ubiquitylation of Hairy to break up the Hairy–Gro complex and allow corepressor exchange (Abed *et al*, 2011a; 2011b). For Slx5/Slx8, Euc1 represents the first example of bipartite substrate recognition and the insights gained in this study might serve as a guide for future research investigating the manifold functions of STUbLs in the DNA damage response, oncogene degradation, and early embryonic development.

4.4 Euc1 and Ub-hotspots Function in Tolerance to Cellular Stress

What could be the cellular function of Euc1 and ub-hotspots? My phenotypic characterization of *EUC1* genetic interactions highlight synthetic growth defects with factors attributed to gene expression control and chromatin maintenance, in particular upon exposure to thermostress (heat/cold) and DMSO (Fig. 24, Fig. 29). Previous studies have established functions in stress adaptation for several of these factors, including the H2A.Z–SWR1-C axis, *NPL3*, *STB5* and the Rpd3L complex, primarily through their roles in gene expression control (de Nadal *et al*, 2004; Ruiz-Roig *et al*, 2010; Gaytán *et al*, 2013; Moehle *et al*, 2012; Kumar & Wigge, 2010). Notably, epistasis analysis revealed that *EUC1* acts in a common pathway with Rpd3S with regards to genetic interactions with the Rpd3L complex (Fig. 24D and Fig. 29). Both complexes form around the catalytic HDAC

subunit Rpd3, of which HDAC1 family enzymes represent homologs in higher eukaryotes (Carrozza *et al*, 2005; Yang & Seto, 2008). Histone deacetylation by Rpd3 typically serves repressive functions, but some heat- or osmo-stress-responsive genes have also been shown to be activated by Rpd3, in particular by the Rpd3L complex (de Nadal *et al*, 2004; Ruiz-Roig *et al*, 2010). In contrast, Rpd3S has its main function in the prevention of aberrant intragenic transcription initiation (Carrozza *et al*, 2005). Mechanistically, Set2 methylates histone H3K36 cotranscriptionally, which signals recruitment of the Rpd3S complex to deacetylate histone H4 and maintain a repressed state after transcription (Carrozza *et al*, 2005). Interestingly, it has recently been demonstrated that Rpd3S-controlled non-coding cryptic transcripts can also regulate the promoters of protein-coding genes, establishing a role for Rpd3S in gene expression control during adaptation to changing nutrient conditions and in aged cells (Sen *et al*, 2015; Kim *et al*, 2016; McDaniel *et al*, 2017).

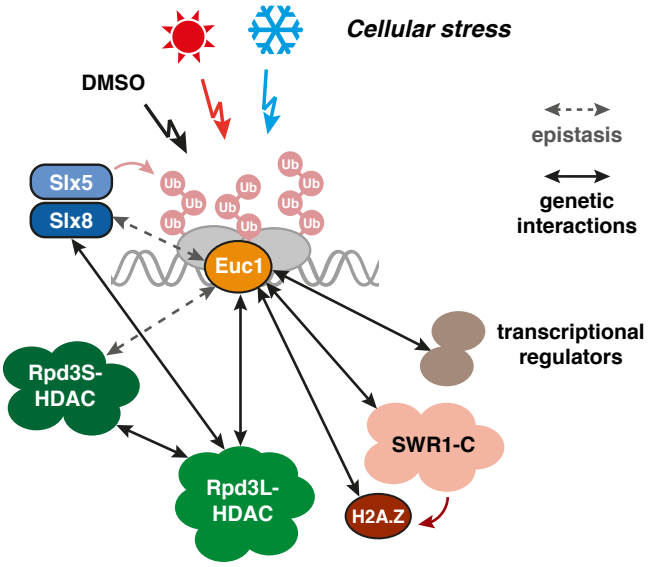

Figure 29. Summary model of genetic interactions of *EUC1* and the ub-hotspot pathway.
Arrows indicated genetic interactions of Euc1, dashed arrows highlight epistatic relationships between Euc1 and Rpd3S or Euc1 and Slx5/Slx8 with regards to genetic interactions with Rpd3L components. See main text for details.

While the precise mechanism by which Euc1 exerts its function in cellular stress responses as part of an Rpd3S-dependent pathway remains a subject of speculation (see below), my data provide cues to guide future research: Transcriptome analysis revealed widespread alterations in *euc1*Δ cells and upon *EUC1* overexpression. Particularly interesting, *RCO1* of the Rpd3S complex was upregulated, and *SIR2*, an HDAC of the sirtuin family, was downregulated in *euc1*Δ cells, which might underlie certain phenotypes or reflect adaptations. Noteworthy, *HSP12*, which gets activated by Rpd3 upon osmotic

stress (de Nadal *et al*, 2004), showed opposing expression changes upon *EUC1* deletion (downregulated) and overexpression (upregulated). Hsp12 binds and stabilizes the plasma membrane and is induced in various stress conditions, including osmotic, heat, and oxidative stress (Welker *et al*, 2010). Compromised membrane organization could also provide a link to the observed phenotypes of *EUC1*-overexpressing cells upon heat and benzyl alcohol exposure, a drug that is known to impair cellular membrane integrity (Lone *et al*, 2015). On the other hand, DMSO enhances several genetic interactions of *euc1*Δ cells, and it has been described that DMSO modulates membrane structure (Gurtovenko & Anwar, 2007). Moreover, mutants in the H2A.Z–Swr1-C axis are hypersensitive to DMSO treatment (Gaytán *et al*, 2013; Zhang *et al*, 2013). Interestingly, DMSO also acts as a weak inhibitor of HDACs (reviewed in (Marks & Breslow, 2007)), which could lead to an exacerbation of phenotypes in mutants with partially compromised gene expression control.

Taken together, a reasonable interpretation of the genetic and transcriptome data could be as follows: Full adaptation to cellular stress conditions like thermo- and DMSO stress relies on several redundant regulatory pathways, one of them being mediated by Euc1, the ub-hotspots and the Rpd3S complex. If other gene expression control systems fail (Rpd3L, H2A.Z–SWR1-C), the ub-hotspot pathway becomes indispensable under these conditions.

4.5 Euc1 and Ub-hotspots in the Context of the Nucleus

Despite the physiological implications for the functions of ub-hotspots suggested by genetic experiments and a good understanding of the mechanism of ub-hotspot formation, it remains mysterious how Euc1 and ub-hotspots fulfill their functions. In this section, I aim to place the Euc1–ub-hotspot pathway in the cellular context of the yeast nucleus and will discuss functional similarities with other pathways. Although other hypotheses cannot be ruled out, two main concepts for Euc1 function deserve consideration based on the available data: First, Euc1 might act as a transcriptional regulator; second, Euc1 and ub-hotspots could be required to establish a specialized chromatin domain for regulatory purposes.

4.5.1 Euc1 as a Putative Transcription Factor

The domain structure of Euc1 (Fig. 28A) is reminiscent of several other GCR1 domain TFs, which in addition to the defining DNA-binding domain also feature transactivation and coiled-coil dimerization domains (Holland *et al*, 1987; Hohmann, 2002). Sequence

alignments suggested that Cbf2 is more distantly related (not shown). The three GCR1 domain TFs Gcr1, Hot1, and Msn1 all act as transcriptional regulators in the adaptation to various cellular stress conditions, like carbon source switches or in osmotic stress (reviewed in (Hohmann, 2002)). My data show that Euc1 can act as a transcriptional activator in reporter-gene assays as well (Fig. 20). However, there is only very limited evidence for a transcriptional regulation of ub-hotspot adjacent genes by Euc1 (Fig. 21). Transcriptome analysis showed that neither deletion of *EUC1,* nor overexpression of *EUC1*, nor expression of Euc1-KR leads to strong changes in expression of ub-hotspot adjacent genes. Notably, RNAseq with high read numbers also did not reveal strong effects on several annotated non-coding RNAs around ub-hotspots when DNA-binding deficient Euc1-DBD* was expressed (not shown). It remains possible that Euc1's role as transcription factor is only triggered upon a specific, currently elusive stimulus. Moreover, other regulators might be required for triggering transactivation at ub-hotspots, or compensatory mechanisms for misregulated *EUC1* could exist. Hypothetically, the ub-hotspot pathway, and in particular SUMOylation, might then act as negative regulators of Euc1-mediated transactivation, as suggested by reporter-gene assays (Fig. 30, see also Appendix Fig. A4A and D).

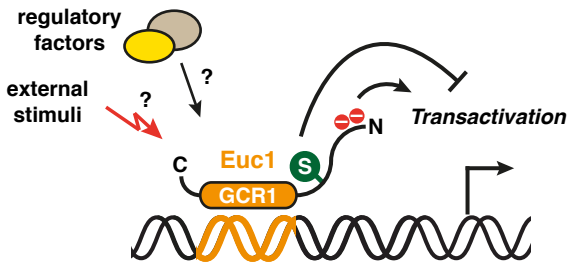

Figure 30. Schematic model of transactivation by Euc1.
In reporter-gene assays, the Euc1 N-terminus comprising an acidic patch can mediate transactivation, while SUMOylation (green) is inhibitory. At ub-hotspots, other factors or external stimuli might be required to activate transactivation. Orange: ub-HS motif/GCR1 domain.

In contrast to metazoan transcriptional regulation, upstream activating sequences or enhancers are usually found close to their target genes in *S. cerevisiae*, typically within several hundred base pairs (Dobi & Winston, 2007). Therefore, it appears unlikely that ub-hotspots act as enhancers for specific, distant genes *in trans*. Since the N-terminal transactivation domain is dispensable for complementation of *EUC1* genetic interactions, a model whereby Euc1 fulfills its major function as key component for the formation of ub-hotspots rather than as TF seems more plausible based on the available data.

4.5.2 Ub-hotspots as Specialized Chromatin Domains

As an alternative, and more complex model than direct transcriptional activation or repression by Euc1, it could be speculated that the ub-hotspots are required for gene expression regulation or chromatin maintenance through a more indirect mechanism. Hypothetically, ub-hotspots could represent a kind of specialized chromatin domain. To regulate and organize the genome, and to separate biochemical activities, several distinct compartments exist in the yeast nucleus, and many (but not all) basic principles are conserved in higher eukaryotes. The yeast interphase nucleus displays several prominent features, which can be visualized as nuclear subcompartments (Fig. 31A). These include centromeres clustered at the spindle pole body (SPB), telomere clusters, the nucleolus, tRNA gene clusters close to nucleoli, so-called "transcription factories" at NPCs, transient foci for DNA replication or repair (reviewed in (Taddei & Gasser, 2012), and the recently described intranuclear quality control compartment (INQ, (Gallina *et al*, 2015)).

Importantly, specific DNA sequences and DNA-binding proteins, or activities such as transcription, replication or other DNA transactions are often required for the formation of these compartments. Of note, several nuclear subcompartments underlie regulation by SUMO or STUbL-mediated ubiquitylation. Examples include the SUMO- and Slx5/Slx8-dependent control of the centromeric histone variant Cse4 upon mislocalization (Ohkuni *et al*, 2016; 2018; Cheng *et al*, 2017). At telomeres, tethering mechanisms are regulated by SUMOylation, and the second *S. cerevisiae* STUbL Uls1 controls unwanted NHEJ by preventing accumulation of polySUMOylated Rap1, a key binding factor of telomeric repeats (Lescasse *et al*, 2013). Within the nucleolus, the SUMO pathway and Slx5/Slx8 critically regulate DNA association of factors involved in rDNA transcription, including Net1 and Tof2 (Gillies *et al*, 2016; Liang *et al*, 2017). Furthermore, in the environmental stress response to ethanol, the SUMO isopeptidase Ulp1 was found to relocate from NPCs to the nucleolus, leading to changes in cellular SUMOylation (Sydorskyy *et al*, 2010). Related to tRNA gene transcription, SUMOylation targets several subunits of RNA Pol III, and their deSUMOylation upon nutrient depletion leads to decreased tRNA gene transcription (Chymkowitch *et al*, 2017). It remains unclear whether this mechanism is connected to the above-mentioned tRNA gene clusters, however. For some inducible RNA Pol II transcribed genes, it has been demonstrated that relocalization to the nuclear pore leads to derepression, which is facilitated by the deSUMOylation activity of the NPC-tethered Ulp1 on transcriptional corepressors (Texari *et al*, 2013). Also Slx5/Slx8 have been reported to localize to the nuclear pore by an interaction with the NPC protein Nup84

(Nagai *et al*, 2008). Interestingly, this localization seems to be important to target irreparable DNA double strand breaks to the NPC via recognition of SUMOylated proteins at the break site. This mechanism has been proposed to enable non-canonical repair pathways (Nagai *et al*, 2008; Horigome *et al*, 2016). SUMOylation and STUbLs also contribute to the regulation of nuclear subcompartments that are specific to mammalian cells, most prominently the SUMO-dependent formation of PML bodies, which also underlie the control of the STUbL RNF4 (Shen *et al*, 2006; Tatham *et al*, 2008).

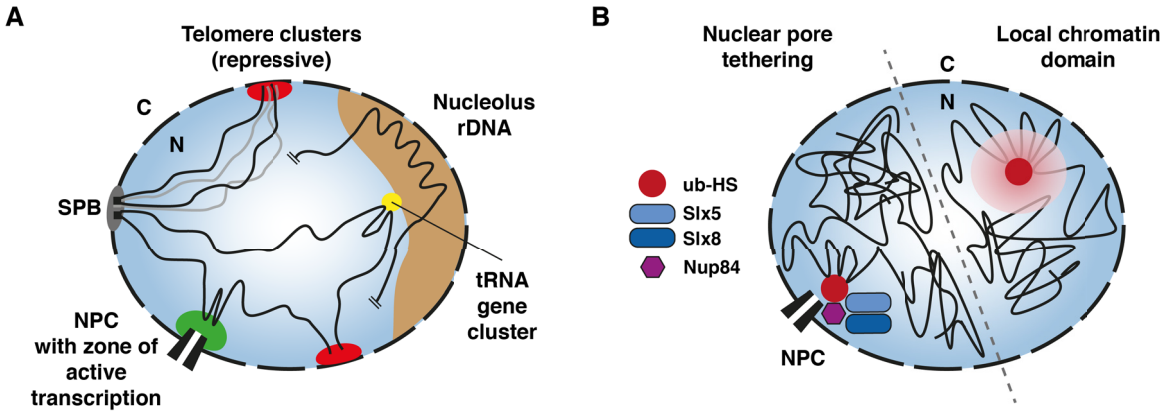

Figure 31. Ub-hotspots in the context of the yeast nucleus.
(A) Schematic drawing of the yeast interphase nucleus. In yeast, centromeres stay attached to short microtubules and the spindle pole body (SPB) throughout interphase, which leads to a permanent V-shaped Rabl conformation of chromosomes. Telomeres cluster into three to six foci at the nuclear envelope, where heterochromatin and a repressive environment are established (red). Opposite of the SPB, the nucleolus forms as a crescent-shaped body around the rDNA repeats (light brown). Many of the approximately 270 tRNA genes from all chromosomes cluster together in RNA Pol III transcription foci close to the nucleolus (yellow). For RNA Pol II-dependent genes, so-called "transcription factories" (green) can form for highly expressed or inducible genes around nuclear pore complexes (NPCs). Adapted from (Taddei & Gasser, 2012). N: nucleus, C: cytoplasm.
(B) Hypothetical representation of putative ub-hotspot chromatin domains. Left: Ub-hotspots could be tethered to the NPC by Slx5/Slx8 via an iteraction with Nup84 (Nagai *et al*, 2008). Right: ub-hotspots could form specific chromatin domains or nuclear territories that mediate specific functions or gene regulation *in trans*.

In the light of the widespread functions of SUMO and STUbLs in the regulation of nuclear subcompartments and their functions, it is attractive to speculate that Euc1-dependent ub-hotspots could localize to a specific subcompartment, or themselves define a discrete chromatin compartment or nuclear territory that mediates gene expression control on a more global level (Fig. 31B). Interestingly, deletion of *NUP84* leads to a loss of ub-hotspots, although it remains unclear whether this is related to a possible association of ub-hotspots with Slx5/Slx8 at NPCs or due to indirect effects (Kern, 2013). A microscopy-based approach to study the localization of ub-hotspots within the nucleus could benefit our further understanding of ub-hotspots. Although published chromosome conformation capture datasets did not reveal a physical association of all the ub-hotspot loci (Duan *et al*, 2010), it remains open whether ub-hotspots might cluster together under certain conditions,

or whether such a putative chromatin domain features epigenetic signatures other than the defining ubiquitylation marks.

4.6 Concluding Remarks

In this study, by investigating the previously poorly characterized yeast "ubiquitin hotspots", I was able to uncover a novel recruitment mechanism for the key yeast SUMO-targeted ubiquitin ligase Slx5/Slx8. The proposed "bipartite recognition mode" sheds light on how specificity might be achieved in the STUbL pathway in *S. cerevisiae*, with important implications for other STUbLs. Furthermore, my data identify not only Euc1 and the ub-hotspots, but also Slx5/Slx8 as part of a cellular stress response pathway that is required in particular in the context of impaired gene expression control. Unresolved questions remain regarding the exact molecular mechanism of ub-hotspot function, however, this study showcases a highly sophisticated mechanism where the SUMO and ubiquitin pathways are tightly interlinked to control ub-hotspots on chromatin. Collectively, my data add an intriguing new facet to the variegated functions of the SUMO and ubiquitin systems in cellular stress adaptation (Tempé *et al*, 2008; Enserink, 2015; Dikic, 2017).

5 Appendix Figures

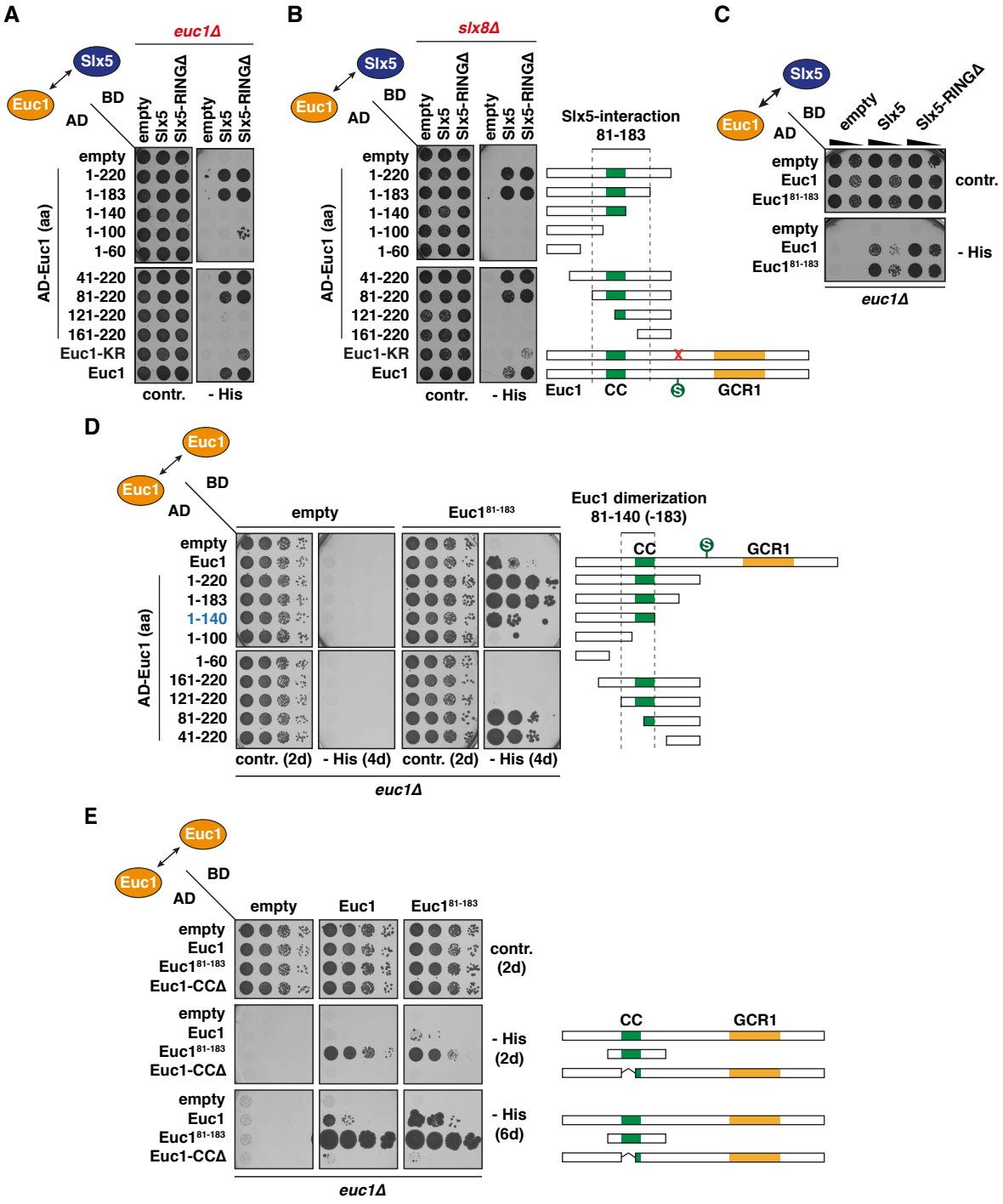

Appendix Figure A1, related to Fig. 13.
(A–B) Endogenous Euc1 and Slx8 are not required for the Euc1–Slx5 interaction in Y2H. Experiment was performed as in Fig. 13B in an *euc1*Δ (A) or an *slx8*Δ genetic background (B). Cells were grown at 30°C for 2 days (A) or 3 days (B).
(C) Euc1$^{81-183}$ is sufficient for Slx5 binding in Y2H assays. Y2H assay performed as in (A). Two dilutions were spotted for each plasmid combination and cells were grown at 30°C for 2 days.
(D) The minimal region of Euc1 required for dimerization maps to aa 81–140. Y2H assay to map the stretch required for dimerization of Euc1 around the CC domain. To avoid artifacts by interactions with endogenous Euc1, I used an *euc1*Δ strain. Note that the region between aa 140–183 likely also contributes to dimerization. Serial dilutions were spotted and cells were grown at 30°C for 2 (control) or 4 days (- His).
(E) The Euc1 CC domain is required for dimerization. Y2H assay to test the requirement for the Euc1 CC domain for dimerization. Euc1-CCΔ: Δaa 104–129. Serial dilutions were spotted and cells were grown at 30°C for 2 or 6 days as indicated.

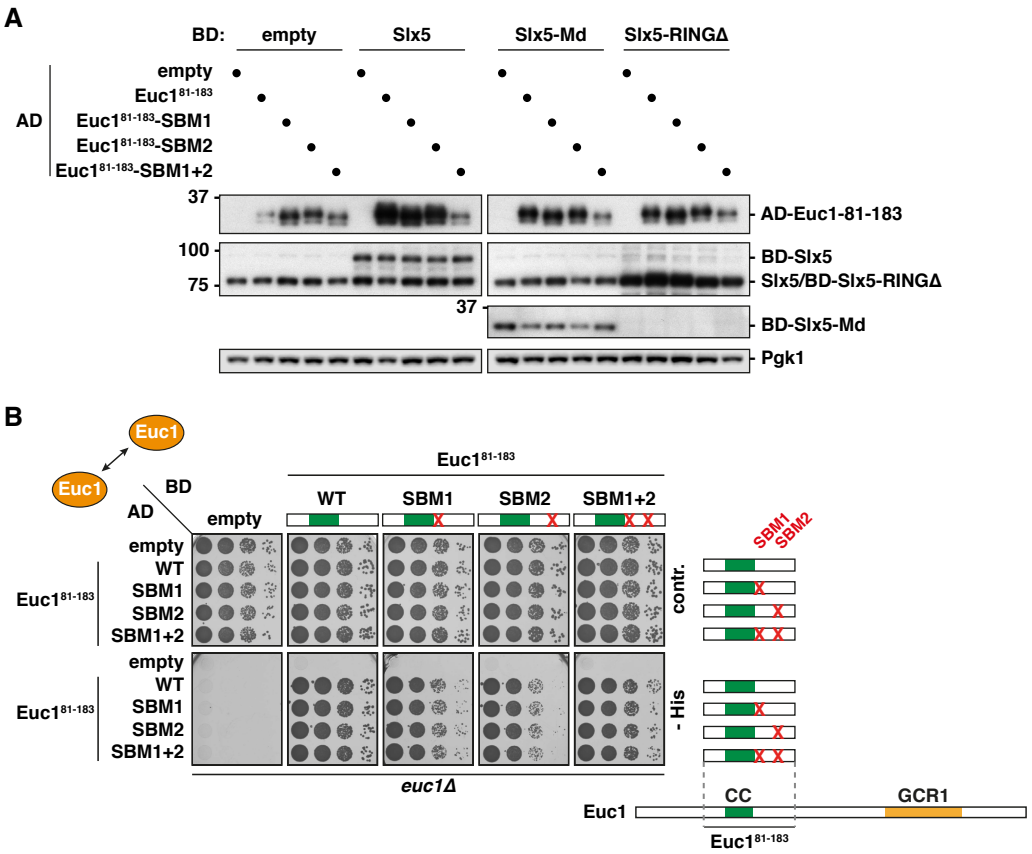

Appendix Figure A2, related to Fig. 14–15.
(A) Expression levels of the constructs expressed for Y2H assays in Fig. 14A and 15C analyzed by WB. AD-Euc1 constructs were probed with a Gal4-AD-specific antibody, BD-Slx5-constructs were probed with a polyclonal Slx5 antibody (raised against Slx5 aa 1–487). Note that for BD-Slx5-Md constructs levels cannot be directly compared with full length or Slx5-RINGΔ constructs, because the polyclonal Slx5 antibody might recognize more epitopes in the latter constructs. Pgk1 was probed to ensure equal amounts of cell material.
(B) Euc1-SBM1/2 constructs are proficient for dimerization. Y2H assay to test the effects of Slx5-binding site mutations on Euc1 dimerization.

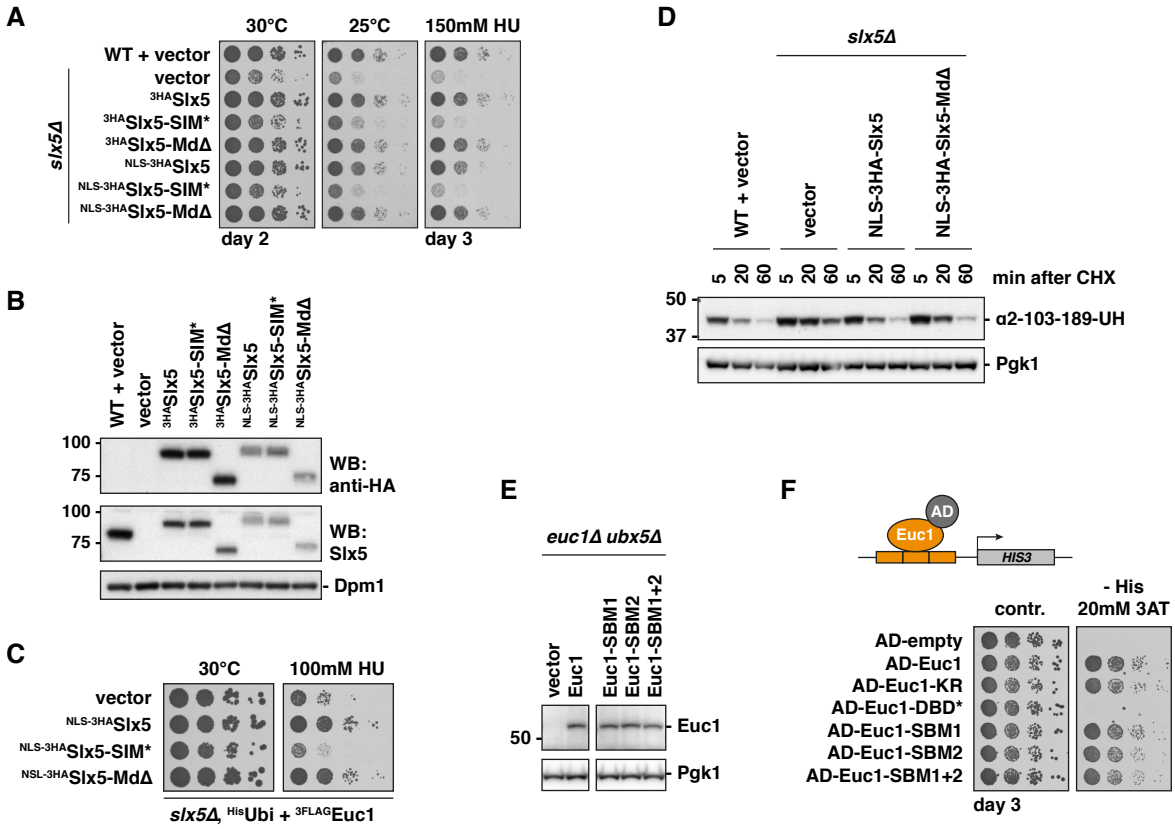

Appendix Figure A3, related to Fig. 16–17.
(A) The Slx5-Md is not required to rescue the *slx5*Δ replication stress phenotype caused by hydroxyurea (HU) or cold sensitivity. WT or *slx5*Δ cells were transformed with plasmids expressing the indicated constructs and spotted in serial dilutions. Cells were grown for 2 days (30°C, 25°C) or 3 days (150 mM HU at 30°C). Note that addition of an N-terminal NLS did not affect the complementation.
(B) Expression levels of Slx5 constructs in cells used in (A) probed by WB against the HA-tag (top), Slx5 (middle) and Dpm1 as loading control (bottom).
(C) HU-complementation assay as described in (A) for cells used in Fig. 16B.
(D) The Slx5-Md is dispensable for Matα2 degradation. Degradation of a Matα2 fragment (α2-103–189-UH (Ura3-3HA)) that has previously been shown to rely on Slx5 for rapid degradation (Hickey & Hochstrasser, 2015), has been monitored in CHX-chase experiments (0.5 mg/ml cycloheximide from t=0). An *slx5*Δ strain was complemented with the indicated constructs expressed from plasmids under the *SLX5* promoter. WB for α2-103–189-UH was probed with an HA antibody and Pgk1 levels are shown as loading control.
(E) Expression levels of Euc1 constructs in cells used in (E) and Fig. 6C–D probed by WB against Euc1. Pgk1 served as loading control. Sections were cropped from the same exposure.
(F) Euc1-SBM1/2 constructs bind the ub-HS-motif in Y1H assays. Gal4-AD fusions with the indicated constructs were used in a Y1H assay as described in Fig. 18B.

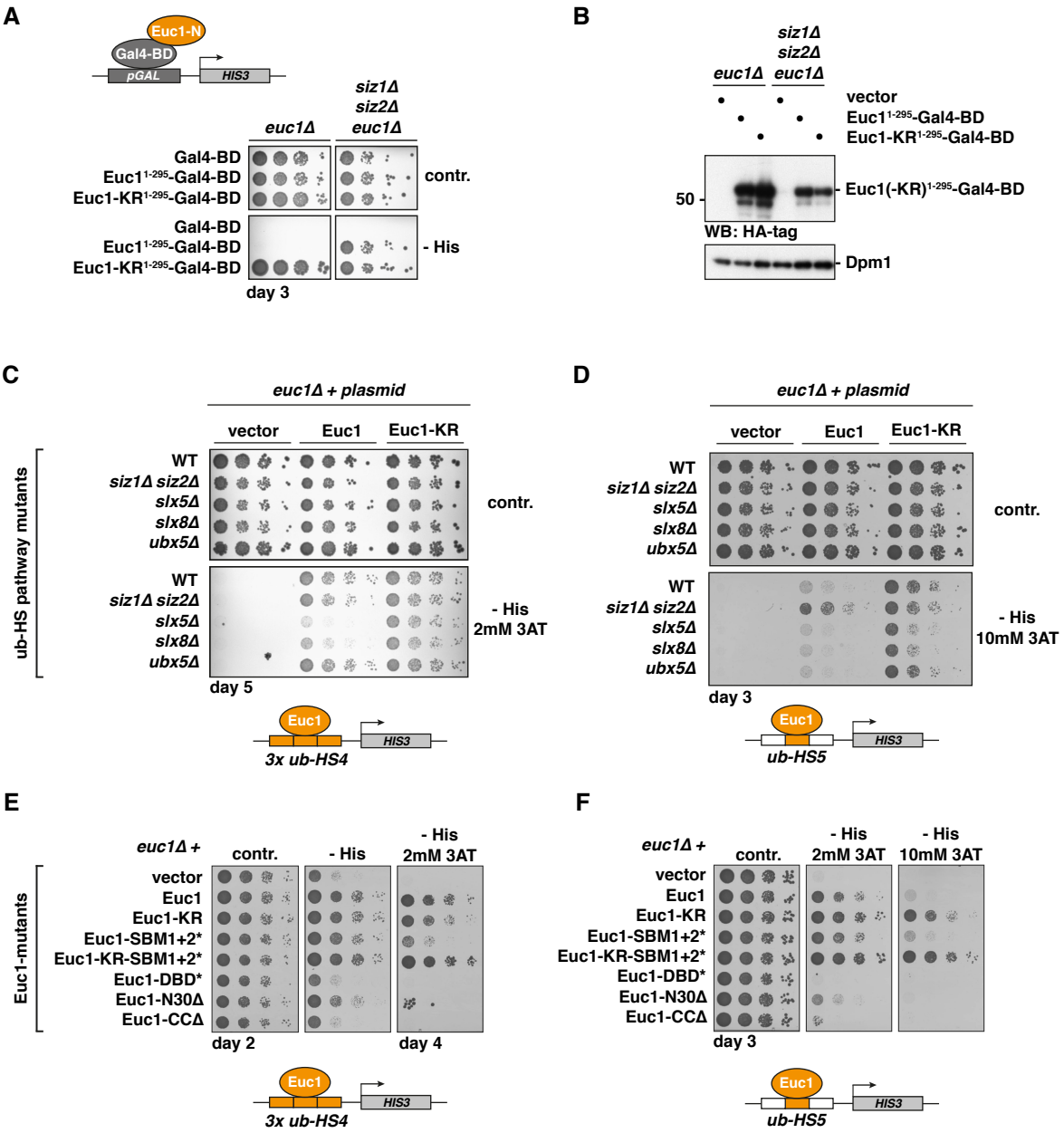

Appendix Figure A4, related to Fig. 21.
(A) SUMOylation controls TF activity of an Euc1$^{1\text{-}295}$-Gal4-BD hybrid construct. Euc1-Gal4-BD fusion constructs as described in 20D were expressed and *HIS3* activation was monitored. Data for Gal4-BD are reproduced from Fig. 20D for comparison.
(B) Expression levels of constructs used in (B) probed by an HA antibody that recognizes an internal HA tag upstream of Gal4-BD. Dpm1 served as loading control.
(C) Reporter-gene assays using the *3x ub-HS4-HIS3* reporter construct (scheme) in the indicated genetic backgrounds. All strains have *EUC1* deleted and were complemented with plasmids as indicated on the top.
(D) As in (C), but using a different reporter construct featuring *ub-HS5* with 100 bp genomic context flanking on both sides (scheme).
(E) The reporter strain used in (A), top row: "WT + *euc1*Δ", was transformed with plasmids expressing the indicated Euc1-constructs and transcriptional activation was tested by *HIS3* activation on selective media.
(F) As in (E), but with the *ub-HS5* reporter strain.
Note that for the *ub-HS5-HIS3* reporter construct transcriptional activation seems to be enhanced when SUMOylation is impaired (*siz1*Δ *siz2*Δ, Euc1-KR construct), comparable to (A). In contrast, SUMOylation does not affect activation of the *3x ub-HS4-HIS3* construct.

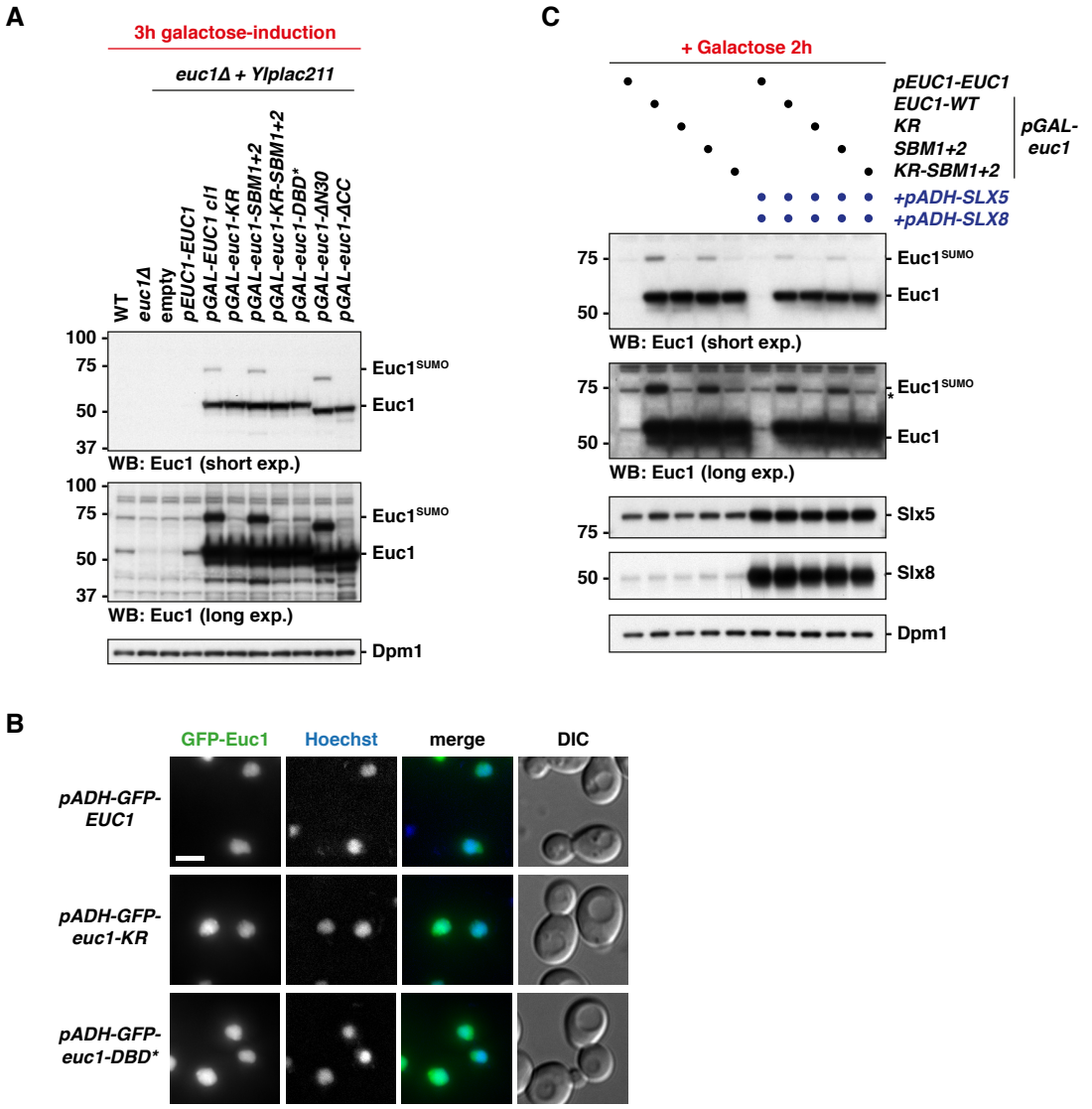

Appendix Figure A5, related to Fig. 22–23.
(A) WB of galactose-induced (3h) *euc1* alleles used in Fig. 22D.
(B) Microscopy of *pADH-GFP-EUC1* cells (or *euc1-KR*, *euc1-DBD**) showing similar nuclear localization of tagged Euc1 constructs. Cells were counterstained with Hoechst 33342 dye to visualize DNA and maximum Z-projections of images recorded on a GE Deltavision Elite are shown. The FIJI software was used for image processing. Scale bar 5µm.
(C) WB for strains used in Fig. 23C–D after 2h galactose induction.

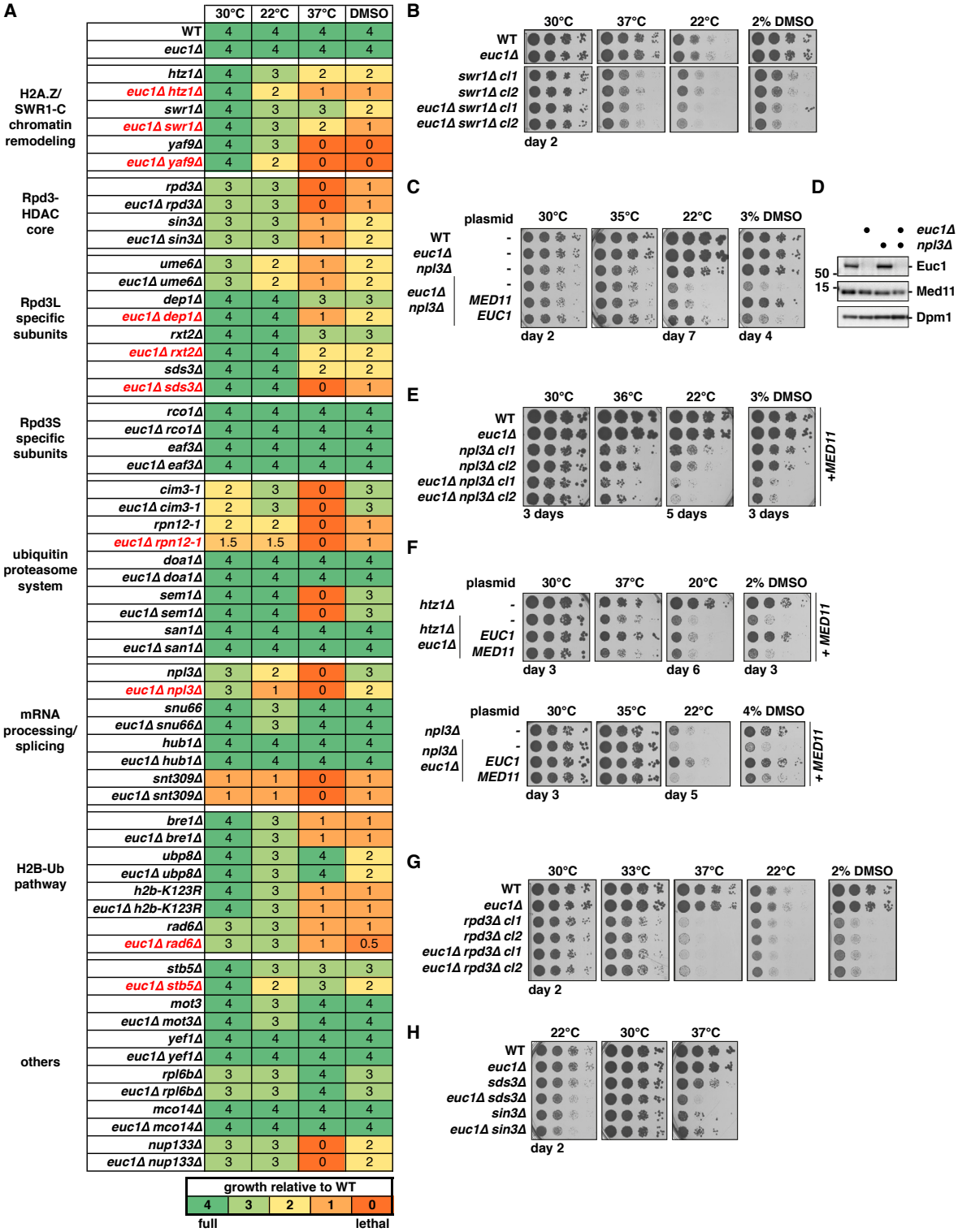

Appendix Figure A6, related to Fig. 24.

(A) Table summarizing genetic interactions manually tested in growth-based spotting assays as shown in Fig. 24A. Scores were given relative to WT growth in the respective conditions. For genetic interactions with *EUC1* (highlighted in red), at least two independent clones were tested. Note that all strains were generated from diploid strains via tetrad dissection and contained an extra copy of *MED11* (see C–F), except for *rpn12-1* strains.

(B) *EUC1* shows genetic interactions with *SWR1*. Spotting assay as described for Fig. 24A.

(C) Certain *euc1*Δ phenotypes can partially be rescued by introducing an extra copy of *MED11* (3% DMSO). Plasmid complementation with *EUC1* or *MED11* plasmids with their endogenous promoters as indicated. I noticed a mild downregulation of the RNA Pol II mediator component *MED11*, which is encoded by the ORF adjacent to *EUC1*, in the *euc1*Δ transcriptome data and on protein level ((D), Fig. 21A). Therefore, I introduced an extra copy of *MED11* at the *URA3* locus (YIplac211) for the genetic analysis. See also (D–F).

(D) Med11 protein levels are mildly reduced in *euc1*Δ *npl3*Δ cells. WB against Euc1, Med11 and Dpm1.

(E) *EUC1* and *NPL3* show genetic interactions also in the presence of an extra copy of *MED11*. Spotting assay as described in Fig. 24A.
(F) Plasmid-borne *EUC1* expression rescues *euc1*Δ phenotypes. Indicated strains were transformed with *EUC1* or *MED11* plasmids and grown on selective media.
(G–H) *EUC1* does not show genetic interactions with the Rpd3S/L core subunits *RPD3* and *SIN3*. Spotting assays as described in Fig. 24A. Note the stronger growth phenotypes of *rpd3*Δ and *sin3*Δ at elevated temperatures or on DMSO compared to *sds3*Δ.

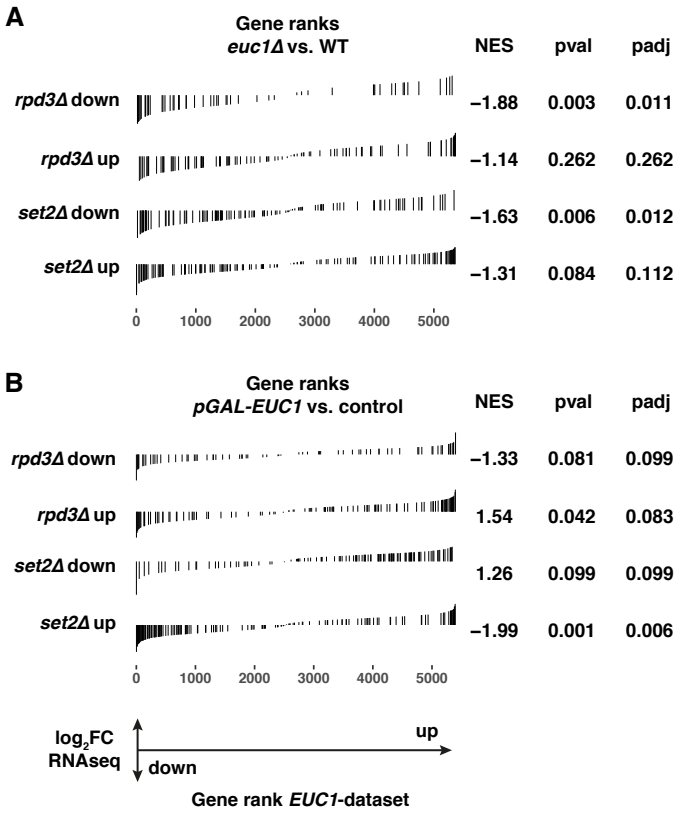

Appendix Figure A7, related to Fig. 21 and 24.
Genes deregulated in *euc1*Δ (A), see Fig. 21A, or upon *EUC1* overexpression (B), *pGAL-EUC1*, see Fig. 21C, show correlations with genes deregulated in published *rpd3*Δ and *set2*Δ transcriptomes. Genes up- or downregulated in the query datasets (*rpd3*Δ*, set2*Δ) were marked in the gene rank plots of *euc1*Δ or *pGAL-EUC1* datasets. NES: normalized enrichment score (negative values for a correlation with genes downregulated in *euc1*Δ*/pGAL-EUC1*, positive values for correlation with upregulated genes), padj: adjusted *p*-value. See Appendix Supplementary Methods for details. Data analysis was performed by Tobias Straub.

A

	30°C vs. 37°C		WT vs. *sds3Δ*	
	WT	*sds3Δ*	30°C	37°C
	p-value ChIP Euc1			
ub-HS3	5.90E-02	3.03E-03	5.07E-02	9.07E-03
ub-HS5	8.41E-02	2.83E-05	3.40E-01	1.56E-02
ub-HS7	2.40E-02	7.99E-05	7.56E-02	3.53E-02
ub-only-site1	2.15E-01	5.71E-01	4.19E-01	3.32E-02
	p-value ChIP ub-K48			
ub-HS3	3.33E-01	5.81E-01	3.75E-01	7.50E-01
ub-HS5	1.97E-03	3.37E-03	1.40E-01	1.05E-01
ub-HS7	8.53E-04	2.76E-03	9.12E-01	5.45E-02
ub-only-site1	3.65E-03	7.12E-03	3.63E-01	2.61E-01

B

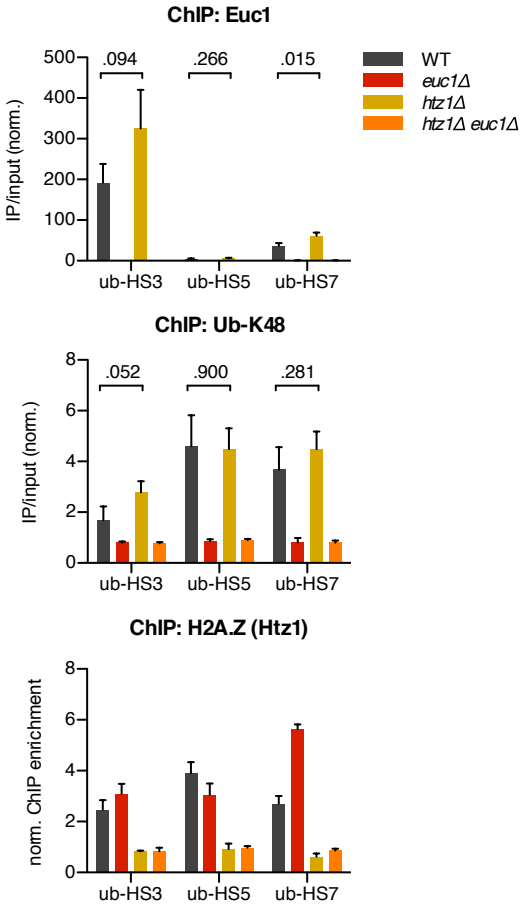

C

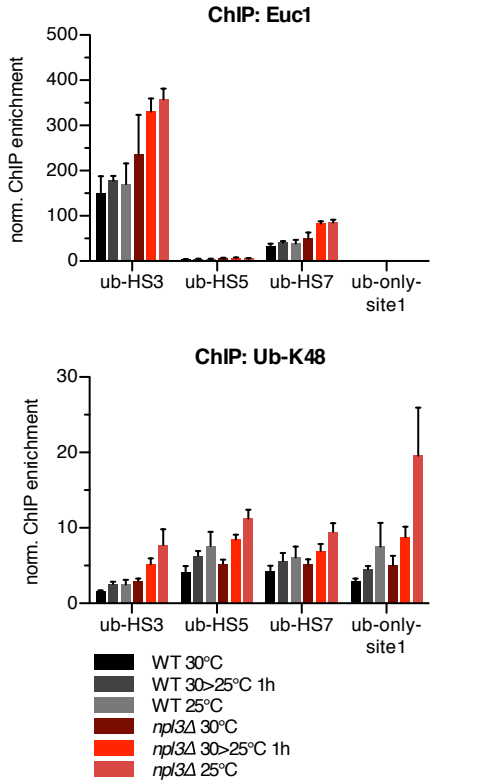

D

	30°C vs. 25°C		WT vs. *npl3Δ*	
	WT	*npl3Δ*	30°C	25°C
	p-value ChIP Euc1			
ub-HS3	5.77E-01	8.21E-02	1.95E-01	3.48E-03
ub-HS5	5.47E-01	8.20E-01	1.10E-01	1.70E-01
ub-HS7	3.78E-01	1.73E-02	1.29E-01	1.84E-03
ub-only-site1	4.66E-01	8.55E-02	9.83E-01	2.36E-01
	p-value ChIP ub-K48			
ub-HS3	6.94E-02	1.67E-02	4.94E-03	1.38E-02
ub-HS5	4.02E-02	1.34E-03	1.26E-01	4.71E-02
ub-HS7	1.27E-01	5.05E-03	2.23E-01	3.45E-02
ub-only-site1	1.71E-01	8.62E-02	1.65E-01	1.38E-01

Appendix Figure A8, related to Fig. 25.
(A) Euc1 is recruited to ub-hotspots upon heat stress. Statistical analysis of ChIP-qPCR data presented in Fig. 25. An unpaired, two-tailed Student's *t*-test was performed ($n = 4$).
(B) Euc1 is recruited to ub-hotspots in *htz1*Δ cells. ChIP-qPCR analysis of ubiquitin-K48, Euc1 and H2A.Z enrichments at selected ub-hotspots. *p*-values for comparisons of ubiquitin and Euc1 enrichments in WT ant *htz1*Δ are indicated. For ub-K48 and Euc1 experiments $n = 3$, for H2A.Z $n = 2$. For statistical analysis an unpaired, two-tailed Student's *t*-test was performed.
(C–D) Euc1 is recruited to ub-hotspots in *npl3*Δ cells upon cold stress. ChIP-qPCR for cells grown at 30°C, shifted to 25°C for 1h, or grown at 25°C. Note that ubiquitin is enriched at 25°C also at the Euc1-independent *ub-only-site1*, arguing for an Euc1-independent effect. Statistical analysis was performed for triplicate experiments (duplicates for *ub-only-site1*) using an unpaired, two-tailed Student's *t*-test (D).

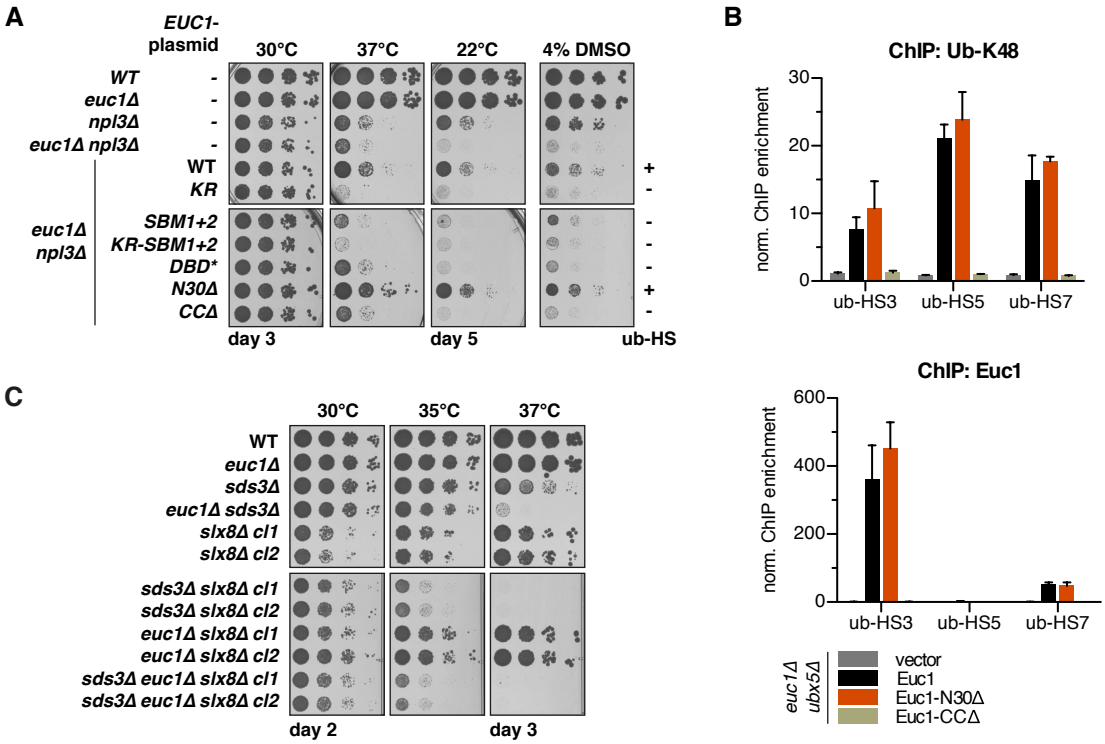

Appendix Figure A9, related to Fig. 26.
(A) Complementation of *euc1*Δ *npl3*Δ phenotypes with plasmid-borne *EUC1* alleles as in Fig. 26A.
(B) Euc1-N30Δ, but not Euc1-CCΔ is proficient in forming ub-hotspots. ChIP-qPCR quantification of ubiquitin and Euc1 in *euc1*Δ *ubx5*Δ cells complemented with the indicated plasmids. Data represent means ± SD (n = 3), for Euc1-CCΔ n = 2.
(C) *SLX8* shows genetic interactions with *SDS3* upon heat stress. Spotting as in Fig. 26B, but with *slx8*Δ strains as indicated.

6 Materials and Methods

All molecular biology and cloning techniques followed standard procedures (Ausubel *et al*, 1988; Green & Sambrook, 2012), unless described specifically, and were commonly used in the Jentsch department, as described previously (Kern, 2013). Sterilized flasks, glassware, solutions and deionized water were used for all experiments. Unless stated otherwise, analytical grade chemicals and reagents were purchased from Agilent, Applied Biosystems, BD, Biomol, Bioneer, Bio-Rad, GE Healthcare, Life Technologies, Merck Millipore, New England Biolabs (NEB), PeqLab, Promega, Qiagen, Roth, Roche, Serva, Sigma-Aldrich, or Thermo Scientific.

All *Escherichia coli* strains, *Saccharomyces cerevisiae* strains, plasmids and vectors, primary antibodies, and primers used for qPCR are listed in Tables 1–5 in section 6.6.

6.1 *Escherichia Coli* (*E. coli*) Methods

E. Coli Media

LB Medium/Plates	1% (w/v) Bacto tryptone 0.5% (w/v) Bacto yeast extract 0.5% (w/v) NaCl 1.5% (w/v) agar (for plates) sterilized by autoclaving

To select for plasmids harboring antibiotic resistance genes, ampicillin (100 µg/ml), kanamycin (30 µg/ml), or chloramphenicol (34 µg/ml) were added.

Competent E. Coli Cells and Transformation

Chemically competent *E. coli* cells were prepared by inoculating 1 l LB medium with a fresh overnight (o/n) culture to an optical density at 600 nm wavelength (OD_{600}) of 0.05, and cells were grown at 37°C with shaking to OD_{600} ~0.5. The culture was then chilled on ice for 15 minutes (min) and cells were pelleted by centrifugation (3500 rpm, 15 min, 4°C). The pellet was resuspended in 300 ml Tfb1 solution (30 mM KOAc, 50 mM $MnCl_2$, 100 mM KCl, 15% (v/v) glycerol, pH adjusted to 5.8 with HOAc) and incubated on ice for 15 min. Bacteria were pelleted again (1500 rpm, 15min, 4°C) and resuspended in 40 ml Tfb2 solution (10 mM MOPS, 7.5 mM $CaCl_2$, 10 mM KCl, 15% (v/v) glycerol, pH adjusted to 7 with NaOH). Competent cells were aliquoted on ice and stored at -80°C.

For transformation, cells were thawed on ice and ~50–500 ng plasmid DNA or 5–30 µl of a cloning product were mixed with 50–100 µl of competent cells. The mixture was incubated on ice for 20 min and subsequently heat-shocked (45 seconds (sec), 42°C waterbath) and chilled on ice again. Cells were either plated directly (for ampicillin resistance) or allowed to recover in 1 ml LB for 1 hour (h) shaking at 37°C before plating.

6.2 *Saccharomyces Cerevisiae* (*S. cerevisiae*) Methods

Buffers and Solutions

YP media/plates:	1% (w/v) Bacto yeast extract 2% (w/v) Bacto peptone 2% (w/v) carbon source (glucose (D), galactose (Gal), raffinose (Raf)) 2% (w/v) agar (only for plates) sterilized by autoclaving
YP-lactate medium:	1% (w/v) Bacto yeast extract 2% (w/v) Bacto peptone 3% (w/v) lactic acid pH adjusted to 5.5 with NaOH (ca. 12 g/l final) sterilized by autoclaving
YPD G418/NAT/Hph plates:	after autoclaving, YPD medium with 2% (w/v) agar was cooled to 50°C, and 200 mg/l G418 (geneticine disulphate, PAA Laboratories), 100 mg/l NAT (nourseothricin, HK Jena) or 500 mg/l Hph (hygromycin B, PAA Laboratories) were added.
Synthetic dropout media:	0.67% (w/v) yeast nitrogen base 0.133% (w/v) amino acid master mix -8 + amino acid supplements (omitting individual ones) 2% (w/v) glucose 2% (w/v) agar (for plates) sterilized by autoclaving
Amino acid master mix -8 stock:	25 g each: Ala, Asn, Asp, Cys, Gln, Glu, Gly, Ile, Phe, Pro, Ser, Thr, Tyr, Val, myo-Inositol 2.5 g para-Aminobenzonic acid

Amino acid supplements:	0.0175% (w/v) final: Leu 0.00875% (w/v) final: His, Met, Arg, Trp, Uracil, Lys-monohydrate 0.00225% (w/v) final: Adenine hemisulfate salt
Sporulation medium:	2% (w/v) KAc, sterilized by autoclaving
SORB Buffer:	100 mM LiOAc 10 mM Tris-HCl, pH 8.0 1 mM EDTA, pH 8.0 1 M sorbitol sterilized by filtration
PEG Solution:	100 mM LiOAc 10 mM Tris-HCl, pH 8 1 mM EDTA, pH 8.0 40% (w/v) PEG-3350 sterilized by filtration stored at 4°C
One-step mix	40% (w/v) PEG-3350 or -6000 200 mM LiAc 0.5 mg/ml herring sperm DNA (Invitrogen)

Basic Yeast Protocols

Yeast cells were typically streaked freshly from glycerol stocks (saturated yeast culture with 15% v/v glycerol, stored at -80°C) on YPD or selective media plates and grown for 1–3 days at 30°C, or 25°C for temperature-sensitive (ts) alleles. Plates were stored for up to 2 weeks for consecutive experiments. For experiments, precultures were inoculated in 5–25 ml appropriate liquid media and incubated with shaking (150–220 rpm) o/n at 25°C/30°C. For main experimental cultures, cells were diluted to an OD_{600} of 0.1–0.2 in fresh medium and incubated in Erlenmeyer flasks or glass tubes with continuous shaking at 30°C (110–220 rpm). Temperature-sensitive mutants were also grown at the semi-permissive temperature of 30°C unless stated otherwise. Of note, all used ts-alleles showed phenotypes at this temperature and an increase in temperature did not substantially change the results. Cells were typically allowed to go through at least two division cycles before any treatment was applied, and cells were harvested in mid-log phase (OD_{600} = 0.6–1). Within experiments, equal amounts of cells were harvested according to cell density, and 1 OD_{600} unit (i.e. 1 ml culture at OD_{600} = 1) corresponds to ~3*10^7 cells.

For galactose induction, cells were cultured in YP + 2% raffinose (or YP-lactate for ChIP-chip experiments), grown to OD_{600} = 0.4–0.5 and galactose was added to a final concentration of 2%, typically for 3 h.

Competent Yeast Cells and Transformation

Competent yeast cells were prepared as described (Knop *et al*, 1999). Briefly, cells were grown to mid-log phase in 50 ml YPD and pelleted (1200 *g*, 2–5 min, room temperature (RT)), washed in 25 ml water, and 0.2 volumes of SORB buffer and were finally resuspended in 360 µl SORB buffer and 50 µl carrier DNA (10 mg/ml herring sperm DNA, Invitrogen). Competent cells were aliquoted and stored at -80°C.

For transformation with PCR products or linearized plasmids, 50 µl of competent cells were mixed with 6 volumes of PEG solution and either 10–20 µl PCR product or 0.2–1 µg linearized plasmid and incubated at RT for 30 min. Subsequently, 1 volume of DMSO was added, cells were heat-shocked (42°C, 10–15 min) and chilled on ice. Cells were pelleted (1500 *g*, 1 min, RT) and plated on selective media plates, or allowed to recover in 5 ml YPD for 2–6 h before plating when antibiotic resistance marker cassettes were used (*natNT2, hphNT1, kanMX4*). Plates were incubated at 25°C or 30°C until single colonies appeared, or replica plated using sterile velvet if necessary.

For plasmid transformations, the above method was scaled down (0.2x volumes, ~100ng plasmid DNA). Alternatively, the one-step protocol was used: ~5 OD_{600} of freshly streaked cells were mixed with 50 µl one-step mix, 5 µl of 1 M dithiothreitol (DTT) and 100–200 ng of plasmid DNA. Cells were then heat-shocked (42°C, 20 min), cooled on ice, and streaked on selective plates.

Yeast Genetic Manipulation

Chromosomal deletion or tagging of *S. cerevisiae* genes largely followed published standard procedures (Knop *et al*, 1999; Janke *et al*, 2004). Briefly, marker cassettes (optionally with epitope tags) were amplified by PCR from plasmid vectors of the pYM series using primers that carried 50 basepair (bp) overhangs homologous to the targeted region. Cells were transformed with PCR products and selected for the used marker cassette. Homologous recombination initiated by the 50 bp overhangs directed cassette integration and correct insertion was tested by yeast colony PCR or western blot (WB) to test for absence of a deleted ORF, or correct epitope-tagging.

For transformation of integrative yeast vectors (*YIplac211, YIplac128*) to integrate genes at *URA3* or *LEU2* loci, 1 µg of plasmid was linearized by restriction enzyme (RE)

digest and transformed as described. Single integration at the correct locus was tested by yeast colony PCR.

For the introduction of point mutations at endogenous loci (*EUC1-tADH::caURA3* (as WT control), *euc1-K231R-tADH::caURA3, euc1-W333A,R334A-tADH::caURA3, slx8-C206S,C209S-tADH::NatNT2*), the ORFs were cloned into the pGAD-C1 vector, mutations were introduced via site-directed mutagenesis, and a marker cassette was cloned downstream of the *ADH* terminator sequence (pMH201/202/204 for *EUC1* mutations and pMH212 for *slx8-CD*, respectively). Subsequently, the mutated ORF together with the *ADH* terminator and marker cassette were amplified (with 50 bp overhang reverse primers) and cells were transformed as described. Colony PCR was performed to check integration and to amplify the complete ORF, which was purified and sequenced to verify mutations.

Mating, Sporulation and Tetrad Analysis

To mate yeast cells with opposing mating types, similar amounts of yeast cells were mixed from fresh plates or directly from glycerol stocks and incubated on a YPD plate for ~3 h or o/n. Cells were then restreaked or replica plated on selective media plates to select diploid cells. If selection was not feasible, zygotes were picked from mating cells using a micromanipulator (Singer MSM Systems) and mating type analysis was performed to test absence of haploid mating types in diploid cells.

For sporulation, cells were grown o/n in YPD and 500 µl of culture was pelleted, cells were washed 4 times with water and resuspended in 5 ml 2% KAc. Cells were incubated for 3–5 days with shaking (220 rpm) at 25°C. To dissect tetrads, 10–20 µl of sporulation culture was mixed with an equal amount of zymolase solution (Amsbio 100T, 1 mg/ml in water) and incubated at RT for 7 min. Individual cells from tetrads were separated using a micromanipulator, grown on YPD plates for 2–5 days, plates were scanned (optionally), and genotypes were tested by replica plating on selective media and mating type test plates.

Mating Type Analysis

To identify mating types, the RH448 (*Mat a*, Y0934) and RC757 (*Mat α*, Y0933), which are hypersensitive to the opposing mating type pheromones, were used as test strains. Cells from freshly streaked test strains were dissolved in 1% melted agar or agarose (precooled to ~45°C) and a layer of the mixture was poured on top of a regular YPD plate. Strains to be tested were then streaked or replica plated on the a/α test plates and mating types were identified by halos of inhibited growth of the opposing mating type test strains.

Spotting or Cell Growth/Survival Assay

Spotting assays were used for qualitative and semi-quantitative assessment of yeast survival and growth rates, e.g. for testing cellular fitness under different growth conditions or drug/chemical treatments, for growth-based readouts of yeast one-/two-hybrid assays or for reporter-gene assays. Typically, cells were freshly streaked from glycerol stocks and grown for 1–3 days, or several clones from plasmid-transformed cells were mixed, resuspended in water and adjusted to OD_{600} = 0.5. Optionally, serial five-fold dilutions were prepared to better visualize differences in growth/survival rates. Cell suspensions were arranged in 96-well plates and spotted on plates using a custom-made stamp, which transfers approximately 5 µl per spot.

Yeast Two-Hybrid (Y2H) Assay

To test *in vivo* protein–protein interactions and for mapping of interaction domains, a yeast two-hybrid assay was employed. Genes encoding proteins to be tested for interaction were cloned into pGAD-C1/pGBD-C1 vectors to allow their expression with N-terminally fused Gal4 transactivation/DNA-binding domains (AD/BD). AD/BD plasmid combinations were then transformed into a Y2H test strain (Pj69-7a or derivatives thereof) that features *GAL*-promoter-controlled reporter genes (*HIS3, ADE2, lacZ*) (James *et al*, 1996). In some cases, the endogenous genes of the proteins to be tested or of binding partners were deleted to avoid interference with the assay (e.g. *EUC1, SLX8*). Transformed cells were then prepared for spotting assays as described and spotted on control (SC-Leu-Trp) or selective media plates (SC-Leu-Trp-His) and growth was scored after 2–5 days. To test for auto-activation artifacts, control combinations for all constructs with an empty vector of the complementary domain (AD-empty, BD-empty) were included.

Yeast One-Hybrid (Y1H) and Reporter Gene Assays

Yeast one-hybrid assays were performed to test binding of query proteins to a specific DNA sequence. Briefly, sequences of interest (3x ub-HS4: chromosome XIII 308901–308939 (Kern, 2013), ub-HS5 + 100 bp flanking: chromosome XIII 413497–413733) were cloned into *YIplac211* vectors upstream of a minimal promoter followed by a *HIS3* reporter gene obtained from *pHISi-1* (Clontech). The plasmid with the reporter construct was then integrated into a reporter strain (derived from YM4271, Clontech) and Gal4-AD-fusion constructs were expressed to assess their binding to the query sequences. Cells were then spotted on control (SC-Leu) or selective media plates (SC-Leu-His). To suppress

background activity of the *HIS3* reporter gene due to the leaky minimal promoter, variable amounts of 3-amino-1,2,4-triazole (2–40 mM) were added to selection plates.

For reporter-gene assays to test transactivation by Euc1 constructs (without any fused AD) the same reporter genes were used and *EUC1* alleles were expressed from plasmids under the control of the *EUC1* promoter. Optionally, the endogenous *EUC1* ORF or other ub-hotspot-pathway genes were deleted to test their influence on reporter-gene activation.

A modified reporter-gene assay was used to test transactivation of isolated N-terminal Euc1 fragments fused to a C-terminal Gal4 BD. Here, Euc1 fragments were cloned into *YEplac195-pADH-BD-tADH* (Moldovan *et al*, 2006) and plasmids were transformed into a PJ69-7a derived Y2H strain with *EUC1* deleted. *GAL*-promoter-controlled *HIS3* expression was used as a readout for transactivation by Euc1 fragments in spotting assays on SC-His plates.

6.3 Molecular Biological Methods

6.3.1 DNA Purification and Analysis

DNA purification methods followed standard procedures and, if commercially available kits were used, they were performed according to the manufacturer's instructions unless stated otherwise. Briefly, for plasmid purification from XL1-Blue *E. coli* cells (mini prep), single colonies of transformed cells were inoculated in 2–5 ml LB supplemented with appropriate antibiotics and grown for 8 h to o/n. Cells were pelleted and plasmid DNA was extracted (AccuPrep Plasmid Mini Extraction Kit, Bioneer).

Genomic DNA from *S. cerevisiae* cells for use as PCR template for cloning was extracted using the MasterPure Yeast DNA Purification kit (Epicentre). Linear DNA fragments from PCR or cloning reactions were purified using the Qiagen PCR purification kit. DNA fragments separated on agarose gels were purified using the AccuPrep Gel Purification Kit (Bioneer). DNA concentrations were measured using a NanoDrop ND-1000 instrument (PeqLab), and sequencing service was typically performed by Eurofins.

Agarose Gel Electrophoresis

For separation of DNA fragments to visualize PCR product size or for cloning, gel electrophoresis was performed. Low-melt agarose (Invitrogen) was dissolved at 0.7–2% (w/v) in 1x TBE buffer (89 mM Tris, 89 mM boric acid, 2 mM EDTA) and melted by boiling. Ethidium bromide was added before polymerization, 6x DNA loading dye

(Invitrogen) was added to DNA and gels were run at 100–120 V in 1x TBE buffer. The 1 kb plus DNA ladder (Invitrogen) was used as size marker and DNA bands were visualized using a UV transilluminator (VWR GenoSmart).

6.3.2 Polymerase Chain Reaction (PCR)

PCR was used to amplify fragments for cloning (Phusion PCR, NEB) or to test genetic modifications of *S. cerevisiae* (yeast colony PCR/Taq polymerase, MPI Biochemistry Core Facility) as detailed below. For amplification of deletion/epitope tagging cassettes, the Taq/Vent (NEB) protocol was used as described (Janke *et al*, 2004) and plasmids of the pYM collection were used as templates (Knop *et al*, 1999; Janke *et al*, 2004). Primers were designed manually or assisted by web-based applications (http://tmcalculator.neb.com/#!/main, https://www.ncbi.nlm.nih.gov/tools/primer-blast/) and purchased from Eurofins. PCR reactions were performed in a thermal cycler (Applied Biosystems).

PCR reaction setups

Reagent	Phusion PCR	Taq PCR
DNA template	2 µl*	2 µl**
dNTPs (10 mM)	1 µl	0.9 µl
Primer for (10 µM)	2.5 µl	1.6 µl
Primer rev (10 µM)	2.5 µl	1.6 µl
Polymerase buffer	10 µl[§]	2.5 µl[§§]
Water	31.5 µl	16.15 µl
Polymerase	0.5 µl	0.25 µl
Total	50 µl	25 µl

*10 ng plasmid or 200 ng genomic DNA, **typically yeast colony PCR template
[§] 5x Phusion HF or GC buffer (NEB), [§§] 10x ThermoPol reaction buffer (Thermo)

PCR amplification protocols

	Phusion PCR		Taq PCR	
Step	**Temperature**	**Duration**	**Temperature**	**Duration**
Initial Denaturation	98 °C	2 min	94°C	5 min
Denaturation	98°C	20 sec	94°C	30 sec
Annealing	60°C*	20 sec	55°C*	30 sec
Elongation	72°C	30–60 sec/kb	72°C	1 min/kb
Final extension	72°C	7 min	72°C	5 min
Cooling	4°C	hold	4°C	hold

*variable, shaded steps were cycled (30x)

Yeast Colony PCR

To test correct integration of deletion/tagging cassettes, yeast colony PCR was performed. For template DNA extraction, a single yeast colony was resuspended in 50 µl 0.02 M

NaOH and heated to 99°C for 10 min in a thermal cycler. Cell debris was pelleted by a 10-sec spin in a micro centrifuge and 2 µl were used as template for Taq PCR as detailed above.

Site-Directed Mutagenesis

Site-directed mutagenesis was performed using the Pfu Turbo polymerase (Stratagene) and according to instructions of the QuikChange Site-Directed Mutagenesis Kit manual (Stratagene). Primers were designed according to the manual and PCR was performed as detailed below, or optimized if necessary. After the PCR, template DNA was digested using the methylation specific restriction enzyme DpnI (NEB, 1 µl, 1 h, 37°C) and 5 µl of the reaction were used for transformation of 80 µl chemically competent XL1-Blue *E. coli* cells. Before plating on selective plates, cells were allowed to recover for 3 h in 1 ml LB at 37°C.

Pfu Turbo PCR protocol

Step	Temperature	Duration
Initial Denaturation	95 °C	2 min
Denaturation	95°C	30 sec
Annealing	50°C	45 sec
Elongation	68°C	15 min
Final extension	68°C	15 min
Cooling	4°C	hold

shaded steps were cycled (19x)

6.3.3 Molecular Cloning

Ligation-based Cloning

For traditional ligation-based cloning, a vector (2.5 µg) and an insert (typically a PCR product, a synthesized gene strand (Eurofins), or annealed oligos) were digested in a 50 µl reaction using restriction enzymes (NEB) according to the manufacturer's instructions. Vectors were dephosphorylated by addition of 1µl calf intestine phosphatase (CIP, NEB; 30 min, 37°C) and purified using a PCR purification kit (Qiagen). Digested PCR products were separated on an agarose gel and purified (AccuPrep Gel Purification Kit, Bioneer). 50–150 ng vector DNA were mixed with a 3–10-fold molar excess of insert DNA and ligated in a 30 µl reaction using T4 ligase (NEB) for 30 min at RT according to the manufacturer's instructions. Subsequently, the complete ligation reaction was used for transformation of 80 µl chemically competent XL1-Blue *E. coli* cells.

Gibson Cloning

For recombination-based Gibson cloning, primers for PCR or gene strands were designed with 15–25 bp overhangs that were homologous to the target vector sequence. Vector DNA was digested, dephosphorylated and purified as above, while insert DNA (PCR product, gene strand) was purified from a gel without digest. 50 ng vector DNA was mixed with 3–10-fold molar excess of insert DNA and an equal volume of Gibson Assembly Master Mix (NEB) was added (typically in a 10 µl reaction). The reaction was performed for 15–60 min at 50°C and half of the reaction was used for transformation of 50 µl chemically competent XL1-Blue *E. coli* cells.

6.4 Biochemical and Cell Biological Methods

6.4.1 Protein Biochemical Methods

Buffers and Solutions

HU buffer	200 mM Tris, pH 6.8 8 M urea 5% (w/v) SDS 1 mM EDTA 0.1% (w/v) bromophenol blue 100 mM DTT added before use
2x SDS loading buffer (Laemmli sample buffer)	120 mM Tris pH 6.8 4% (w/v) SDS 20% (w/v) glycerol 0.02% (w/v) bromophenol blue 10% (v/v) β-mercaptoethanol added before use
MOPS buffer	50 mM MOPS 50 mM Tris base 3.5 mM SDS 1 mM EDTA
Blotting buffer	250 mM Tris base 1.92 M glycine 0.1% (w/v) SDS 20% (v/v) methanol
Blotting buffer (commercial)	5% (v/v) 20x Swift buffer (G-Bioscience) 10% (v/v) Methanol

TBS-T solution	25 mM Tris, pH 7.5 137 mM NaCl 2.6 mM KCl 0.1% (v/v) Tween 20
PBS	10 mM phosphate, pH 7.4 137 mM NaCl 2.7 mM KCl
FLAG-IP buffer (FIPB)	100 mM HEPES-KOH pH 7.6 200 mM KOAc 10% (v/v) glycerol 0.1% (v/v) NP-40

Total Protein Analysis from Yeast Cell Lysates

Proteins for analysis by SDS-PAGE and western blot analysis from yeast whole cell extracts (WCE) were prepared using the trichloroacetic acid (TCA) precipitation method (Knop *et al*, 1999). Cells were grown to mid-log phase and 1 OD_{600} unit was harvested by centrifugation. For cycloheximide (CHX) chase experiments, mid-log phase cells were pelleted gently, resuspended at OD_{600} = 1 in fresh medium supplemented with 0.5mg/ml CHX and samples were taken at the indicated time-points and harvested.

The cell pellet was resuspended in 1 ml cold water and mixed with 150 µl freshly prepared lysis solution (1.85 M NaOH, 7.5% β-mercaptoethanol) and incubated for 15 min on ice. 150 µl of cold 55% TCA were added to precipitate proteins for 10 min on ice. Proteins were pelleted by centrifugation (10 min, 14000 rpm, 4°C), the supernatant (SN) was removed and a second 5 min centrifugation step was performed to remove residual SN. Protein pellets were then resuspended in 40–100 µl HU buffer and denatured at 65°C for 10 min with shaking (1400 rpm).

Separation of Proteins via SDS-PAGE

Sodium dodecyl sulfate polyacrylamide gel electrophoresis (SDS-PAGE) was performed to separate proteins according to their molecular weight. Typically, pre-cast NuPage gels were used (Invitrogen, 4–12% or 12% Bis-Tris, or 3–8% Tris-Acetate for GST-Euc1/6His-Slx5 pull-down samples). Protein samples were prepared in HU buffer (denaturation for 10 min, 65°C) or Laemmli sample buffer (denaturation for 5 min, 99°C), loaded, and gels were run in MOPS running buffer (Bis-Tris gels) or Tris-Acetate SDS running buffer (Invitrogen) at 120–200 V constant voltage. For molecular weight estimation of proteins,

the Precision Plus All Blue Standard (Bio-Rad) was used. For direct visualization of proteins, gels were stained with PageBlue Protein Staining Solution (Thermo Scientific).

Western Blot (WB)

For protein analysis via western blot, proteins separated by SDS-PAGE were transferred to a polyvinylidene difluoride (PVDF) membrane using a wet blot protocol. Briefly, the membrane was activated in methanol, the gel was placed on top and filter paper (Whatman) soaked in blotting buffer was added on the top and bottom in a sandwich-like fashion. Blots were assembled in a cassette and blotting was performed in Amersham Biosciences blot chambers at 75 V constant voltage at 4°C for 1:45 h. The membrane was then blocked in 5% (w/v) skim milk powder in TBS-T for 15–60 min at RT and subsequently incubated o/n with primary antibody dissolved in 5% milk/TBS-T (optionally with 0.02% sodium azide). Afterwards, the membrane was washed twice briefly with TBS-T and incubated with secondary antibody coupled to horseradish peroxidase in 5% milk/TBS-T for 1–6 h (at least 3 h for Euc1 and Slx5 WBs). Lastly, the membrane was washed four times for 7 min in TBS-T, and detection of proteins was performed using chemiluminescence reagents (ECL or ECL plus, Thermo Scientific). Signals were detected using Amersham Hyperfilm ECL (GE Healthcare) or a camera-based detection system (LI-COR Odyssey Fc) and processed in Adobe Photoshop or quantified using the ImageStudio Lite package (LI-COR).

Co-immunoprecipitation (Co-IP)

For FLAG-IPs, 300 OD_{600} units of cells were harvested (1500 *g*, 10 min, 4°C) from a mid-log phase culture, washed once with 50 ml 1 M sorbitol/25 mM HEPES pH7.6, and pelleted again (3500 *g*, 5 min, 4°C). Cells were then resuspended in 3 ml FLAG-IP buffer (FIPB), freshly supplemented with 2 mM β-mercaptoethanol, 1x protease inhibitors (Roche cOmplete EDTA-free), 0.02 M N-ethylmaleimide (NEM), 1 mg/ml Pefabloc SC (Roche) and 2 mM $MgCl_2$. Resuspended cells were snap-frozen as “yeast popcorn” in liquid nitrogen and stored at -80°C or processed directly in a Freezer/Mill (FM6870, SPEX SamplePrep). Cell lysates were thawed in a water bath, incubated on ice with 1.5 µl benzonase (Merck/Millipore) to digest nucleic acids for 15 min, and cleared by centrifugation (2000 *g*, 20 min, 4°C). Input samples were set aside and 50 µl slurry of anti-FLAG agarose beads (M2, Sigma) pre-equilibrated in FIPB were added per sample. Co-immunoprecipitation of FLAG-tagged proteins and binding partners was carried out for 2 h at 4°C on a rotating wheel and beads were then washed five times with 1 ml ice-cold FIPB

supplemented with inhibitors (as above). Finally, beads were eluted with 50 µl HU buffer (65°C, 10 min shaking 1400 rpm) and samples analyzed by SDS-PAGE and WB.

GST-pulldown Assay

For GST-pulldown assays, indicated recombinant proteins (8 µg GST, 15 µg GST-Euc1 or 20 µg 6His-Slx5) were mixed in binding buffer (50 mM Tris pH 7.5, 5 mM DTT, 150 mM NaCl, 0.5% NP-40, 20 mM imidazole) and incubated for 30 min at room temperature to allow binding. Input samples were set aside, 50 µl magnetic glutathione bead slurry (ThermoFisher) were added and samples rotated for one hour at 4°C. Beads were washed four times with wash buffer (as binding buffer, but 300 mM NaCl) and eluted with 30 µl 5 mM glutathione in wash buffer for 5 min at RT. All samples were dried in a vacuum concentrator (Eppendorf) and resuspended in 3 µl water and 12 µl Laemmli sample buffer. Finally, samples were separated by SDS-PAGE on 3–8% Tris-Acetate gels and stained with PageBlue (ThermoFisher).

NiNTA Pulldown

To investigate proteins covalently modified with either 7His-SUMO (^{His}SUMO) or 6His-ubiqutin (^{His}Ubi), nickel-nitrilotriacetic acid (NiNTA) pulldowns of yeast cell lysates were performed under denaturing conditions as described (Psakhye & Jentsch, 2016). Typically, 200 OD_{600} units of cells from a mid-log phase culture were harvested by centrifugation (3500 *g*, 5 min, 4°C), washed with 25 ml cold PBS and pellets were snap-frozen in liquid nitrogen and optionally stored at -80°C. Cells were lysed on ice for 15 min in 6 ml 1.85 M NaOH with 7.5% β-mercaptoethanol freshly added. To precipitate proteins, 6 ml of cold 55% TCA was added, samples were incubated on ice for 15 min, and proteins were pelleted by centrifugation (3000 *g*, 30 min, 4°C). Pellets were carefully washed twice (without resuspending) using ice-cold water and subsequently resuspended in buffer A (6 M guanidinium hydrochloride, 100 mM NaH_2PO_4, 10 mM Tris-HCl, pH 8) supplemented with 0.05% Tween-20. To fully dissolve pellets, samples were incubated for 1–3 h at RT with shaking (220 rpm) and subsequently centrifuged to remove insoluble particles (23000 *g*, 20 min, 4°C). The SN was transferred to 15 ml Falcon tubes and imidazole (final concentration of 20 mM) and NiNTA beads were added (50–100 µl agarose or magnetic agarose slurry, both Qiagen). Samples were incubated on a rolling platform o/n at 4°C and beads were recovered by centrifugation (1000 *g*, 5 min, 4°C, magnetic beads) or loaded on filter columns (Bio-Rad, for NiNTA agarose beads). For magnetic beads, beads were washed using a magnetic rack: 3 times with 1 ml buffer A (+ 20 mM imidazole, 0.05%

Tween-20), 5 times with 1 ml buffer C (8 M urea, 100 mM NaH_2PO_4, 10 mM Tris-HCl, pH 6.3) with 0.05% Tween-20, and once with 125µl buffer C without Tween-20. To elute proteins, beads were incubated for 10 min at 65°C shaking (1400 rpm) with 1% SDS (w/v) in water. Beads were discarded and the solution was dried in a vacuum concentrator (Eppendorf, 45°C, 30 min). Samples were resuspended in 10 µl water and 15 µl HU buffer and analyzed by SDS-PAGE and WB.

NiNTA agarose beads were washed in filter columns twice with 7.5 ml buffer A (+ 20 mM imidazole, 0.05% Tween-20), twice with 7.5 ml buffer C (+ 0.05% Tween-20), and once with 10 ml buffer C. To elute proteins, the column was sealed and beads were incubated twice with 1 ml elution buffer (0.75x buffer C, 250 mM imidazole) for 10 min. Proteins were then precipitated with the TCA method, pellets were optionally washed with cold acetone (-20°C), and resuspended in HU buffer for SDS-PAGE and WB.

Antibodies

All primary antibodies used in this study are listed in Table 4 in section 6.6. Primary antibodies against Slx5 (aa 1–487) and Slx8 were produced by Alexander Strasser (MPI of Biochemistry) using standard procedures. Briefly, GST-tagged proteins were expressed from pGEX-4T3 vectors in Rosetta 2 cells and purified, rabbits were immunized with several boosts (MPI Animal Facility), blood was collected, and serum was passed over columns with 6His-tagged proteins (expressed from pET28a vectors in Rosetta 2 (DE3) cells) to enrich specific antibodies. Columns were eluted, antibody specificity was tested in WBs and antibodies were stored in PBS/50% glycerol at -20°C. Notably, Slx5 and Slx8 antibodies detect several non-specific targets besides their primary antigen. However, re-using the antibody solution (in 5% milk/TBS-T) several times significantly improved the signal ratio between specific versus non-specific bands. Note that for all WBs using anti-Euc1 antibody, 5% (w/v) BSA was used instead of milk powder for blocking and primary/secondary antibody dilutions. Secondary antibodies for WB detection were all purchased from Dianova and coupled to horseradish peroxidase (HRP, goat anti-mouse/rabbit/rat).

Recombinant Proteins

Recombinant 6His-Slx5 for GST-pulldowns was produced by the MPI Biochemistry Core Facility exactly following a published protocol (Yang *et al*, 2006). Purified GST and GST-Euc1 were kind gifts from A. Strasser and M. J. Kern and had been purified by standard procedures.

6.4.2 Chromatin immunoprecipitation (ChIP)

ChIP Buffers

FA lysis buffer (FA-LB)	50 mM Hepes, pH 7.5 150 mM NaCl 1 mM EDTA 1% (v/v) Triton X-100 0.1% (w/v) Deoxycholic acid, Na-salt 0.1% (w/v) SDS
FA lysis buffer 500 mM NaCl (FA-LB500)	50 mM Hepes, pH 7.5 500 mM NaCl 1 mM EDTA 1% (v/v) Triton X-100 0.1% (w/v) Deoxycholic acid, Na-salt 0.1% (w/v) SDS
ChIP wash buffer	10 mM Tris, pH 8 250 mM LiCl 1 mM EDTA 0.5% (v/v) NP-40 0.5% (w/v) Deoxycholic acid, Na-salt
ChIP elution buffer	50 mM Tris, pH 7.5 10 mM EDTA 1% (w/v) SDS
TE	10 mM Tris, pH 8 1 mM EDTA

ChIP Protocol

ChIP was performed based on a published protocol (Aparicio *et al*, 2005), with minor modifications as described (Kalocsay *et al*, 2009; Renkawitz *et al*, 2013; Kern, 2013). Briefly, cells were grown to mid-log phase and for each IP, yeast cells equivalent to 75 OD_{600} units were crosslinked with formaldehyde (1% final) for 16 minutes and the reaction was quenched by adding glycine (325 mM final) for 15 min. Cells were pelleted (3500 *g*, 5 min, 4°C) and washed in 25 ml ice-cold PBS, transferred to 2-ml Eppendorf tubes (eppis), pelleted and snap-frozen in liquid nitrogen. Cells were resuspended in 800 µl FA lysis buffer freshly supplemented with protease inhibitors (PIs: cOmplete EDTA-free protease inhibitors and Pefabloc SC (1 mg/ml final), both Roche), and lysed by beat-beating (MM301 or MM200, Retsch GmbH) with zirconia/silica beads (BioSpec Inc.) for 6 cycles

with 3 min shaking (30/s) and 3 min breaks at 4°C. Lysates were transferred to fresh 2-ml eppis by the piggy-back elution method and pelleted by centrifugation (15 min, 14000 rpm, 4°C). The SN was discarded and the chromatin pellet was resuspended in 1 ml fresh FA-LB+PIs and transferred to 15 ml TPX tubes (Sumilon/Diagenode).

Chromatin was sheared to 200–500 bp fragments using a Bioruptor UCD-200 sonication system (Diagenode, 3 10-min cycles, high power, 30 sec on/off intervals, ice-water bath). Cell debris was pelleted by centrifugation (6150 *g*, 30 min, 4°C), input samples (20 µl) were collected and 800 µl chromatin was subjected to immunoprecipitation with specific antibodies (90 min, RT) and pre-equilibrated Protein A Sepharose CL-4B (GE Healthcare, 10 µl bead volume per sample) was added for 30 min precipitation (RT). Beads were pelleted (500 *g*, 2 min, RT) and washed with 400 µl of FA-LB (3x, 200 *g*, 1 min), FA-LB500 (1x), ChIP wash buffer (1x), and TE (1x). Elution was performed with 110 µl ChIP elution buffer for 10 min at 65 °C with shaking (1400 rpm). Beads were pelleted (8000 *g*, 2 min) and 100 µl SN were collected and mixed with 80 µl TE and 20 µl proteinase K (Sigma, 20 mg/ml in 10 mM Tris pH 8). Input samples were mixed with 100 µl ChIP elution buffer, 60 µl TE and 20 µl proteinase K. Protein digest and de-crosslinking was performed for 3 h at 42°C and 8 h at 65°C followed by cooling to 4°C. DNA was recovered using the PCR purification kit (Qiagen) according to the manufacturer's instructions. Elution was performed with a 5 min incubation step and typically 75 µl of elution buffer. Enriched DNA was subjected to qPCR-analysis or processed for genome-wide quantification using NimbleGen arrays as detailed below.

Quantitative Real-time PCR (qPCR)

qPCR was performed to quantify DNA contents of ChIP samples (ChIP-qPCR) or cDNA levels of reverse-transcribed RNA samples (RT-qPCR) using a LightCycler 480 system (Roche). All qPCR primers used in this study are listed in Table 5 in section 6.6. For ChIP quantification, input DNA samples were diluted 1:10 and 2 µl of input or ChIP DNA were mixed with 10 µl KAPA-Mix (KAPA SYBR FAST qPCR Master Mix 2x, Roche), 7.92 µl water, and 0.04 µl forward and reverse primers each (100 µM stock). Reactions were set up in technical triplicates in 384-well LightCycler plates (Roche). To control for primer-specific amplification efficiencies, a standard curve was set up using input DNA (1:3, 1:30, 1:300, 1:3000 dilutions) for each primer pair and every experiment. The PCR was carried out as detailed below, including a melt-curve analysis to ensure amplification of a single PCR product. Quantification was performed using the "second-derivative maximum"

mode of the LightCycler 480 software. To calculate relative enrichments at selected loci, ratios of IP/input signals were calculated and, unless stated otherwise, subsequently normalized to an unrelated control region that showed low fluctuations of ubiquitin, Euc1 and Slx8 signals in ChIP-chip experiments (chromosome II, *TOS1* promoter). Hence, background levels were defined as 1.

Reaction conditions were the same for quantification of reverse-transcribed cDNA, which was diluted 1:5 prior to qPCR. A standard curve using ChIP input DNA (from a WT strain) as described above was also included for RT-qPCR, but normalization was carried out relative to expression of housekeeping genes (*ACT1, PGK1*) and to control strains/conditions as detailed in the respective figure legends.

qPCR protocol (KAPA-Mix)

Step	Temperature	Duration
Initial Denaturation	95 °C	3 min
Denaturation	95°C	10 sec
Annealing	57°C	20 sec
Elongation	72°C	1 sec
Melt-curve analysis	95°C	5 sec
	65°C	1 min
	65–97°C	0.11°C/sec
Cooling	4°C	hold

shaded steps were cycled (40x)

ChIP-chip

Microarray-based genome-wide ChIP quantification (ChIP-chip) was performed as described before (Kalocsay *et al*, 2009; Renkawitz *et al*, 2013). Briefly, input and ChIP DNA samples were treated with RNase (Sigma) and amplified with the GenomePlex Complete Whole Genome Amplification kit (Sigma) in two steps as described (O'Geen *et al*, 2006). Labeling of input and ChIP DNA (Cy3 or Cy5), hybridization to *S. cerevisiae* tiling arrays, array scanning and raw data extraction was performed by Source BioScience Berlin (formerly imaGenes, NimbleGen ChIP-chip service). Custom-designed c12plex NimbleGen arrays with 84 bp median genomic probe spacing were used and only unique probes were analysed. A dye-swap was included for replicate experiments and genome-wide binding profiles were generated from two independent experiments. Data presented in figures is on $\log_2$-scale, normalized to input DNA and plots were generated using IGB (Integrated Genome Browser).

Bioinformatic Analysis of ChIP-chip Data[5]

Data analysis was performed using R/Bioconductor as previously described (https://www.epigenesys.eu/images/stories/protocols/pdf/20111025114444_p43.pdf). Raw tiling array signals were $\log_2$ transformed and quantile normalized (library "preprocessCore"). For peak calling first a t statistic using the 90% rule of Efron (function "efron.stat", library "st") was calculated on IP versus background for the signals of each probe. Then the local false discovery rate (lfdr, library "locfdr") on the t values for each probe was determined. Probes less than 350 bp apart with a lfdr < 0.2 and a $\log_2$ (IP/background ratio) > 0.5 (1 in case of Euc1/Ymr111c) were merged. Merged regions broader than 500 bp were defined as peaks (enriched regions, ER).

6.4.3 RNA Methods

mRNA Quantification (RT-qPCR)

Yeast total RNA was isolated form 4 OD_{600} units of yeast cells using the RNeasy Kit (Qiagen) following the manufacturer's instruction, with beat-beating for cell lysis (MM301 or MM200, Retsch GmbH) with zirconia/silica beads (BioSpec Inc.) for 6 cycles with 3 min shaking (30/s) and 3 min breaks at 4°C. Before the on-column DNase I digest step, an optional wash step (buffer RW1, 5 min incubation) was included, all other steps followed

[5] Bioinformatic analysis was performed by Tobias Straub (LMU/BMC)

the provided protocol and RNA was eluted in 50 µl RNase-free water and concentration was measured on a NanoDrop ND-1000 instrument (PeqLab).

For qPCR-based quantification of mRNA, two alternative methods were used to remove residual genomic DNA contamination. For both methods, isolated RNA was treated with an additional in solution DNase I digest (Qiagen DNaseI, NEB DNaseI incubation buffer) for 15 min at 25°C. For method 1, RNA was then precipitated with NaOAc pH 5.2 (0.3M final) and 70% EtOH (final) for >2 h at -20°C, pelleted by centrifugation (14000 rpm, 15 min, 4°C), washed with 70% EtOH, and resuspended in RNase-free water. For method 2, DNase I was inactivated by denaturation at 75°C for 10 min and RNA was immediately processed for cDNA synthesis. To this end, a Transcriptor First Strand cDNA Synthesis Kit (Roche) was used according to the manufacturer's instructions with oligo dT primers (55°C, 30 min synthesis). Resulting cDNA was diluted 1:5 and qPCR (RT-qPCR) was performed on a Light Cycler 480 instrument (Roche). mRNA-levels were normalized to *ACT1* (in case of *HIS3*) or *PGK1*-levels (others) for each sample and then normalized to the reference sample.

Transcriptome Analysis (RNAseq)[6,7]

Total RNA was isolated as detailed above and samples were further processed and sequenced by the MPI Biochemistry Core Facility (Marja Driessen). Briefly, polyA RNA was enriched (NEBNext Poly(A) mRNA Magnetic Isolation Module #E7490), libraries were prepared for sequencing (NEBNext Ultra II RNA library prep Set for Illumina #E7770L) and barcoded (NEBNext Multiplex Oligo for Illumina #E7335L, #E7500L, #E7710L, #E7730L), all according to the manufacturer's instructions. 75bp single-end reads were obtained by sequencing on an Illumina NextSeq 500 instrument using a NextSeq500/550 High Output kit v2 (75 cycles, Illumina).

Sequencing reads were aligned to the yeast transcriptome (ENSEMBL R64-1-1, annotation version 94) using STAR (v. 2.6.0a). Read counts per gene were provided by STAR and TPM expression values were calculated with RSEM (v. 1.3.0). An unfiltered count table was used for differential expression analysis in DESeq2 (v. 1.22.2). Based on the standard pipeline, size factors and dispersion values were estimated for each gene and a generalized linear model was fitted with a single factor "genotype". Significance testing

[6] Generation of sequencing libraries and sequencing performed by Marja Driessen (MPI Biochemistry Core Facility)
[7] Bioinformatic analysis including gene enrichment analysis performed by Tobias Straub (LMU/BMC)

was based on the Wald test (default parameters). The results were extracted with an alpha of 0.1, an lfcThreshold of 0, and independent filtering (default parameters).

For gene enrichment analysis, sets of up- and downregulated genes upon deletion of *RPD3* (GEO: GSE67151) and *SET2* (GEO: GSE89265) were defined by an adjusted *p*-value cutoff of < 0.1 and a $\log_2$ fold-change cutoff of 1.5 (*rpd3*Δ) and 2 (*set2*Δ). The four gene sets were tested for enrichment on the expression changes observed upon *EUC1* deletion (*euc1*Δ) or overexpression (*pGAL-EUC1*) using fgsea (v. 1.8.0) with 1000 permutations.

6.5 Other Bioinformatic Methods and Software

Slx5 binding site prediction[8]

To identify the putative Euc1 sites responsible for interaction with Slx5, a *de novo* motif prediction was performed with a development version of HH-MOTiF (Prytuliak *et al*, 2017). The input dataset consisted of putative Slx5 substrates identified in a mass spectrometry experiment (I. Psakhye). Additionally, Euc1 as putative Slx5/Slx8 substrate was included. From the obtained candidate motifs, only those containing an instance in the region aa 81–183 of Euc1 were retained. As a result, only three motif candidates passed the filtering procedure. Upon replacement of several charged/hydrophobic residues with alanines in Euc1 aa 81–183, mutations in two candidate binding sites led to decreased interaction with Slx5 in Y2H experiments (Slx5-binding mutant 1/2, SBM1/2).

Online Resources and Software Packages

To retrieve information about and sequences of *S. cerevisiae* genes or proteins, mainly the webpages of the *S. cerevisiae* Genome Database (https://www.yeastgenome.org/), the UniProt Consortium (https://www.uniprot.org/), the National Center for Biotechnology Information (https://www.ncbi.nlm.nih.gov/) were used. Protein structure prediction for Euc1 was performed using Phyre2 (http://www.sbg.bio.ic.ac.uk/phyre2/html/page.cgi?id=index) (Kelley *et al*, 2015), *EUC1* homologs were identified using the Yeast Gene Order Browser (http://ygob.ucd.ie/) (Byrne & Wolfe, 2005), sequence homology was calculated using Clustal Omega (https://www.ebi.ac.uk/Tools/msa/clustalo/) and displayed using Jalview (http://www.jalview.org/), and ub-hotspot sequence conservation was investigated using the 7 yeast Multiz Alignment & Conservation tool of the USCS Genome Browser

[8] Binding site prediction was performed by Roman Prytuliak (MPI Computational Biology Group)

(https://genome.ucsc.edu/). For *in silico* DNA and protein sequence handling, the DNASTAR package (DNASTAR Inc.) or the ApE software (http://jorgensen.biology.utah.edu/wayned/ape/) was used. ChIP-chip data were visualized using R/Bioconductor and the Integrated Genome Browser (https://bioviz.org/). For analysis and presentation of quantitative data, Microsoft Excel or and GraphPad Prism were used routinely. Contrast adjustment for WBs was performed in Adobe Photoshop (Adobe Inc.) with linear adjustment and without highlight/shadow clipping, unless underexposed regions were of specific interest. Alternatively, the ImageStudio Lite software (LI-COR) for WB image processing/quantification and the FIJI software (https://fiji.sc/) for microscopy image processing were used. To create figures and schematics, Adobe Illustrator (Adobe Inc.) was used, and software of the Microsoft Office package (Microsoft Corp.) was used for text and tables. Papers 3 (Digital Science & Research Solution Inc.) was used for reference management.

Data Availability

ChIP-chip and RNAseq data are available from Gene Expression Omnibus (GEO, https://www.ncbi.nlm.nih.gov/geo/) entry GSE118818.

6.6 Material Tables

Table 1. E. Coli Strains

Strain	Genotype	Source
XL1-Blue	*recA1 endA1 gyrA96 thi-1 hsdR17 supE44 relA1 lac* [F´ *proAB lacI*^{q} *ZΔM15* Tn*10* (Tet^{r})]	Agilent
Rosetta 2	F^{-} *ompT hsdS*$_B$(r_B^- m_B^-) *gal dcm* pRARE2 (Cam^R)	Novagen
Rosetta 2 (DE3)	F^{-} *ompT hsdS*$_B$(r_B^- m_B^-) *gal dcm* (DE3) pRARE2 (Cam^R)	Novagen

Table 2. S. Cerevisiae Strains

All yeast strains used in this study are isogenic to DF5 (Finley *et al*, 1987), unless noted otherwise in the table below. If possible, all strains were generated by mating and sporulation, or by genetic modification of diploid strains and subsequent sporulation (see below). Diploid strains marked with (*) were sporulated and haploid strains were used for testing of genetic interactions (not listed).

Strain	Relevant Genotype	Ref./Source
DF5	*trp1-1 ura3-52 his3Δ200 leu2-3,11 lys2-801*	(Finley et al, 1987)
MJK102	*DF5, Mata ubx5::kanMX4*	(Kern, 2013)
MJK503	*DF5, MATα cdc48-3::LEU2*	(Kern, 2013)
MJK354	*DF5, MATα cdc48-6 YIplac128-Ub-HS4-F7::LEU2*	(Kern, 2013)
MJK355	*DF5, MATα cdc48-6 YIplac128-Ub-HS4-F7-Mut::LEU2*	(Kern, 2013)
YM4271	*MATa, ura3-52, his3-200, ade2-101, ade5, lys2-801, leu2-3, 112, trp1-901, tyr1-501, gal4D, gal8D, ade5::hisG*	Clontech
MJK391	*YM4271, ubx5::hphNT1 YIplac211-3xUb-HS4-F7-min.promoter-HIS3::URA3*	(Kern, 2013)
MJK447	*YM4271, ubx5::hphNT1 YIplac211-3xUb-HS4-F7-min.promoter-HIS3::URA3 euc1::natNT2*	(Kern, 2013)
MJK448	*DF5, MATa euc1::natNT2*	(Kern, 2013)
PJ69-7A	*trp-901-, leu2-3,112 ura3-53 his3-200 gal4 gal80 GAL1::HIS GAL2-ADE2 met2::GAL7-lacZ*	(James et al, 1996)
MH093	*PJ69-7A, euc1::natNT2*	This study
MH443	*PJ69-7A, slx8::caURA3MX4*	This study
MH719	*PJ69-7A, euc1::hphNT1*	This study
MH725	*PJ69-7A, siz1::kanMX4 siz2::natNT2 euc1::hphNT1*	This study
MJK612	*DF5, MATa euc1-K231R::URA3*	(Kern, 2013)
MJK567	*DF5, MATa Slx8-9myc::kanMX4*	(Kern, 2013)
MJK569	*DF5, MATa Slx8-9myc::kanMX4 euc1::natNT2*	(Kern, 2013)
MJK609	*DF5, MATa Slx8-9myc::kanMX4 ubc9-1::URA3*	(Kern, 2013)
MJK617	*DF5, MATa Slx8-9myc::kanMX4 euc1-K231R::URA3*	(Kern, 2013)
MJK571	*DF5, MATa Slx8-9myc::kanMX4 cdc48-3::LEU2*	(Kern, 2013)
MJK579	*DF5, MATa slx5::HIS3MX6*	(Kern, 2013)
MJK595	*DF5, MATa slx8::hphNT1*	(Kern, 2013)
MJK604	*DF5, MATa pSMT3-smt3KRall-tSMT3*	I. Psakhye
MJK621	*DF5, MATa pSMT3-smt3KRall-tSMT3 ubx5::NatMX*	M. J. Kern
MH491	*DF5, MATa pADH-3HA-Slx5::NatNT2*	This study
MH499	*DF5, MATa pADH-3HA-Slx5::NatNT2 cdc48-3::LEU2*	This study
MH470	*DF5, MATa pADH-3HA-Slx5::NatNT2 euc1::kanMX4*	This study
MH497	*DF5, MATa pADH-3HA-Slx5::NatNT2 Euc1-K231R::URA3*	This study
MH493	*DF5, MATa pADH-3HA-Slx5::NatNT2 slx8::HIS3MX4*	This study
MH489	*DF5, MATa slx5::HIS3MX6 Slx8-9myc::kanMX4*	This study
MH745	*DF5, MATα euc1::kanMX4*	This study
MH743	*DF5, MATα euc1::kanMX4 YIplac211-pADH-HisSUMO-tADH::URA3*	This study
MH744	*DF5, MATa euc1::kanMX4 YIplac211-pADH-HisUb-tADH::URA3*	This study

MH747	*DF5, MATa euc1::kanMX4 slx8-C206S,C209S::NatNT2 YIplac211-pADH-HisUb-tADH::URA3*	This study
MH649	*DF5, MATa euc1::kanMX4 slx8-C206S,C209S-tADH::NatNT2*	This study
MH845	*DF5, MATa euc1::kanMX4 YIplac211-pADH-HisUbi-tADH::URA3 slx5::HIS3MX4*	This study
MH850	*DF5, MATa euc1::kanMX4 YIplac211-pADH-HisUbi-tADH::URA3 cdc48-3::LEU2*	This study
MH629-1a1	*DF5, MATa EUC1-tADH::caURA3*	This study
MH630-2a1	*DF5, MATa euc1-K231R-tADH::caURA3*	This study
MH632-2a1	*DF5, MATa euc1-W333A,R334A-tADH::caURA3*	This study
MHY501 = MH934	*MATα his3-Δ200 leu2-3,112 ura3-52 lys2-801 trp1-1*	(Chen et al, 1993)
MHY3712 = MH935	*MATα his3-Δ200 leu2-3,112 ura3-52 lys2-801 trp1-1 slx5::kanMX4*	(Xie et al, 2007)
MH1047	*DF5, Mata YIplac211-MED11::URA3*	This study
MH1074	*DF5, Mata YIplac211-MED11::URA3 euc1::natNT2*	This study
MH1172	*DF5, Mata YIplac211-MED11::URA3 htz1::hphNT1*	This study
MH1173	*DF5, Mata YIplac211-MED11::URA3 htz1::hphNT1 euc1::natNT2*	This study
MH1174	*DF5, Mata YIplac211-MED11::URA3 stb5::hphNT1*	This study
MH1175	*DF5, Mata YIplac211-MED11::URA3 euc1::natNT2 stb5::hphNT1*	This study
MH1221	*DF5, Mata YIplac211-MED11::URA3 npl3::hphNT1*	This study
MH1222	*DF5, Mata YIplac211-MED11::URA3 euc1::natNT2 npl3::hphNT1*	This study
MH1158	*DF5, Mata YIplac211-MED11::URA3 dep1::kanMX4*	This study
MH1159	*DF5, Mata YIplac211-MED11::URA3 euc1::natNT2 dep1::kanMX4*	This study
MH1160	*DF5, Mata YIplac211-MED11::URA3 rxt2::kanMX4*	This study
MH1161	*DF5, Mata YIplac211-MED11::URA3 euc1::natNT2 rxt2::kanMX4*	This study
MH1164	*DF5, Mata YIplac211-MED11::URA3 sds3::kanMX4*	This study
MH1165	*DF5, Mata YIplac211-MED11::URA3 euc1::natNT2 sds3::kanMX4*	This study
MH1229	*DF5, Mata YIplac211-MED11::URA3 rco1::hph*	This study
MH1230	*DF5, Mata YIplac211-MED11::URA3 euc1::natNT2 rco1::hph*	This study
MH1231	*DF5, Mata YIplac211-MED11::URA3 sds3::kanMX4 rco1::hph*	This study
MH1232	*DF5, Mata YIplac211-MED11::URA3 euc1::natNT2 sds3::kanMX4 rco1::hph*	This study
MH1233	*DF5, Mata YIplac211-MED11::URA3 eaf3::hph*	This study
MH1234	*DF5, Mata YIplac211-MED11::URA3 euc1::natNT2 eaf3::hph*	This study
MH1235	*DF5, Mata YIplac211-MED11::URA3 sds3::kanMX4 eaf3::hph*	This study
MH1236	*DF5, Mata YIplac211-MED11::URA3 euc1::natNT2 sds3::kanMX4 eaf3::hph*	This study
MH1189	*DF5, Mata YIplac211-MED11::URA3 swr1::hphNT1*	This study
MH1190	*DF5, Mata YIplac211-MED11::URA3 euc1::natNT2 swr1::hphNT1*	This study
MH1237	*DF5, Mata YIplac211-MED11::URA3 yaf9::hph*	This study
MH1238	*DF5, Mata YIplac211-MED11::URA3 euc1::natNT2 yaf9::hph*	This study
MH578	*DF5, Mata npl3::hphNT1*	This study
MH580	*DF5, Mata npl3::hphNT1 euc1::natNT2*	This study
MH1162	*DF5, Mata YIplac211-MED11::URA3 sin3::kanMX4*	This study
MH1163	*DF5, Mata YIplac211-MED11::URA3 euc1::natNT2 sin3::kanMX4*	This study
MH1203	*DF5, Mata YIplac211-MED11::URA3 rpd3::kanMX4*	This study
MH1204	*DF5, Mata YIplac211-MED11::URA3 euc1::natNT2 rpd3::kanMX4*	This study
MH1151*	*DF5, Mata/α YIplac211-MED11::URA3 euc1::natNT2 ume6::kanMX4*	This study
MH1178*	*DF5, Mata/α cim3-1 YIplac211-MED11::URA3 euc1::natNT2*	This study
Y0351	*DF5, Matα ura3, his3, trp1, rpn12-1*	Kominami 1994
MH1184	*DF5, Matα ura3, his3, trp1, rpn12-1 euc1::natNT2*	This study

MH1180*	*DF5, Mata/α YIplac211-MED11::URA3 euc1::natNT2 doa1::kanMX4*	This study
MH1181*	*DF5, Mata/α YIplac211-MED11::URA3 euc1::natNT2 sem1::kanMX4*	This study
MH1182*	*DF5, Mata/α YIplac211-MED11::URA3 euc1::natNT2 san1::kanMX4*	This study
MH1126*	*DF5, Mata/α YIplac211-MED11::URA3 euc1::natNT2 snu66::kanMX6*	This study
MH1127*	*DF5, Mata/α YIplac211-MED11::URA3 euc1::natNT2 hub1::LEU2*	This study
MH1146*	*DF5, Mata/α YIplac211-MED11::URA3 euc1::natNT2 snt309::kanMX4*	This study
MH1129*	*DF5, Mata/α YIplac211-MED11::URA3 euc1::natNT2 bre1::kanMX4*	This study
MH1130*	*DF5, Mata/α YIplac211-MED11::URA3 euc1::natNT2 ubp8::hphNT1*	This study
MH1131*	*DF5, Mata/α YIplac211-MED11::URA3 euc1::natNT2 rad6::HIS3*	This study
MH1132*	*DF5, Mata/α YIplac211-MED11::URA3 euc1::natNT2 htb2::hphNT1 htb1-K123R::kanMX4*	This study
MH1227	*DF5, Mata YIplac211-MED11::URA3 mot3::kan*	This study
MH1228	*DF5, Mata YIplac211-MED11::URA3 euc1::natNT2 mot3::kan*	This study
MH1153*	*DF5, Mata/α YIplac211-MED11::URA3 euc1::natNT2 yef1::kanMX4*	This study
MH1154*	*DF5, Mata/α YIplac211-MED11::URA3 euc1::natNT2 rpl6b::kanMX4*	This study
MH1155*	*DF5, Mata/α YIplac211-MED11::URA3 euc1::natNT2 mco14::kanMX4*	This study
MH1176	*DF5, Mata YIplac211-MED11::URA3 nup133::hphNT1*	This study
MH1177	*DF5, Mata YIplac211-MED11::URA3 euc1::natNT2 nup133::hphNT1*	This study
MH063	*DF5, Mata pGPD-EUC1::natNT2*	This study
Y2726	*W303 (RAD5), Mata leu2-3,112 ade2-1 can1-100 his3-11,15 ura3-1 trp1-1*	Xiaolan Zhao
MH1125	*W303 (RAD5), Mata euc1::natNT2 leu2-3,112 ade2-1 can1-100 his3-11,15 ura3-1 trp1-1*	This study
MH1133	*W303 (RAD5), Mata euc1::natNT2 YIplac211-pGAL-empty-tADH::URA3*	This study
MH1134	*W303 (RAD5), Mata euc1::natNT2 YIplac211-pEUC1-EUC1::URA3*	This study
MH1135	*W303 (RAD5), Mata euc1::natNT2 YIplac211-pGAL-EUC1-tADH::URA3*	This study
MH1136	*W303 (RAD5), Mata euc1::natNT2 YIplac211-pGAL-euc1-KR-tADH::URA3*	This study
MH1137	*W303 (RAD5), Mata euc1::natNT2 YIplac211-pGAL-euc1-SBM1+2-tADH::URA3*	This study
MH1138	*W303 (RAD5), Mata euc1::natNT2 YIplac211-pGAL-euc1-KR-SBM1+2-tADH::URA3*	This study
MH1139	*W303 (RAD5), Mata euc1::natNT2 YIplac211-pGAL-euc1-333WR>AA334-tADH::URA3*	This study
MH1140	*W303 (RAD5), Mata euc1::natNT2 YIplac211-pGAL-euc1-ΔN30-tADH::URA3*	This study
MH1141	*W303 (RAD5), Mata euc1::natNT2 YIplac211-pGAL-euc1-Δ104-129(F104>L)-tADH::URA3*	This study
MH1191	*DF5, Mata YIplac211-MED11::URA3 slx5::HIS3MX6*	This study
MH1192	*DF5, Mata YIplac211-MED11::URA3 sds3::kanMX4 slx5::HIS3MX6*	This study
MH1193	*DF5, Mata YIplac211-MED11::URA3 euc1::natNT2 slx5::HIS3MX6*	This study
MH1194	*DF5, Mata YIplac211-MED11::URA3 euc1::natNT2 sds3::kanMX4 slx5::HIS3MX6*	This study
MH417	*DF5, Mata/α Slx8::hphNT1 pGPD-EUC1::NatNT2*	This study
MH1239	*DF5, Mata/α slx5::HIS3MX4 pGPD-EUC1::natNT2*	This study
MH709	*YM4271, Mata YIplac211-3xub-HS4-pHIS3min-HIS3 euc1::kanMX4*	This study
MH713	*YM4271, Mata YIplac211-3xub-HS4-pHIS3min-HIS3 euc1::kanMX4 ubx5::hphNT1*	This study
MH714	*YM4271, Mata YIplac211-3xub-HS4-pHIS3min-HIS3 euc1::kanMX4 slx5::natNT2*	This study
MH715	*YM4271, Mata YIplac211-3xub-HS4-pHIS3min-HIS3 euc1::kanMX4 slx8-C206S,C209S-tADH::natNT2*	This study
MH727	*YM4271, Mata YIplac211-3xub-HS4-pHIS3min-HIS3 euc1::kanMX4 siz1::hphNT1 siz2::natNT2*	This study
MH868	*YM4271, Mata YIplac211-ub-HS5-100bp-flanking-pHIS3min-HIS3 euc1::kanMX4*	This study
MH965	*YM4271, Mata YIplac211-ub-HS5-100bp-flanking-pHIS3min-HIS3 euc1::kanMX4 siz1::hphNT1 siz2::natNT2*	This study
MH966	*YM4271, Mata YIplac211-ub-HS5-100bp-flanking-pHIS3min-HIS3 euc1::kanMX4 slx5::natNT2*	This study
MH967	*YM4271, Mata YIplac211-ub-HS5-100bp-flanking-pHIS3min-HIS3 euc1::kanMX4 slx8::hphNT1*	This study

MH968	*YM4271, Mata YIplac211-ub-HS5-100bp-flanking-pHIS3min-HIS3 euc1::kanMX4 ubx5::hphNT1*	This study
MH1109	*DF5, Mata natNT2::pADH-GFP-EUC1*	This study
MH1166	*DF5, Matα natNT2::pADH-GFP-euc1-K231R-tADH::caURA3*	This study
MH1169	*DF5, Mata natNT2::pADH-GFP-euc1-333WR>AA334-tADH::caURA3*	This study
MJK347	*W303 (RAD5), Mata YIplac211-pGAL-empty-tADH::URA3*	(Kern, 2013)
MJK534	*W303 (RAD5), Mata YIplac211-pGAL-EUC1-tADH::URA3*	(Kern, 2013)
MH1199	*DF5, Mata YIplac211-MED11::URA3 slx8::hphNT1*	This study
MH1200	*DF5, Mata YIplac211-MED11::URA3 sds3::kanMX4 slx8::hphNT1*	This study
MH1201	*DF5, Mata YIplac211-MED11::URA3 euc1::natNT2 slx8::hphNT1*	This study
MH1202	*DF5, Matα YIplac211-MED11::URA3 euc1::natNT2 sds3::kanMX4 slx8::hphNT1*	This study

Table 3. Plasmids and Vectors

Standard yeast vectors were used for molecular cloning procedures as described (Mumberg *et al*, 1995; James *et al*, 1996; Gietz & Sugino, 1988). Positions for all protein truncation constructs refer to amino acid (aa) positions in WT proteins.

Plasmid	**Construct**	**Ref./Source**
pMax144	*YIplac128-Ub-HS4-F7*	(Kern, 2013)
pMax145	*YIplac128-Ub-HS4-F7-mut*	(Kern, 2013)
pMax197	*YIplac211-min.promotor-HIS3*	(Kern, 2013)
pMax193	*YIplac211-3xUb-HS4-F7-min.promoter-HIS3*	(Kern, 2013)
pGAD-C1	*Gal4-AD*	(James *et al*, 1996)
pGBD-C1	*Gal4-BD*	(James *et al*, 1996)
pMax209	*pGAD-EUC1*	(Kern, 2013)
pMax198	*pGBD-EUC1*	(Kern, 2013)
pMax242	*pGAD-euc1-K231R*	(Kern, 2013)
pMH237	*pGAD-EUC1-aa16-end*	This study
pMH238	*pGAD-EUC1-aa31-end*	This study
p415-ADH	*p415-pADH-empty*	(Mumberg *et al*, 1995)
pMH281	*p415-ADH-3FLAG-EUC1*	This study
pMH282	*p415-ADH-3FLAG-EUC1-K231R*	This study
pMH120	*pGAD-EUC1-81-183*	This study
pMH53	*pGBD-SLX5*	This study
pMH55	*pGBD-SLX5-1-487 (RINGΔ)*	This study
pMH11	*p415-pEUC1-empty*	This study
pMH197	*p415-pEUC1-3FLAG-EUC1*	This study
pMH198	*p415-pEUC1-3FLAG-EUC1-KR*	This study
pMH217	*p415-pEUC1-3FLAG-EUC1-W333A,R334A (DBD*)*	This study
pMH294	*p415-pEUC1-3FLAG-EUC1-SBM1*	This study
pMH295	*p415-pEUC1-3FLAG-EUC1-SBM2*	This study
pMH296	*p415-pEUC1-3FLAG-EUC1-SBM1+2*	This study
pMH300	*p415-pEUC1-3FLAG-EUC1-KR-SBM1*	This study
pMH301	*p415-pEUC1-3FLAG-EUC1-KR-SBM2*	This study
pMH302	*p415-pEUC1-3FLAG-EUC1-KR-SBM1+2*	This study
pMH124	*pGAD-EUC1-81-183_SBM1*	This study

pMH125	*pGAD-EUC1-81-183_SBM2*	This study
pMH135	*pGAD-EUC1-81-183_SBM1+2*	This study
pMH57	*pGBD-SLX5-1-337*	This study
pMH264	*pGBD-SLX5-201-335 (Md)*	This study
pMH266	*pGBD-SLX5-1-200,339-end (MdΔ)*	This study
pMH318	*p415-pADH-3FLAG-EUC1-SBM1*	This study
pMH319	*p415-pADH-3FLAG-EUC1-SBM2*	This study
pMH320	*p415-pADH-3FLAG-EUC1-SBM1+2*	This study
pMH321	*p415-pADH-3FLAG-EUC1-KR-SBM1*	This study
pMH322	*p415-pADH-3FLAG-EUC1-KR-SBM2*	This study
pMH323	*p415-pADH-3FLAG-EUC1-KR-SBM1+2*	This study
p414-ADH	*p414-pADH-empty*	(Mumberg *et al*, 1995)
pMH326	*p414-pSLX5-NLS-3HA-SLX5*	This study
pMH327	*p414-pSLX5-NLS-3HA-SLX5_SIM1-5mut (SIM*)*	This study
pMH330	*p414-pSLX5-NLS-3HA-SLX5_1-200_339-end (MdΔ)*	This study
pMH146	*pGAD-EUC1-240-462*	This study
pMH147	*pGAD-EUC1-291-462*	This study
pMH148	*pGAD-EUC1-291-335*	This study
pMH149	*pGAD-EUC1-291-385*	This study
pMH150	*pGAD-EUC1-291-425*	This study
pMH151	*pGAD-EUC1-336-462*	This study
pMH152	*pGAD-EUC1-386-462*	This study
pMH153	*pGAD-EUC1-426-462*	This study
pMH157	*pGAD-EUC1-W333A,R334A (DBD*)*	This study
D2431	*YEplac195-pADH-BD-tADH*	(Moldovan *et al*, 2006)
pMH273	*YEplac195-pADH-EUC1-1-30-HA-BD-tADH*	This study
pMH268	*YEplac195-pADH-EUC1-1-295-HA-BD-tADH*	This study
pMH269	*YEplac195-pADH-EUC1-1-295KR-HA-BD-tADH*	This study
pMH63	*pGAD-EUC1-1-220*	This study
pMH77	*pGAD-EUC1-1-183*	This study
pMH78	*pGAD-EUC1-1-140*	This study
pMH79	*pGAD-EUC1-1-100*	This study
pMH64	*pGAD-EUC1-1-60*	This study
pMH68	*pGAD-EUC1-161-220*	This study
pMH82	*pGAD-EUC1-121-220*	This study
pMH81	*pGAD-EUC1-81-220*	This study
pMH80	*pGAD-EUC1-41-220*	This study
pMH222	*pGBD-EUC1-81-183*	This study
pMH261	*pGAD-EUC1_Δ104-129 (F104>L), (CCΔ)*	This study
pMH222	*pGBD-EUC1-81-183*	This study
pMH223	*pGBD-EUC1-81-183_SBM1*	This study
pMH224	*pGBD-EUC1-81-183_SBM2*	This study
pMH225	*pGBD-EUC1-81-183_SBM1+2*	This study
pMH249	*pGBD-SLX5-1-275*	This study
pMH250	*pGBD-SLX5-1-200*	This study

pMH251	*pGBD-SLX5-1-145*	This study
pMH252	*pGBD-SLX5-1-90*	This study
pMH253	*pGBD-SLX5-1-50*	This study
pMH324	*p414-pSLX5-NLS-3HA*	This study
pMH333	*p414-pSLX5-3HA-SLX5*	This study
pMH334	*p414-pSLX5-3HA-SLX5_SIM1-5mut (SIM*)*	This study
pMH337	*p414-pSLX5-3HA-SLX5_1-200_339-end (MdΔ)*	This study
pMH14	*p415-pEUC1-EUC1*	This study
pMH291	*p415-pEUC1-EUC1-SBM1*	This study
pMH292	*p415-pEUC1-EUC1-SBM2*	This study
pMH293	*p415-pEUC1-EUC1-SBM1+2*	This study
pMH368	*p415-pGAD-C1-EUC1-SBM1*	This study
pMH369	*p415-pGAD-C1-EUC1-SBM2*	This study
pMH370	*p415-pGAD-C1-EUC1-SBM1+2*	This study
pMH365	*p415-pMET25-a2(103-189)-URA3-3HA-6His*	(Hickey & Hochstrasser, 2015)
pMH190	*YCplac111-MED11 (ORF + 479us-307ds)*	This study
pMH191	*YCplac111-EUC1 (ORF + 403us-328ds)*	This study
pMH447	*p413-pADH-SLX5-tCYC1*	This study
pMH218	*p414-pADH-SLX8-tADH*	This study
pMH15	*p415-pEUC1-euc1-K231R*	This study
pMH299	*p415-pEUC1-euc1-K231R-SBM1+2**	This study
pMH367	*p415-pEUC1-euc1-W333A,R334A (DBD*)*	This study
pMH244	*p415-pEUC1-euc1-aa31-end (N30Δ)*	This study
pMH260	*p415-pEUC1-euc1-Δ104-129 (F104>L) (CCΔ)*	This study
pMH101	*pET28a-6His-Slx5*	(Yang *et al*, 2006)
pGEX-4T3	*pGEX-4T3-GST*	GE Healthcare
pMax212	*pGEX-4T3-GST-EUC1*	M. J. Kern
V0001	*YIplac211-pGAL-empty-tADH*	Jentsch vector collection
pMH405	*YIplac211-pEUC1-EUC1 (ORF + 403us-328ds)*	This study
pMH430	*YIplac211-pGAL-EUC1-tADH*	This study
pMH431	*YIplac211-pGAL-euc1-KR-tADH*	This study
pMH432	*YIplac211-pGAL-euc1-SBM1+2-tADH*	This study
pMH433	*YIplac211-pGAL-euc1-KR-SBM1+2-tADH*	This study
pMH434	*YIplac211-pGAL-euc1-W333A,R334A-tADH*	This study
pMH435	*YIplac211-pGAL-euc1-ΔN30-tADH*	This study
pMH436	*YIplac211-pGAL-euc1-Δ104-129(F104>L)-tADH*	This study
pMH311	*YIplac211-ub-HS5-100bp-flanking-pHIS3min-HIS3*	This study
pMH201	*pGAD-EUC1-tADH-pTEF1-caURA3-tTEF1*	This study
pMH202	*pGAD-euc1-K231R-tADH-pTEF1-caURA3-tTEF1*	This study
pMH204	*pGAD-euc1-W333A,R334A -tADH-pTEF1-caURA3-tTEF1*	This study
pMH212	*pGAD-slx8-C206S,C209S-tADH-natNT2*	This study
pMH39	*pET28a-6His-Slx5_1-487*	This study
pMH40	*pGEX-4T3-GST-Slx5_1-487*	This study
pMH41	*pET28a-6His-Slx8*	This study
pMH42	*pGEX-4T3-GST-Slx8*	This study

Table 4. Primary Antibodies

Antigen	Use	Type	Source
anti-Myc (9E10)	ChIP (3–5 µl)	monoclonal (mouse IgG)	Sigma
anti-HA (ab9110)	ChIP (3 µl)	polyclonal (rabbit IgG)	Abcam
anti-HA (3F10)	WB (1:500-1:1000)	monoclonal (rat IgG)	Roche
anti-FLAG-HRP (M2)	WB (1:3000)	monoclonal (mouse, HRP-coupled)	Sigma (F8592)
anti-ubiquitin-K48 (Apu2)	ChIP (4 µl)	monoclonal (rabbit IgG)	Merck/Millipore
anti-ubiquitin (P4D1)	WB (1:1000)	monoclonal (mouse IgG)	Santa Cruz
anti-H2A.Z (= Htz1)	ChIP (3 µl)	polyclonal (rabbit IgG)	Active Motif
anti-Med11 (ab221200)	WB (1:500-1:1000)	polyclonal (rabbit IgG)	Abcam
anti-Dpm1 (5C5A7)	WB (1:500)	monoclonal (mouse IgG)	Invitrogen
anti-Pgk1 (22C5D8)	WB (1:15000)	monoclonal (mouse IgG)	Invitrogen
anti-Gal4-BD (RK5C1)	WB (1:1000)	monoclonal (mouse IgG)	Santa Cruz
anti-Gal4-AD (14-7E10G10)	WB (1:1000)	monoclonal (mouse IgG)	Abcam
IgG (mouse)	ChIP (1.5 µl)	monoclonal (mouse IgG)	Bethyl Laboratories Inc.
anti-Smt3	WB (1:10000)	polyclonal (rabbit IgG)	(Hoege *et al*, 2002)
anti-Ymr111c/Euc1 (aa 292-462)	WB (1:5000/5% BSA) ChIP (1.5 µl)	polyclonal (rabbit IgG)	(Kern, 2013)
anti-Slx5 (aa 1–487)	WB (1:10000) ChIP (2.5 µl)	polyclonal (rabbit IgG)	A. Strasser (self-made)
anti-Slx8	WB (1:10000) ChIP (0.5 µl)	polyclonal (rabbit IgG)	A. Strasser (self-made)

Table 5. Primers for qPCR

Primers for qPCR were typically designed using an online tool (https://www.ncbi.nlm.nih.gov/tools/primer-blast/index.cgi) to amplify 100–200 bp amplicons. All primers used for ChIP-qPCR and RT-qPCR are listed in the table below. Primers labeled with IH- or Max-prefixes were kind gifts from I. Heckmann or M. J. Kern, respectively.

Name	Label	Position	Sequence
ub-HS1_F	Max_420	ChrIII_123537	TTTCTGCCAGTAGCGACACCACACAT
ub-HS1_R	Max_421	ChrIII_123719	ATGACGATGGCAGGGAAAATAGGGCTGT
ub-HS1_motif1_F	MaH_67	ChrIII_123811	GTAACCCTGCGTCACACATGAGAA
ub-HS1_motif1_R	MaH_68	ChrIII_123985	TCACAGTTTACCCGGAGGTCATCA
ub-HS1_motif2_F	MaH_69	ChrIII_125415	TGTTTTATGCGGAAATTGCAGTGGA
ub-HS1_motif2_R	MaH_70	ChrIII_125547	ATGTATGGTTAAGCAGGCTTTGCG
ub-HS2_F	Max_769	ChrIV_358238	CCTTGTCAGATAATGTATGGGTGGTGTG
ub-HS2_R	Max_770	ChrIV_358367	TATTCTTTGTGTTCGCATTCGCTTCCC
ub-HS3_F	Max_698	ChrIV_1087121	AACAATAGAAAAACGCGGGACTCGAT
ub-HS3_R	Max_699	ChrIV_1087280	TGCTAATTTTCAGCCACATCACATGC
ub-HS4_F	Max_373	ChrXIII_309445	TGGAAGCATCACATCGTATGCTACTAGA
ub-HS4_R	Max_374	ChrXIII_309647	TATGTATGCGGCAATGAACTACTCCGA
ub-HS4_motif1+2_F	MaH_71	ChrXIII_308867	TAAAGTGCATTCAAACATCGGCAGG

ub-HS4_motif1+2_R	MaH_72	ChrXIII_309021	CCCACGACAGCGGTATCTATCTTT
ub-HS4_motif3_F	MaH_73	ChrXIII_309619	TTTCGGAGTAGTTCATTGCCGCAT
ub-HS4_motif3_R	MaH_74	ChrXIII_309760	ACGCATCCATGTCGTGTACATTTC
ub-HS5_A_F	Max_437	ChrXIII_413843	AACGACGTACCCACTACGCGTTTGAA
ub-HS5_A_R	Max_438	ChrXIII_414033	AACTGTTGGAATGTGAGGGCGACCTAGT
ub-HS5_B_F	MaH_75	ChrXIII_413474	ATCTGAGCACACACTTCCTCCTGA
ub-HS5_B_R	MaH_76	ChrXIII_413659	GAAATCCTAGCTGCGAACGGGAAA
ub-HS6_F	Max_717	ChrXIII_433645	TCTTTGCACAATGCATTACGTGGGAG
ub-HS6_R	Max_718	ChrXIII_433789	GAGAAATAGATTCAATGCCGTGGCGA
ub-HS7_F	Max_702	ChrXV_168011	TGTTACGCGTTCCATTTGAGAAGCAA
ub-HS7_R	Max_703	ChrXV_168209	CGGCTTTAAACACCCGTGCCTATATT
contr_F (*pTOS1*)	Max_342	ChrII_564535	ACCGACTAATGCGGTCATGGAAAGC
contr_R (*pTOS1*)	Max_343	ChrII_564727	CTTTTCTCGCAAGAAGACTCCAGAATCA
ect-ub-HS_F	Max_433	YI128 backbone	CATTAATGCAGCTGGCACGACAGGTT
ect-ub-HS_R	Max_434	YI128 backbone	ACAATTCCACACAACATACGAGCCGGA
ACT1_F	MaH_90	ORF	GAAATGCAAACCGCTGCTCAATCTTC
ACT1_R	MaH_91	ORF	CAATACCGGCAGATTCCAAACCCAAA
HIS3_F	MaH_557	ORF	TTACCCTCCACGTTGATTGTCTGC
HIS3_R	MaH_558	ORF	AACACCTTTGGTGGAGGGAACATC
ub-only-site1_F	Max_371	ChrIV_1117000	GCATCTATCGTATTCTTGAGTTATTGCGAC
ub-only-site1_R	Max_372	ChrIV_1117000	ATGTCAATACCATCAGGATCTTGCATGA
STI1-CIN5_F	MaH_769	ChrXV_382999	GGACCATCTTTCCTGTCGTTCTCC
STI1-CIN5_r	MaH_770	ChrXV_383175	GCTTAGCGAATGTTGTCATGGAGC
TEC1-us_F	MaH_773	ChrII_408761	TGAATTCGGGAATGTGCGTGTTTC
TEC1-us_R	MaH_774	ChrII_408921	AGCACCATGGATTGCTGATGGTAG
PGK1_F	IH_316	ORF	GTAAGGCTTTGGAGAACCCAACCA
PGK1_R	IH_317	ORF	TGAAGGTGAAAGCCATACCACCAC
ILV5_F	IH_320	ORF	AACTCTTCTTACGCCGTCTGGAAC
ILV5_R	IH_321	ORF	AGAACATACCGTGGATACCACCCA
SSF2_F	MaH_559	ORF	GGCTGTTAAAGATGCTAAAAAGCAACG
SSF2_R	MaH_560	ORF	GAAGATCCATCATCGCTCATTGCAC
EUC1_F	MaH_480	ORF	CCGTCAGTTCTTTCCCTTGAGAGG
EUC1_R	MaH_481	ORF	CGACAACCTTGATGGCTTGGTTTC
HSP12_F	MaH_783	ORF	TGTCCACGACTCTGCCGAAA
HSP12_R	MaH_784	ORF	CAACTTGGACTTGGCGGCTC
SIR2_F	MaH_785	ORF	CCTTCCCACGTTCCCCAAGT
SIR2_R	MaH_786	ORF	TATGCGGAATCGTCCAGCCA
SBH2_F	MaH_787	ORF	AGTTCCACCAGGAGGTCAGC
SBH2_R	MaH_788	ORF	AAGACCCACCGTAACCAGCC
RCO1_F	MaH_794	ORF	CCCAAAATGGCAATAGCGAGGA
RCO1_R	MaH_795	ORF	GTTCGTTCGGCACGACTACG
PFK1_F	MaH_796	ORF	ACTGCTATCCCAGGCCATGT
PFK1_R	MaH_797	ORF	AGCGTCAGTGTTTGGAGAAGC
ALD5_F	MaH_798	ORF	GGGCTCGTCTTGTGACTGGA
ALD5_R	MaH_799	ORF	TGGGACCAAACACTTCCTCCT

CIN5_F	MaH_800	ORF	TGCAAGGCCGGTGACAATAA
CIN5_R	MaH_801	ORF	ATGAAGCTGCCGGTTGGCTA
MRH1_F	MaH_802	ORF	CGGTGCTGACAAATTGGGCT
MRH1_R	MaH_803	ORF	TGGTGTAGCAGCAGGTCTTGG
ADH2_F	MaH_804	ORF	CGTTAAGGCTACCAACGGCG
ADH2_R	MaH_805	ORF	TTCCCCACGTAAGAGCCGAC
CDC19_F	IH_312	ORF	TTACAACCCAAGACCAACCAGAGC
CDC19_R	IH_313	ORF	CTTGTTCAGCAATGACAGCGGTTT

Table 6. Ub-hotspot Name Conversion

Note that for this study and a recent publication (Höpfler *et al*, 2019), the previously described ubiquitin hotspots (Kern, 2013) have been renamed according to the following conversion table.

Ub-hotspot name conversion

This study	Kern 2013, PhD thesis
ub-HS1	ubiquitin hotspot 1
ub-HS2	ubiquitin hotspot 2
ub-HS3	ubiquitin hotspot 3
ub-HS4	ubiquitin hotspot 5
ub-HS5	ubiquitin hotspot 6
ub-HS6	ubiquitin hotspot 7
ub-HS7	ubiquitin hotspot 8
ub-only-site1	ubiquitin hotspot 4
ub-only-site2	ubiquitin hotspot 9

Abbreviations

Abbreviations for nucleotides and amino acids were used according to the standard definitions (1-letter or 3-letter code) and are not specifically listed in this section.

3AT	3-amino-1,2,4-triazol
A. U.	arbitrary units
aa	amino acid(s)
AAA+	ATPases associated with various cellular activities
Ac	acetyl group or acetate
AD	Gal4 (trans-) activation domain
ARM	arginine-rich motif
ATP	adenosine 5'-triphosphate
BD	Gal4 DNA-binding domain
BenzAlc	benzyl alcohol
BER	base excision repair
BMC	Biomedizinisches Centrum München
bp	base pair(s)
C	carboxy (C-terminal/-terminus), also cytoplasm
°C	degree Celsius
CC	coiled-coiled
cDNA	complementary DNA
ChIP	chromatin immunoprecipitation
ChIP-chip	ChIP combined with genome-wide tiling microarrays
CHX	cycloheximide
cl	clone
contr.	control
CRL	Cullin RING ligase
Cy3	cyanine dye 3
Cy5	cyanine dye 5
d	day(s)
D	dextrose
DMSO	dimethyl sulfoxide
DNA	deoxyribonucleic acid
DNase	deoxyribonuclease
dNTP	2'-deoxyribonucleoside-5'-triphosphate
DUB	deubiquitylating enzyme
DSB	DNA double-strand break
DTT	dithiothreitol
E. coli	*Escherichia coli*
e.g.	exempli gratia, for example
E1	activating enzyme
E2	conjugating enzyme
E3	ligase
E4	chain elongating ligase
ECL	enhanced chemiluminescence
EDTA	ethylenediaminetetraacetic acid
ER	endoplasmic reticulum
ERAD	ER-associated degradation
EtOH	ethyl alcohol
Euc1	Enriches ubiquitin on chromatin 1
FDR	false discovery rate
g	gram
g	gravity
G1	gap 1 (cell cycle phase)
G2	gap 2 (cell cycle phase)
G418	geneticine disulfate
Gal	galactose
GEO	Gene Expression Omnibus
GFP	green fluorescent protein
GINS	go-ichi-ni-san
GST	glutathione S-transferase
h	hour(s)
H. sapiens	*Homo sapiens*
HA	influenza hemagglutinin epitope
HAT	histone acetyltransferase
HDAC	histone deacetylase
HECT	homologous to the E6-AP carboxyl terminus
HEPES	(4-(2-hydroxyethyl)-1-piperazineethanesulfonic acid
His	histidine
HMW	high molecular weight
Hph	hygromycin B
hphNT1	gene conferring resistance to hygromycin
HR	homologous recombination
HRP	horseradish peroxidase
HU	hydroxyurea
i.e.	id est, in other words
IgG	immunoglobulin G
INQ	intranuclear quality control compartment
IP	immunoprecipitation
JAMM	JAB1/MPN/MOV34
kanMX6	gene conferring resistance to G418
kb	kilo base pair(s)
kDa	kilo Dalton
l	liter(s)
LB	lysogeny broth

LMU	Ludwig-Maximilians-University Munich
log	logarithmic
M	molar
m	milli (x10^{-3})
Md	middle domain
$M_{N/C}$	middle domain N-/C-terminal
M-phase	mitotic phase
µ	micro (x10^{-6})
µm	micrometre(s)
MCM	minichromosome maintenance
MDa	mega Dalton
min	minute(s)
MINDY	motif interacting with ubiquitin DUB family
MOPS	3-(N-morpholino) propanesulfonic acid
MPI	Max-Planck-Institute
mRNA	messenger RNA
Myc	c-Myc epitope
N	amino (N-terminal/-terminus), also nucleus
n	nano (x10^{-9})
n	sample size
NAT	nourseothricin
natNT2	gene conferring resistance to nourseothricin
NEB	New England Biolabs
NEM	N-ethylmaleimide
NER	nucleotide excision repair
NES	normalized enrichment score
NFκB	nuclear factor kappa-light-chain-enhancer of activated B cells
NHEJ	non-homologous end joining
NiNTA	Ni^{2+} nitrilotriacetic acid
NLS	nuclear localization signal
norm.	normalized
nm	nanometre(s)
NP-40	nonidet p-40
NPC	nuclear pore complex
OD_{600}	optical density at 600 nm wavelength
ORF	open reading frame
OTU	ovarian tumor protease
p	promoter (with gene names)
p-value, pval	probability value
padj	adjusted *p*-value
PAGE	polyacrylamide gel electrophoresis
PBS	phosphate buffered saline
PCNA	proliferating cell nuclear antigen
PCR	polymerase chain reaction
PD	pulldown
PEG	polyethylene glycol
PH	pleckstrin homology
PhD	doctor of philosophy
PML	promyelocytic leukaemia
PNGase	peptide N-glycanase
Pol	polymerase
PRC1	polycomb repressive complex 1
PTM	post-translational modification
PUB	PNGase/ubiquitin-associated
PUL	PLAP, Ufd3 and Lub1
PVDF	polyvinylidene fluoride
QC	quality control
qPCR	quantitative real-time PCR
Rad	radiation
Raf	raffinose
RBR	RING-between-RING
rDNA	ribosomal DNA
Ref.	reference
RING	really interesting new gene
RMA	Robust Multiarray Analysis
RNA	ribonucleic acid
RNase	ribonuclease
RNF	Ring finger protein
rpm	rounds per minute
RT	room temperature
RT-qPCR	reverse transcription followed by qPCR
S	Svedberg
S	SUMO (in figures)
S-phase	synthesis phase
S. cerevisiae	*Saccharomyces cerevisiae*
S. pombe	*Schizosaccharomyces pombe*
SAP	SAF-A/B, Acinus, PIAS
SBM	Slx5-binding mutant
SC	synthetic complete
SCF	Skp, Cullin, F-box
SDS	sodium dodecyl sulfate
sec	second(s)
SENP	sentrin specific protease
SHP	suppressor of high-copy PP1
SIM	SUMO-interacting motif
SPB	spindle pole body
STUbL	SUMO-targeted ubiquitin ligase
Sub	substrate
SUMO	small ubiquitin-like modifier
Swi/Snf	switch/sucrose non-fermentable
t	terminator (with gene names)
TBE	tris, boric acid, EDTA

TBS-T	tris-buffered saline with Tween-20
TCA	trichloro acidic acid
TE	Tris, EDTA
TF	transcription factor
TGFβ	transforming growth factor β
Tris	Tris(hydroxymethyl)-aminomethane
tRNA	transfer RNA
Ub, ub	ubiquitin
ub-HS	ubiquitin hotspot
UBA	ubiquitin-associated domain
Ubc	ubiquitin conjugating
UBD	ubiquitin-binding domain
UBL	ubiquitin-like
UBX	ubiquitin regulatory X
UBZ	ubiquitin-binding zing finger
UCH	ubiquitin C-terminal hydrolase
Ufd	ubiquitin-fusion degradation
UIM	ubiquitin-interacting motif
ULP	ubiquitin-like protease
UPS	ubiquitin–proteasome system
us	upstream
USP	ubiquitin-specific protease
UTR	untranslated region
UV	ultraviolet
V	Volt
v/v	volume per volume
VBM	VCP binding motif
VCP	valosine-containing protein
VIM	VCP-interacting motif
vs.	versus
WB	western blot
WCE	whole cell extract
WGA	Whole Genome Amplification
WT	wild-type
w/v	weight per volume
Y1H	yeast one-hybrid
Y2H	yeast two-hybrid
YPD	yeast extract, peptone, dextrose
ZnF	zinc finger

References

Abbas T & Dutta A (2017) Regulation of Mammalian DNA Replication via the Ubiquitin-Proteasome System. *Adv. Exp. Med. Biol.* **1042:** 421–454

Abed M, Barry KC, Kenyagin D, Koltun B, Phippen TM, Delrow JJ, Parkhurst SM & Orian A (2011a) Degringolade, a SUMO-targeted ubiquitin ligase, inhibits Hairy/Groucho-mediated repression. *EMBO J* **30:** 1289–1301

Abed M, Bitman-Lotan E & Orian A (2011b) A fly view of a SUMO-targeted ubiquitin ligase. *Fly (Austin)* **5:** 340–344

Ahner A, Gong X, Schmidt BZ, Peters KW, Rabeh WM, Thibodeau PH, Lukacs GL & Frizzell RA (2013) Small heat shock proteins target mutant cystic fibrosis transmembrane conductance regulator for degradation via a small ubiquitin-like modifier–dependent pathway. *Mol Biol Cell* **24:** 74–84

Aparicio O, Geisberg JV, Sekinger E, Yang A, Moqtaderi Z & Struhl K (2005) Chromatin immunoprecipitation for determining the association of proteins with specific genomic sequences in vivo. *Curr Protoc Mol Biol* **Chapter 21:** Unit 21.3

Armstrong AA, Mohideen F & Lima CD (2012) Recognition of SUMO-modified PCNA requires tandem receptor motifs in Srs2. *Nature* **483:** 59–63

Auld KL, Brown CR, Casolari JM, Komili S & Silver PA (2006) Genomic association of the proteasome demonstrates overlapping gene regulatory activity with transcription factor substrates. *Mol Cell* **21:** 861–871

Ausubel FM, Brent R, Kingston RE, Moore DD, Seidman JG, Smith JA & Struhl K eds. (1988) Current Protocols in Molecular Biology. 1st ed. Wiley & Sons, Inc.

Baker LA, Ueberheide BM, Dewell S, Chait BT, Zheng D & Allis CD (2013) The Yeast Snt2 Protein Coordinates the Transcriptional Response to Hydrogen Peroxide-Mediated Oxidative Stress. *Mol Cell Biol* **33:** 3735–3748

Banerjee S, Bartesaghi A, Merk A, Rao P, Bulfer SL, Yan Y, Green N, Mroczkowski B, Neitz RJ, Wipf P, Falconieri V, Deshaies RJ, Milne JLS, Huryn D, Arkin M & Subramaniam S (2016) 2.3 Å resolution cryo-EM structure of human p97 and mechanism of allosteric inhibition. *Science* **351:** 871–875

Bard JAM, Goodall EA, Greene ER, Jonsson E, Dong KC & Martin A (2018) Structure and Function of the 26S Proteasome. *Annu Rev Biochem* **87:** 697–724

Bergink S & Jentsch S (2009) Principles of ubiquitin and SUMO modifications in DNA repair. *Nature* **458:** 461–467

Bergink S, Ammon T, Kern M, Schermelleh L, Leonhardt H & Jentsch S (2013) Role of Cdc48/p97 as a SUMO-targeted segregase curbing Rad51-Rad52 interaction. *Nat Cell Biol* **15:** 526–532

Berner N, Reutter K-R & Wolf DH (2018) Protein Quality Control of the Endoplasmic Reticulum and Ubiquitin–Proteasome-Triggered Degradation of Aberrant Proteins: Yeast Pioneers the Path. *Annu Rev Biochem* **87:** 751–782

Bhogaraju S, Kalayil S, Liu Y, Bonn F, Colby T, Matic I & Dikic I (2016) Phosphoribosylation of Ubiquitin Promotes Serine Ubiquitination and Impairs Conventional Ubiquitination. *Cell* **167:** 1–28

Biedenkapp H, Borgmeyer U, Sippel AE & Klempnauer KH (1988) Viral myb oncogene encodes a sequence-specific DNA-binding activity. *Nature* **335:** 835–837

Biggins S, Bhalla N, Chang A, Smith DL & Murray AW (2001) Genes involved in sister chromatid separation and segregation in the budding yeast Saccharomyces cerevisiae. *Genetics* **159:** 453–470

Billon P & Côté J (2013) Precise deposition of histone H2A.Z in chromatin for genome expression and maintenance. *Biochim Biophys Acta* **1819:** 290–302

Blythe EE, Olson KC, Chau V & Deshaies RJ (2017) Ubiquitin- and ATP-dependent unfoldase activity of P97/VCP•NPLOC4•UFD1L is enhanced by a mutation that causes multisystem proteinopathy. *Proc Natl Acad Sci USA* **4:** 201706205–9

Bodnar NO & Rapoport TA (2017) Molecular Mechanism of Substrate Processing by the Cdc48 ATPase Complex. *Cell* **169:** 722–730.e9

Branigan E, Plechanovová A, Jaffray EG, Naismith JH & Hay RT (2015) Structural basis for the RING-catalyzed synthesis of K63-linked ubiquitin chains. *Nat Struct Mol Biol* **22:** 597–602

Braun S & Madhani HD (2012) Shaping the landscape: mechanistic consequences of ubiquitin modification of chromatin. *EMBO Rep* **13:** 619–630

Buchberger A, Schindelin H & Hänzelmann P (2015) Control of p97 function by cofactor binding. *FEBS Lett* **589:** 2578–2589

Byrne KP & Wolfe KH (2005) The Yeast Gene Order Browser: combining curated homology and syntenic context reveals gene fate in polyploid species. *Genome Res* **15:** 1456–1461

Cadwell K & Coscoy L (2005) Ubiquitination on nonlysine residues by a viral E3 ubiquitin ligase. *Science* **309:** 127–130

Cal-Bąkowska M, Litwin I, Bocer T, Wysocki R & Dziadkowiec D (2011) The Swi2-Snf2-like protein Uls1 is involved in replication stress response. *Nucleic Acids Res* **39:** 8765–8777

Cappadocia L & Lima CD (2018) Ubiquitin-like Protein Conjugation: Structures, Chemistry, and Mechanism. *Chem Rev* **118:** 889–918

Carrozza MJ, Li B, Florens L, Suganuma T, Swanson SK, Lee KK, Shia W-J, Anderson S, Yates J, Washburn MP & Workman JL (2005) Histone H3 methylation by Set2 directs deacetylation of coding regions by Rpd3S to suppress spurious intragenic transcription. *Cell* **123:** 581–592

Catic A, Suh CY, Hill CT, Daheron L, Henkel T, Orford KW, Dombkowski DM, Liu T, Liu XS & Scadden DT (2013) Genome-wide Map of Nuclear Protein Degradation Shows NCoR1 Turnover as a Key to Mitochondrial Gene Regulation. *Cell* **155:** 1380–1395

Chen P, Johnson P, Sommer T, Jentsch S & Hochstrasser M (1993) Multiple ubiquitin-conjugating enzymes participate in the in vivo degradation of the yeast MAT alpha 2 repressor. *Cell* **74:** 357–369

Cheng H, Bao X, Gan X, Luo S & Rao H (2017) Multiple E3s promote the degradation of histone H3 variant Cse4. *Sci Rep* **7:** 1–8

Cheng J, Wang D, Wang Z & Yeh ETH (2004) SENP1 enhances androgen receptor-dependent transcription through desumoylation of histone deacetylase 1. *Mol Cell Biol* **24:** 6021–6028

Churikov D, Charifi F, Eckert-Boulet N, Silva S, Simon M-N, Lisby M & Géli V (2016) SUMO-Dependent Relocalization of Eroded Telomeres to Nuclear Pore Complexes Controls Telomere Recombination. *Cell Rep* **15:** 1–13

Chymkowitch P, Nguéa P A & Enserink JM (2015a) SUMO-regulated transcription: Challenging the dogma. *BioEssays* **37:** 1095–1105

Chymkowitch P, Nguéa P A, Aanes H, Koehler CJ, Thiede B, Lorenz S, Meza-Zepeda LA, Klungland A & Enserink JM (2015b) Sumoylation of Rap1 mediates the recruitment of TFIID to promote transcription of ribosomal protein genes. *Genome Res* **25:** 897–906

Chymkowitch P, Nguéa P A, Aanes H, Robertson J, Klungland A & Enserink JM (2017) TORC1-dependent sumoylation of Rpc82 promotes RNA polymerase III assembly and activity. *Proc Natl Acad Sci USA* **114:** 1039–1044

Cook CE, Hochstrasser M & Kerscher O (2009) The SUMO-targeted ubiquitin ligase subunit Slx5 resides in nuclear foci and at sites of DNA breaks. *Cell Cycle* **8:** 1080–1089

Costanzo A, Gaudio N, Conte L, Dell'Aversana C, Vermeulen M, Thé H, Migliaccio A, Nebbioso A & Altucci L (2018) The HDAC inhibitor SAHA regulates CBX2 stability via a SUMO- triggered ubiquitin-mediated pathway in leukemia. *Oncogene* **37:** 1–14

Costanzo M, Baryshnikova A, Bellay J, Kim Y, Spear ED, Sevier CS, Ding H, Koh JLY, Toufighi K, Mostafavi S, Prinz J, St Onge RP, VanderSluis B, Makhnevych T, Vizeacoumar FJ, Alizadeh S, Bahr S, Brost RL, Chen Y, Cokol M, et al (2010) The genetic landscape of a cell. *Science* **327:** 425–431

Costanzo M, VanderSluis B, Koch EN, Baryshnikova A, Pons C, Tan G, Wang W, Usaj M, Hanchard J, Lee SD, Pelechano V, Styles EB, Billmann M, van Leeuwen J, van Dyk N, Lin Z-Y, Kuzmin E, Nelson J, Piotrowski JS, Srikumar T, et al (2016) A global genetic interaction network maps a wiring diagram of cellular function. *Science* **353:** aaf1420–aaf1420

Cubeñas-Potts C & Matunis MJ (2013) SUMO: a multifaceted modifier of chromatin structure and function. *Dev Cell* **24:** 1–12

Dantuma NP & Hoppe T (2012) Growing sphere of influence: Cdc48/p97 orchestrates ubiquitin-dependent extraction from chromatin. *Trends Cell Biol*. **22:** 483–491

Dantuma NP & van Attikum H (2016) Spatiotemporal regulation of posttranslational modifications in the DNA damage response. *EMBO J* **35:** 6–23

David G, Neptune MA & DePinho RA (2002) SUMO-1 modification of histone deacetylase 1 (HDAC1) modulates its biological activities. *J Biol Chem* **277:** 23658–23663

de Nadal E, Zapater M, Alepuz PM, Sumoy L, Mas G & Posas F (2004) The MAPK Hog1 recruits Rpd3 histone deacetylase to activate osmoresponsive genes. *Nature* **427:** 370–374

DeLaBarre B & Brunger AT (2003) Complete structure of p97/valosin-containing protein reveals communication between nucleotide domains. *Nat Struct Mol Biol* **10:** 856–863

Denison C, Rudner AD, Gerber SA, Bakalarski CE, Moazed D & Gygi SP (2005) A Proteomic Strategy for Gaining Insights into Protein Sumoylation in Yeast. *Mol Cell Proteomics* **4:** 246–254

Deshaies RJ & Joazeiro CAP (2009) RING Domain E3 Ubiquitin Ligases. *Annu Rev Biochem* **78:** 399–434

Desterro JM, Rodriguez MS & Hay RT (1998) SUMO-1 modification of IkappaBalpha inhibits NF-kappaB activation. *Mol Cell* **2:** 233–239

Deveraux Q, Ustrell V, Pickart C & Rechsteiner M (1994) A 26 S protease subunit that binds ubiquitin conjugates. *J Biol Chem* **269:** 7059–7061

Dewar JM & Walter JC (2017) Mechanisms of DNA replication termination. *Nat Rev Mol Cell Biol* **18:** 507–516

Dewar JM, Low E, Mann M, Räschle M & Walter JC (2017) CRL2Lrr1 promotes unloading of the vertebrate replisome from chromatin during replication termination. *Genes Dev* **31:** 275–290

Dikic I (2017) Proteasomal and Autophagic Degradation Systems. *Annu Rev Biochem* **86:** 193–224

Dikic I, Wakatsuki S & Walters KJ (2009) Ubiquitin-binding domains - from structures to functions. *Nat Rev Mol Cell Biol* **10:** 659–671

Dobi KC & Winston F (2007) Analysis of Transcriptional Activation at a Distance in Saccharomyces cerevisiae. *Mol Cell Biol* **27:** 5575–5586

Duan Z, Andronescu M, Schutz K, McIlwain S, Kim YJ, Lee C, Shendure J, Fields S, Blau CA & Noble WS (2010) A three-dimensional model of the yeast genome. *Nature* **465:** 363–367

Elsasser S, Gali RR, Schwickart M, Larsen CN, Leggett DS, Müller B, Feng MT, Tübing F, Dittmar GAG & Finley D (2002) Proteasome subunit Rpn1 binds ubiquitin-like protein domains. *Nat Cell Biol* **4:** 725–730

Enserink JM (2015) Sumo and the cellular stress response. *Cell Division* **10:** 1–13

Erker Y, Neyret-Kahn H, Seeler J-S, Dejean A, Atfi A & Levy L (2013) Arkadia, a novel SUMO-targeted ubiquitin ligase involved in PML degradation. *Mol Cell Biol* **33:** 2163–2177

Espelin CW, Simons KT, Harrison SC & Sorger PK (2003) Binding of the essential Saccharomyces cerevisiae kinetochore protein Ndc10p to CDEII. *Mol Biol Cell* **14:** 4557–4568

Everett RD, Boutell C & Hale BG (2013) Interplay between viruses and host sumoylation pathways. *Nat Rev Microbiol* **11:** 400–411

Finley D, Ozkaynak E & Varshavsky A (1987) The yeast polyubiquitin gene is essential for resistance to high temperatures, starvation, and other stresses. *Cell* **48:** 1035–1046

Finley D, Ulrich HD, Sommer T & Kaiser P (2012) The ubiquitin-proteasome system of Saccharomyces cerevisiae. *Genetics* **192:** 319–360

Flick K, Ouni I, Wohlschlegel JA, Capati C, McDonald WH, Yates JR & Kaiser P (2004) Proteolysis-independent regulation of the transcription factor Met4 by a single Lys 48-linked ubiquitin chain. *Nat Cell Biol* **6:** 634–641

Flotho A & Melchior F (2013) Sumoylation: a regulatory protein modification in health and disease. *Annu Rev Biochem* **82:** 357–385

Franz A, Ackermann L & Hoppe T (2016) Ring of Change: CDC48/p97 Drives Protein Dynamics at Chromatin. *Front Genet* **7:** 73

Franz A, Orth M, Pirson PA, Sonneville R, Blow JJ, Gartner A, Stemmann O & Hoppe T (2011) CDC-48/p97 coordinates CDT-1 degradation with GINS chromatin dissociation to ensure faithful DNA replication. *Mol Cell* **44:** 85–96

Funakoshi M, Sasaki T, Nishimoto T & Kobayashi H (2002) Budding yeast Dsk2p is a polyubiquitin-binding protein that can interact with the proteasome. *Proc Natl Acad Sci USA* **99:** 745–750

Galanty Y, Belotserkovskaya R, Coates J & Jackson SP (2012) RNF4, a SUMO-targeted ubiquitin E3 ligase, promotes DNA double-strand break repair. *Genes Dev* **26:** 1179–1195

Gallagher PS, Oeser ML, Abraham A-C, Kaganovich D & Gardner RG (2013) Cellular maintenance of nuclear protein homeostasis. *Cell Mol Life Sci* **71:** 1865–1879

Gallina I, Colding C, Henriksen P, Beli P, Nakamura K, Offman J, Mathiasen DP, Silva S, Hoffmann E, Groth A, Choudhary C & Lisby M (2015) Cmr1/WDR76 defines a nuclear genotoxic stress body linking genome integrity and protein quality control. *Nat Commun* **6:** 6533

Gareau JR & Lima CD (2010) The SUMO pathway: emerging mechanisms that shape specificity, conjugation and recognition. *Nat Rev Mol Cell Biol* **11:** 861–871

Gaytán BD, Loguinov AV, La Rosa De VY, Lerot J-M & Vulpe CD (2013) Functional genomics indicates yeast requires Golgi/ER transport, chromatin remodeling, and DNA repair for low dose DMSO tolerance. *Front Genet* **4:** 154

Geng F, Wenzel S & Tansey WP (2012) Ubiquitin and Proteasomes in Transcription. *Annu Rev Biochem* **81:** 177–201

Geoffroy M-C, Jaffray EG, Walker KJ & Hay RT (2010) Arsenic-induced SUMO-dependent recruitment of RNF4 into PML nuclear bodies. *Mol Biol Cell* **21:** 4227–4239

Gietz RD & Sugino A (1988) New yeast-Escherichia coli shuttle vectors constructed with in vitro mutagenized yeast genes lacking six-base pair restriction sites. *Gene* **74:** 527–534

Gillies J, Hickey CM, Su D, Wu Z, Peng J & Hochstrasser M (2016) SUMO Pathway Modulation of Regulatory Protein Binding at the Ribosomal DNA Locus in Saccharomyces cerevisiae. *Genetics* **202:** 1377–1394

Goebl MG, Yochem J, Jentsch S, McGrath JP, Varshavsky A & Byers B (1988) The yeast cell cycle gene CDC34 encodes a ubiquitin-conjugating enzyme. *Science* **241:** 1331–1335

Goldknopf IL, French MF, Musso R & Busch H (1977) Presence of protein A24 in rat liver nucleosomes. *Proc Natl Acad Sci USA* **74:** 5492–5495

Green MR & Sambrook J eds. (2012) Molecular Cloning. 4 ed. Cold Spring Harbor Laboratory Press

Groocock LM, Nie M, Prudden J, Moiani D, Wang T, Cheltsov A, Rambo RP, Arvai AS, Hitomi C, Tainer JA, Luger K, Perry JJP, Lazzerini-Denchi E & Boddy MN (2014) RNF4 interacts with both SUMO and nucleosomes to promote the DNA damage response. *EMBO Rep* **15:** 601–608

Guo B & Sharrocks AD (2009) Extracellular signal-regulated kinase mitogen-activated protein kinase signaling initiates a dynamic interplay between sumoylation and ubiquitination to regulate the activity of the transcriptional activator PEA3. *Mol Cell Biol* **29:** 3204–3218

Guo L, Giasson BI, Glavis-Bloom A, Brewer MD, Shorter J, Gitler AD & Yang X (2014) A Cellular System that Degrades Misfolded Proteins and Protects against Neurodegeneration. *Mol Cell* **55:** 15–30

Gurtovenko AA & Anwar J (2007) Modulating the structure and properties of cell membranes: the molecular mechanism of action of dimethyl sulfoxide. *J Phys Chem B* **111:** 10453–10460

Guzzo CM, Berndsen CE, Zhu J, Gupta V, Datta A, Greenberg RA, Wolberger C & Matunis MJ (2012) RNF4-dependent hybrid SUMO-ubiquitin chains are signals for RAP80 and thereby mediate the recruitment of BRCA1 to sites of DNA damage. *Sci Signal* **5:** ra88

Hammond-Martel I, Yu H & Affar EB (2012) Roles of ubiquitin signaling in transcription regulation. *Cell Signal* **24:** 410–421

Hannich JT, Lewis A, Kroetz MB, Li S-J, Heide H, Emili A & Hochstrasser M (2005) Defining the SUMO-modified proteome by multiple approaches in Saccharomyces cerevisiae. *J Biol Chem* **280:** 4102–4110

Hari KL, Cook KR & Karpen GH (2001) The Drosophila Su(var)2-10 locus regulates chromosome structure and function and encodes a member of the PIAS protein family. *Genes Dev* **15:** 1334–1348

Harrigan JA, Jacq X, Martin NM & Jackson SP (2018) Deubiquitylating enzymes and drug discovery: emerging opportunities. *Nat Rev Drug Discov* **17:** 57–78

Hänzelmann P & Schindelin H (2017) The Interplay of Cofactor Interactions and Post-translational Modifications in the Regulation of the AAA+ ATPase p97. *Front Mol Biosci* **4:** 875–22

Hendriks IA & Vertegaal ACO (2016) A comprehensive compilation of SUMO proteomics. *Nat Rev Microbiol* **17:** 581–595

Hetzer M, Meyer HH, Walther TC, Bilbao-Cortes D, Warren G & Mattaj IW (2001) Distinct AAA-ATPase p97 complexes function in discrete steps of nuclear assembly. *Nat Cell Biol* **3:** 1086–1091

Hickey CM & Hochstrasser M (2015) STUbL-mediated degradation of the transcription factor MATα2 requires degradation elements that coincide with corepressor binding sites. *Mol Biol Cell* **26:** 3401–3412

Hickey CM, Xie Y & Hochstrasser M (2018) DNA binding by the MATα2 transcription factor controls its access to alternative ubiquitin-modification pathways. *Mol Biol Cell* **29:** 542–556

Hochstrasser M & Varshavsky A (1990) In vivo degradation of a transcriptional regulator: the yeast alpha 2 repressor. *Cell* **61:** 697–708

Hochstrasser M, Ellison MJ, Chau V & Varshavsky A (1991) The short-lived MAT alpha 2 transcriptional regulator is ubiquitinated in vivo. *Proc Natl Acad Sci USA* **88:** 4606–4610

Hoege C, Pfander B, Moldovan G-L, Pyrowolakis G & Jentsch S (2002) RAD6-dependent DNA repair is linked to modification of PCNA by ubiquitin and SUMO. *Nature* **419:** 135–141

Hofmann K & Bucher P (1996) The UBA domain: a sequence motif present in multiple enzyme classes of the ubiquitination pathway. *Trends Biochem Sci* **21:** 172–173

Hohmann S (2002) Osmotic stress signaling and osmoadaptation in yeasts. *Microbiol Mol Biol Rev* **66:** 300–372

Holland MJ, Yokoi T, Holland JP, Myambo K & Innis MA (1987) The GCR1 gene encodes a positive transcriptional regulator of the enolase and glyceraldehyde-3-phosphate dehydrogenase gene families in Saccharomyces cerevisiae. *Mol Cell Biol* **7:** 813–820

Horigome C, Bustard DE, Marcomini I, Delgoshaie N, Tsai-Pflugfelder M, Cobb JA & Gasser SM (2016) PolySUMOylation by Siz2 and Mms21 triggers relocation of DNA breaks to nuclear pores through the Slx5/Slx8 STUbL. *Genes Dev* **30:** 931–945

Höhfeld J & Hoppe T (2018) Ub and Down: Ubiquitin Exercise for the Elderly. *Trends Cell Biol*. **28:** 512–522

Höpfler M, Kern MJ, Straub T, Prytuliak R, Habermann BH, Pfander B & Jentsch S (2019) Slx5/Slx8-dependent ubiquitin hotspots on chromatin contribute to stress tolerance. *EMBO J***:** e100368

Huie MA, Scott EW, Drazinic CM, Lopez MC, Hornstra IK, Yang TP & Baker HV (1992) Characterization of the DNA-binding activity of GCR1: in vivo evidence for two GCR1-binding sites in the upstream activating sequence of TPI of Saccharomyces cerevisiae. *Mol Cell Biol* **12:** 2690–2700

Husnjak K & Dikic I (2012) Ubiquitin-binding proteins: decoders of ubiquitin-mediated cellular functions. *Annu Rev Biochem* **81:** 291–322

Husnjak K, Elsasser S, Zhang N, Chen X, Randles L, Shi Y, Hofmann K, Walters KJ, Finley D & Dikic I (2008) Proteasome subunit Rpn13 is a novel ubiquitin receptor. *Nature* **453:** 481–488

Ii T, Fung J, Mullen JR & Brill SJ (2007) The yeast Slx5-Slx8 DNA integrity complex displays ubiquitin ligase activity. *Cell Cycle* **6:** 2800–2809

Inoue Y & Imamura T (2008) Regulation of TGF-β family signaling by E3 ubiquitin ligases. *Cancer Science* **99:** 2107–2112

Inui M, Manfrin A, Mamidi A, Martello G, Morsut L, Soligo S, Enzo E, Moro S, Polo S, Dupont S, Cordenonsi M & Piccolo S (2011) USP15 is a deubiquitylating enzyme for receptor-activated SMADs. *Nat Cell Biol* **13:** 1368–1375

James P, Halladay J & Craig EA (1996) Genomic libraries and a host strain designed for highly efficient two-hybrid selection in yeast. *Genetics* **144:** 1425–1436

Janke C, Magiera MM, Rathfelder N, Taxis C, Reber S, Maekawa H, Moreno-Borchart A, Doenges G, Schwob E, Schiebel E & Knop M (2004) A versatile toolbox for PCR-based tagging of yeast genes: new fluorescent proteins, more markers and promoter substitution cassettes. *Yeast* **21:** 947–962

Jentsch S & Psakhye I (2013) Control of nuclear activities by substrate-selective and protein-group SUMOylation. *Annu Rev Genet* **47:** 167–186

Jentsch S & Rumpf S (2007) Cdc48 (p97): a 'molecular gearbox' in the ubiquitin pathway? *Trends Biochem Sci* **32:** 6–11

Jentsch S, McGrath JP & Varshavsky A (1987) The yeast DNA repair gene RAD6 encodes a ubiquitin-conjugating enzyme. *Nature* **329:** 131–134

Johnson ES & Blobel G (1999) Cell cycle-regulated attachment of the ubiquitin-related protein SUMO to the yeast septins. *J. Cell Biol*. **147:** 981–994

Kalocsay M, Hiller NJ & Jentsch S (2009) Chromosome-wide Rad51 spreading and SUMO-H2A.Z-dependent chromosome fixation in response to a persistent DNA double-strand break. *Mol Cell* **33:** 335–343

Kaplun L, Tzirkin R, Bakhrat A, Shabek N, Ivantsiv Y & Raveh D (2005) The DNA damage-inducible UbL-UbA protein Ddi1 participates in Mec1-mediated degradation of Ho endonuclease. *Mol Cell Biol* **25:** 5355–5362

Kelley LA, Mezulis S, Yates CM, Wass MN & Sternberg MJE (2015) The Phyre2 web portal for protein modeling, prediction and analysis. *Nat Protoc* **10:** 845–858

Kern M (2013) Cdc48-dependent Chromatin Ubiquitylation Hotspots in *Saccharomyces Cerevisiae*. Dissertation der Fakultät für Biologie der Ludwig-Maximilians-Universität München. Available at: https://edoc.ub.uni-muenchen.de/21812/1/Kern_Maximilian_Josef.pdf

Kerscher O, Felberbaum R & Hochstrasser M (2006) Modification of proteins by ubiquitin and ubiquitin-like proteins. *Annu Rev Cell Dev Biol* **22:** 159–180

Keusekotten K, Bade VN, Meyer-Teschendorf K, Sriramachandran AM, Fischer-Schrader K, Krause A, Horst C, Schwarz G, Hofmann K, Dohmen RJ & Praefcke GJK (2014) Multivalent interactions of the SUMO-interaction motifs in RING finger protein 4 determine the specificity for chains of the SUMO. *Biochem J* **457:** 207–214

Kim JH, Lee BB, Oh YM, Zhu C, Steinmetz LM, Lee Y, Kim WK, Lee SB, Buratowski S & Kim T (2016) Modulation of mRNA and lncRNA expression dynamics by the Set2–Rpd3S pathway. *Nat Commun* **7:** 1–11

Kirsh O, Seeler J-S, Pichler A, Gast A, Muller S, Miska E, Mathieu M, Harel-Bellan A, Kouzarides T, Melchior F & Dejean A (2002) The SUMO E3 ligase RanBP2 promotes modification of the HDAC4 deacetylase. *EMBO J* **21:** 2682–2691

Knop M, Siegers K, Pereira G, Zachariae W, Winsor B, Nasmyth K & Schiebel E (1999) Epitope tagging of yeast genes using a PCR-based strategy: more tags and improved practical routines. *Yeast* **15:** 963–972

Koegl M, Hoppe T, Schlenker S, Ulrich HD, Mayer TU & Jentsch S (1999) A novel ubiquitination factor, E4, is involved in multiubiquitin chain assembly. *Cell* **96:** 635–644

Koltun B, Shackelford E, Bonnay F, Matt N, Reichhart JM & Orian A (2017) The SUMO-targeted ubiquitin ligase, Dgrn, is essential for Drosophila innate immunity. *Int. J. Dev. Biol.* **61:** 319–327

Komander D & Rape M (2012) The ubiquitin code. *Annu Rev Biochem* **81:** 203–229

Kosoy A, Calonge TM, Outwin EA & O'Connell MJ (2007) Fission yeast Rnf4 homologs are required for DNA repair. *J Biol Chem* **282:** 20388–20394

Kramarz K, Litwin I, Cal-Bąkowska M, Szakal B, Branzei D, Wysocki R & Dziadkowiec D (2014) Swi2/Snf2-like protein Uls1 functions in the Sgs1-dependent pathway of maintenance of rDNA stability and alleviation of replication stress. *DNA Repair (Amst.)* **21:** 24–35

Kumar R, González-Prieto R, Xiao Z, Verlaan-de Vries M & Vertegaal ACO (2017) The STUbL RNF4 regulates protein group SUMOylation by targeting the SUMO conjugation machinery. *Nat Commun* **8:** 1809

Kumar SV & Wigge PA (2010) H2A.Z-containing nucleosomes mediate the thermosensory response in Arabidopsis. *Cell* **140:** 136–147

Kunz K, Piller T & Muller S (2018) SUMO-specific proteases and isopeptidases of the SENP family at a glance. *Journal of Cell Science* **131:** jcs211904

Kuo C-Y, Li X, Kong X-Q, Luo C, Chang C-C, Chung Y, Shih H-M, Li KK & Ann DK (2014) An arginine-rich motif of ring finger protein 4 (RNF4) oversees the recruitment and degradation of the phosphorylated and SUMOylated Krüppel-associated box domain-associated protein 1 (KAP1)/TRIM28 protein during genotoxic stress. *J Biol Chem* **289:** 20757–20772

Kuroha K, Zinoviev A, Hellen CUT & Pestova TV (2018) Release of Ubiquitinated and Non-ubiquitinated Nascent Chains from Stalled Mammalian Ribosomal Complexes by ANKZF1 and Ptrh1. *Mol Cell* **72:** 286–302.e8

Leggett DS, Hanna J, Borodovsky A, Crosas B, Schmidt M, Baker RT, Walz T, Ploegh H & Finley D (2002) Multiple associated proteins regulate proteasome structure and function. *Mol Cell* **10:** 495–507

Lescasse R, Pobiega S, Callebaut I & Marcand SEP (2013) End-joining inhibition at telomeres requires the translocase and polySUMO-dependent ubiquitin ligase Uls1. *EMBO J* **32:** 805–815

Lewicki MC, Srikumar T, Johnson E & Raught B (2014) The S. cerevisiae SUMO stress response is a conjugation-deconjugation cycle that targets the transcription machinery. *J Proteomics*

Li G, Zhao G, Zhou X, Schindelin H & Lennarz WJ (2006) The AAA ATPase p97 links peptide N-glycanase to the endoplasmic reticulum-associated E3 ligase autocrine motility factor receptor. *Proc Natl Acad Sci USA* **103:** 8348–8353

Liakopoulos D, Doenges G, Matuschewski K & Jentsch S (1998) A novel protein modification pathway related to the ubiquitin system. *EMBO J* **17:** 2208–2214

Liang J, Singh N, Carlson CR, Albuquerque CP, Corbett KD & Zhou H (2017) Recruitment of a SUMO isopeptidase to rDNA stabilizes silencing complexes by opposing SUMO targeted ubiquitin ligase activity. *Genes Dev* **31:** 802–815

Lindstrom KC, Vary JC, Parthun MR, Delrow J & Tsukiyama T (2006) Isw1 functions in parallel with the NuA4 and Swr1 complexes in stress-induced gene repression. *Mol Cell Biol* **26:** 6117–6129

Lone MA, Atkinson AE, Hodge CA, Cottier S, Martínez-Montañés F, Maithel S, Mène-Saffrané L, Cole CN & Schneiter R (2015) Yeast Integral Membrane Proteins Apq12, Brl1, and Brr6 Form a Complex Important for Regulation of Membrane Homeostasis and Nuclear Pore Complex Biogenesis. *Eukaryot Cell* **14:** 1217–1227

Lu K, Brave den F & Jentsch S (2017) Receptor oligomerization guides pathway choice between proteasomal and autophagic degradation. *Nat Cell Biol* **11:** 497–20

Lu K, Psakhye I & Jentsch S (2014) Autophagic clearance of polyQ proteins mediated by ubiquitin-Atg8 adaptors of the conserved CUET protein family. *Cell* **158:** 549–563

Luo K, Zhang H, Wang L, Yuan J & Lou Z (2012) Sumoylation of MDC1 is important for proper DNA damage response. *EMBO J* **31:** 3008–3019

Maculins T, Nkosi PJ, Nishikawa H & Labib K (2015) Tethering of SCFDia2 to the Replisome Promotes Efficient Ubiquitylation and Disassembly of the CMG Helicase. *Curr Biol***:** 1–7

Mahajan R, Delphin C, Guan T, Gerace L & Melchior F (1997) A small ubiquitin-related polypeptide involved in targeting RanGAP1 to nuclear pore complex protein RanBP2. *Cell* **88:** 97–107

Marcomini I, Shimada K, Delgoshaie N, Yamamoto I, Seeber A, Cheblal A, Horigome C, Naumann U & Gasser SM (2018) Asymmetric Processing of DNA Ends at a Double-Strand Break Leads to Unconstrained Dynamics and Ectopic Translocation. *Cell Rep* **24:** 2614–2628.e4

Maric M, Maculins T, De Piccoli G & Labib K (2014) Cdc48 and a ubiquitin ligase drive disassembly of the CMG helicase at the end of DNA replication. *Science* **346:** 1253596

Marks PA & Breslow R (2007) Dimethyl sulfoxide to vorinostat: development of this histone deacetylase inhibitor as an anticancer drug. *Nat Biotechnol* **25:** 84–90

Matunis MJ, Coutavas E & Blobel G (1996) A novel ubiquitin-like modification modulates the partitioning of the Ran-GTPase-activating protein RanGAP1 between the cytosol and the nuclear pore complex. *J. Cell Biol*. **135:** 1457–1470

Maytal-Kivity V, Reis N, Hofmann K & Glickman MH (2002) MPN+, a putative catalytic motif found in a subset of MPN domain proteins from eukaryotes and prokaryotes, is critical for Rpn11 function. *BMC Biochem*. **3:** 28

McDaniel SL & Strahl BD (2013) Stress-free with Rpd3: a unique chromatin complex mediates the response to oxidative stress. *Mol Cell Biol* **33:** 3726–3727

McDaniel SL, Hepperla AJ, Huang J, Dronamraju R, Adams AT, Kulkarni VG, Davis IJ & Strahl BD (2017) H3K36 Methylation Regulates Nutrient Stress Response in Saccharomyces cerevisiae by Enforcing Transcriptional Fidelity. *Cell Rep* **19:** 2371–2382

McKnight JN, Boerma JW, Breeden LL & Tsukiyama T (2015) Global Promoter Targeting of a Conserved Lysine Deacetylase for Transcriptional Shutoff during Quiescence Entry. *Mol Cell* **59:** 732–743

McLean JR, Chaix D, Ohi MD & Gould KL (2011) State of the APC/C: organization, function, and structure. *Critical Reviews in Biochemistry and Molecular Biology* **46:** 118–136

Mevissen TET & Komander D (2017) Mechanisms of Deubiquitinase Specificity and Regulation. *Annu Rev Biochem* **86:** 159–192

Meyer H, Bug M & Bremer S (2012) Emerging functions of the VCP/p97 AAA-ATPase in the ubiquitin system. *Nat Rev Microbiol* **14:** 117–123

Meyer H-J & Rape M (2014) Enhanced protein degradation by branched ubiquitin chains. *Cell* **157:** 910–921

Moehle EA, Ryan CJ, Krogan NJ, Kress TL & Guthrie C (2012) The yeast SR-like protein Npl3 links chromatin modification to mRNA processing. *PLoS Genet*. **8:** e1003101

Moldovan G-L, Pfander B & Jentsch S (2006) PCNA controls establishment of sister chromatid cohesion during S phase. *Mol Cell* **23:** 723–732

Moreno SP, Bailey R, Campion N, Herron S & Gambus A (2014) Polyubiquitylation drives replisome disassembly at the termination of DNA replication. *Science* **346:** 477–481

Morreale FE & Walden H (2016) Types of Ubiquitin Ligases. *Cell* **165:** 248–248.e1

Mukhopadhyay D, Arnaoutov A & Dasso M (2010) The SUMO protease SENP6 is essential for inner kinetochore assembly. *J. Cell Biol.* **188:** 681–692

Mullen JR, Kaliraman V, Ibrahim SS & Brill SJ (2001) Requirement for three novel protein complexes in the absence of the Sgs1 DNA helicase in Saccharomyces cerevisiae. *Genetics* **157:** 103–118

Mumberg D, Müller R & Funk M (1995) Yeast vectors for the controlled expression of heterologous proteins in different genetic backgrounds. *Gene* **156:** 119–122

Nagai S, Dubrana K, Tsai-Pflugfelder M, Davidson MB, Roberts TM, Brown GW, Varela E, Hediger F, Gasser SM & Krogan NJ (2008) Functional targeting of DNA damage to a nuclear pore-associated SUMO-dependent ubiquitin ligase. *Science* **322:** 597–602

Ndoja A, Cohen RE & Yao T (2014) Ubiquitin signals proteolysis-independent stripping of transcription factors. *Mol Cell* **53:** 893–903

Neyret-Kahn H, Benhamed M, Ye T, Le Gras S, Cossec J-C, Lapaquette P, Bischof O, Ouspenskaia M, Dasso M, Seeler J, Davidson I & Dejean A (2013) Sumoylation at chromatin governs coordinated repression of a transcriptional program essential for cell growth and proliferation. *Genome Res* **23:** 1563–1579

Ng CH, Akhter A, Yurko N, Burgener JM, Rosonina E & Manley JL (2015) Sumoylation controls the timing of Tup1-mediated transcriptional deactivation. *Nat Commun* **6:** 6610

Nie M & Boddy M (2016) Cooperativity of the SUMO and Ubiquitin Pathways in Genome Stability. *Biomolecules* **6:** 14–13

Nie M, Aslanian A, Prudden J, Heideker J, Vashisht AA, Wohlschlegel JA, Yates JR & Boddy MN (2012) Dual recruitment of Cdc48 (p97)-Ufd1-Npl4 ubiquitin-selective segregase by small ubiquitin-like modifier protein (SUMO) and ubiquitin in SUMO-targeted ubiquitin ligase-mediated genome stability functions. *J Biol Chem* **287:** 29610–29619

Niskanen EA, Malinen M, Sutinen P, Toropainen S, Paakinaho V, Vihervaara A, Joutsen J, Kaikkonen MU, Sistonen L & Palvimo JJ (2015) Global SUMOylation on active chromatin is an acute heat stress response restricting transcription. *Genome Biol.* **16:** 1–19

O'Geen H, Nicolet CM, Blahnik K, Green R & Farnham PJ (2006) Comparison of sample preparation methods for ChIP-chip assays. *Biotechniques* **41:** 577–580

Oh E, Akopian D & Rape M (2018) Principles of Ubiquitin-Dependent Signaling. *Annu Rev Cell Dev Biol* **34:** annurev–cellbio–100617–062802

Ohkuni K, Levy-Myers R, Warren J, Au W-C, Takahashi Y, Baker RE & Basrai MA (2018) N-terminal Sumoylation of Centromeric Histone H3 Variant Cse4 Regulates Its Proteolysis To Prevent Mislocalization to Non-centromeric Chromatin. *G3 (Bethesda)* **8:** 1215–1223

Ohkuni K, Takahashi Y, Fulp A, Lawrimore J, Au W-C, Pasupala N, Levy-Myers R, Warren J, Strunnikov A, Baker RE, Kerscher O, Bloom K & Basrai MA (2016) SUMO-Targeted Ubiquitin Ligase (STUbL) Slx5 regulates proteolysis of centromeric histone H3 variant Cse4 and prevents its mislocalization to euchromatin. *Mol Biol Cell* **27:** 1500–1510

Panse VG, Kressler D, Pauli A, Petfalski E, Gnädig M, Tollervey D & Hurt E (2006) Formation and nuclear export of preribosomes are functionally linked to the small-ubiquitin-related modifier pathway. *Traffic* **7:** 1311–1321

Pao K-C, Wood NT, Knebel A, Rafie K, Stanley M, Mabbitt PD, Sundaramoorthy R, Hofmann K, Aalten DMF & Virdee S (2018) Activity-based E3 ligase profiling uncovers an E3 ligase with esterification activity. *Nature* **556:** 1–27

Papouli E, Chen S, Davies AA, Huttner D, Krejci L, Sung P & Ulrich HD (2005) Crosstalk between SUMO and ubiquitin on PCNA is mediated by recruitment of the helicase Srs2p. *Mol Cell* **19:** 123–133

Parker JL & Ulrich HD (2012) A SUMO-interacting motif activates budding yeast ubiquitin ligase Rad18 towards SUMO-modified PCNA. *Nucleic Acids Res* **40:** 11380–11388

Pfander B, Moldovan G-L, Sacher M, Hoege C & Jentsch S (2005) SUMO-modified PCNA recruits Srs2 to prevent recombination during S phase. *Nature* **436:** 428–433

Pickles S, Vigié P & Youle RJ (2018) Mitophagy and Quality Control Mechanisms in Mitochondrial Maintenance. *Curr Biol* **28:** R170–R185

Plechanovová A, Jaffray EG, McMahon SA, Johnson KA, Navrátilová I, Naismith JH & Hay RT (2011) Mechanism of ubiquitylation by dimeric RING ligase RNF4. *Nat Struct Mol Biol* **18:** 1052–1059

Plechanovová A, Jaffray EG, Tatham MH, Naismith JH & Hay RT (2012) Structure of a RING E3 ligase and ubiquitin-loaded E2 primed for catalysis. *Nature* **489:** 115–120

Potts PR & Yu H (2007) The SMC5/6 complex maintains telomere length in ALT cancer cells through SUMOylation of telomere-binding proteins. *Nat Struct Mol Biol* **14:** 581–590

Poulsen SL, Hansen RK, Wagner SA, van Cuijk L, van Belle GJ, Streicher W, Wikstrom M, Choudhary C, Houtsmuller AB, Marteijn JA, Bekker-Jensen S & Mailand N (2013) RNF111/Arkadia is a SUMO-targeted ubiquitin ligase that facilitates the DNA damage response. *J. Cell Biol.* **201:** 797–807

Prudden J, Pebernard S, Raffa G, Slavin DA, Perry JJP, Tainer JA, McGowan CH & Boddy MN (2007) SUMO-targeted ubiquitin ligases in genome stability. *EMBO J* **26:** 4089–4101

Prytuliak R, Volkmer M, Meier M & Habermann BH (2017) HH-MOTiF: de novo detection of short linear motifs in proteins by Hidden Markov Model comparisons. *Nucleic Acids Res* **45:** W470–W477

Psakhye I & Jentsch S (2012) Protein group modification and synergy in the SUMO pathway as exemplified in DNA repair. *Cell* **151:** 807–820

Psakhye I & Jentsch S (2016) Identification of Substrates of Protein-Group SUMOylation. *Methods Mol Biol* **1475:** 219–231

Qiu J, Sheedlo MJ, Yu K, Tan Y, Nakayasu ES, Das C, Liu X & Luo Z-Q (2016) Ubiquitination independent of E1 and E2 enzymes by bacterial effectors. *Nature* **533:** 1–17

Ramadan K, Bruderer R, Spiga FM, Popp O, Baur T, Gotta M & Meyer HH (2007) Cdc48/p97 promotes reformation of the nucleus by extracting the kinase Aurora B from chromatin. *Nature* **450:** 1258–1262

Raman M, Havens CG, Walter JC & Harper JW (2011) A genome-wide screen identifies p97 as an essential regulator of DNA damage-dependent CDT1 destruction. *Mol Cell* **44:** 72–84

Rape M, Hoppe T, Gorr I, Kalocay M, Richly H & Jentsch S (2001) Mobilization of processed, membrane-tethered SPT23 transcription factor by CDC48(UFD1/NPL4), a ubiquitin-selective chaperone. *Cell* **107:** 667–677

Ravarani CN, Erkina TY, De Baets G, Dudman DC, Erkine AM & Babu MM (2018) High-throughput discovery of functional disordered regions: investigation of transactivation domains. *Mol Syst Biol* **14:** e8190

Rendón OZ, Fredrickson EK, Howard CJ, Van Vranken J, Fogarty S, Tolley ND, Kalia R, Osuna BA, Shen PS, Hill CP, Frost A & Rutter J (2018) Vms1p is a release factor for the ribosome- associated quality control complex. *Nat Commun* **9:** 1–9

Renkawitz J, Lademann CA, Kalocsay M & Jentsch S (2013) Monitoring homology search during DNA double-strand break repair in vivo. *Mol Cell* **50:** 261–272

Richly H, Rape M, Braun S, Rumpf S, Hoege C & Jentsch S (2005) A series of ubiquitin binding factors connects CDC48/p97 to substrate multiubiquitylation and proteasomal targeting. *Cell* **120:** 73–84

Ritz D, Vuk M, Kirchner P, Bug M, Schütz S, Hayer A, Bremer S, Lusk C, Baloh RH, Lee H, Glatter T, Gstaiger M, Aebersold R, Weihl CC & Meyer H (2011) Endolysosomal sorting of ubiquitylated caveolin-1 is regulated by VCP and UBXD1 and impaired by VCP disease mutations. *Nat Cell Biol* **13:** 1116–1123

Rojas-Fernandez A, Plechanovová A, Hattersley N, Jaffray E, Tatham MH & Hay RT (2014) SUMO Chain-Induced Dimerization Activates RNF4. *Mol Cell* **53:** 880–892

Rosonina E, Akhter A, Dou Y, Babu J & Sri Theivakadadcham VS (2017) Regulation of transcription factors by sumoylation. *Transcription* **8:** 220–231

Rosonina E, Duncan SM & Manley JL (2010) SUMO functions in constitutive transcription and during activation of inducible genes in yeast. *Genes Dev* **24:** 1242–1252

Rosonina E, Duncan SM & Manley JL (2012) Sumoylation of transcription factor Gcn4 facilitates its Srb10-mediated clearance from promoters in yeast. *Genes Dev* **26:** 350–355

Ruiz-Roig C, Viéitez C, Posas F & de Nadal E (2010) The Rpd3L HDAC complex is essential for the heat stress response in yeast. *Mol Microbiol* **76:** 1049–1062

Rumpf S & Jentsch S (2006) Functional Division of Substrate Processing Cofactors of the Ubiquitin-Selective Cdc48 Chaperone. *Mol Cell* **21:** 261–269

Ryu T, Spatola B, Delabaere L, Bowlin K, Hopp H, Kunitake R, Karpen GH & Chiolo I (2015) Heterochromatic breaks move to the nuclear periphery to continue recombinational repair. *Nat Cell Biol* **17:** 1401–1411

Sato Y, Yoshikawa A, Mimura H, Yamashita M, Yamagata A & Fukai S (2009) Structural basis for specific recognition of Lys 63-linked polyubiquitin chains by tandem UIMs of RAP80. *EMBO J* **28:** 2461–2468

Schauber C, Chen L, Tongaonkar P, Vega I, Lambertson D, Potts W & Madura K (1998) Rad23 links DNA repair to the ubiquitin/proteasome pathway. *Nature* **391:** 715–718

Scheffner M, Nuber U & Huibregtse JM (1995) Protein ubiquitination involving an E1-E2-E3 enzyme ubiquitin thioester cascade. *Nature* **373:** 81–83

Schreiner P, Chen X, Husnjak K, Randles L, Zhang N, Elsasser S, Finley D, Dikic I, Walters KJ & Groll M (2008) Ubiquitin docking at the proteasome through a novel pleckstrin-homology domain interaction. *Nature* **453:** 548–552

Schwanhäusser B, Busse D, Li N, Dittmar G, Schuchhardt J, Wolf J, Chen W & Selbach M (2011) Global quantification of mammalian gene expression control. *Nature* **473:** 337–342

Schweiggert J, Stevermann L, Panigada D, Kammerer D & Liakopoulos D (2016) Regulation of a Spindle Positioning Factor at Kinetochores by SUMO-Targeted Ubiquitin Ligases. *Dev Cell* **36:** 415–427

Schwertman P, Bekker-Jensen S & Mailand N (2016) Regulation of DNA double-strand break repair by ubiquitin and ubiquitin-like modifiers. *Nat Rev Mol Cell Biol* **17:** 379–394

Seifert A, Schofield P, Barton GJ & Hay RT (2015) Proteotoxic stress reprograms the chromatin landscape of SUMO modification. *Sci Signal* **8:** rs7–rs7

Sen P, Dang W, Donahue G, Dai J, Dorsey J, Cao X, Liu W, Cao K, Perry R, Lee JY, Wasko BM, Carr DT, He C, Robison B, Wagner J, Gregory BD, Kaeberlein M, Kennedy BK, Boeke JD & Berger SL (2015) H3K36 methylation promotes longevity by enhancing transcriptional fidelity. *Genes Dev* **29:** 1362–1376

Shah PP, Zheng X, Epshtein A, Carey JN, Bishop DK & Klein HL (2010) Swi2/Snf2-related translocases prevent accumulation of toxic Rad51 complexes during mitotic growth. *Mol Cell* **39:** 862–872

Shalizi A, Gaudillière B, Yuan Z, Stegmüller J, Shirogane T, Ge Q, Tan Y, Schulman B, Harper JW & Bonni A (2006) A calcium-regulated MEF2 sumoylation switch controls postsynaptic differentiation. *Science* **311:** 1012–1017

Sharma P, Mullen JR, Li M, Zaratiegui M, Bunting SF & Brill SJ (2017) A Lysine Desert Protects a Novel Domain in the Slx5-Slx8 SUMO Targeted Ub Ligase To Maintain Sumoylation Levels in Saccharomyces cerevisiae. *Genetics* **206:** 1807–1821

Shen TH, Lin H-K, Scaglioni PP, Yung TM & Pandolfi PP (2006) The mechanisms of PML-nuclear body formation. *Mol Cell* **24:** 331–339

Shibata Y & Morimoto RI (2014) How the nucleus copes with proteotoxic stress. *Curr Biol* **24:** R463–74

Shiio Y & Eisenman RN (2003) Histone sumoylation is associated with transcriptional repression. *Proc Natl Acad Sci USA* **100:** 13225–13230

Shimizu Y, Okuda-Shimizu Y & Hendershot LM (2010) Ubiquitylation of an ERAD substrate occurs on multiple types of amino acids. *Mol Cell* **40:** 917–926

Sigler PB (1988) Transcriptional activation. Acid blobs and negative noodles. *Nature* **333:** 210–212

Sims JJ & Cohen RE (2009) Linkage-specific avidity defines the lysine 63-linked polyubiquitin-binding preference of rap80. *Mol Cell* **33:** 775–783

Skaar JR, Pagan JK & Pagano M (2013) Mechanisms and function of substrate recruitment by F-box proteins. *Nat Rev Mol Cell Biol* **14:** 369–381

Song J, Durrin LK, Wilkinson TA, Krontiris TG & Chen Y (2004) Identification of a SUMO-binding motif that recognizes SUMO-modified proteins. *Proc Natl Acad Sci USA* **101:** 14373–14378

Sri Theivakadadcham VS, Bergey BG & Rosonina E (2019) Sumoylation of DNA-bound transcription factor Sko1 prevents its association with nontarget promoters. *PLoS Genet*. **15:** e1007991

Sriramachandran AM & Dohmen RJ (2014) SUMO-targeted ubiquitin ligases. *Biochim Biophys Acta* **1843:** 75–85

Steinacher R & Schär P (2005) Functionality of human thymine DNA glycosylase requires SUMO-regulated changes in protein conformation. *Current Biology* **15:** 616–623

Stingele J & Jentsch S (2015) DNA-protein crosslink repair. *Nat Rev Microbiol* **16:** 455–460

Stingele J, Schwarz MS, Bloemeke N, Wolf PG & Jentsch S (2014) A DNA-Dependent Protease Involved in DNA-Protein Crosslink Repair. *Cell*

Su XA, Dion V, Gasser SM & Freudenreich CH (2015) Regulation of recombination at yeast nuclear pores controls repair and triplet repeat stability. *Genes Dev* **29:** 1006–1017

Sun H & Hunter T (2012) Poly-Small Ubiquitin-like Modifier (PolySUMO)-binding Proteins Identified through a String Search. *J Biol Chem* **287:** 42071–42083

Sun H, Leverson JD & Hunter T (2007) Conserved function of RNF4 family proteins in eukaryotes: targeting a ubiquitin ligase to SUMOylated proteins. *EMBO J* **26:** 4102–4112

Sun H, Liu Y & Hunter T (2014) Multiple Arkadia/RNF111 Structures Coordinate Its Polycomb Body Association and Transcriptional Control. *Mol Cell Biol* **34:** 2981–2995

Sydorskyy Y, Srikumar T, Jeram SM, Wheaton S, Vizeacoumar FJ, Makhnevych T, Chong YT, Gingras A-C & Raught B (2010) A novel mechanism for SUMO system control: regulated Ulp1 nucleolar sequestration. *Mol Cell Biol* **30:** 4452–4462

Taddei A & Gasser SM (2012) Structure and Function in the Budding Yeast Nucleus. *Genetics* **192:** 107–129

Talhaoui I, Bernal M, Mullen JR, Dorison H, Palancade B, Brill SJ & Mazón G (2018) Slx5-Slx8 ubiquitin ligase targets active pools of the Yen1 nuclease to limit crossover formation. *Nat Commun* **9:** 1–14

Tan W, Wang Z & Prelich G (2013) Physical and Genetic Interactions Between Uls1 and the Slx5-Slx8 SUMO-Targeted Ubiquitin Ligase. *G3 (Bethesda)* **3:** 771–780

Tatham MH, Geoffroy M-C, Shen L, Plechanovová A, Hattersley N, Jaffray EG, Palvimo JJ & Hay RT (2008) RNF4 is a poly-SUMO-specific E3 ubiquitin ligase required for arsenic-induced PML degradation. *Nat Cell Biol* **10:** 538–546

Tatham MH, Matic I, Mann M & Hay RT (2011) Comparative proteomic analysis identifies a role for SUMO in protein quality control. *Sci Signal* **4:** rs4

Tempé D, Piechaczyk M & Bossis G (2008) SUMO under stress. *Biochem. Soc. Trans.* **36:** 874–878

Texari L, Dieppois G, Vinciguerra P, Contreras MP, Groner A, Letourneau A & Stutz F (2013) The nuclear pore regulates GAL1 gene transcription by controlling the localization of the SUMO protease Ulp1. *Mol Cell* **51:** 807–818

Thomas JJ, Abed M, Heuberger J, Novak R, Zohar Y, Lopez APB, Trausch-Azar JS, Ilagan MXG, Benhamou D, Dittmar G, Kopan R, Birchmeier W, Schwartz AL & Orian A (2016) RNF4-Dependent Oncogene Activation by Protein Stabilization. *Cell Rep* **16:** 3388–3400

Thu YM, Van Riper SK, Higgins L, Zhang T, Becker JR, Markowski TW, Nguyen HD, Griffin TJ & Bielinsky AK (2016) Slx5/Slx8 Promotes Replication Stress Tolerance by Facilitating Mitotic Progression. *Cell Rep* **15:** 1–13

Tsuchiya H, Ohtake F, Arai N, Kaiho A, Yasuda S, Tanaka K & Saeki Y (2017) In Vivo Ubiquitin Linkage-type Analysis Reveals that the Cdc48-Rad23/Dsk2 Axis Contributes to K48-Linked Chain Specificity of the Proteasome. *Mol Cell* **66:** 488–502.e7

Tutucci E & Stutz F (2011) Keeping mRNPs in check during assembly and nuclear export. *Nat Rev Mol Cell Biol* **12:** 377–384

Ulrich HD & Walden H (2010) Ubiquitin signalling in DNA replication and repair. *Nat Rev Mol Cell Biol* **11:** 479–489

Uzunova K, Göttsche K, Miteva M, Weisshaar SR, Glanemann C, Schnellhardt M, Niessen M, Scheel H, Hofmann K, Johnson ES, Praefcke GJK & Dohmen RJ (2007) Ubiquitin-dependent proteolytic control of SUMO conjugates. *J Biol Chem* **282:** 34167–34175

van de Pasch LAL, Miles AJ, Nijenhuis W, Brabers NACH, van Leenen D, Lijnzaad P, Brown MK, Ouellet J, Barral Y, Kops GJPL & Holstege FCP (2013) Centromere binding and a conserved role in chromosome stability for SUMO-dependent ubiquitin ligases. *PLoS ONE* **8:** e65628

van den Boom J & Meyer H (2017) VCP/p97-Mediated Unfolding as a Principle in Protein Homeostasis and Signaling. *Mol Cell* **69:** 1–13

Van der Veen AG & Ploegh HL (2012) Ubiquitin-Like Proteins. *Annu Rev Biochem* **81:** 323–357

van Hagen M, Overmeer RM, Abolvardi SS & Vertegaal ACO (2010) RNF4 and VHL regulate the proteasomal degradation of SUMO-conjugated Hypoxia-Inducible Factor-2alpha. *Nucleic Acids Res* **38:** 1922–1931

van Nocker S, Sadis S, Rubin DM, Glickman M, Fu H, Coux O, Wefes I, Finley D & Vierstra RD (1996) The multiubiquitin-chain-binding protein Mcb1 is a component of the 26S proteasome in Saccharomyces cerevisiae and plays a nonessential, substrate-specific role in protein turnover. *Mol Cell Biol* **16:** 6020–6028

Varadan R, Assfalg M, Raasi S, Pickart C & Fushman D (2005) Structural determinants for selective recognition of a Lys48-linked polyubiquitin chain by a UBA domain. *Mol Cell* **18:** 687–698

Varshavsky A (2012) The ubiquitin system, an immense realm. *Annu Rev Biochem* **81:** 167–176

Verma R, Aravind L, Oania R, McDonald WH, Yates JR, Koonin EV & Deshaies RJ (2002) Role of Rpn11 metalloprotease in deubiquitination and degradation by the 26S proteasome. *Science* **298:** 611–615

Verma R, Chen S, Feldman R, Schieltz D, Yates J, Dohmen J & Deshaies RJ (2000) Proteasomal proteomics: identification of nucleotide-sensitive proteasome-interacting proteins by mass spectrometric analysis of affinity-purified proteasomes. *Mol Biol Cell* **11:** 3425–3439

Verma R, Oania R, Fang R, Smith GT & Deshaies RJ (2011) Cdc48/p97 mediates UV-dependent turnover of RNA Pol II. *Mol Cell* **41:** 82–92

Verma R, Reichermeier KM, Burroughs AM, Oania RS, Reitsma JM, Aravind L & Deshaies RJ (2018) Vms1 and ANKZF1 peptidyl-tRNA hydrolases release nascent chains from stalled ribosomes. *Nat Rev Microbiol* **557:** 446–451

Wang X, Herr RA & Hansen TH (2012) Ubiquitination of substrates by esterification. *Traffic* **13:** 19–24

Wang Z & Prelich G (2009) Quality Control of a Transcriptional Regulator by SUMO-Targeted Degradation. *Mol Cell Biol* **29:** 1694–1706

Wang Z, Wu C, Aslanian A, Yates JR & Hunter T (2018) Defective RNA polymerase III is negatively regulated by the SUMO-Ubiquitin-Cdc48 pathway. *Elife* **7:** 526

Wei Y, Diao L-X, Lu S, Wang H-T, Suo F, Dong M-Q & Du L-L (2017) SUMO-Targeted DNA Translocase Rrp2 Protects the Genome from Top2-Induced DNA Damage. *Mol Cell* **66:** 1–36

Welker S, Rudolph B, Frenzel E, Hagn F, Liebisch G, Schmitz G, Scheuring J, Kerth A, Blume A, Weinkauf S, Haslbeck M, Kessler H & Buchner J (2010) Hsp12 is an intrinsically unstructured stress protein that folds upon membrane association and modulates membrane function. *Mol Cell* **39:** 507–520

Westerbeck JW, Pasupala N, Guillotte M, Szymanski E, Matson BC, Esteban C & Kerscher O (2014) A SUMO-targeted ubiquitin ligase is involved in the degradation of the nuclear pool of the SUMO E3 ligase Siz1. *Mol Biol Cell* **25:** 1–16

Wilcox AJ & Laney JD (2009) A ubiquitin-selective AAA-ATPase mediates transcriptional switching by remodelling a repressor-promoter DNA complex. *Nat Cell Biol* **11:** 1481–1486

Wohlschlegel JA, Johnson ES, Reed SI & Yates JR (2004) Global analysis of protein sumoylation in Saccharomyces cerevisiae. *J Biol Chem* **279:** 45662–45668

Xie Y, Kerscher O, Kroetz MB, McConchie HF, Sung P & Hochstrasser M (2007) The yeast Hex3.Slx8 heterodimer is a ubiquitin ligase stimulated by substrate sumoylation. *J Biol Chem* **282:** 34176–34184

Xie Y, Rubenstein EM, Matt T & Hochstrasser M (2010) SUMO-independent in vivo activity of a SUMO-targeted ubiquitin ligase toward a short-lived transcription factor. *Genes Dev* **24:** 893–903

Xu Y, Plechanovová A, Simpson P, Marchant J, Leidecker O, Kraatz S, Hay RT & Matthews SJ (2014) Structural insight into SUMO chain recognition and manipulation by the ubiquitin ligase RNF4. *Nat Commun* **5:** 4217

Yang L, Mullen JR & Brill SJ (2006) Purification of the yeast Slx5-Slx8 protein complex and characterization of its DNA-binding activity. *Nucleic Acids Res* **34:** 5541–5551

Yang X-J & Seto E (2008) The Rpd3/Hda1 family of lysine deacetylases: from bacteria and yeast to mice and men. *Nat Rev Mol Cell Biol* **9:** 206–218

Yao T & Ndoja A (2012) Regulation of gene expression by the ubiquitin-proteasome system. *Semin Cell Dev Biol* **23:** 523–529

Yau RG, Doerner K, Castellanos ER, Haakonsen DL, Werner A, Wang N, Yang XW, Martinez-Martin N, Matsumoto ML, Dixit VM & Rape M (2017) Assembly and Function of Heterotypic Ubiquitin Chains in Cell-Cycle and Protein Quality Control. *Cell* **171:** 1–37

Yin Y, Seifert A, Chua JS, Maure J-F, Golebiowski F & Hay RT (2012) SUMO-targeted ubiquitin E3 ligase RNF4 is required for the response of human cells to DNA damage. *Genes Dev* **26:** 1196–1208

Yu H, Braun P, Yildirim MA, Lemmens I, Venkatesan K, Sahalie J, Hirozane-Kishikawa T, Gebreab F, Li N, Simonis N, Hao T, Rual J-F, Dricot A, Vazquez A, Murray RR, Simon C, Tardivo L, Tam S, Svrzikapa N, Fan C, et al (2008) High-quality binary protein interaction map of the yeast interactome network. *Science* **322:** 104–110

Zhang H, Roberts DN & Cairns BR (2005) Genome-wide dynamics of Htz1, a histone H2A variant that poises repressed/basal promoters for activation through histone loss. *Cell* **123:** 219–231

Zhang L, Liu N, Ma X & Jiang L (2013) The transcriptional control machinery as well as the cell wall integrity and its regulation are involved in the detoxification of the organic solvent dimethyl sulfoxide in Saccharomyces cerevisiae. *FEMS Yeast Res*. **13:** 200–218

Zhao X (2018) SUMO-Mediated Regulation of Nuclear Functions and Signaling Processes. *Mol Cell* **71:** 409–418

Zheng J, Benschop JJ, Shales M, Kemmeren P, Greenblatt J, Cagney G, Holstege F, Li H & Krogan NJ (2010) Epistatic relationships reveal the functional organization of yeast transcription factors. *Mol Syst Biol* **6:** 420

Zheng N & Shabek N (2017) Ubiquitin Ligases: Structure, Function, and Regulation. *Annu Rev Biochem* **86:** 129–157

Zhou W, Ryan JJ & Zhou H (2004) Global Analyses of Sumoylated Proteins in Saccharomyces cerevisiae. *J Biol Chem* **279:** 32262–32268

Danksagung

Zuallererst gilt mein Dank Stefan Jentsch, der mir die Möglichkeit gegeben hat an diesem Projekt zu arbeiten, und der mit seiner Neugier, seiner Offenheit und seiner großzügigen Art eine unvergleichliche Umgebung für wissenschaftliche Forschung in seinem Labor geschaffen hat. Er war ein inspirierender Mentor, und ich bedauere es sehr, dass er die Vollendung dieser Arbeit nicht erleben kann.

Mein großer Dank und meine Wertschätzung gelten ebenso Boris Pfander, der mich in allen Belangen in den Jahren nach Stefans Tod unterstützt hat. Ich bin dankbar für die Freiheit, die auch er mir gewährt hat, für den regen Austausch von Ideen sowie die geduldige Unterstützung bei der Vollendung unserer Publikation und dieser Arbeit.

Außerdem gilt mein Dank besonders Peter Becker, der sich großzügig bereiterklärt hat als mein Doktorvater zu agieren und der schon in meinem Thesis Advisory Committee wertvolle Ideen eingebracht hat. Auch Christof Osman, der als Zweitgutachter fungiert, sowie den anderen Mitgliedern meines TACs, Alexander Buchberger und Stephan Gruber und allen Angehörigen der Prüfungskommission möchte ich für ihre Zeit und ihre Anregungen danken.

Auch Max Kern ist an dieser Stelle besonders hervorzuheben, seine Doktorarbeit hat den Grundstein für diese Arbeit gelegt und ich konnte von seinen Ideen und Anregungen, aber auch von vorhandenen Ergebnissen und Materialien immens profitieren. Für die exzellente wissenschaftliche Zusammenarbeit möchte ich mich auch besonders bei Tobias Straub bedanken, der geduldig und fachkundig die bioinformatische Analyse vieler Datensätze übernommen hat. Auch mit Roman Prytuliak sowie Bianca Habermann hat sich eine sehr gute Zusammenarbeit bei der Slx5-Bindemotif-Vorhersage ergeben.

Neben den wissenschaftlichen Ideengebern und Kollaborationspartnern wäre diese Arbeit auch ohne handfeste Hilfe im Labor nicht möglich gewesen. Besonders für ihren Einsatz an der Bench möchte ich daher Alexander Strasser, Katrin Strasser, Jochen Rech und Ludwig Rieger danken, auch von der MPI Biochemistry Core Facility, besonders von Marja Driessen (RNA Sequenzierung), Nagarjuna Nagaraj (Proteomik), sowie von Assa Yeroslaviz (Bioinformatik) habe währen meiner Doktorarbeit wertvolle Hilfe bekommen. Auch Florian Paasch, Florian Wilfling, und Johannes Heipke haben mich bei wichtigen Experimenten unterstützt. Besonders wichtig für die Arbeit war auch die exzellente Arbeit der Mitarbeiter in der Medienküche, besonders Massimo Bossi hat mit seiner Arbeit vieles überhaupt erst möglich gemacht. Auch Klara und Dirk danke ich speziell für ihre Hilfe mit organisatorischen Aufgabenund Bestellungen.

Bei allen Laborkollegen möchte ich mich nicht nur für ein exzellentes wissenschaftliches Umfeld mit bereichernden Diskussionen bedanken (besonders mit Julian, Claudio, Sittinan, Fabian, Flo W., Flo P.), sondern auch für eine einmalige Laboratmosphäre, die immer Spaß gemacht hat und frustrierende Ergebnisse meist schnell vergessen ließ. Speziell mit meinen Benchnachbarn Irina und André, sowie den Labornachbarn Claudio, Matías und Ben ist die Zeit im Labor meist schnell vergangen. Nachdem das Labor etwas geschrumpft ist, haben auch besonders Kenny und Flo W. noch für eine gute Stimmung gesorgt. Auch alle anderen Jentsch Lab Mitglieder sowie besonders die Mitarbeiter der Pfander Gruppe und der anderen MCB Gruppen haben für eine gute wissenschaftliche Atmosphäre und gute Stimmung gesorgt.

Speziell bei Julian, Max, Neysan, Flo P., Claudio und Ivan möchte ich mich auch für das Korrekturlesen und ihre Ideen für das Manuskript und diese Arbeit bedanken!

Neben all der Unterstützung im und um das Labor war auch die persönliche Unterstützung meiner Familie und Freunde von unschätzbarem Wert. Speziell meine Schwestern Karin und Lisa haben mir immer Rückhalt gegeben, und meine Nichte und meine Neffen Valerie, Moritz und Jakob haben mich während der Doktorarbeit zum stolzen Onkel gemacht und für viel Abwechslung gesorgt. Ein großes Danke auch an Papa und Helga, sie haben mich immer unterstützt wenn ich sie gebraucht habe, und Papa hat mir immer die Freiheit gegeben das zu tun, was mich am meisten begeistert hat. Auch dem Rest meiner Familie möchte ich danken, der große Zusammenhalt nach einigen schwierigen Jahren war für uns alle wichtig!

Leider können Mama und Oma die Fertigstellung dieser Arbeit nicht miterleben – ihnen habe ich viel zu verdanken, sie haben mich immer auf meinem Weg in der Wissenschaft unterstützt und wären sicher stolz wenn sie dabei sein könnten.

Last but not least, I would like to express my endless gratitute to Natalia, her love, encouragement and patient support when I spent many evenings working were key ingredients to the success of this work. Besides that, she makes each and every day we spend together so much better!

Curriculum Vitae
Markus Höpfler

University Education & Research Experience

09/2013 - present	**PhD thesis with Prof. Stefan Jentsch** (deceased 10/2016) and Dr. Boris Pfander, Max Planck Institute of Biochemistry, Martinsried/Munich. Thesis title: "Slx5/Slx8-dependent ubiquitin hotspots on chromatin contribute to stress tolerance in *Saccharomyces Cerevisiae*"
04/2012 - 05/2013	**Research associate position with Prof. Andrea Barta**, Max F. Perutz Laboratories, Medical University of Vienna. Work on alternative splicing regulation in *A. thaliana.*
10/2006 - 06/2012	**Medical School** of the Medical University of Vienna (parallel studies), finished three years of MD curriculum.
11/2010 - 08/2011	**Diploma thesis with Prof. Jochen Guck**, Cavendish Laboratory, University of Cambridge, UK. Thesis title: "Connections between Cell Mechanics and Chromatin Dynamics in Embryonic Stem Cells"
10/2005 - 12/2011	**Diploma in Molecular Biology** (equivalent to MSc), University of Vienna. Focus on Genetics, Cell Biology and Microbiology. Graduation with distinction.
09/1996 - 07/2004	**Highschool** Stiftsgymnasium Kremsmünster, Austria. Matura (graduation) with distinction.

Publications

Markus Höpfler, Maximilian J. Kern, Tobias Straub, Roman Prytuliak, Bianca H. Habermann, Boris Pfander, and Stefan Jentsch (2019). **Slx5/Slx8-dependent ubiquitin hotspots on chromatin contribute to stress tolearance.** *EMBO J.*
http://emboj.embopress.org/content/early/2019/04/23/embj.2018100368

Yamile Marquez, Markus Höpfler, Zahra Ayatollahi, Andrea Barta, and Maria Kalyna (2015). **Unmasking alternative splicing inside protein-coding exons defines exitrons and their role in proteome plasticity.** *GENOME RES.*
http://genome.cshlp.org/content/25/7/995.long

Kevin J. Chalut*, Markus Höpfler*, Franziska Lautenschläger, Lars Boyde, Joseph Chang, Andrew Ekpenyong, Alfonso Martinez-Arias, and Jochen Guck (2012). **Chromatin Decondensation and Nuclear Softening Accompany Nanog Downregulation in Embryonic Stem Cells.** *BIOPHYS J.*
* equal contribution
https://www.cell.com/biophysj/fulltext/S0006-3495(12)01120-4

Awards & Scholarships

2015	Poster prize, International Max Planck Research School Seminar, Martinsried/Munich
2013	Selected for Max Planck International Research School for Molecular Life Sciences, Martinsried/Munich
2013	Selected for Life Science Zurich Graduate School (declined)
2013	Selected for FMI Basel International PhD Program (declined)
2010	Research scholarship to support my diploma thesis in Cambridge, UK, granted from the University of Vienna
2010	Performance scholarship for excellent grades (University of Vienna)
2009	Performance scholarship for excellent grades (University of Vienna)
2008	Performance scholarship for excellent grades (University of Vienna)
2007	Performance scholarship for excellent grades (Medical University of Vienna)